

UNIVERSITÉ DE NANTES
FACULTÉ DES SCIENCES ET DES TECHNIQUES

ÉCOLE DOCTORALE 3MPL
MATIERE, MOLECULES, MATERIAUX EN PAYS DE LOIRE

Année 2014

Caractérisation des interactions entre le dioxyde de titane et les phospholipides en milieu aqueux

THÈSE DE DOCTORAT
Discipline : Sciences des Matériaux
Spécialité : Physico-Chimie des Matériaux

*Présentée
et soutenue publiquement par*

Quoc Chon LE

Le 01 Décembre 2014, devant le jury ci-dessous

Président	Hynd REMITA, Directeur de Recherche, CNRS
Rapporteurs	Dominique COSTA, Chargé de Recherche, CNRS Sylvie BEGIN-COLIN, Professeur, Université de Strasbourg
Examineurs	Hynd REMITA, Directeur de Recherche, CNRS Mireille RICHARD, Chargé de Recherche, CNRS Luc BROHAN, Chargé de Recherche, CNRS

Directeur de thèse : Bernard HUMBERT

Co-encadrant : Marie-Hélène ROPERS et Hélène TERRISSE

Preface

This dissertation is the result of 3-years work in collaboration between “Institut des Matériaux de Nantes” (IMN, France) and “Biopolymère, Interactions, Assemblages” (BIA) group at INRA (Nantes, France). There are 5 chapters in this dissertation. The study started in October 2011 and finished in November 2014.

Some results from this work have been published and presented:

1. Quoc-Chon Le, Marie-Hélène Ropers, Hélène Terrisse, Bernard Humbert. Interactions between phospholipids and titanium dioxide particles. Accepted for *Journal of Colloids and Surfaces B: Biointerfaces*. DOI: 10.1016/j.colsurfb.2014.09.010
2. Oral presentation in European Conference on Surface Science 2014 (Antalya, Turkey).
3. Poster presentation in 27th Conference of European Colloid and Interface Society 2013 (Sofia, Bulgaria).

Abstract

Characterizing the interactions between titanium dioxide and phospholipids in aqueous medium.

Quoc Chon LE

October 2014

The interaction of titanium dioxide nanoparticles with phospholipids, components of living membranes, was investigated in aqueous medium. The aim of this study was to understand (i) how metal-oxide (TiO_2) affinity chromatography can separate phospholipids and (ii) TiO_2 -living cells interactions at molecular level. At the macroscopic level, Langmuir film technique coupled with Laser Doppler Velocimetry revealed that the interactions between TiO_2 -P25 particles and phospholipids are essentially charge-dependent. TiO_2 -P25 particles interact strongly at acidic pH with 1,2-dimyristoyl-sn-glycero-3-phosphate (DMPA), 1,2-dimyristoyl-sn-glycero-3-phospho-rac-1-glycerol (DMPG) and 1',3'-bis[1,2-dimyristoyl-sn-glycero-3-phospho]-sn-glycerol (TMCL), and weakly with 1,2-dimyristoyl-sn-glycero-3-phospho-L-serine (DMPS). Other membrane lipids such as 1,2-dimyristoyl-sn-glycero-3-phosphocholine (DMPC), 1,2-dimyristoyl-sn-glycero-3-phosphoethanolamine (DMPE) and sphingomyelin (SM) did not interact with TiO_2 -P25 regardless of pH. The interactions of DMPA and DMPG, the main phospholipid adsorbing on TiO_2 -P25 particles, with pure anatase and rutile crystallites were evidenced by surface tension measurements, batch adsorption experiments, Infrared spectroscopy, Raman spectroscopy and ^{31}P NMR. DMPA adsorbs solely at acidic pH on anatase and rutile, through electrostatic interactions implying the phosphate moiety. In contrast, DMPG adsorbs on TiO_2 at both acidic and basic pH mainly by non-electrostatic interactions, through the glycerol moiety and weakly through the phosphate group. The Ti (IV) sites and surface hydroxyl groups on TiO_2 were suggested to be involved into the interaction with phospholipids.

Keywords: titanium dioxide, phospholipid, adsorption, surface charge, electrostatic, inner-sphere complex, Langmuir trough, Infrared spectroscopy, Raman spectroscopy, ^{31}P solid-state NMR.

Acknowledgments

First and foremost, all credit and acknowledgment go to my supervisors: Bernard HUMBERT, Marie-Hélène ROPERS and Hélène TERRISSE. They have been sharing with me so many ideas, knowledge and skills. They keep constant giving me advices and supports for this long walk. I could not have asked for more dedicated supervisors, a better work environment than here in IMN and INRA.

I thank for the financial support from French Ministry of Higher Education and Research.

I thank to the permanent support from IMN. Especially, people in direction board, administration team. They arranged for me to be in IMN and achieved the Ph.D. degree. Special thanks to the enduring help from group CESES. In particular, I appreciate the advices and discussions from Mireille Richard and Luc Brohan related to TiO_2 . I am so grateful for the help from Chris Ewels for his English corrections to my oral presentation and proofreading for the article. I thank Gildas Guignard for funny discussions and for his corrections to my poor communication skills in French.

I took a lot technical supports from Eric Gautron for TEM, Jean-Yves Mevellec for Infrared & Raman spectroscopy, Florin Popa and Pierre-Emmanuel Petit for XRD, Stéphane Grolleau for BET, Jonathan Hamon for XPS, Pascal Janvier (CEISAM) for phosphate dosage. I am so grateful for their invaluable assistance.

About 50% of experiments in this thesis were conducted in BIA-INRA Nantes. There, I got strong support not only from administrative procedure but also technical help linked to Langmuir film. I appreciate their hospitality and enduring support.

There are other peoples, who help me by some ways through these three years. In limited space, it is hard to mention everyone. I sincerely say “Cam on” (thanks in Vietnamese) to you all.

Finally, I thank my family for their constant encouragements.

Quoc Chon LE, October 2014, Nantes

Table of contents

Abbreviations	v
French summary	1
General introduction.....	13
Chapter 1 – Background and the state-of-the-art	17
Chapter 2 – Materials and methods.....	95
Chapter 3 – Probing the interaction between phospholipids and TiO ₂ particles through surface tension measurement	147
Chapter 4 – Effect of TiO ₂ crystallinity on the interaction with phospholipids	181
Chapter 5 – Spectroscopic study of the interaction between phospholipids and TiO ₂	203
General conclusion and outlook.....	239

Abbreviations

Phospholipids

DHP	Dihexadexyl phosphate
DMPA	1,2-dimyristoyl-sn-glycero-3-phosphate
DMPC	1,2-dimyristoyl-sn-glycero-3-phosphocholine
DMPE	1,2-dimyristoyl-sn-glycero-3-phosphoethanolamine
DMPG	1,2-dimyristoyl-sn-glycero-3 phospho-rac-1-glycerol
DMPS	1,2-dimyristoyl-sn-glycero-3-phosphoserine
SM	Sphingomyelin
TMCL	1,3-bis(sn-3'-phosphatidyl)-sn-glycerol

Titanium dioxide (TiO₂)

TiO ₂ -A	Anatase from MTI Corporation
TiO ₂ -P25	Mixture of anatase and rutile from Degussa Company
TiO ₂ -PC10	Anatase from Millennium company (Crystal Corporation)
TiO ₂ -PC100	Anatase from Millennium company (Crystal Corporation)
TiO ₂ -PC50	Anatase from Millennium company (Crystal Corporation)
TiO ₂ -R	Rutile from Sigma Aldrich company

Techniques

DLS	Dynamic Light Scattering
DRIFTS	Diffuse Reflectance Infrared Fourier Transform Spectroscopy
FT-IR	Fourier Transform Infrared Spectroscopy
FT-Raman	Fourier Transform Raman Spectroscopy
LDV	Laser Doppler Velocimetry
NMR	Nuclear Magnetic Resonance spectroscopy

QCM-D	Quartz Crystal Microbalance Dissipation
TEM	Transmission Electron Microscopy
XPS	X-ray Photoelectron Spectroscopy
XRD	X-ray Diffraction

Parameters

IEP	Isoelectric point
PZC	Point of zero charge

Résumé Français

Introduction

Le dioxyde de titane (TiO_2) est un oxyde métallique utilisé dans des biens de consommation aussi variés que les cosmétiques, les aliments, les produits pharmaceutiques, les peintures, les ciments et les fenêtres autonettoyantes.¹⁻³ Il est également utilisé en chromatographie d'affinité métal-oxyde où il permet de séparer les phosphopeptides⁴⁻⁶ et en médecine où il recouvre en fine couche les implants à base de titane et permet le contact avec les tissus⁷. Il fait également l'objet de nombreuses recherches quant à sa toxicité en tant que nanomatériau vis-à-vis des organismes vivants.⁸

Maîtriser les domaines d'application du dioxyde de titane ou son innocuité pour l'environnement repose en bonne partie sur notre connaissance de son affinité pour son environnement. Par exemple, l'utilisation de particules de dioxyde de titane en chromatographie d'affinité métal-oxyde repose sur l'affinité de la surface des particules pour les espèces phosphatées. Il a été souvent affirmé que le groupe phosphate des phosphopeptides se lie à la surface de TiO_2 de la même façon que les ions phosphate. Comme il a été montré que les ions phosphate peuvent former des liaisons covalentes avec la surface de TiO_2 ,^{9,10} ce mode d'accrochage n'est en revanche pas compatible avec la libération de phosphopeptides par élution⁴⁻⁶. De même, l'utilisation de dioxyde de titane pour séparer les phospholipides du lait par extraction en phase solide semble être efficace.¹¹ Toutefois, lorsque la composition de la fraction séparée est comparée à la composition du lait, certains phospholipides sont manquants. Ceci soulève la question de l'affinité de l'ensemble des classes de phospholipides pour le dioxyde de titane. En toxicologie, il a été montré que le dioxyde de titane colle à la membrane des érythrocytes humains et induit leur coalescence.¹² Quand ces expériences ont été reproduites sur une membrane modèle avec un seul composant de phospholipides, aucune coalescence n'a pu être observée. On peut alors se demander si ce phospholipide était la véritable cible du dioxyde de titane, ou bien si un phospholipide d'une autre classe pourrait avoir une plus grande affinité pour TiO_2 . Ces trois exemples illustrent la façon dont les connaissances sur l'affinité de dioxyde de titane pour les molécules phosphorylées biologiques sont encore obtenues par tâtonnement.

L'objectif de cette thèse est donc de déterminer quels phospholipides ont une affinité pour le dioxyde de titane et la nature de ces interactions. Les interactions ont été détectées en milieu aqueux. Le criblage des interactions avec des particules de TiO₂-P25, forme commercialisée de l'oxyde de titane souvent prise comme référence dans la littérature, a d'abord été effectué sur un large panel de phospholipides identifiés dans les membranes biologiques et qui diffèrent par la nature des substituants portés par le groupe phosphate. Passée cette étape, les interactions ont été analysées pour chacune des phases constituant les particules de TiO₂-P25 puis ces interactions ont été analysées à l'état solide par spectroscopie infrarouge et RMN.

Ce document comprend 5 chapitres. Le chapitre 1 rappelle les propriétés physico-chimiques des oxydes métalliques et en particulier celles du dioxyde de titane, les propriétés des phospholipides, et fait le bilan des connaissances sur les affinités entre le dioxyde de titane et les phospholipides. Il y est notamment mis en évidence les lacunes concernant la caractérisation du dioxyde de titane dans ces études, la nature des phospholipides interagissant avec le dioxyde de titane et la nature controversée des liaisons. Dans le chapitre 2, une attention particulière est portée à la caractérisation des particules de dioxyde de titane sélectionnées. Les chapitres 3 et 4 portent respectivement sur les résultats du criblage et l'effet de la nature des oxydes de titane, cristallinité, aire spécifique, forme structurale, etc.... Le chapitre 5 tente d'élucider à l'échelle moléculaire à l'aide de spectroscopies, la nature des interactions et montre combien les interactions sont spécifiques à chaque tête polaire.

Résultats du criblage - Chapitre 3

À pH 2 et 5, les isothermes π -A des monocouches de DMPA, DMPG, TMCL et DHP (figures 1 et S8, panneaux a-d) diffèrent en présence de particules de TiO₂-P25 dans la sous-phase, tandis que les isothermes π -A des monocouches de DMPE, SM et DMPC sont identiques sur l'eau et sur la suspension de TiO₂-P25 (Figure S6). Les isothermes π -A de monocouches de DMPS (figure 2, tableau b) diffèrent aussi en présence de particules de TiO₂-P25 dans la sous-phase mais seulement à pH 5. Pour DHP, l'effet de TiO₂-P25 est plus net à pH 5 (figure 2) qu'à pH 2 (Figure 1). En revanche, la plupart des isothermes π -A réalisées avec des suspensions de particules de TiO₂-P25 à pH 9 se superposent avec celles réalisées sur l'eau pure (Figure S8), sauf celles des couches de DMPG, TMCL et DMPS. Un petit décalage vers les plus grandes aires moléculaires a été observé pour DMPG et une transition de phase plus prononcée a été observée pour TMCL et DMPS. En fonction de la nature de la tête polaire, l'effet des particules de TiO₂-P25 a pu être supprimé à des forces

ioniques faibles ($\text{NaCl } 10^{-2} \text{ mol/L}$) (Figure S10) ou à des concentrations plus élevées en sel (10^{-1} mol/L) (Figure S7). Le déplacement des isothermes vers des aires moléculaires plus faibles est le signe d'une perte de molécules de DMPG, TMCL, ou DMPA à l'interface air-solution, et ceci est attribué à une solubilisation partielle des lipides dans la sous-phase par l'intermédiaire d'une adsorption sur les particules de $\text{TiO}_2\text{-P25}$. Pour les molécules de DMPA, DMPG et TMCL restant à l'interface, l'apparition d'un nouveau point de transition sur les isothermes de compression lorsque la sous-phase contient $\text{TiO}_2\text{-P25}$ (figure 1a, 1c), l'extension du plateau de coexistence, et les pentes plus douces dans la phase cristallisée de DMPG (figure 1b), sont les signes de la présence de particules de $\text{TiO}_2\text{-P25}$ encore ancrées à l'interface.

Pour interpréter ces résultats qui dépendent du pH, le potentiel zêta de tous les phospholipides étudiés a été mesuré en fonction du pH sur des suspensions de vésicules. Les valeurs sont reportées sur la figure 3 avec celles des particules de $\text{TiO}_2\text{-P25}$. En milieu acide ($\text{pH} < 6,6$), les particules de $\text{TiO}_2\text{-P25}$ sont chargées positivement, alors que leur charge de surface devient négative en milieu basique ($\text{pH} > 6,6$). En revanche, DMPA, DMPG, DMPS, DHP et TMCL portent des charges négatives sur l'ensemble de la gamme de pH entre 2 et 10. DMPA, DMPG et TMCL sont fortement chargés sur toute la gamme de pH de 2 à 10, conduisant à des potentiels zêta fortement négatifs (variant entre - 60 et - 80 mV) (Figure 3, panneaux a, b, c). Au contraire, les vésicules de DMPS et DHP sont moins chargées, en particulier à pH 2 (- 20 mV et - 15 mV respectivement) (figure 3, les panneaux d et e). Ainsi, les particules de $\text{TiO}_2\text{-P25}$ et les vésicules lipidiques de DMPA, DMPG, TMCL, DMPS et DHP possèdent des charges opposées dans la gamme de pH de 2 à 6,6, et de même signe au-dessus de pH 6,6. Par ailleurs, la figure 3f montre que les vésicules de DMPE portent une charge de surface positive à des valeurs de pH inférieures à 5. Au-delà, la mobilité des vésicules de DMPE est négative, en particulier pour des valeurs de pH supérieures à 8. Ainsi, les particules de $\text{TiO}_2\text{-P25}$ et les vésicules de DMPE sont de charge opposée seulement dans un petit intervalle de pH entre 5 et 6,6. Le comportement des vésicules de SM (figure 3, panneau g) est proche de celui des vésicules de DMPE. Le potentiel zêta est nul autour de pH 5. En dessous de cette valeur, les vésicules de SM portent une charge positive comme les particules de $\text{TiO}_2\text{-P25}$. Au-dessus de pH 6,6, les deux composés portent des charges de surface négatives. Par conséquent, DMPE et SM portent une charge opposée à celle du dioxyde de titane seulement entre pH 5 et 6,6. Enfin, la courbe de mobilité électrophorétique des vésicules de DMPC en fonction du pH (figure 3h) présente une faible variation entre les valeurs de potentiel zêta de + 20 mV à pH 2 et - 10 mV à pH 10. Entre pH 2 et 5, les vésicules

de DMPC sont chargées positivement comme les particules de TiO₂-P25, et elles sont chargées négativement comme les particules de TiO₂-P25 au-dessus de pH 6,6. Par conséquent, les deux composés présente une charge opposée entre pH 5 et 6,6.

La comparaison des courbes de mobilités électrophorétiques en fonction du pH (Figure 3) avec les isothermes π -A à pH 2 (figures 1 et S5), pH 5 (figures 2 et S8), et pH 9 (figure S8) démontre que les lipides DMPA, DMPG, DMPS, DHP et TMCL interagissent avec les particules de TiO₂-P25 lorsque l'oxyde et les lipides portent des charges opposées. Le tableau 1 résume ces résultats avec la gamme de pH où les charges sont opposées entre chaque lipide et TiO₂-P25, et les valeurs de pH à laquelle les interactions ont été effectivement observées. Contrairement à ces lipides, les interactions sont faibles ou absentes à pH 2 pour DHP ou DMPS avec TiO₂-P25, mais deviennent plus fortes à pH 5. Etant donné que la valeur du potentiel zêta des vésicules de DMPS est d'environ - 17 mV à pH 2 et - 60 mV à pH 5, nous supposons que le lipide n'est pas suffisamment chargé à pH 2 pour permettre une interaction significative avec les particules de TiO₂-P25 dispersées. Ce même raisonnement s'applique à DHP, pour lequel la charge de surface des vésicules à pH 2 (potentiel zêta - 15 mV) est inférieure à celle à pH 5 (potentiel zêta - 30 mV). Ces deux cas montrent que le signe et l'amplitude de la charge de surface déterminent si des interactions peuvent ou non se produire entre les lipides et TiO₂-P25. Cette charge seuil (correspondant à un potentiel zêta d'au moins 20 mV) peut également être appliquée aux interactions entre DMPE, SM ou DMPC et le dioxyde de titane. Les faibles valeurs absolues de potentiel zêta de DMPE, SM (près de - 10 mV) et DMPC (proche de 0) à pH 5,8 indiquent que les vésicules sont trop faiblement chargées et par conséquent, aucune interaction n'a été observée dans ces conditions. Nos résultats ne sont pas en contradiction avec l'affirmation récente que la lécithine d'œuf s'adsorbe à la surface de TiO₂ par des interactions hydrophobes et électrostatiques.¹³ En effet, la lécithine d'œuf (principalement composée de PC et PE) contient également de petites quantités de cholestérol (très hydrophobe) et de plasmalogène,¹⁴ qui pourraient favoriser l'adsorption et, en outre, le dépôt a été effectué dans du chloroforme avant le séchage et la dispersion.¹³

Tableau 1. Conditions d'interactions entre les phospholipides et les particules de TiO₂-P25: la première colonne est la gamme de pH où les charges de surface sont opposées et la seconde indique si des interactions ont été effectivement observées à l'interface air-eau. Les lettres S (pour strong), w (pour weak) and vw (very weak) indiquent l'amplitude de l'effet. La dernière colonne donne la concentration en sel qui permet d'annuler l'interaction.

Lipides	Gamme de pH avec des charges opposées	Amplitude de l'effet et valeurs de pH testées	Concentration en sel (mol/L) permettant de supprimer l'interaction
DMPA	2 – 6.6	S (pH 2, 5)	10 ⁻¹
DMPG	2 – 6.6	S (pH 2, 5)	10 ⁻¹
TMCL	2 – 6.6	S (pH 2)	10 ⁻¹
DHP	2 – 6.6	vw (pH 2) w (pH 5)	10 ⁻²
DMPS	2 – 6.6	w (pH 5)	10 ⁻²
DMPE	5 – 6.6	–	–
SM	5 – 6.6	–	–
DMPC ^(a)	5 – 6.6	–	–

^(a) une étude antérieure à pH 6 ± 1 avec du dipalmitoylphosphatidylcholine (DPPC) a montré une faible interaction entre DPPC et TiO₂-P25.¹⁵

Pour conclure, les expériences démontrent clairement qu'une interaction efficace entre les lipides et TiO₂-P25 peut avoir lieu lorsque deux conditions sont remplies : les deux composés doivent être à la fois de charges opposées et suffisamment chargés en surface. Le potentiel zêta doit présenter une valeur absolue au minimum égale à 20 mV, compte tenu de l'approximation appliquée pour son calcul. Ceci suggère que les interactions entre TiO₂ et les molécules de phospholipides sont gouvernées en premier lieu par des forces électrostatiques.

Toutefois, dans le cas de DMPG, TMCL et DMPS, d'autres interactions fortes existent, mises en évidence au travers des isothermes π -A.

D'après les résultats de la littérature concernant l'adsorption des phosphates d'alkyles sur les surfaces d'oxyde de titane, on peut supposer que l'adsorption de DMPA sur TiO₂-P25 est réalisée via un pontage des atomes d'oxygène par l'atome de phosphore, pour former des complexes mono- et bidentés.¹⁶ Pour DHP (Figure S1d), les interactions faibles avec les particules de TiO₂-P25 à pH 2 (tableau 1) sont expliquées par la faible déprotonation du groupe phosphate à pH 2, ce qui, d'après la littérature, limite la bonne délocalisation électronique sur les deux atomes d'oxygène libres qui sont impliqués dans l'adsorption des groupes phosphate sur la surface de TiO₂.^{9,10,17,18} A pH 5, les deux atomes d'oxygène sont déprotonés, permettant une interaction plus forte qu'à pH 2. Pour les autres phospholipides, à savoir DMPG, TMCL et DMPS, où les atomes de phosphore sont également liés à deux substituants, les interactions sont similaires ou même plus fortes que pour DHP. La formation d'un complexe de surface pontant bidenté entre DMPG, TMCL ou DMPS et les particules de TiO₂-P25 peut se produire à condition qu'il y ait une bonne délocalisation électronique sur les deux atomes d'oxygène libres liés à P. Cependant, cette hypothèse n'est pas suffisante pour expliquer les interactions plus fortes que pour DHP, ni les interactions faibles observés à pH 9 pour ces molécules. Pour expliquer cette différence, il faut tenir compte de la présence de groupes hydroxyle et carboxylate dans le substituant polaire du phosphore. Les groupes hydroxyle terminaux du glycérol pourraient interagir avec la surface de TiO₂, comme mentionné dans la littérature, où l'adsorption sur TiO₂ de molécules par le biais de groupes hydroxyle a été rapportée.¹⁹ Cela expliquerait aussi que les interactions subsistent à un pH de 9, ou bien à pH 2 en présence de NaCl 0,1 mol L⁻¹ pour TMCL et DMPG. De même, l'adsorption de carboxylate a également été signalée sur TiO₂ avec un ancrage monodenté.^{20,21} Cela pourrait faciliter les interactions entre DMPS et TiO₂, car le groupe phosphate est dans ce cas plus enchevêtré dans la structure moléculaire et moins libre pour une adsorption directe sur la surface de TiO₂. L'implication des groupes carboxylate de DMPS dans les interactions avec les particules de TiO₂-P25 peut également être comprise d'après les résultats obtenus avec DMPE. La structure moléculaire de DMPS dérive en effet de DMPE via la substitution d'un atome d'hydrogène par un groupe carboxyle -COOH. Considérant que DMPE n'a aucune interaction avec TiO₂-P25, la mise en place d'un groupe chargé négativement -COO⁻ crée un environnement favorable pour l'adsorption sur la surface inorganique. Les changements dans les propriétés interfaciales de DMPS à pH 5 et à pH 2 confirment que les interactions de DMPS avec l'oxyde de titane sont favorisées par la déprotonation du groupe carboxylate (pH

> 4). Cela suggère que le phosphate dans le DMPS n'est pas impliqué dans l'interaction avec l'oxyde de titane. La suppression de l'interaction entre l'oxyde de titane et le DMPS à des concentrations en NaCl inférieures à celles nécessaires dans le cas du DMPA peut alors être expliquée par la plus faible adsorption des espèces carboxylate sur des surfaces de TiO₂ que celle des espèces phosphate.²²

Etudes ciblées sur la nature des oxydes à deux valeurs de pH pour deux molécules de phospholipides - Chapitre 4

Comme les particules de TiO₂-P25 contiennent à la fois des grains de structure anatase et rutile, la contribution de chacune d'entre elles a été analysée. Mais l'impossibilité de séparer les différentes phases dans la poudre de P25 nous a obligés à considérer des particules de fabrication différente permettant l'obtention de l'une ou l'autre des phases. Les isothermes de compression des films de DMPA et DMPG, complétées par la construction des isothermes d'adsorption à pH 2 et pH 9 ont donné des résultats parfaitement cohérents. Les molécules de DMPA et de DMPG s'adsorbent sur les deux surfaces d'anatase et de rutile. DMPA s'absorbe uniquement à pH acide, probablement par des interactions électrostatiques qui impliquent le groupement phosphate. DMPG s'adsorbe sur TiO₂ dans des quantités similaires en milieu acide ou basique par des interactions non électrostatiques, probablement par l'intermédiaire du groupement glycérol. Quel que soit le mode d'accroche, l'adsorption est plus forte sur la surface de rutile que sur la surface d'anatase. Ceci peut être relié à la nature des sites en surface et à la prépondérance de certaines faces. Les interactions fortes entre TiO₂-P25 et DMPA ou DMPG à pH 2, et les autres interactions observées entre DMPG et TiO₂-P25 à pH 9 et à pH 2 en présence de sel (chapitre 3) peuvent ainsi être comprises par les interactions de DMPA et DMPG avec l'anatase et la rutile à pH 2, et avec le rutile à pH 9. Cependant nos conclusions ne peuvent pas être appliquées à tout type d'anatase. Une étude approfondie des propriétés de surface des anatases de type TiO₂-PC devra être entreprise.

Vision à l'échelle moléculaire des interactions - Chapitre 5.

Les analyses par spectroscopie RMN du ³¹P, infrarouge et Raman des liaisons entre le DMPA ou le DMPG et les surfaces d'anatase et rutile ont été réalisées sur des échantillons qui ont été soigneusement lavés, mais dans des conditions différentes de celles du chapitre 4, afin d'obtenir des signaux spectroscopiques suffisamment exploitables pour, dans un premier temps, démontrer la faisabilité de cette approche moléculaire. La faisabilité de notre démarche

est effectivement bien démontrée dans ce chapitre, mais certaines conclusions ne peuvent être directement transférées et appliquées aux interprétations du chapitre 4. Cependant la qualité des signaux laissent clairement envisager un prolongement de cette forme d'étude aux échantillons contrôlés du chapitre 4. Les études spectroscopiques montrent de manière évidente que DMPA et DMPG se lient fortement à la surface de la phase anatase en impliquant les têtes phosphates. Cependant, malgré la modification de l'environnement chimique observée en RMN, les évolutions de la symétrie locale de la tête phosphate mises en évidence en spectroscopie Raman, ainsi que l'implication des groupes de surface $\text{Ti-OH}_2^{\delta+}$ démontrée par spectroscopie infrarouge, il n'est pas simple de conclure à la formation à l'interface en solution aqueuse d'une liaison chimique covalente Ti-O-P. Le substrat rutile montre un comportement différent notamment parce qu'une plus grande partie des OH de surface sont de nature pontante, Ti-OH-Ti, avec un caractère plus acide que les OH terminaux, type Ti-OH ou $\text{Ti-OH}_2^{\delta+}$, qui sont, eux, plus abondants pour la phase anatase utilisée ici (résultat démontré au chapitre 2 par spectroscopie IR). La tête phosphate semble, avec l'échantillon de rutile utilisé ici, beaucoup moins perturbée lors de l'adsorption que dans le cas de la phase anatase, avec une implication plus importante du groupement glycérol dans le cas de DMPG. Cette étude est également faisable pour caractériser les interactions dans des conditions basiques, à des valeurs de pH d'équilibre de 9, ce qui n'a pas pu être réalisé dans le cadre de ce travail. Il serait donc maintenant intéressant de poursuivre cette approche dans les conditions des isothermes d'adsorption recueillies et interprétées au chapitre 4. La difficulté viendra alors de la façon de recueillir la phase solide dans ces conditions.

Conclusion

Cette étude a consisté à examiner l'interaction entre les nanoparticules de TiO_2 -P25, anatase, ou rutile et les phospholipides en milieu aqueux. L'étape de criblage, fondée sur la mesure de la charge de surface et la sensibilité de l'organisation des phospholipides à leur environnement à l'interface air-liquide, a permis d'identifier deux groupes de phospholipides. Dans le premier groupe, on trouve les phospholipides qui sont suffisamment chargés et qui interagissent avec les particules de TiO_2 -P25 uniquement en milieu acide (l'acide phosphatidique DMPA, la phosphatidylsérine DMPS), et ceux qui interagissent avec les particules de TiO_2 -P25 sur une large gamme de pH (phosphatidylglycérol DMPG et cardiolipine TMCL). Les phospholipides DMPA et DMPS interagissent avec les particules de TiO_2 -P25 par des interactions électrostatiques qui sont écrantées par la force ionique à des concentrations de 10^{-1} mol/L et 10^{-2} mol/L respectivement. De toute évidence, le groupe

phosphate de DMPA est impliqué dans l'adsorption sur les particules de TiO₂-P25 tandis que le groupement carboxylate du DMPS est au moins l'un des groupes impliqués dans l'adsorption sur les particules de TiO₂-P25. Pour DMPG et TMCL, nous avons émis l'hypothèse que les groupes hydroxyles jouent un rôle dans l'adsorption sur les particules de TiO₂-P25, ce qui a pu être confirmé par spectroscopie infrarouge.

Dans le second groupe, on trouve les lipides zwitterioniques comme la phosphatidylcholine DMPC, la phosphatidyléthanolamine DMPE et la sphingomyéline SM, qui n'interagissent pas avec TiO₂-P25 quel que soit le pH. Ces phospholipides, largement présents dans la composition des membranes biologiques ne favorisent pas, par conséquent, la fixation des particules de TiO₂-P25 sur les membranes.

Les affinités différentes des molécules de phospholipides pour le dioxyde de titane nous aident maintenant à comprendre la séparation des seules molécules PC, PE et SM, lors de la séparation des phospholipides du lait sur colonne de TiO₂. En effet, les phospholipides chargés présents dans le lait n'ont pas été retrouvés après la séparation sur colonne de TiO₂. Ce résultat peut s'expliquer par leur rétention dans la colonne, via la formation de liaison covalente avec les particules de dioxyde de titane.

Les particules de TiO₂-P25 étant constituée de cristaux de rutile et anatase, le rôle de la structure cristalline a été étudié sur des échantillons séparés d'anatase et de rutile. Les isothermes de compression et d'adsorption à pH 2 et pH 9 ont séparément montré que le DMPA et le DMPG, principaux phospholipides à s'adsorber sur les particules de TiO₂-P25, pouvaient s'adsorber sur les deux types de cristaux anatase et rutile. DMPA s'adsorbe uniquement en milieu acide sur anatase et rutile, tandis que DMPG s'adsorbe sur anatase et rutile, à la fois en milieu acide et basique, et dans des quantités similaires : il s'agit donc d'interactions non électrostatiques. Les interactions fortes observées entre TiO₂-P25 et DMPA ou DMPG à pH 2 correspondent donc à l'adsorption des phospholipides sur les phases anatase et rutile à la fois. Les interactions entre DMPG et TiO₂-P25 à pH 9 en présence de sel peuvent être maintenant comprises par l'adsorption de DMPG principalement sur le rutile à pH 9. Bien que les isothermes d'adsorption n'aient pas été réalisées en présence de sel, on peut supposer que les interactions entre DMPG et TiO₂-P25 à pH 2 en présence de sel résultent du même type d'interactions qu'à pH 9.

La caractérisation des liaisons par spectroscopie de vibration infrarouge ou Raman et spectroscopie RMN du ³¹P n'a pas pu aller jusqu'à prouver la formation de liaisons covalentes via le groupe phosphate. Les phospholipides DMPA et DMPG s'adsorbent sur TiO₂ en déplaçant la couche d'eau adsorbée et les groupes OH de la surface. Ils forment clairement

des complexes de sphère interne. Alors que le groupe phosphate est le seul groupement impliqué dans l'adsorption du DMPA sur TiO_2 , il est moins impliqué dans l'interaction du DMPG pour TiO_2 . Dans ce cas, les groupements alcool primaire et secondaire du glycérol substitué sur le groupe phosphate sont les principaux groupements impliqués dans l'adsorption. En dépit de nos efforts, il reste beaucoup de questions à résoudre. Il faut maintenant valider ces résultats dans des milieux physiologiques précis : ceux de la peau, des milieux aquatiques ou ceux des cellules biologiques. L'effet de la lumière ultraviolette sur l'interaction entre les phospholipides et le dioxyde de titane est intéressant à étudier en raison de l'activité photocatalytique du TiO_2 et sa présence dans les environnements aquatiques. L'absence d'interactions entre certaines anatases et les phospholipides est assez surprenante et la description fine de la surface de ces anatases pourrait nous aider à comprendre ce phénomène. Si on sait maintenant que les phospholipides s'adsorbent sur les phases anatase et rutile, l'utilisation de monocristaux à faces contrôlées sera nécessaire pour déterminer si certaines faces permettent mieux que d'autres d'adsorber ces molécules. En ce qui concerne les phospholipides, un système plus complexe (mélange de phospholipides, protéines ...) peut être maintenant étudié, en tenant compte de l'organisation des phospholipides (qui ne se mélangent pas les uns avec les autres dans toutes les conditions), et de la formation de radeaux lipidiques avec le cholestérol.

Cette thèse peut avoir des retombées potentielles dans le domaine des biomatériaux car les phospholipides pourraient, en s'adsorbant sur le dioxyde de titane, rendre la surface de TiO_2 plus biocompatible. Elle pourrait également permettre d'améliorer la séparation des phospholipides sur colonne de TiO_2 et de trouver un moyen de récupérer les phospholipides fortement fixés. En outre, la compréhension de l'interaction TiO_2 -phospholipides peut servir à évaluer l'interaction de cet oxyde avec les cellules, lors des études toxicologiques.

Références

1. Fujishima, A., Zhang, X. & Tryk, D. TiO₂ photocatalysis and related surface phenomena. *Surf. Sci. Rep.* **63**, 515–582 (2008).
2. Labille, J. *et al.* Aging of TiO₂ nanocomposites used in sunscreen. Dispersion and fate of the degradation products in aqueous environment. *Environ. Pollut.* **158**, 3482–9 (2010).
3. Weir, A., Westerhoff, P., Fabricius, L., Hristovski, K. & von Goetz, N. Titanium dioxide nanoparticles in food and personal care products. *Environ. Sci. Technol.* **46**, 2242–50 (2012).
4. Larsen, M. R., Thingholm, T. E., Jensen, O. N., Roepstorff, P. & Jørgensen, T. J. D. Highly selective enrichment of phosphorylated peptides from peptide mixtures using titanium dioxide microcolumns. *Mol. Cell. Proteomics* **4**, 873–86 (2005).
5. Engholm-Keller, K. & Larsen, M. R. Titanium dioxide as chemo-affinity chromatographic sorbent of biomolecular compounds--applications in acidic modification-specific proteomics. *J. Proteomics* **75**, 317–28 (2011).
6. Leitner, A., Sturm, M. & Lindner, W. Tools for analyzing the phosphoproteome and other phosphorylated biomolecules: a review. *Anal. Chim. Acta* **703**, 19–30 (2011).
7. Collier, J. H. & Messersmith, P. B. Phospholipid strategies in Biomineralization and biomaterials research. *Annu. Rev. Mater. Res.* **31**, 237–263 (2001).
8. Shi, H., Magaye, R., Castranova, V. & Zhao, J. Titanium dioxide nanoparticles: a review of current toxicological data. *Part. Fibre Toxicol.* **10**, 15 (2013).
9. Connor, P. A. & Mcquillan, A. J. Phosphate Adsorption onto TiO₂ from Aqueous Solutions: An in Situ Internal Reflection Infrared Spectroscopic Study. *Langmuir* **15**, 2916–2921 (1999).
10. Gong, W. A real time in situ ATR-FTIR spectroscopic study of linear phosphate adsorption on titania surfaces. *Int. J. Miner. Process.* **63**, 147–165 (2001).
11. Calvano, C. D., Jensen, O. N. & Zambonin, C. G. Selective extraction of phospholipids from dairy products by micro-solid phase extraction based on titanium dioxide microcolumns followed by MALDI-TOF-MS analysis. *Anal. Bioanal. Chem.* **394**, 1453–1461 (2009).
12. Šimundić, M. *et al.* Effect of engineered TiO₂ and ZnO nanoparticles on erythrocytes, platelet-rich plasma and giant unilamellar phospholipid vesicles. *BMC Vet. Res.* **9**, 7 (2013).
13. Wiącek, A. E., Anitowska, E., Delgado, A. V., Hołysz, L. & Chibowski, E. The electrokinetic and rheological behavior of phosphatidylcholine-treated TiO₂ suspensions. *Colloids Surfaces A Physicochem. Eng. Asp.* **440**, 110–115 (2014).

14. Palacios, L. E. & Wang, T. Egg-yolk lipid fractionation and lecithin characterization. *J. Am. Oil Chem. Soc.* **82**, 571–578 (2005).
15. Chibowski, E., Holysz, L., Terpilowski, K. & Wiacek, A. E. Influence of Ionic Surfactants and Lecithin on Stability of Titanium Dioxide in Aqueous Electrolyte Solution. *Croat. Chem. Acta* **80**, 395–403 (2007).
16. Spori, D. M. *et al.* Influence of alkyl chain length on phosphate self-assembled monolayers. *Langmuir* **23**, 8053–60 (2007).
17. Myller, A. T., Karhe, J. J. & Pakkanen, T. T. Preparation of aminofunctionalized TiO₂ surfaces by binding of organophosphates. *Appl. Surf. Sci.* **257**, 1616–1622 (2010).
18. Raj, K. J. A., Shanmugam, R., Mahalakshmi, R. & Viswanathan, B. XPS and IR spectral studies on the structure of phosphate and sulphate modified titania – A combined DFT and experimental study. *Indian J. Chem.* **49A**, 9–17 (2010).
19. Zhou, C.-H. *et al.* Effect of poly (ethylene glycol) on coarsening dynamics of titanium dioxide nanocrystallites in hydrothermal reaction and the application in dye sensitized solar cells. *J. Colloid Interface Sci.* **374**, 9–17 (2012).
20. Thomas, A. G. & Syres, K. L. Adsorption of organic molecules on rutile TiO₂ and anatase TiO₂ single crystal surfaces. *Chem. Soc. Rev.* **41**, 4207–17 (2012).
21. Mpandou, A. & Siffert, B. Sodium Carboxylate Adsorption onto TiO₂: Shortest Chain Length Allowing Hemimicelle Formation and Shear Plane Position in the Electric Double Layer. *J. Colloid Interface Sci.* **102**, 138–145 (1984).
22. Lushtinetz, R., Gemming, S. & Seifert, G. Anchoring functional molecules on TiO₂ surfaces: A comparison between the carboxylic and the phosphonic acid group. *Eur. Phys. J. Plus* **126**, 98 (2011).

General introduction

The application of metal oxides in commercial products is widespread. Among them, Titanium dioxide (TiO_2) is widely used in consumer goods like cosmetics, food, pharmaceuticals, paints, buildings (cements and self-cleaning windows).¹⁻⁴ It is also used in metal-oxide affinity chromatography to separate phosphorylated molecules⁵⁻⁷ and focuses also the interest in medicine for the biocompatibility of titanium-based implants⁸. Besides commercial applications, it focuses also a lot of research to solve its potential toxicity as nanoparticles in living organisms, including humans⁹.

The applications and the toxicological concern are based on the knowledge of the affinity of titanium dioxide for species. For example, the use of titanium dioxide in metal-oxide affinity chromatography lies on the strong affinity of titanium dioxide for phosphate species. It is often claimed that the phosphate group of phosphopeptides anchors to TiO_2 similarly as phosphate ions do. As it was claimed that phosphate ions could form covalent bonds with the surface of TiO_2 ,^{10,11} this grafting is not consistent with the release of phosphopeptides by elution⁶. The use of titanium dioxide for separating phospholipids from dairy products by micro-solid phase extraction seems to be efficient.¹² However, when the composition of the separated fraction is compared with the composition of milk, some phospholipids are missing. This raises the question of the affinity of the whole classes of phospholipids for titanium dioxide. In toxicology, it was shown that titanium dioxide adhered to the membrane of human erythrocytes and induced their coalescence.¹³ When they checked their result on a model membrane with a single phospholipid component, they could not induce any notable effect. This raises the question whether this phospholipid was the right target of titanium dioxide or if a phospholipid of another class had a higher affinity for TiO_2 . These three examples illustrate how the knowledge about the affinity of titanium dioxide for biological phosphorylated molecules is still based on trial and error.

The objective of this thesis was thus to determine the affinity of phospholipids for titanium dioxide and the nature of these interactions. The interactions have been screened in the aqueous medium, in relation with chromatography and toxicology. A screening was first performed on a large panel of phospholipids that bear the same skeleton with a phosphate function substituted by different functions. Then, the interactions were analyzed in the solid state by infrared, Raman and NMR spectroscopies.

The dissertation comprises 5 chapters. *Chapter 1* reviews the literature relevant to first the physical chemistry of oxide surface, especially titanium dioxide, in aqueous medium, and second the principal characteristics of phospholipids in aqueous solution and at the air-water interface. The state-of-the-art related to the TiO₂-phospholipids interaction is also introduced and discussed. In *Chapter 2* the materials and methods are described. Furthermore, a specific part is devoted to the fine characterization of the selected titanium dioxide particles. *Chapter 3* displays the results of phospholipid screening while *Chapter 4* presents complementary results related to the crystalline phase of titanium dioxide. Finally *Chapter 5* focuses on the nature of bonds between titanium dioxide and phospholipids.

References

1. Labille, J. *et al.* Aging of TiO₂ nanocomposites used in sunscreen. Dispersion and fate of the degradation products in aqueous environment. *Environ. Pollut.* **158**, 3482–9 (2010).
2. Fujishima, A., Zhang, X. & Tryk, D. TiO₂ photocatalysis and related surface phenomena. *Surf. Sci. Rep.* **63**, 515–582 (2008).
3. Weir, A., Westerhoff, P., Fabricius, L., Hristovski, K. & von Goetz, N. Titanium dioxide nanoparticles in food and personal care products. *Environ. Sci. Technol.* **46**, 2242–50 (2012).
4. Prasad, R. Y. *et al.* Effect of Treatment Media on the Agglomeration of Titanium Dioxide Nanoparticles: Impact on Genotoxicity, Cellular Interaction, and Cell Cycle. *ACS Nano* **7**, 1929–1942 (2013).
5. Larsen, M. R., Thingholm, T. E., Jensen, O. N., Roepstorff, P. & Jørgensen, T. J. D. Highly selective enrichment of phosphorylated peptides from peptide mixtures using titanium dioxide microcolumns. *Mol. Cell. Proteomics* **4**, 873–86 (2005).
6. Engholm-Keller, K. & Larsen, M. R. Titanium dioxide as chemo-affinity chromatographic sorbent of biomolecular compounds--applications in acidic modification-specific proteomics. *J. Proteomics* **75**, 317–28 (2011).
7. Leitner, A., Sturm, M. & Lindner, W. Tools for analyzing the phosphoproteome and other phosphorylated biomolecules: a review. *Anal. Chim. Acta* **703**, 19–30 (2011).
8. Collier, J. H. & Messersmith, P. B. Phospholipid strategies in Biomineralization and biomaterials research. *Annu. Rev. Mater. Res.* **31**, 237–263 (2001).
9. Shi, H., Magaye, R., Castranova, V. & Zhao, J. Titanium dioxide nanoparticles: a review of current toxicological data. *Part. Fibre Toxicol.* **10**, 15 (2013).
10. Gong, W. A real time in situ ATR-FTIR spectroscopic study of linear phosphate adsorption on titania surfaces. *Int. J. Miner. Process.* **63**, 147–165 (2001).
11. Connor, P. A. & Mcquillan, A. J. Phosphate Adsorption onto TiO₂ from Aqueous Solutions: An in Situ Internal Reflection Infrared Spectroscopic Study. *Langmuir* **15**, 2916–2921 (1999).
12. Calvano, C. D., Jensen, O. N. & Zamboni, C. G. Selective extraction of phospholipids from dairy products by micro-solid phase extraction based on titanium dioxide microcolumns followed by MALDI-TOF-MS analysis. *Anal. Bioanal. Chem.* **394**, 1453–1461 (2009).
13. Šimundić, M. *et al.* Effect of engineered TiO₂ and ZnO nanoparticles on erythrocytes, platelet-rich plasma and giant unilamellar phospholipid vesicles. *BMC Vet. Res.* **9**, 7 (2013).

Chapter 1

Background and the-state-of-the-art

Table of contents

1.	Background and the-state-of-the-art	20
1.1	The metal oxide surface	20
1.1.1	Under vacuum and at ambient conditions	20
1.1.2	Sorption on the metal oxide surface	21
1.2	The metal oxide - aqueous solution interface.....	22
1.2.1	Hydration and surface charge of metal oxide.....	22
1.2.2	Modeling of the metal oxide – aqueous solution interface	24
1.2.3	Sorption of aqueous species at metal oxide surfaces	30
1.3	Titanium dioxide (TiO ₂)	36
1.3.1	Crystal structures.....	36
1.3.2	Surface chemistry	42
1.3.3	TiO ₂ – aqueous solution interface.....	53
1.3.4	TiO ₂ – electrolyte solution interface	55
1.4	Sorption of species on TiO ₂ surface in aqueous solution	59
1.4.1	Sorption of phosphate and phosphate-containing molecules	59
1.4.2	Sorption of carboxyl-containing molecules	60
1.4.3	Sorption of hydroxyl-containing molecules	61
1.5	Phospholipids (PLs)	63
1.5.1	Structure of phospholipids	63
1.5.2	Characteristics of phospholipids in aqueous medium	67
1.5.3	Characteristics of phospholipids at the air-water interface	72
1.6	Literature review on TiO ₂ -phospholipids interactions.....	76
1.6.1	TiO ₂ -supported phospholipid bilayers	77

1.6.2	Role of divalent cations	77
1.6.3	Chemisorption or physisorption?.....	78
1.6.4	Role of the surface characteristics	78
1.6.5	Nature of the head polar group	78
1.7	Gaps of knowledge and objective of the thesis.....	79
	References.....	81

1. Background and the-state-of-the-art

This chapter briefly reviews the general physico-chemical characteristics of metal oxides – water interfaces, and that of metal oxide - molecules interactions in aqueous solution. More importantly, the detailed physico-chemical characteristics of TiO₂ surface in vacuum and in aqueous solution with the presence of sorbed species will be reviewed. Because this thesis aims at understanding the interaction TiO₂ – phospholipids, some background information concerning characteristics of phospholipids and their arrangement in aqueous medium are also given. Finally, the state-of-the-art related to TiO₂-phospholipids interactions is introduced and discussed.

1.1 The metal oxide surface

1.1.1 Under vacuum and at ambient conditions

In the bulk structure of metal oxides, all metal cations present coordinative saturation. At the surface, they are, however, unsaturated. This low coordination of surface atoms is not energetically favorable and metal cations will generally prefer to increase their coordination number. As a consequence, these surface atoms present a high reactivity toward surrounding environment. Moreover, the surface generally presents some defects such as kink, adatom, step, terrace and vacancy (Figure 1.1) that will play a crucial role in the reactivity of the surface to surrounding environment.

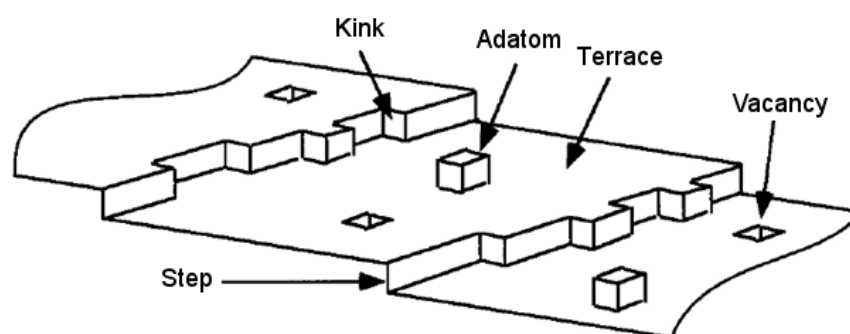


Figure 1.1. Defect sites model on single – crystal surface. Reproduced from Brown 1999¹

Under dried state, an oxide surface treated in ultrahigh vacuum (UHV) is called a clean surface. Once the surface enters into contact with atmosphere, it can interact with chemicals like H₂O vapor or CO₂.

Interaction of H₂O with the oxide surface leads to an increase of the coordination number of surface atoms because H₂O and OH groups fill the missing place around the cation. As a result, the surface functional groups and the relaxation of surface atoms and ions on oxide surface are changed upon interaction with water.¹ Thus, the surface physico-chemical features might be strongly altered compared to the clean surface, and vary greatly with the chemical composition of the medium (nature of electrolyte, presence of molecules...) and its physical conditions (pH, ionic strength...). For example, re-crystallization of the oxide surface can occur upon contact with water and protonation/deprotonation of surface functional groups can change as a function of pH, as well as competing interactions of different substances adsorbed from the medium to the surface.

1.1.2 Sorption on the metal oxide surface

Inorganic or organic species may adsorb to metal oxide surfaces, and this process is called sorption. The sorbed species are termed adsorbate, the surface is called adsorbent. The amount of adsorbate retained onto a surface unit of area is called the coverage. Depending on the nature of the binding mode of adsorbate to the surface, the sorption is termed either chemisorption or physisorption. In the former case, the adsorbate bonds directly to the surface via chemical bonds and the sorbed species is referred as inner-sphere adsorption complex (Figure 1.2). The sites where adsorbate binds to the oxide surface are called sorption sites. In the latter, the adsorbate is not directly bound to the surface, but through hydrogen bonds (H-bonds), hydrophobic interactions, electrostatic and van der Waals attraction forces. The resulting adsorbate is named outer-sphere adsorption complex. Theory related to the adsorption at solid surface in detail can be consulted in literature.²

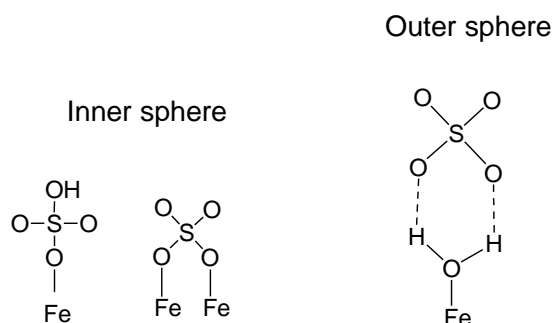


Figure 1.2. Models of the outer- and inner-sphere Fe-sulfate complexes in water.

The sorption process is complex and related to many variables including the nature of oxide surface, the nature of sorbed species, and the environmental conditions. In addition, the sophisticated interactions among these variables not only determine the nature of sorption but also significantly affect it. The sorption, according to its nature, can proceed through several steps. For examples, these steps in heterogeneous catalysis process are: diffusion of species from bulk solution to the surface, adsorption on surface, interaction among adsorbates, desorption and release from the surface.

Understanding the clean surface is a prerequisite before considering the surface in the presence of water and other constituents of the medium. Various issues must be considered: (i) characterization of the metal oxide – water interface, (ii) determination of the amount of adsorbed species, (iii) study of thermodynamics and kinetics of adsorption, (iv) identification of the adsorbate – adsorbent interactions. Additionally, the interaction among adsorbates can render the sorption even more complex to study. To investigate the sorption, many popular techniques are used. These techniques and the obtained information from them are well described and documented in literature.^{1,3}

1.2 The metal oxide - aqueous solution interface

1.2.1 Hydration and surface charge of metal oxide

As an adsorbed molecule, water can bind to the metal oxide surface via H-bonds, chemical bonds or electrostatic forces.⁴ Studies show that there are two binding modes of H₂O to metal oxides: molecular and dissociative. Depending on the nature of metal oxide, one binding mode can be more favorable than the other, or both can occur simultaneously. Literature data indicates that some metal oxide surfaces such as Al₂O₃ and zeolites seem to be inactive for H₂O dissociation.⁵ Studies also show that dissociative adsorption is more favorable at defect sites.^{4,6}

The extent of H₂O adsorption to oxide surface varies with surface nature. With the assumption that hard-sphere diameter of H₂O molecule is around 2.5 – 3 Å, several molecular layers of H₂O can form on the metal oxide surface, and the layer thickness can go up to about 10 Å.^{1,7} These layers (Figure 1.3) bind to the surface through different mechanisms. The innermost layer of H₂O (first layer) can bind directly to oxide surface and form surface M-OH groups. This first important chemical reaction at the metal oxide-water interface is called hydroxylation. This generally takes place on the surface reactive sites such as cation (Lewis

acid) or anion (Brønsted base). The second layer of H₂O can create H-bonds with the first layer, and likewise the third one links to the second via H-bonds. In addition, lateral H-bonds might form among H₂O molecules in the same layer resulting in a network of H-bonds.⁵ These layers are named interfacial water layers.

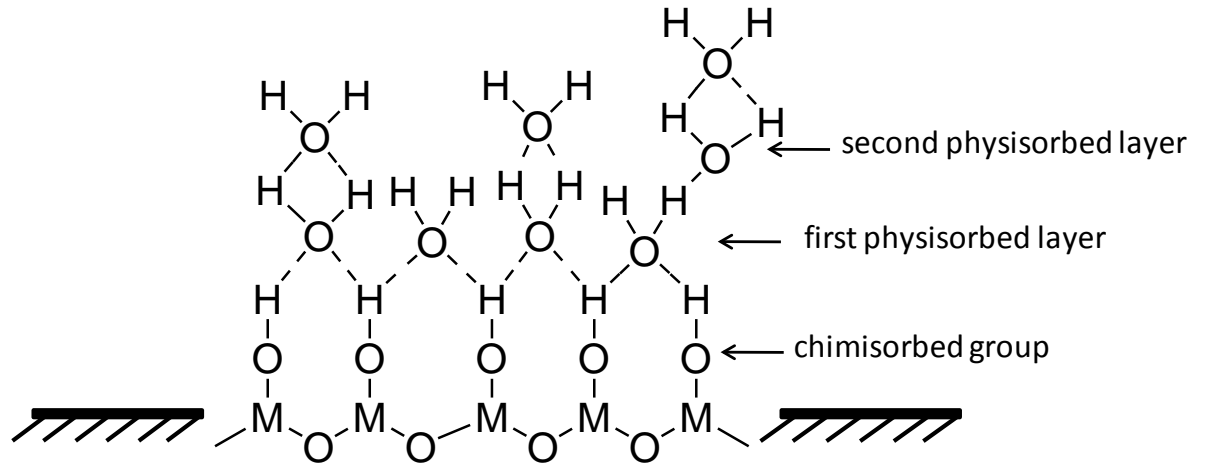
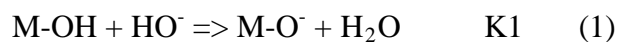


Figure 1.3. Interfacial layers of water adsorbed on metal oxide surface

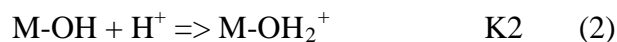
The structure and properties of this interfacial water layer have been the subjects of numerous experimental and theoretical studies from different disciplines such as geochemistry, soil science and environmental science, and which were extensively reviewed.^{1,4,5} The most important fact is that interfacial water molecules are more ordered relative to those of liquid water in bulk phase.¹ Therefore, The hydration of oxide surface also impacts directly the hydrodynamic size of particles and agglomeration phenomena. As a result, the interactions between oxide particles with aqueous species, and the other suspension properties (viscosity, rheological behavior) are controlled by the interfacial properties. This can be described through the electrical double-layer theory.⁸

In the presence of acid or base in aqueous medium, protonation or deprotonation reactions occur on surface hydroxyl groups and induce surface charges. The protonation and deprotonation reactions of surface hydroxyl groups are often schematized as:

in basic condition



and in acid condition



Depending on pH values of aqueous medium, charges on the oxide surfaces can be positive, negative or zero according to the density ratio of “M-OH₂⁺” and “M-O⁻” groups. The pH value where net surface charge equals zero is called Point of Zero Charge (PZC). Surface charge of oxide can be predicted to be positive if pH < PZC, and in this situation M-OH₂⁺ groups are in majority on the surface. In contrast, surface charge is negative at pH > PZC, and M-O⁻ groups are then in majority. Concentration of both HO⁻ and H⁺ ions in solution determines the surface charge of oxide, and they are responsible for the created electrostatic potential. It is noteworthy to remind that only proton (H⁺) is chemisorbed on oxide surface and form M-OH or M-OH₂⁺ groups. Hydroxide (HO⁻) ions are proton acceptors and induce surface M-O⁻ groups. Both hydroxyl ions and protons are called potential determining ions (PDIs).

PZC is an important characteristic of the oxide surface, and there are different approaches to measure it, for instance acid/base titration, pH drift technique, mass titration.⁹ Literature data well documents PZC values for a large variety of metal oxides, as reported by Parks and recently by Kosmulski.^{10,11} PZC value is dependent on the nature of oxide and many factors such as polarization of surface groups, crystal structure, particle morphology, history of oxide and electrolyte nature.¹¹⁻¹⁴ Particularly, for a given oxide, the adsorption of electrolyte on surface sites may shift the PZC, depending on the nature of the interaction.

A correlation between this PZC value and proton affinity can only result in a single proton affinity thermodynamic phenomenological constant.^{10,15} However if one wants to relate this value to the chemical natures of the various surface chemical groups, one needs for each one of these groups the affinity constants. Few attempts have been made to predict proton affinity constants of individual surface groups.¹⁶ We discuss of this approach applied specifically to the TiO₂ surface particles in the next section.

1.2.2 Modeling of the metal oxide – aqueous solution interface

Understanding the detailed structure of the interface is important to control oxide surface properties. However, it is usually difficult to directly measure or investigate the interface at atomic/molecular scale from experimental studies. Therefore, building models to describe the interface have been developed.

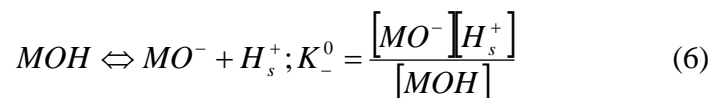
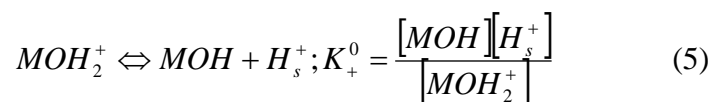
The chemical composition of the oxide-aqueous medium interface is very complex. In addition to the possible permanent functional surface charged groups, there can be adsorbed

molecules, adsorbed ions, free ions, bound water and unbound water. For these reasons, metal oxide surfaces in contact with water develop surface charges, which determine the surface potential. The interface includes the constituent ions of the solid. Those species create an electrical multiple layer around the charged oxide particles, which can be described by double-layer or triple-layer models. The family of “electrical double-layer” (EDL) models is based on simplifying assumptions such as inner – sphere complex, outer – sphere complex, and adsorption of counterions to neutralize the surface charge. These assumptions may be tested by direct measurements the spatial distribution of ions in the EDL as a function of pH, ionic strength, solution metal ion concentration, and other variables for a given sorbent and sorbate.¹ According to this model, bound ions (chemically or physically bound to the surface groups of oxide particles) should be limited to a single layer close to the surface (the Helmholtz model), while ions accumulated Coulombically should appear in a diffuse cloud that decays exponentially with distance from the surface (the Gouy-Chapman-Stern model). Some aspects of the models have been testing by theoretical calculation and available tools. Nonetheless, more investigations are required because of the complexity of the interfaces. Some tools, which have been used to study the interface, are Atomic Force Microscopy, X-ray Standing Wave, Sum Frequency Generation. The details about experiments with these techniques are described in the excellent review of Brown et al. and references therein.¹

Modeling the oxide-solution interface requires an understanding of the characteristics of oxide surface. These are surface acidity and the related intrinsic constants, the relationship between surface charge and potential within surrounding medium (inner layer and diffuse layer of electrical double layer).

1.2.2.1 Surface acidity and intrinsic constant

The surface group acidity is characterized by equilibria:



H_s^+ is the local concentration of protons in equilibrium with surface groups. These protons are subjected to the electrical potential (ψ_0) at the oxide surface:

$$[H_s^+] = [H^+] \exp\left(\frac{-F\psi_0}{RT}\right) \quad (7)$$

where $[H^+]$ is the concentration of protons in the solution far from the oxide – solution interface.

Therefore, the constants for equation (5) and (6) can be written as:

$$K_+^0 = \frac{[MOH][H^+]}{[MOH_2^+]} \exp\left(\frac{-F\psi_0}{RT}\right) \quad \text{and} \quad K_+^0 = \frac{[MO^-][H^+]}{[MOH]} \exp\left(\frac{-F\psi_0}{RT}\right)$$

Or

$$K_+^0 = K^+ \exp\left(\frac{-F\psi_0}{RT}\right) \quad \text{and} \quad K_+^0 = K^- \exp\left(\frac{-F\psi_0}{RT}\right) \quad (8)$$

K^+ and K^- are the intrinsic constants, which characterize the acidity of surface groups in the absence of electrical potential ($\psi_0 = 0$).

1.2.2.2 Surface charge-potential relationship

The double layer is divided into two layers: inner and outer. Within the inner layer, under given conditions of solution, surface charge density σ_0 is described by equation (3):

$$\sigma_0 = \frac{F}{A} ([MOH_2^+] - [MO^-])$$

Where F is the Faraday constant (96500 C.mol⁻¹) and A is the total surface area of oxide particles in solution (m²/L). The total number of surface groups per unit area, N_s (mol/m²) is:

$$N_s = \frac{([MOH_2^+] + [MOH] + [MO^-])}{A}$$

Surface charge density can be rewritten:

$$\sigma_0 = FN_s \frac{[MOH_2^+] - [MO^-]}{[MOH_2^+] + [MOH] + [MO^-]}$$

Taking into account the intrinsic constants from equation (8):

$$\sigma_0 = FN_s \frac{([H^+]/K^+) \exp(-F\psi_0/RT) - (K^-/[H^+]) \exp(F\psi_0/RT)}{1 + ([H^+]/K^+) \exp(-F\psi_0/RT) + (K^-/[H^+]) \exp(F\psi_0/RT)} \quad (9)$$

This equation (9) describes the relation between surface charge (σ_0) and electric potential (ψ_0) at the surface at a given pH.

In the outer layer (diffuse layer), counter-ions are subjected to the surface potential as well as thermal agitation. The net charge (σ_d) of the diffuse layer is determined by Graham's relation:

$$\sigma_d = -(8\varepsilon CRT)^{1/2} \sin\left(\frac{zF\psi_d}{2RT}\right) \quad (10)$$

Where ε is the dielectric permittivity of the medium. It is the product of permittivity of water with that of the vacuum. C is the electrolyte concentration (mol/L), z is the charge of electrolyte ions. Equation (10) indicates that a variation of electrolyte concentration induces changes in σ_d and ψ_d .

The electrostatic potential (ψ_d) caused by the charge at the end of the Stern layer is considered to be very close to the zeta potential (ζ), which is normally measured through electrophoretic mobility determination.

The electric potential at the distance r, from the surface is written by Poisson-Boltzmann equation:

$$\psi(r) = \frac{2RT}{\varepsilon} \ln \frac{1 + \gamma[-\kappa(r-d)]}{1 - \gamma[-\kappa(r-d)]} \quad \text{with} \quad \gamma = \frac{\exp(zF\psi_d/2RT) + 1}{\exp(zF\psi_d/2RT) - 1} \quad (11)$$

The thickness of the diffuse layer is termed Debye-Huckel length. It corresponds to the distance from the surface for which the electrostatic potential reaches the value of ψ_0/e (with $\ln e = 1$). It is noted κ^{-1} , and calculated from equation (4).

$$\kappa = \left(\frac{2 \cdot e^2 N_A \cdot I}{\varepsilon \cdot k \cdot T} \right)^{1/2} \quad (12)$$

Where N_A is Avogadro number, I is the ionic strength (mol.L⁻¹), k is Boltzmann constant, T is the absolute temperature.

As it can be noted from equation (12), this length is very sensitive to ionic strength (I). When I increases, the diffuse layer is compressed and therefore the length (κ^{-1}) is smaller.

1.2.2.3 Models of metal oxide–solution interface

To interpret experimental data and to accurately describe the relation between surface charge as a function of pH: $\sigma_0 = f(\text{pH})$, several models have been proposed. These models use mass-action law and matter balance to describe surface reactions. An electrostatic model is used to characterize relationship between potential and surface charge, in which aqueous species are placed in the interfacial zone. Among the models, triple layer model (TLM) is the most general model, which accounts for adsorption of electrolyte ions on surface by complexing with protonated and deprotonated surface groups.¹² TLM is illustrated in figure 1.4.

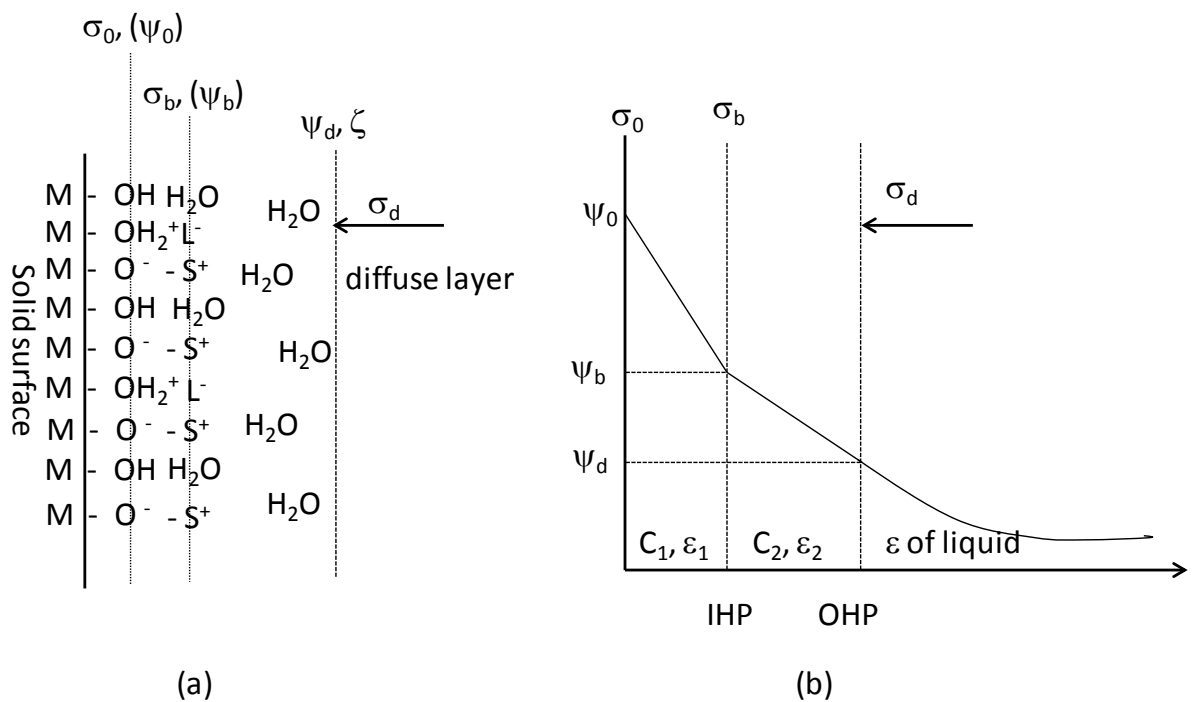
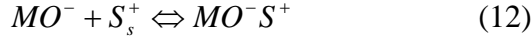


Figure 1.4. Oxide – solution interface where (a) represents surface species position in triple layer model and (b) shows the decay of potential from the surface and the charge-potential relationship. There are three planes in the model: the first one is positioned at the oxide surface with pair charge and potential (σ_0, ψ_0), the second one is called IHP (σ_b, ψ_b) and the third one corresponds to OHP (σ_d, ψ_d).

TLM is established partly on the equilibria (5) and (6) accounting for protons adsorption. In addition, the complexation between electrolyte ions with surface groups is taken into account. The equilibria of these complexation reactions are displayed by:

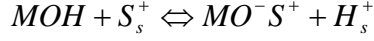
For cations from solution S_s^+



For anions from solution L_s^-



Combining (12) with (6), we have:



$$K_s = \frac{[MO^-S^+][H^+]}{[MOH][S_s^+]} \exp\left(\frac{-F(\psi_0 - \psi_b)}{RT}\right) \quad (14)$$

And (13) with (5):



$$K_L = \frac{[MOH][L_s^-][H^+]}{[MOH_2^+L^-]} \exp\left(\frac{-F(\psi_0 - \psi_b)}{RT}\right) \quad (15)$$

Equilibria (14) and (15) show the relation between the complexation reactions and acid-base ones. The equilibria also relates to the charge generation processes via protons adsorption/desorption.

The surface charge σ_0 , the shielding charge due to complexation σ_b and the compensating charge of the diffuse layer σ_d are written as:

$$\sigma_0 = \frac{F}{A} ([MOH_2^+] + [MOH_2^+L^-] - [MO^-] - [MO^-S^+]) \quad (16)$$

$$\sigma_b = \frac{F}{A} ([MO^-S^+] - [MOH_2^+L^-]) \quad (17)$$

$$\sigma_d = \frac{F}{A} ([MOH_2^+] - [MO^-]) \quad (18)$$

Electroneutrality for the whole system imposes: $\sigma_0 + \sigma_b + \sigma_d = 0$

The total density of charged sites expressed in unit of charge density is

$$N_s = \frac{F}{A} ([MOH_2^+] + [MOH_2^+L^-] + [MO^-] + [MO^-S^+]) \quad (19)$$

The potentials ψ_0 and $(\psi_0 - \psi_b)$ are related to the surface charge via capacitances C_1 and C_2 . C_1 is the capacitance of zone 1 between surface and IHP, C_2 is that of zone 2 between IHP and OHP. The capacitances are linked to potentials as following:

$$C_1 = \frac{\sigma_0}{\psi_0 - \psi_b} \text{ and } C_2 = \frac{\sigma_d}{\psi_d - \psi_b}$$

The metal oxide – aqueous solution interface is very complex because there are many variables. Particularly, calculating equilibrium constants of surface ionization is very difficult. Nonetheless, literature data shows that this model is quite good for many oxides, such as TiO_2 , SiO_2 and Al_2O_3 with every electrolyte 1:1 over a wide range of ionic strengths at standard condition (298 K and 1 bar). This model is considered to be more useful and flexible than any other models.¹

1.2.3 Sorption of aqueous species at metal oxide surfaces

Sorption of aqueous species on metal oxides have attracted many studies because of numerous interests such as in geochemistry, environmental sciences, biomaterials and particularly for heterogeneous catalysis applications.¹⁷⁻²⁰ Aqueous species are either inorganic or organic. Inorganic species are cations and anions, which might adsorb through physisorption or chemisorption.²¹⁻²³ Organic species are polar or nonpolar with functional groups such as hydroxyl, carboxylate, amine etc. Sorption energy involved in processes depends on the involved interaction forces: for physisorption, the energy is lower than 50 kJ/mol, whereas that for chemisorption is several hundred kJ/mol.

Considering ionic species, the interaction can whether be strong or weak, depending on the nature of these ions. The relatively weak charge density ions, for instance Cs^+ , ClO_4^- , cannot penetrate the physisorbed H_2O layers. In this case, the minimum distance that these ions can reach from the surface corresponds to the thickness of Stern layer, and these ions are then positioned at the outer limit of this layer, which is named outer Helmholtz plane (OHP). Some other ions, such as Na^+ , have stronger interaction with surface charged sites, and can penetrate the physisorbed layer of H_2O on oxide surface. Nevertheless, these ions do not form ion pairs or complexes with surface charged sites. The interaction does not affect the solvation layers around these ions, which are constrained within the hydration layer of oxide surface. It is thought that these ions form hydrogen bonds with surface charged sites.¹²

The last kind of ions can even penetrate the Stern layer and adsorb chemically on surface sites. These ions are complexing anion or easily hydrolysable cations. Some neutral molecules forming coordination complexes can behave similarly.

All these ions are situated near the oxide surface, therefore they can shield the mutual interactions between surface charged groups, and might also modify the surface charge. Hence, at a given pH, surface charge of oxide is dependent on the concentration of counter-ions and the level of created shielding. This phenomenon is termed salt effect, and is related to PZC measurement experiments. Through these experiments, the effect of ionic strength on surface charge and PZC of oxide is analyzed. In short, if the ions just Coulombically accumulate in the water layer, all curves $\sigma_0 = f(\text{pH})$ intersect at PZC. On the contrary, if chemical adsorption occurs, the PZC is shifted whether to lower pH in the case of cations, or to higher pH in the case of anions. The strength of ions affinity to the surface determines the extent to which PZC is shifted.

1.2.3.1 Effect of oxide surface nature

The sorption process depends on oxide surface characteristics, particularly on the charge density and on the structure of coordination sites.¹² Defective sites are the most reactive on metal oxide surface¹ and they are crucial adsorption and reaction sites for molecules.^{24,25} Moreover, coordination environment of surface atoms, redox properties of the oxide and oxidation state of the surface, have significant influence on the sorption at the metal oxide surface.¹⁷ Thus, the nature of oxide determines the adsorption of species. For instance aspartic acid presents weak interactions with fused SiO_2 , whereas stronger with TiO_2 in the same conditions.²⁶

Moreover, properties of metal oxide particles such as particle size, shape, porosity, surface roughness, that have consequences on the surface chemical heterogeneity, the surface charges, and the chemical nature of surface sites (defects, acid or basic properties) strongly affect their interaction with molecules. Porous materials allow the molecules to penetrate into pores and precipitate inside. Particle surfaces possessing a higher number of surface active sites tend to adsorb more molecules, thus the coverage is higher. Particles with smaller size usually possess a higher specific area, thus relatively more active sites available for interaction.²⁷ Effect of particle size on the adsorption behavior of species is obviously demonstrated by the adsorption of proteins on metal oxide. For instance, experimental data

reported that the amount of fetal bovine serum adsorbed on nanosized alumina (24 nm) is significantly higher than that on alumina with bigger size (167 nm) in the same conditions.²⁸ Adsorption of sulfate ion on $\alpha\text{-Fe}_2\text{O}_3$ was found to be dependent on the shape of oxide particles. This ion adsorbed strongly on ellipsoid particles, whereas weakly on thin platelets and moderate on thick platelets.²⁹

Adsorption of aqueous species is dependent on the oxide crystal faces. Reasons for this rely on the differences in quantity and quality of reactive sites existing on. An experimental study illustrates that adsorption of sulphate species is favoured on some specific facets of $\alpha\text{-Fe}_2\text{O}_3$. Sugimoto and al. shows that SO_4^{2-} ions strongly adsorb on (110), (100) and (012) faces where they bind to Fe ions through bidentate mode, whereas they are weakly adsorbed on (001) face, via monodentate binding mode.²⁹ Citrate was found to adsorb strongly on (0001) face of ZnO and more weakly on $(10\bar{1}0)$ faces, whereas for ethylenediamine the opposite behavior was observed.³⁰ Those phenomena result from the distribution of active sites and the coordination number of surface atoms which are different on various crystal faces.

The surface reactive sites are not easy to define, since they depend on the involved reaction with the adsorbing chemical species. If we consider the solvated OH^- anion, a surface metal atom may be the reactive site. For instance, it has been demonstrated that 5-fold coordinated Ti atoms on some crystallographic facets of TiO_2 rutile constitute Lewis acids for lone-pair electron molecules, and 2-fold coordinated O^{2-} sites are Brønsted base sites which can capture protons from molecules.²⁴ Some of these sites are simply sketched in figure 1.5.

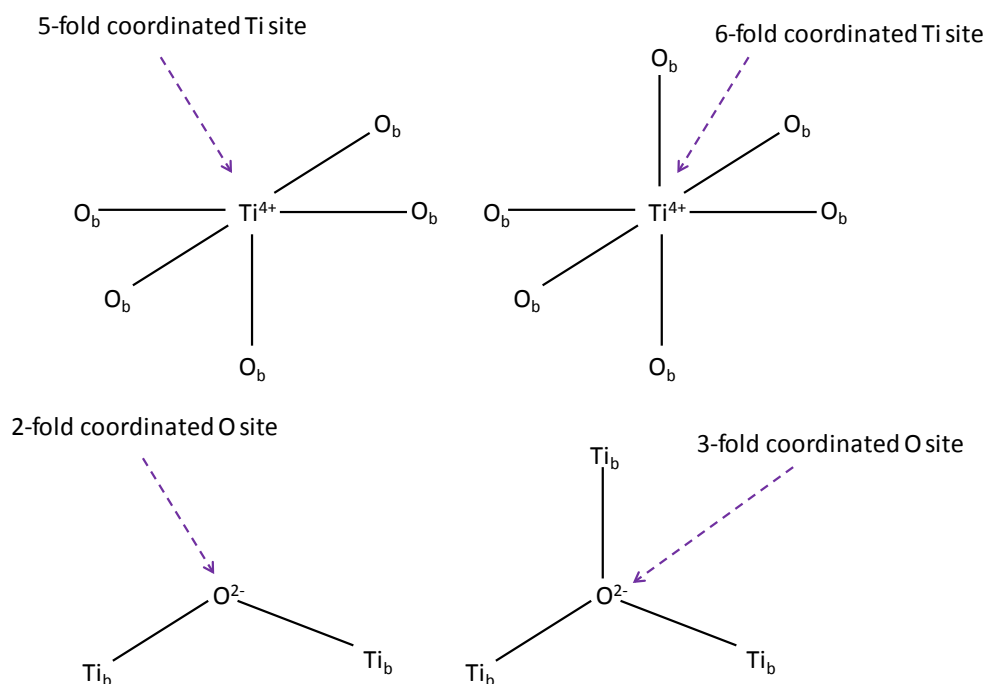


Figure 1.5. Model for Titanium sites and Oxygen sites on surface and in the bulk lattice of TiO_2 crystal. Ti_b and O_b are Oxygen and Titanium in the bulk lattice, respectively. In the bulk lattice, Ti is 6-fold coordinated, and O needs a 3-fold coordination to be saturated. However, on the surface Ti can exist as 5-fold coordinated atoms and similarly oxygen atoms can be 2-fold coordinated.

1.2.3.2 Effect of sorbed species

In addition, the nature of aqueous species significantly affects the sorption mechanism. A popular case is the sorption of nonpolar organic compounds on metal oxide, the binding mechanism involving hydrophobic interactions. Some organic species are surface active, as they have tendency to gather at the air – water interface or to adsorb strongly on metal oxide – water interface.¹ Sorption behavior of these surface active species on metal oxide is very particular, as they bind via their polar group to the surface and point the nonpolar chains outwards solution. Surfactant adsorption on metal oxide is an apparent example.³¹

Some macromolecules such as polyelectrolytes, polymers, with various structures and functional groups interacting differently with metal oxide, have been investigated for applications in colloidal stabilization.^{32,33} The functional groups of these species are responsible for the adsorption onto oxide surface, as illustrated by the binding role of hydroxyl groups of catechol family on oxides.³⁴ Long chain molecules, with polar moiety adsorbed on surfaces, present lateral interactions between apolar chains, and can reorient the position of their chains from horizontal to vertical, forming clusters or bilayers on the surface

at high coverage.^{1,31} The large structure of the apolar chains points towards solution and hinders agglomeration of oxide particles. This phenomenon is applied in steric stabilization technique for metal oxide suspensions.

1.2.3.3 Effect of environmental condition

The medium where oxides and molecules are dispersed has a vital role on the interactions existing between them. The state of molecules in H₂O medium is affected by various interactions (hydration forces, hydrophobic or hydrophilic interactions). Strong binding of molecules by H₂O increases the intrinsic volume of the molecules and reduces their flexibility in diffusion processes, therefore affecting the sorption process. Furthermore, molecules can self-assemble to form various structures in aqueous medium, and these structures can compete with sorption processes on oxide surfaces. Adsorption of non-ionic surfactant on silica surface comprises three steps: monomer diffusion, micelle diffusion and micelle dissociation.³¹ At pre-micellar concentration, the adsorption rate presents a linear relationship with bulk concentration, whereas, beyond critical micellar concentration, this relation is not linear. Micelles are assumed not to adsorb on surface, and they only release monomers in the diffusive step.

In many systems, pH and ionic strength of the solution control sorption of species on oxide surfaces. A study of Cesarano et al. about the adsorption of polymetacrylic acid (PA) on α -Al₂O₃ in aqueous suspension³² showed the strong effect of medium, particularly the pH, on the chemical sorption of PA on α -Al₂O₃ particle surfaces. In fact, the functional groups of PA are carboxylic moieties, which deprotonate when pH increases. Deprotonation level increases and get almost 100% at pH around 8.5. Concerning the oxide surface, the point of zero charge of Al₂O₃ is about 8.5. As a result, in pH 4 – 8, electrostatic forces between PA and Al₂O₃ are attractive, and become repulsive at pH > 8.5. Another example is the dependence on pH of phosphate complexes formation on goethite studied with diffuse reflectance infrared spectroscopy.³⁵ This study found that though phosphate coordinated to iron (III) cation on goethite surface via monodentate binding mode whether in acid or alkaline pH condition, the difference among complexes is the protonation level which depends on pH. Theoretical study also demonstrates that the coordination mode of phosphate to iron hydroxyde is significantly pH dependent.³⁶ The authors demonstrated that bidentate binding formed at pH 4 – 6, while monodentate formed at pH 7.9 and 12.8. Jeon and coworkers proved that chemical adsorption coverage of alkyl phosphates on alumina decreases when pH of solution increases.³⁷ Both

theoretical and experimental studies indicated that adsorption coverage of orthophosphate species on goethite increases when pH decreases from 11 to 3.³⁸ A similar conclusion was driven from the adsorption of sulphate ions on α -Fe₂O₃ at 100°C, when pH decreases from 4 to 2.²⁹

The organization of species in aqueous solution also influences the sorption process. Indeed, the molecular solubility, the interaction between the molecules themselves, and the competition effects during the sorption have to be considered. An apparent example is the effect of organic ligands on the adsorption of metal ions on oxide surface in metal – organic complexes. In this case, the ligands control the adsorption instead of the metal cations. A pronounced illustration is the adsorption of complexes of Co(II) with ethylenediaminetetraacetic acid (EDTA) on metal oxides.¹ Conversely, without competition phenomenon, it is possible to have cooperative effects. For instance, the presence of some components in the medium can hinder or enhance the sorption processes: these components are called modifiers. According to Rossetti et al., Ca²⁺ ions enhance the adsorption of phospholipid vesicles on TiO₂ substrate, leading to the formation of a supported phospholipid bilayer (SPB).³⁹ Authors suggested that Ca²⁺ ions may bind to both the negatively charged phospholipid vesicles and the oxide surface, subsequently facilitating the formation of SPB.

At last, light can have effect on the adsorption of aqueous species on metal oxide surface. Indeed, the photosensitivity of some oxides under presence of H₂O and light can lead to oxidation or reduction of the adsorbate into different species. Thus, the sorption mechanisms can change completely. Titanium dioxide is very sensitive to ultraviolet light and can degrade many organic molecules. This oxide is widely used as a photocatalyst for water and air purification, for example. Therefore, the investigation of sorption processes with photosensitive oxides must carefully take into account the effect of light.

1.2.3.4 Tendencies and challenges

There are two approaches to describe the adsorption of aqueous species on metal oxide surface. From a macroscopic point of view, quantitative and qualitative analysis were used to investigate the adsorption as a function of several factors. These factors are typical conditions of environment such as pH, ionic strength, effect of modifiers, temperature or concentration of adsorbed species. In order to distinguish the nature of adsorption, whether chemisorption or physisorption, modifying environmental conditions is a conventional choice. Nevertheless, to

understand the interactions occurring at the oxide – aqueous solution interface at molecular level, a microscopic approach is required. For this purpose, both theoretical and experimental studies are essential. Calculating adsorption energy either by classic model or by quantum mechanics is crucial to differentiate the mode of adsorption based on the bonding energy. For experimenters, to probe the adsorption nature, vibrational spectroscopy and other techniques such as Sum Generation Frequency or Nuclear Magnetic Resonance are powerful choice. With these techniques, nature of adsorption can be elucidated and furthermore, the structural information of adsorbed species can be predicted.

1.3 Titanium dioxide (TiO₂)

Understanding the surface properties of TiO₂ before investigating the interactions of this material with phospholipids or other molecules is essential. However, a complete review regarding the surface studies of TiO₂ is out of the scope of this thesis; detailed information can be found in some excellent reviews.⁴⁰⁻⁴² Herein, only a brief review relevant to the thesis is summarized and discussed.

1.3.1 Crystal structures

Titanium dioxide exists in three primary crystalline phases: anatase, rutile and brookite.⁴³⁻⁴⁵ Macroscopically, rutile is the most stable and the most abundant phase.⁴⁶ At the nanoscale, the anatase phase is found to be dominant both in synthesis and nature. Nevertheless, both anatase and rutile play a vital role in the applications of TiO₂.⁴⁰ Figure 1.6 depicts the bulk structure of anatase and rutile.

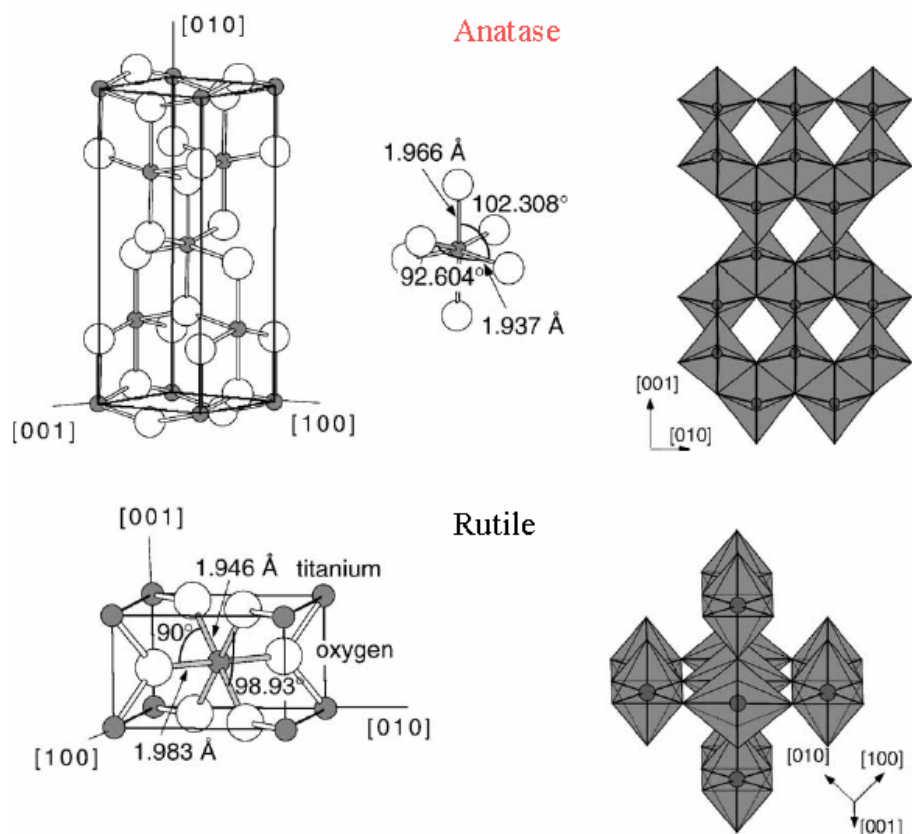


Figure 1.6. Bulk structure of anatase (top row) and rutile (down), taken from Diebold 2003⁴⁰.

Both structures can be described through TiO_6 octahedra, where Ti^{4+} is fully coordinated by six O atoms (6-fold coordinated Ti). Each O atom is fully coordinated to three Ti atoms (3-fold coordinated O). The difference between anatase and rutile is the assembly of these octahedra and the distortion of each of them. Anatase is significantly distorted in comparison with rutile. In rutile, each octahedron is in contact with ten neighboring octahedra (two sharing an edge, eight sharing a corner), whereas in the anatase structure each octahedron has only eight neighbors (four sharing an edge, four sharing a corner). These differences in lattice structure result in differences in physical and chemical behavior between polymorphs.⁴⁷ Density (kg/m^3) of rutile is 4240, a little higher than that of anatase, which is 3830. The estimated band-gap energies are 3.0 eV and 3.2 eV for rutile and anatase respectively.⁴²

The suitability of TiO_2 for any industrial application depends not only on the phase of the TiO_2 particles, but also on their morphology.⁴⁸ The morphology of anatase and rutile particles was predicted by shape dependent thermodynamic models. They are sketched in

Figure 1.7. The faces exposed by these morphologies are found to be dominant on nanocrystals of anatase and rutile.

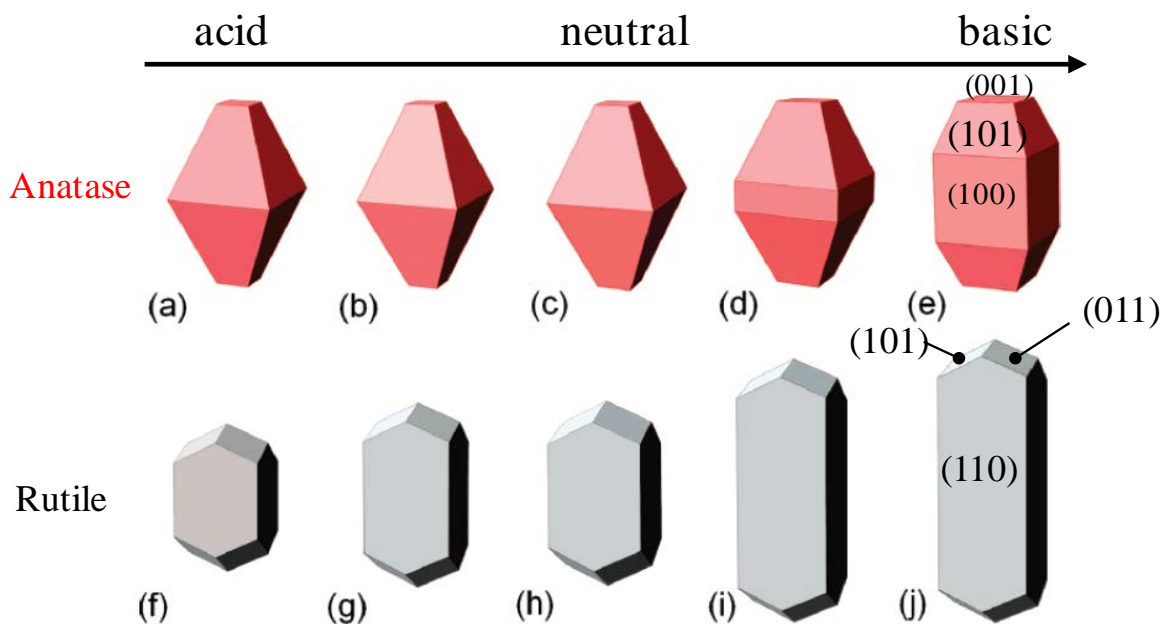


Figure 1.7. Morphology of anatase and rutile crystals for different degrees of surface acidity, from strong acid to strong basic condition. (Taken from Barnard 2005⁴⁸).

Preparation techniques and procedures determining the crystal morphology, this in turn defines the exposed faces. In acid medium, the main faces of anatase crystal are (101) and to a less extent (001) faces. In basic condition, area of (001) face increases, whereas that of (101) decreases and a new face, (100), appears. In contrast, when acidity of medium decreases, the formation of rutile crystal does not give rise to new faces, but the crystal seems to lengthen, thus (110) face expands. Anatase is considered to possess higher photocatalytic activity than rutile.⁴³ Reactive sites being located on faces, the reactivity of each face is different from the others.

The surface physico-chemical properties of TiO_2 drastically depend on several parameters: the crystalline phase, the shape, the crystal faces, the state of crystal faces (defects, edges, impurities), and the degree of hydration of TiO_2 surface.⁴⁶ Theoretical studies find that the (110) is the most thermodynamically stable among (110), (001) and (100) faces of rutile, based on the fact that the (110) face has the least dangling bond number, and that this crystal face has the lowest energy. These faces are modeled in figure 1.8

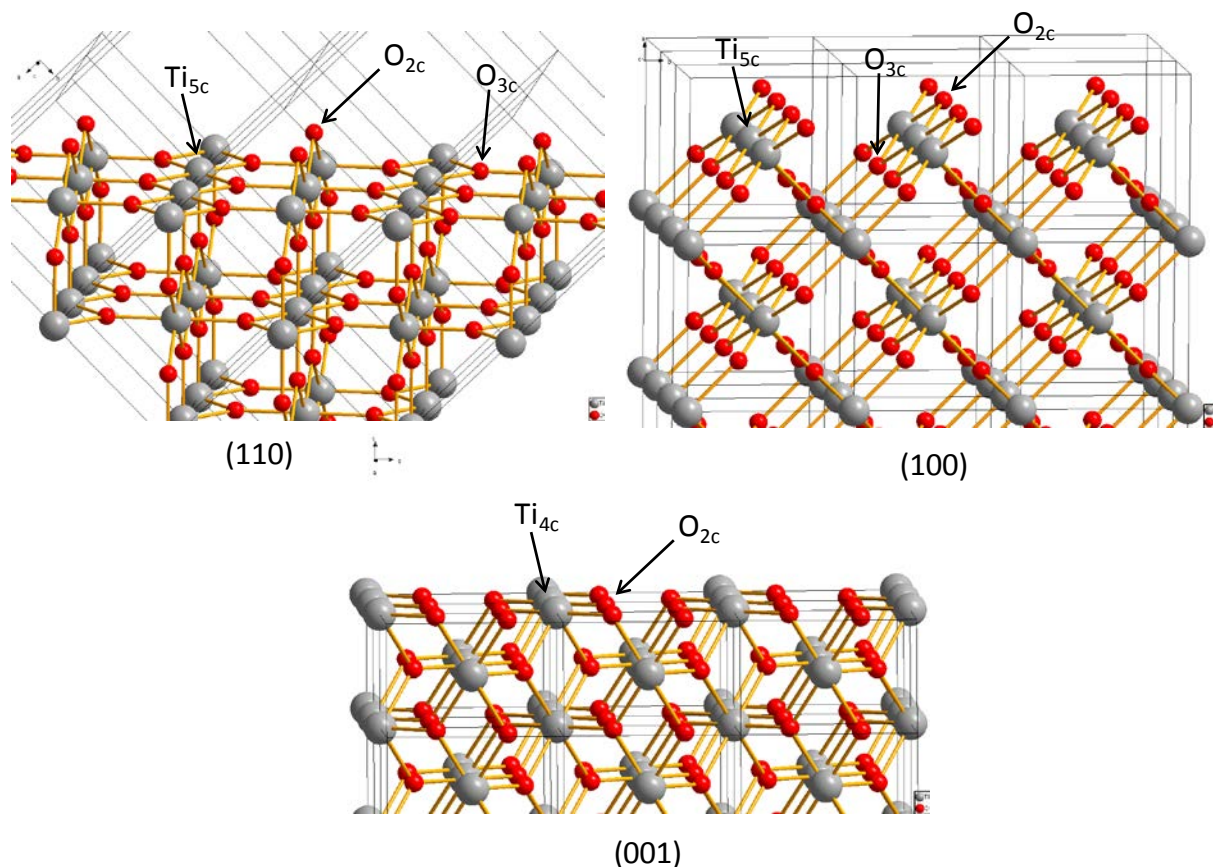


Figure 1.8. Three main faces of rutile.⁴⁹ Both faces (110) and (100) expose 5-fold coordinated Ti^{4+} . Face (001) exposes 4-fold coordinated Ti^{4+} , that are theoretically more active than 5-fold coordinated Ti^{4+} . The bridging oxygen (O_{2c}) is present on three faces.

On the (110) face of rutile, rows of 6-fold coordinated Ti atoms alternate with rows of 5-fold coordinated Ti. There is a row of 2-fold coordinated O atoms located on the row of 6-fold coordinated Ti and perpendicular to the plane (110). These 2-fold O is called bridging oxygen, and is suggested to be very active. If this bridging O atom is removed from the surface, by thermal treatment for example, a vacancy is formed and significantly affects surface reactivity of rutile (110). In addition, 3-fold coordinated O atoms are also present on (110) faces; this type of O is inert to chemical reaction because its coordination is saturated.

Rutile (100) and (001) faces are less studied than (110). The (100) face is strongly corrugated with a row of 2-fold coordinated O atoms on the outermost ridges. The (001) face is very particular, as all atoms of Ti and O are located in the plane. Only 4-fold coordinated Ti and 2-fold coordinated O atoms are present on this face, whereas on the rutile (110) face, 50% of total surface Ti atoms are 5-fold coordinated and 50% are 6-fold coordinated. Therefore, the (001) face is more reactive than the others.

Anatase nanocrystal primarily exposes (101), (100) and (001) faces (see Figure 1.9). In anatase, the (101) crystal face was proven to have the lowest energy in comparison to the (100) and (001) faces.⁵⁰ Based on the calculated surface formation energy, the stability of faces is in the order from high to low: (101) > (100) > (001). Hence, anatase (101) face is more stable than (100) and (001) faces. It was demonstrated that the presence of low coordinated Ti atoms induces higher surface energy.⁴³ Compared with rutile faces, the average surface energy of an equilibrium-shape anatase crystal is smaller than that of rutile; this can be a hint to explain why the nanoscale of rutile crystal is less stable than that of anatase.⁶ All three faces expose 5-fold coordinated Ti and 2-fold coordinated O atoms. (101) and (100) faces present 3-fold coordinated O atoms, whereas the (001) face does not. The (101) face is the most corrugated among the three. Both Ti and O atoms on anatase (001) face lack a ligand, which is perpendicular to the (001) plane. With this geometry, Ti and O atoms should be easily targeted for chemical reaction compared to the other faces of anatase. Experimental studies have indeed demonstrated that the (001) face is more reactive than the (101) face in anatase.⁵¹ New synthesis methods have been developed to control exposed faces of anatase, aiming at increasing the percentage of (001) faces.^{52,53}

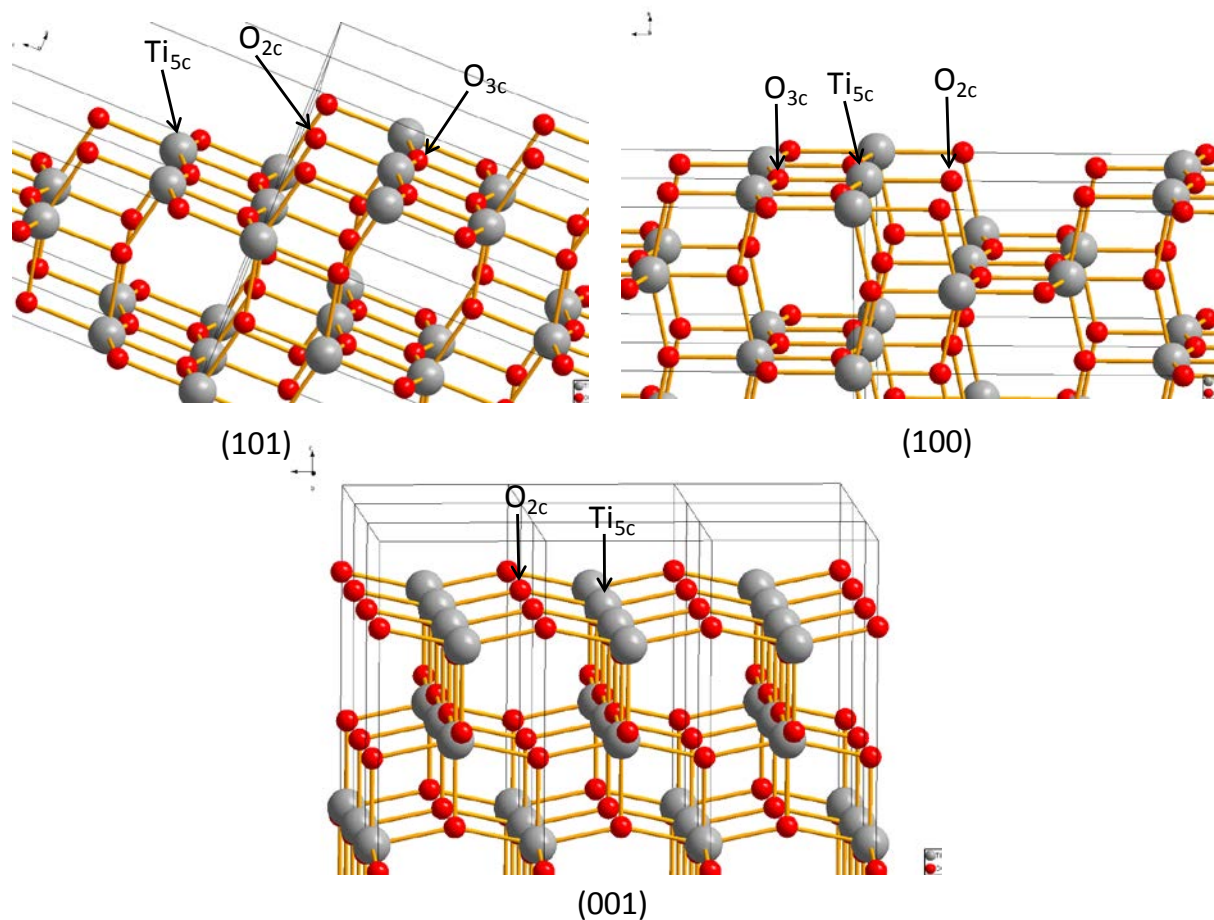


Figure 1.9. The three main faces of anatase crystal. All faces expose 5-fold coordinated Ti⁴⁺.

In reality, because of the presence of H₂O and other molecules in atmosphere, all under-coordinated Ti and O atoms on TiO₂ surfaces are saturated by H₂O and hydroxyl groups. The interaction of H₂O with TiO₂ gives rise to the presence of hydroxyl groups which dominate the chemistry of TiO₂ surface. The physical or chemical processes that take place on the surface of TiO₂ are significantly affected by these hydroxyl groups and H₂O layers. Understanding the interaction of H₂O with the surface of TiO₂ will give more insights about the surface chemistry of TiO₂, which is developed in the next section.

1.3.2 Surface chemistry

1.3.2.1 Interaction of TiO₂ with inorganic molecules

In this part we will discuss first the interactions between vapor H₂O and TiO₂ surfaces, which will allow describing some active surface sites. Next, other small molecules will be studied as molecular probes to investigate the reactivity of TiO₂ surfaces.

1.3.2.1.1 Interaction with vapor H₂O

Water is the most important adsorbate at TiO₂ surfaces due to the vital role of H₂O in photocatalytic applications of TiO₂ (in aqueous conditions). H₂O molecules adsorb on TiO₂ surface either molecularly (surface water) or dissociatively (formation of surface hydroxyl groups). Subsequently, these surface species strongly influence the physical and chemical processes at the interface. In well-controlled conditions like experiments in ultra high vacuum (UHV) chambers, vapor H₂O is the main component of residual gas. There has been extensive researches, to determine how H₂O adsorbs (whether dissociatively or molecularly), how it controls the properties of TiO₂, what is the driving force to form the adsorbed layer, how the adsorbed layer is arranged on the surface, and how H₂O co-adsorbs with other substances. For a complete description, see the extensive reviews by Henderson and Diebold.^{40,54} The present chapter will only give a brief overview of the adsorption of H₂O on the surface of TiO₂.

a) Vapor H₂O adsorption on rutile

Many studies dealt with specific facets, defects or non-defects on single crystals.⁶ The most studied facet is the (110) surface of rutile,⁵⁵ the (100) and finally (001) faces of rutile.

- Rutile (110) surface

On stoichiometric rutile (110) surface, evidence of molecular adsorption of H₂O was demonstrated by Scanning Tunneling Microscope (STM) works, which were reviewed by several authors.^{40,41,54} Molecular adsorption of H₂O was dominant.⁵⁶ Figure 1.10 illustrates molecular adsorption of H₂O on 5-fold coordinated Ti⁴⁺ sites (acid sites), with oxygen atom of H₂O directly bound to Ti⁴⁺, the O-H bond pointing outward from the surface. Henderson suggested that, on rutile (110) face, the distance between the adsorbed-hydrogen atom of adsorbed H₂O and the nearest bridging oxygen (basic site) atom is too long (3.2 Å), so that H-bonds cannot form between them. Subsequently, only molecular adsorption of H₂O was

observed on perfect (110) surface. Dissociative adsorption only occurs at defect sites (kinks and steps) and oxygen vacancies with a close distance between acidic sites (5-fold coordinated Ti^{4+}) and basic sites (2-fold coordinated bridging O^{2-} , noted O_b), that favors the weakening of H-OH bond, resulting in the dissociation of adsorbed H_2O . Nearly all experimental studies of water adsorption on the TiO_2 (110) 1×1 surface indicate that water dissociates only at O_b -vacancies, as shown in the reaction scheme in figure 1.11. Water fills the vacancy and one of the hydrogen atoms splits off, leaving a bridging hydroxyl group (OH_b) at the vacancy. The hydrogen atom sits on a nearby bridging O atom, forming another OH_b species.⁵⁷ This is in accordance with several theoretical studies, which suggest that the (110) surface of rutile favors dissociation of H_2O .⁵⁷

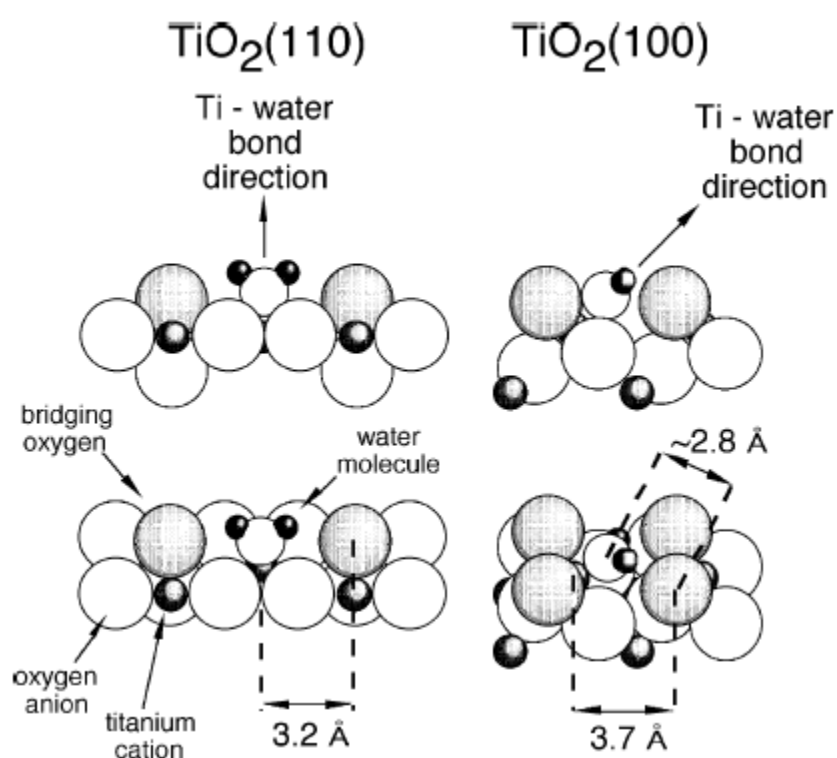


Figure 1.10. Molecular adsorption on (110) and dissociative adsorption on (100) faces of H_2O on TiO_2 (rutile). Adapted from Henderson 1996⁵⁶

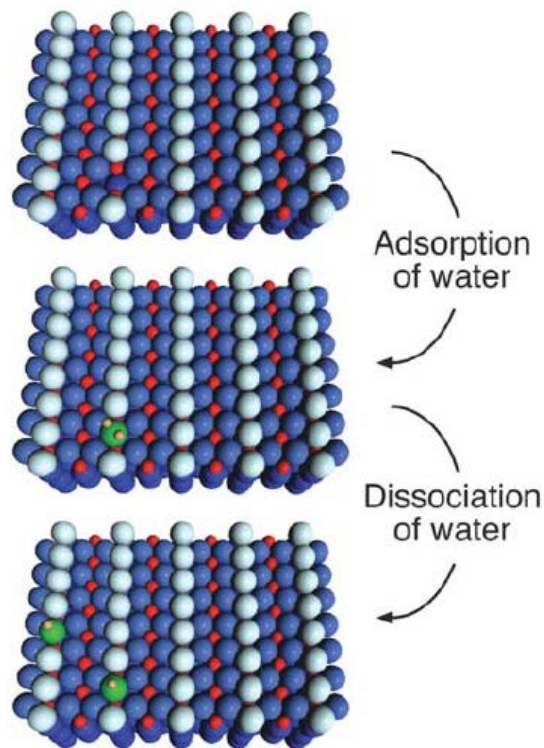


Figure 1.11. Model illustrating the dissociation of adsorbed H_2O at oxygen vacancy on rutile (110). Blue and red spheres represent respectively O and Ti atoms in the crystal lattice. Slight blue denotes bridging O atoms. Green spheres bearing two small shade pink spheres indicate O atoms binding two H atoms. Adapted from Pang 2008⁵⁷

- Rutile (100) surface

On perfect rutile (100) face, the adsorption of H_2O is dissociative at lower coverage followed by molecular adsorption at higher coverage.⁶ The dissociation of adsorbed H_2O on rutile (100) face is induced by the close distance between acidic and basic sites on this face (2.8 Å). The shorter distance facilitates the possible formation of weak H-bonds and induces the dissociation of adsorbed H_2O .

b) Vapor H_2O adsorption on anatase

In contrast with rutile, studies on the adsorption of H_2O on anatase are limited and mostly theoretical due to the unavailability of single crystal.⁶ Anatase (001) and (101) faces were the main targets of research on this crystalline phase: the latter is the main exposed surface of natural anatase, whereas the (001) is a minor surface for most anatase samples.⁵⁸ Density functional calculations showed that H_2O was molecularly adsorbed on the (101) face, while dissociatively adsorbed on the minor (001) surface. Experimental study (Herman 2003) with temperature-programmed desorption and X-ray photoelectron spectroscopy indicated

that multilayer of H₂O adsorbed on (101) and H₂O molecules bind directly to 2-fold coordinated O and 5-fold coordinated Ti sites. There are no evidence for the dissociative adsorption.

1.3.2.1.2 Interaction with CO: molecular probe of the sorption sites

One powerful way to investigate the Lewis acid and base centers consisted in the use of a molecular probe such as CO.⁵⁹⁻⁶² The majority of these studies were conducted on the rutile (110) face.

a) CO adsorption on rutile

The adsorption of CO on the surface of TiO₂ is dependent on the characteristics of the surface.⁶³ Adsorption of CO occurs at defective sites and is enhanced by the presence of oxygen vacancies. In contrast, the interaction of adsorbed CO with adjacent bridging oxygen or with pre-adsorbed oxygen leads to desorption of CO₂. Stoichiometric and defective (110) faces of rutile showed the same coverage for both faces. Saturation coverage is reached at about 2.5×10^{14} CO/cm², which approximately accounts for 50% of 5-fold coordinated Ti ions.⁴⁰ Theoretical studies based on density functional theory (DFT) indicated that CO is more preferably adsorbed on the surface by C-end than O-end orientation. The former occurs through the interaction of CO with Ti lattice sites to form Ti-CO configuration, the latter through defect sites to form Ti-OC.⁶⁴ Adsorption energy for Ti-CO configuration at 50% coverage reaches about 11 kcal/mol, whereas for Ti-OC this value is only 2.71 kcal/mol, in good agreement with experimental values.

b) CO adsorption on anatase-rich samples

TiO₂-P25 powder is a mixture of about 80% of anatase and 20% of rutile. The anatase crystals expose mainly (010), (101) and (001) faces. Spoto and co-workers studied the adsorption of CO on a treated TiO₂-P25 powder to get a fully dehydroxylated surface. After exposition to CO, the authors could firmly assign the infrared peak at 2179.5 cm⁻¹ to the adsorption of CO on 5-fold coordinated Ti⁴⁺, which are located on (101) and (010) faces of anatase particles. Once the pressure of CO was reduced, the vibration frequency of CO was red-shifted (Figure 1.12) to 2192.5 cm⁻¹. Peaks ranging from 2211.5 cm⁻¹ to 2207 cm⁻¹ were ascribed to CO bonded to low coordinated Ti⁴⁺ at edge, step and corner positions. The peak at 2153 cm⁻¹ was assigned to CO bonded to residual OH group through H-bonds.

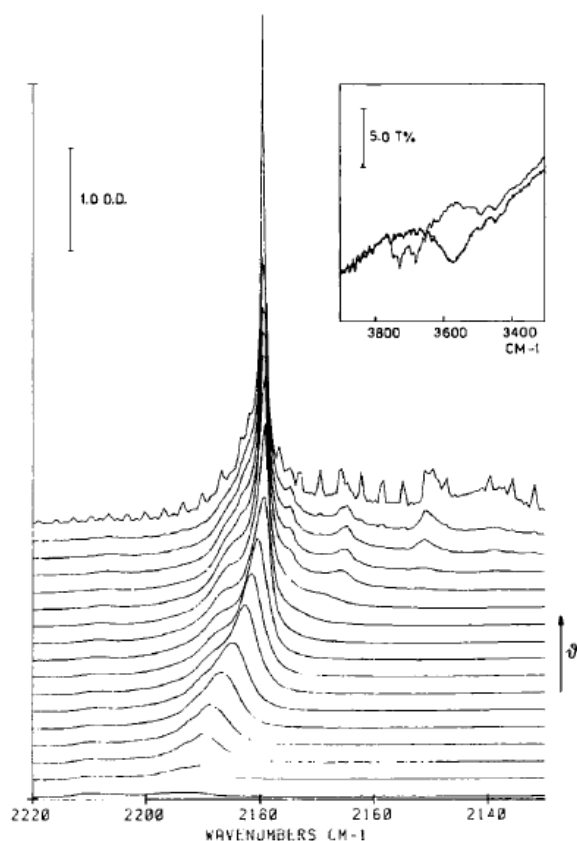


Figure 1.12. Infrared spectra of CO adsorbed at 77K on TiO₂ outgassed at 873 K. The most intense spectrum was recorded at 40 torr of CO. The inset is the spectra in OH region before and after contact with CO. Adapted from Spoto 1990⁶⁵

A very similar study was conducted ten years later by Martra, in which the author compared two types of TiO₂ powders, P25 (80% anatase and 20% rutile) and pure anatase.⁶⁶ These TiO₂ particles also have different morphologies. Indeed, TiO₂-P25 exposes mostly (101) and (001) faces of anatase particles, whereas pure anatase particles expose (101) faces and roundish surfaces. The author found that the Lewis acidity of 5-fold coordinated Ti⁴⁺ on roundish surfaces and (101) faces of pure anatase sample is less strong than that on (001) and (010) anatase faces in TiO₂-P25. The authors postulated that the Ti⁴⁺ centers on pure anatase possess less acidic reactivity due to the effect of surrounding ligands O²⁻. In addition, acidity of Ti⁴⁺ centers located at edge, corner and steps are evidently stronger than that of centers located on regular faces.

These studies demonstrate that the reactivity of TiO₂ towards CO molecules depends on the particles morphology and also on the interaction of Lewis centers (Ti⁴⁺) with oxygen ligands (O²⁻). CO binds directly to Lewis acid sites (Ti⁴⁺) on flat surfaces and terraces, and

also at edge, step and corner positions. Besides, CO may form H-bonds with hydroxyl groups. At high coverage, lateral interactions among CO molecules occur.

1.3.2.1.3 Interaction with CO₂

Interaction of CO₂ with the surface of oxides, has been a very important subject of research because of its key role in industry and was reviewed by Freund and Roberts.⁶⁷

CO₂ interacts weakly with oxygen vacancies of clean (110) surfaces of rutile and even more weakly on regular lattice sites. The binding mode is in linear configuration, as proven by high resolution EELS data. However, the adsorption of CO₂ is blocked in the presence of H₂O on the (110) surface of rutile. Co-adsorption of CO₂ and H₂O on rutile (110) surfaces leads to the formation of bicarbonate species while pre-adsorbed CO₂ is found to be displaced by H₂O.⁶⁸ Oxygen vacancies present on the vacuum annealed rutile TiO₂ (110) surface allows stronger CO₂ binding than the 5-fold coordinated Ti⁴⁺ on nearly perfect surface.

Since CO₂ is more acid than CO, Martra and co-authors investigated the basic centers (O²⁻) of TiO₂-P25 and pure anatase by CO₂ adsorption conducted at low (423 K) and high (873 K) temperatures.⁶⁶ The author showed that CO₂ can create linear bond with O²⁻ centers on TiO₂-P25. On the contrary, spectra of pure anatase do not show the corresponding peaks of these species.

1.3.2.1.4 Interaction with oxygen and nitrogen

Dioxygen plays a key function in photocatalytic processes of TiO₂. It is widely used in photochemical oxidation studies on TiO₂ surface, and is considered as the main scavenger of photoexcited electrons, preventing the accumulation of negative charges on the surface of TiO₂ particles.⁶⁹ The typical species resulting from this scavenging process are O²⁻ and HO₂[•], which probably play a direct role in oxidation of organic compounds.⁷⁰

Many studies investigated the adsorption of dioxygen on the (110) surface of rutile whether theoretically⁷¹ or experimentally⁶⁹⁻⁷³. At temperatures below 150 K, oxygen adsorbs via both molecular and dissociative modes on rutile (110) surface.⁶⁹ Interestingly, molecular adsorption is stable up to 410 K and exists as O²⁻ on surface. Above 150 K, dissociative adsorption is favored. It was suggested that O₂ adsorbed on oxygen vacancy sites of reduced TiO₂ and creates O adatom on neighboring 5-fold coordinated Ti⁴⁺ sites.⁷³ This O adatom can react with neighboring adsorbed H₂O to form two surface hydroxyl groups (Figure 1.13).

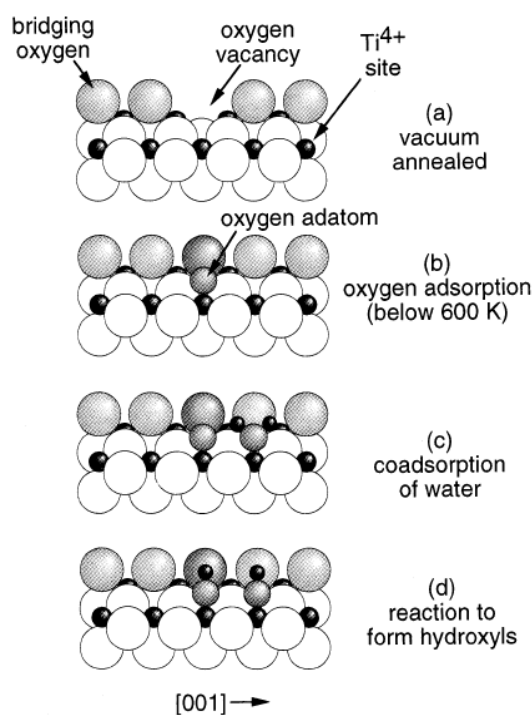


Figure 1.13. Model of oxygen adsorption on the (110) surface of rutile. (a) shows the oxygen vacancy position, where oxygen will adsorb, thus creating oxygen adatom in (b) on acidic site Ti^{4+} . (c) presents the co-adsorption of H_2O to an adjacent Ti^{4+} site. The interaction between oxygen adatom and adsorbed-water molecules leads to the formation of a pair of surface hydroxyl groups (d). Adapted from Epling 1998⁷³

The presence of N_2 with O_2 in atmosphere can lead to the adsorption of N_2 on the surface of TiO_2 . Both theoretical and experimental studies were conducted concerning the physisorption of N_2 on the (110) surface of rutile.⁴⁰ Under vacuum condition (less than 1 Torr), N_2 was found to adsorb at all 5-fold coordinated Ti^{4+} sites, leading to lateral interactions among these adsorbed- N_2 molecules. Surprisingly, theoretical calculations indicated that the area covered by one N_2 molecule (19.2 \AA^2 for monolayer and 9.6 \AA^2 for multilayer regime) is different from the usual value used for BET measurements (16.2 \AA^2). If this finding is confirmed, then surface area measured by BET method is underestimated.⁶

1.3.2.1.5 Interaction with NH_3

Experimental and theoretical studies confirm that at room temperature NH_3 is molecularly adsorbed on rutile (110) and (001) surfaces via N-end binding to 5-fold coordinated Ti^{4+} sites.⁴⁰ NH_3 strongly binds to defect sites and can block the neighboring 5-fold coordinated Ti^{4+} sites. When surfaces with oxygen vacancies are exposed to NH_3 , the latter fills the vacancies and dissociates.

1.3.2.1.6 Surface sites of TiO₂

After describing how probe molecules allowed the identification of surface active sites, let us summarize in figure 1.14 the positions and names of these sites on each crystalline face of rutile and anatase.

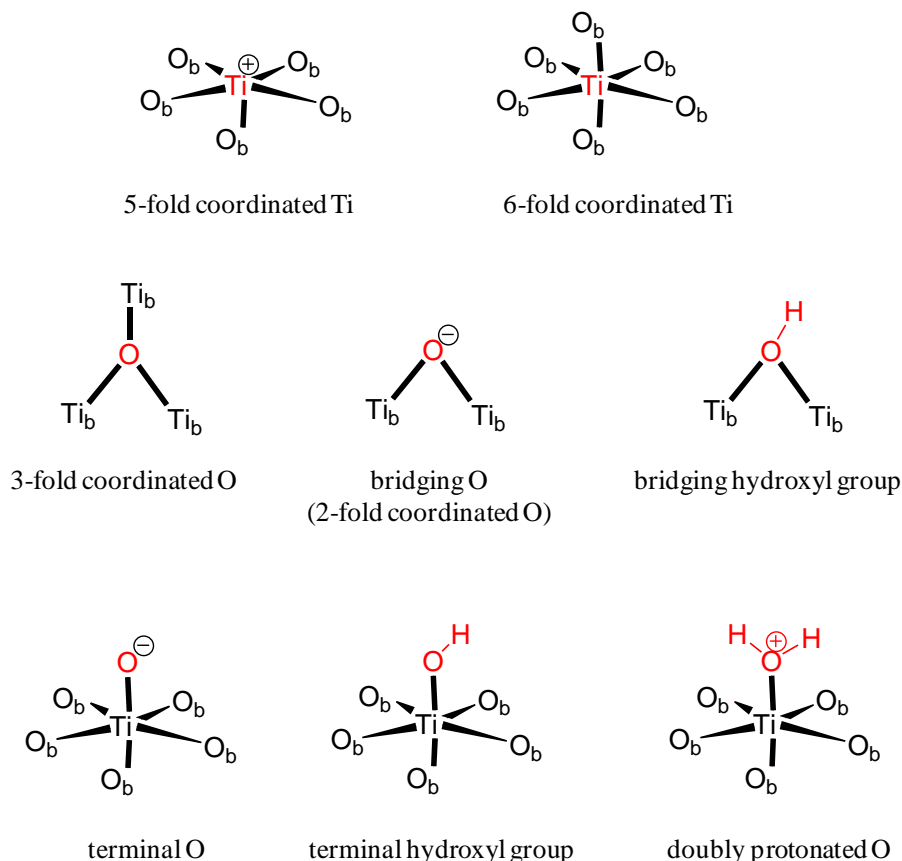


Figure 1.14. Nomenclature of surface sites on TiO₂ surface. Ti_b and O_b designates oxygen and titanium atom in the bulk lattice, respectively.

The active sites of TiO₂ now being precisely described, information about the adsorption modes of some organic molecules will be discussed.

1.3.2.2 Interaction with small organic molecules

1.3.2.2.1 Carboxylic acid

Studies on the adsorption of carboxylic acid on TiO₂ surface have been driven by TiO₂ applicability in various technical fields such as solar cell, catalysis.^{57,74} Formic acid is considered as a representative molecule of organic acids. The adsorption of formic acid on TiO₂ has been well-documented and was exhaustively reviewed by Diebold⁴⁰ and Thomas⁷⁴.

The adsorption of formic acid on the (110) surface of rutile is the most studied among all TiO₂ surfaces and is considered to apply for all monocarboxylic acids adsorbed on TiO₂. Formic acid adsorbs on (110) surface of rutile and dissociates as formate. The binding mode of formate is substantially affected by experimental condition such as temperature, history of oxide surface, dosing concentration of acid formic.⁵⁷ The formate is bound to the surface according to three kinds of bridging geometry, shown in Figure 1.15. In the first one (A), the formate is bound to two surface Ti_{5c} atoms via its two oxygen atoms. The second one involves filling of a bridging oxygen O_b site by one of the carboxyl oxygen atoms and the other bound to Ti_{5c} (B in Figure 1.15). The third binding mode (site C in Figure 1.15) involves only one formate oxygen atom, which fills the oxygen vacancy.⁷⁴

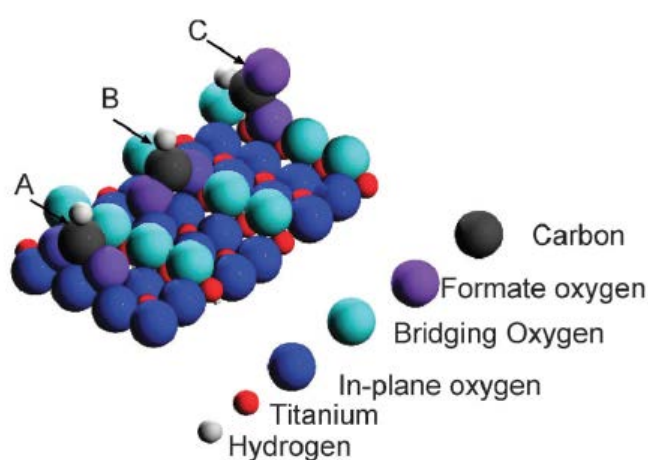


Figure 1.15. Proposed geometries of adsorbed formate on rutile (110). Type A shows the favored geometry for most formate, deduced from near edge X-ray adsorption fine structure spectroscopy (NEXAFS) and Scanned-energy mode photoelectron diffraction (PhD) measurements. Type B was less common and deduced from NEXAFS and STM while C was deduced from STM. Adapted from Thomas 2012⁷⁴

The adsorption of monocarboxylic acids typically follows the room temperature adsorption behavior of formic acid on TiO₂ rutile (110) 1×1, *i.e.* . In this adsorption mode, they form carboxylate moieties on surface through acid hydrogen cleavage, and adopt bidentate binding geometry, which is comparable to that for formate.⁵⁷

Adsorption of small carboxylic acids on the rutile TiO₂ (100) (1×3) and (100) (1×1) surfaces show that the adsorption is similar to that seen for the rutile (110) surface, *i.e.* the acid adsorbs dissociatively. Similar results were obtained for adsorption on the (001) surface. More recently there have been a few experimental and theoretical studies of carboxylic acid

adsorption on the TiO_2 (011) (2×1) surface, which suggest adsorption in a bridging bidentate mode. This bonding mode is favored despite the larger Ti–Ti distances found on the (011) surface relative to the (110) surface.⁷⁴

In contrast to rutile surfaces, far less numerous studies have been carried out on the anatase surfaces. By means of density functional calculation (DFT) on the (101) surface of anatase crystals⁷⁵, Vittadini et al. predicted that acid formic adsorbs preferentially as monodentate species, and that it forms hydrogen-bonds with the bridging oxygen atoms.⁷⁵ When co-adsorbed with water, formic acid keeps a monodentate adsorption mode, but dissociates through interactions with nearby water molecules. Studies also found that formic and acetic acid were adsorbed on anatase (001) – (1 x 4) thin film via bonding with under-coordinated Ti sites on surface.⁷⁴ Adsorbed formate and acetate were stable on surface up to 700 °C. Above this temperature, they were decomposed.

Dicarboxylic acids were suggested to have many possible adsorption modes on surface of TiO_2 that are exhibited in Figure 1.16.

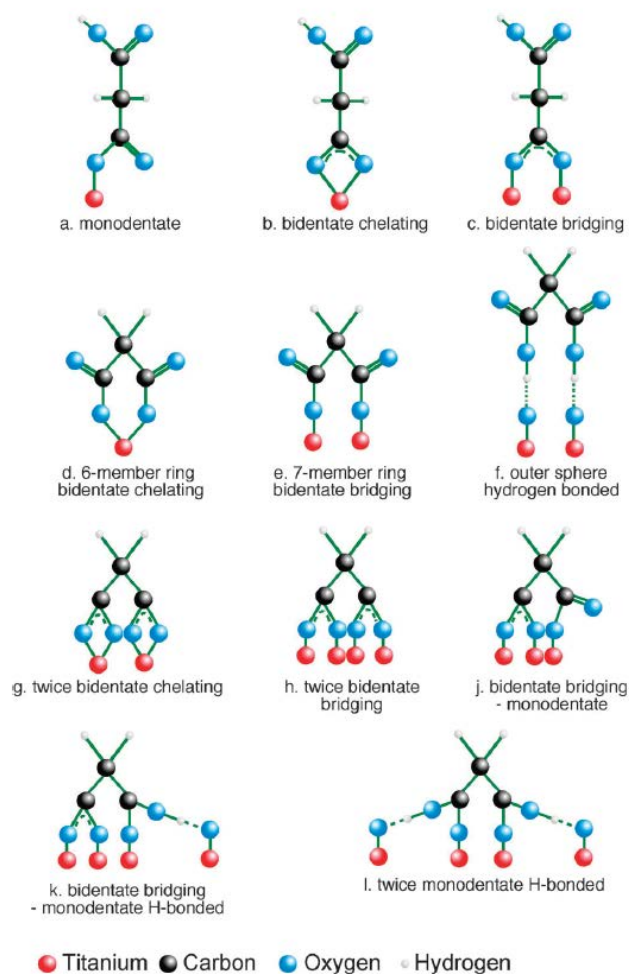


Figure 1.16. Possible binding modes of dicarboxylic acid on TiO_2 surface. Adapted from Thomas 2012⁷⁴

1.3.2.2.2 Alcohol

The interaction of TiO_2 with alcohol have many technological applications. Alcohols are popular models of organic contaminants to study the photocatalytic activity of TiO_2 .⁵⁷ Among the substrates, rutile (110) is the most studied because it is considered as an important model of metal oxide surfaces.⁷⁶ Few other rutile surfaces were investigated, for example the (001), (441) and (100) surfaces.⁴⁰ Both computational and experimental studies led to the same conclusion that the majority of methanol molecules adsorbs molecularly to the (110) surface of rutile and a minor fraction is dissociated.^{6,77} Molecular adsorption of aliphatic alcohols usually takes place on 5-fold coordinated Ti sites whereas dissociative adsorption preferentially occurs on oxygen vacancy sites^{78,79} or on bridging oxygen⁷⁷. The dissociation of methanol takes place through the breaking of the O-H bond of CH_3OH , leading to the adsorption of methoxy species, the bridging oxygen probably being hydroxylated. Arribas and

Madix reported that the formation of methane from methanol adsorption is preferential at oxygen vacancies when both types of active sites (Ti^{4+} sites and oxygen vacancies) are available.⁸⁰ Exposing the methanol-modified TiO_2 surface to O_2 resulted in more methoxy groups on the surface due to cleavage of the $\text{CH}_3\text{O}-\text{H}$ bond. In contrast, co-adsorbed water had little effect on methanol at the surface.⁷⁴

While there are numerous investigations on rutile, far less studies have been conducted on anatase surfaces,⁵¹ due to unavailability of well-defined and high quality single crystals. However, a study revealed both molecular and dissociative adsorption of methanol on 5-fold coordinated Ti sites of (101) anatase surface, as well as the existence of molecular adsorption on bridging oxygen. Dissociative adsorption of methanol was also observed on step edges Ti sites.⁸¹ Molecular dynamic simulation (MD) proved that molecular adsorption of methanol on anatase (101) surface is thermodynamically favorable, which is in agreement with experimental studies. Nevertheless, the presence of defect sites and hydroxyl groups on the surface of anatase can alter the adsorption modes of methanol.⁸²

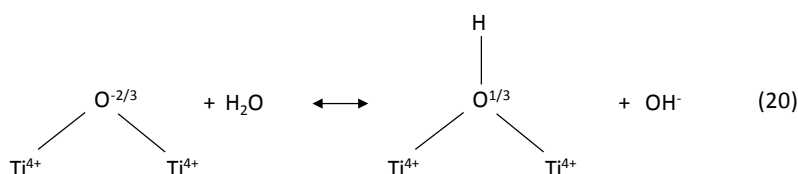
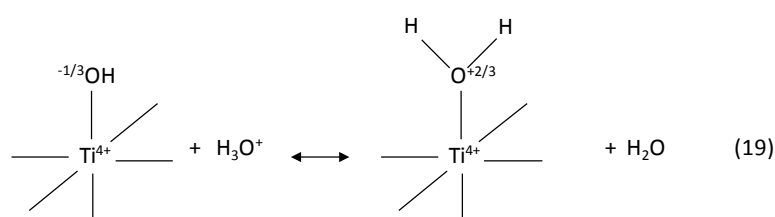
1.3.3 TiO_2 – aqueous solution interface

1.3.3.1 Hydration

Clean surfaces of TiO_2 in ultrahigh vacuum present under-coordinative saturation atoms of Ti and O. However, in ambient conditions and aqueous medium, TiO_2 surface is hydrated and saturated by chemisorbed and physisorbed H_2O . The dissociation combines with protonation/deprotonation on surface TiO_2 hydroxyl group or oxygen atom. There are three types of exposed oxygen: singly coordinative (TiO), doubly coordinative (Ti_2O) and triply coordinative (Ti_3O)³⁸ and consequently three possibilities of hydroxyl groups: terminal hydroxyl (TiOH) on 5-fold coordinative Ti^{4+} sites, bridging hydroxyl (Ti_2OH) on bridging oxygen and triply coordinative hydroxyl (Ti_3OH) on 3-fold coordinative O atom. As a result, each type of surface atom exhibits a defined charge in defined conditions. The surface charges on metal oxides were initially calculated according to Pauling valence bond concept. Recent developments in interfacial chemistry proposed another approach to compute surface charge on TiO_2 .⁸³ Hereafter, a review concerning surface protonation/deprotonation models to calculate surface charge of TiO_2 is proposed.

1.3.3.2 Surface charge according to Pauling valence bond concept

Using Pauling valence bond concept (for local charged neutrality), charge (δ) on oxygen atoms can be calculated with formula: $\delta = n\nu - 2 + p$, where n is the number of bonds O-Ti, p is the number of H atoms binding to an oxygen atom, ν is the formal bond valence ($\nu = z/N$), z is charge of cation and N is coordination number of cation.¹² Charges of exposed oxygen atoms on TiO₂ surface were estimated: -4/3 for singly, -2/3 for doubly and 0 for triply coordinated oxygen.³⁸ This finding implies that the acid – base character of TiO₂ surface can be represented by the protonation/deprotonation equilibria of terminal hydroxyl groups and doubly exposed O atoms. The equilibria equations are simplified as following:

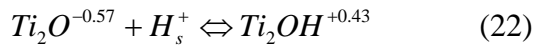


The protonation constant of the exposed oxygen atoms were also calculated, based on multisite complexation model (MUSIC). The logarithm of protonation constants of equations (19) and (20) estimated from MUSIC model and Pauling valence bond approach are 6.7 and 5.1. The results suggested that triply coordinated O cannot be protonated in normal pH range and singly coordinated O is instantly protonated in contact with H₂O.⁸⁴

1.3.3.3 Surface ionization models on TiO₂ surface

Panagiotou et al. developed a surface ionization model of TiO₂-P25 nanocrystallites based on experimental results and quantum mechanical population analysis. There are two types of protonation/deprotonation sites on TiO₂ surfaces. They are bridging and terminal oxygens.

Concerning terminal oxygens, which are generated from dissociation of adsorbed H₂O at 5-fold coordinative Ti⁴⁺ sites. The protonation/deprotonation processes of surface groups on TiO₂ in aqueous suspension can be written as the following:



According to the author, the speciation of these sites on TiO_2 -P25 surface according to pH and for different ionic strengths (Figure 1.17).

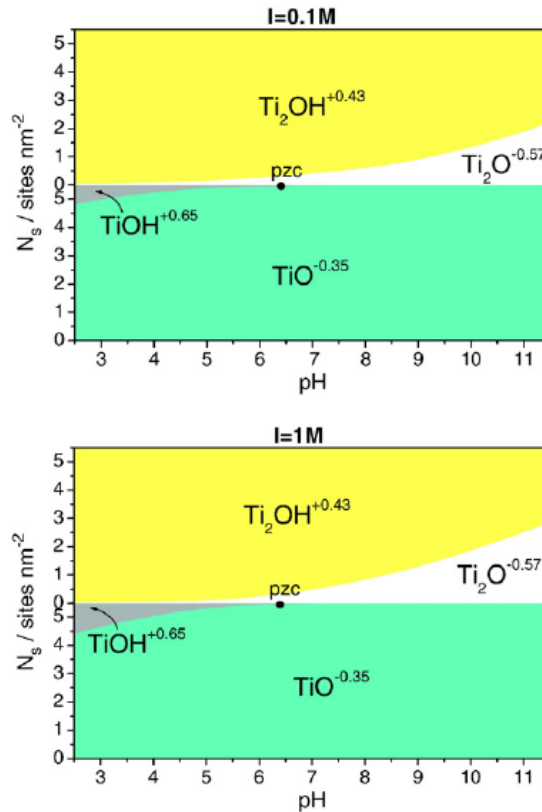


Figure 1.17. Surface sites exposed on TiO_2 P25 as a function of pH at two ionic strengths in aqueous medium. Adapted from Panagiotou 2008⁸⁵

1.3.4 TiO_2 – electrolyte solution interface

1.3.4.1 Arrangement of ions at the interface

The charges developed at the TiO_2 surface generate an electrical double layer at the TiO_2 -solution interface. The location of electrolyte ions at the interface is significantly dependent on their interaction with surface charged groups. The triple layer model (figure 1.18) can be used to map the distribution of these ions inside the interface. This model divides the interfacial region in three planes: the first one (plane 0) is the location of surface groups of oxide ((hydr)oxo groups). The second one (plane 1) is the closest distance that counter-ions

can approach to the surface to create ion-pairs with surface sites of opposite charge. The charge of these counter-ions is distributed in the whole space from plane 1 to plane 2, the latter constituting the beginning of the diffuse layer. Co-ions and the remaining counter-ions stay slightly far away from the surface, within the diffuse layer.

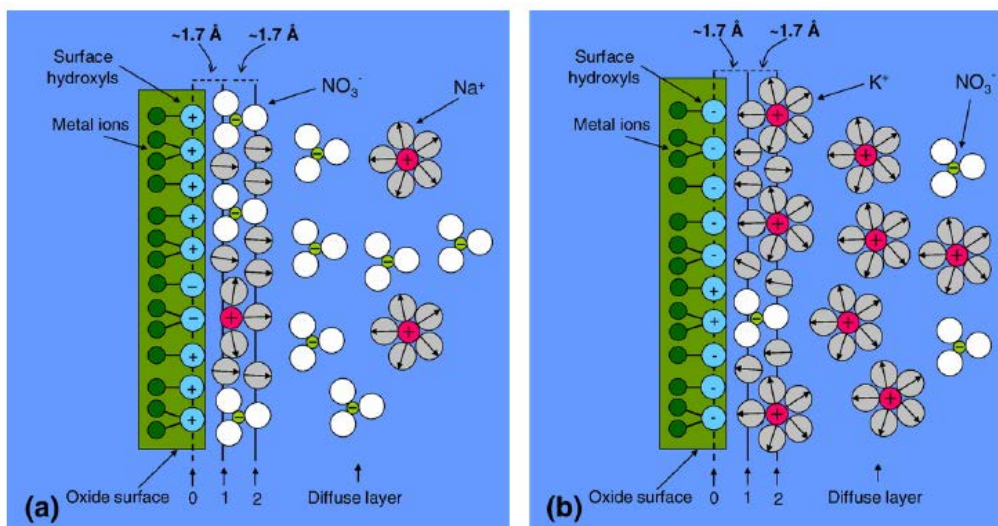


Figure 1.18. Triple layer model showing the location of electrolyte (a) NaNO_3 at the interface of positively charged TiO_2 and (b) KNO_3 at the interface of negatively charged TiO_2 with aqueous solution. From Panagiotou 2008

As illustrated in figure 1.19, the thickness of the compact zone (from surface to plane 2) is about 3.4 \AA .⁸⁵ Na^+ ions in panel (a) get closer to the surface and these ions are partially dehydrated. On the contrary, K^+ ions in (b) panel stay quite far away from the surface and these ions are not dehydrated. It is suggested that as the size of K^+ ions is bigger than that of Na^+ ions, it is difficult for K^+ ions to penetrate the first ordered-water layer at the interface.

1.3.4.2 Shear plane and zeta potential

Within the diffuse layer, there are two regions: the region which is closer to the surface is stagnant and the other one is mobile. The barrier between both regions is named shear plane, where the zeta potential can be determined via electrophoretic mobility measurements (microelectrophoresis technique) or the recently “streaming potential” method developed for high ionic strength values.

Conventionally, the shear plane is assumed to be positioned at the head end of the diffuse part of the electrical double layer (plane 2 in the triple layer model). However, several studies have pointed out that this position is not always true, and depends on the ionic

strength of solution.^{84,85} These two studies indicated that the distance of the shear plane from the head end of the diffuse part is inversely proportional to the square root of ionic strength. It is noteworthy that, on the contrary, the thickness of compact zone is independent on ionic strength of solution. Only the thickness of diffuse layer is compacted when ionic strength increases. Consequently, the position of shear plane is displaced. Increasing ionic strength also leads to the accumulation of counter-ions in the region which is closest to the oxide surface. Panagiotou and others shows that when ionic strength is higher than 0.02 mol.L^{-1} , concentration of counter-ions in the stagnant diffuse layer is higher than that in the mobile part. Additionally, pH also has an effect on the distribution of counter-ions in the interfacial region, which depends on the region within the interface and on the pH value compared to PZC of oxide surface. When pH is far away from PZC, the surface charge is higher, leading to a larger concentration of counter-ions in the compact region and the stagnant diffuse layer. Furthermore, removing pH away from PZC or increasing ionic strength can reduce the mobility of counter-ions in the interfacial region. Nevertheless, in most case, concentration of counter-ions in interfacial region is higher than that in the bulk solution. In addition, concentration of counter-ions in the compact region is lower than that in the diffuse layer because of the hindrance related to ordered – water layer and the big size of solvated ions.

Several models allow the conversion of electrophoretic mobility into zeta potential. First, Von Smoluchowski and Hückel developed a linear relation between electrophoretic mobility and zeta potential, respectively for large particles developing insignificant double layer, and for small particles with a thick double layer, assuming that the electrical conductivity of the particle is the same as that of the surrounding medium. Later, Henry revisited Hückel theory, considering that the conductivity is different for the particle and the liquid phase. This conductivity leads to the mutual distortion of the applied field and the field of the double layer, and hence slows the electrophoretic motion. O'Brien developed a complete picture of the frequency dependent dielectric response of a dilute suspension of spheres with thin double layers. Several electrokinetic models were further elaborated in order to take into account parameters not included in the previous ones: surface conductance for spheroidal particles, polydispersivity of the sample, nanoparticles agglomeration, diffuse layer overlapping. Mangelsdorf and White's numerical model takes into account particle size effects and the adsorption of ions and their mobility in the inner part of the electrical double layer.

However, zeta potential estimations can be erroneous due to the uncertainty concerning the value of the conversion factor used in Henry equation. This could explain the “observed” shift of the shear-plane position as a function of the ionic strength in surface complexation models. Henry and O’Brien considered that only the counterions in the diffuse layer are responsible for the surface conductivity. They did not consider the influence of the Stern layer on particle surface conductivity. Leroy and co-workers⁸⁶ examined the possible influence of the very high TiO₂ nanoparticle surface conductivity, including Stern layer contribution, on its electrophoretic mobility, in order to obtain zeta potential values in agreement with those predicted by electrostatic surface complexation models (without considering large variations of the distance between the outer boundary of the compact layer and the inner boundary of the diffuse layer). This model significantly lowers the amplitude of electrical potential at the OHP compared to that of other recent surface complexation models. Moreover, their modeling results suggest that the shear plane may be located close to the OHP, in contradiction with the hypothesis of a stagnant diffuse layer having a salinity-dependent thickness at the TiO₂ water interface. The same group showed that the repulsive electrostatic force between nanoparticles and their stability ratios can be significantly underestimated if apparent zeta potentials (not corrected with surface conductivity) are used instead of true zeta potentials.⁸⁷

To conclude, surface charge and generated electrical potentials in the interfacial region TiO₂-aqueous solution can be controlled in part by ionic strength and pH of aqueous medium. Consequently, the interaction between oxide particles in suspension can also be controlled. Indeed, electrostatic and van der Waals forces mediate the aggregation and agglomeration of particles in aqueous medium. Increasing or decreasing surface charges or surface potentials can whether enhance or reduce the level of aggregation and agglomeration between particles. This phenomenon has been widely used in stabilization techniques for suspensions of many oxide particles, among them TiO₂. Likewise, steric stabilization is used for the similar purpose. For this, surface particles are grafted by molecules, which have suitable size or charged groups to inhibit the particles getting closer to each other.

The interface of TiO₂-aqueous solution is very complex to understand at a molecular level. There are many variables, which affect the interfacial region. Among them, pH, ionic strength and nature of electrolyte are crucial parameters. They not only affect surface charge, surface potential, and stability of oxide particle suspensions, but also the interaction of the

surface with aqueous species. In the next section, adsorption of species on TiO₂ surface in aqueous medium is discussed.

1.4 Sorption of species on TiO₂ surface in aqueous solution

1.4.1 Sorption of phosphate and phosphate-containing molecules

Due to a variety of interests, there is considerable research investigating the adsorption of phosphate species on TiO₂.⁸⁸⁻⁹² On one hand, phosphate is present in biological systems such as blood, in concentration of approximately 3×10^{-4} mol/L. On the other hand, titanium metal is widely used as implant, which is normally covered by a layer (thickness of a few nm) of TiO₂.⁹³⁻⁹⁵ Consequently, the interaction between phosphate species in biological system and TiO₂ was largely studied. All studies converged to the fact that phosphate ions in aqueous solution adsorb on TiO₂.^{88-90,96} By combining batch experiments and NMR spectroscopic methods at several pH values, Kang et al. found that phosphate ions form inner-sphere surface complexes at the TiO₂ surface. The sorption of phosphate was irreversible at pH 4.5 and pH 7, in contrast to pH 9.⁹⁶ Based on ³¹P solid-state NMR experiments, the authors suggested the formation of a bidentate complex. The sorption of phosphate on TiO₂ through bidentate mode was also suggested by Connor and McQuillan, although they could not distinguish between bridging bidentate or chelating bidentate modes by IR experiments. However, IR technique could bring evidence that sulfate groups, which have similar symmetry as phosphate ones, may bind to TiO₂-P25 through chelating bidentate.⁹⁷ Moreover, Attenuated Total Reflectance - Fourier Transform Infrared Spectroscopy (ATR-FTIR) was successfully used to prove the binding of linear polyphosphate species to TiO₂, with the formation of Ti-O-P bonds.⁹⁰ The presence of Ti-O-P bonds was also demonstrated by XPS.⁹⁸⁻¹⁰¹ Bachinger and Kickelbick conducted a photocatalytic activity study of TiO₂ (mixture of anatase and brookite) modified with phosphonate or phosphate organic molecules, and they found that the Ti-O-P bonds were very stable under UV illumination.¹⁰² Indeed, the organic moiety was totally degraded while the phosphate groups remained anchored to the surface of TiO₂.¹⁰² As a conclusion, the adsorption mechanism seems to depend on both pH and reactivity of the metal oxide surface. Further research is needed to elucidate the influence of each parameter and to reveal the adsorption mode, as sketched in Figure 1.19.

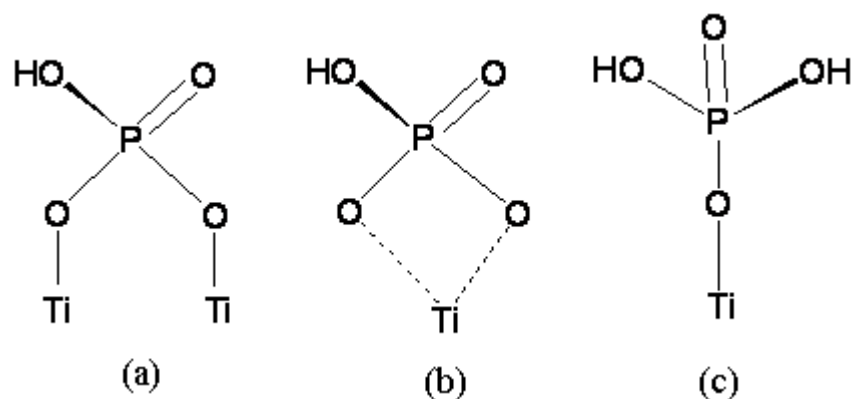


Figure 1.19. Simple binding mode models of phosphate group to Ti^{4+} sites on TiO_2 : bridging bidentate (a), chelating bidentate (b) and monodentate (c). Coordination number of Ti^{4+} may be 5, 4 or 3, depending on the position of Ti sites whether on flat surfaces, corners or steps.

The formation of Ti-O-P bonds gave the opportunity to anchor organic molecules on the surface of TiO_2 through their phosphate group¹⁰³ and to use TiO_2 surface as sorbent to separate and purify phosphorylated biomolecules (Metal Oxide Affinity Chromatography, MOAC). Such molecules, for instance, phosphorylated peptides, glycosylphosphatidylinositol and phospholipids could be well separated and enriched by using TiO_2 micro-column chromatography^{104–106}. The selective and strong interaction of phosphate groups with the TiO_2 surface was claimed as clearly the fundamental basis to separate phosphorylated molecules from the others in the mixture.^{105,106} However, it does not explain the separation of various phospholipids and the binding mode is still rather unclear.

1.4.2 Sorption of carboxyl-containing molecules

Studies on synthesis and applications of TiO_2 require the understanding at a molecular level of the interaction of carboxylic acids with the TiO_2 surface. Indeed, carboxyl groups are used as anchored groups in order to control the particle size in TiO_2 synthesis. Through their adsorption on specific surfaces of growing crystals, they prevent the growth of these faces, leading to anisotropic particles of controlled size. Carboxyl groups also play an essential role as dye-surface contacts in TiO_2 -based dye-sensitive solar cell.⁷⁵

Formic acid is the representative molecule of carboxylic acids, and both theoretical and experimental studies were performed on its adsorption on the TiO_2 surface. In aqueous environment, formic acids and carboxylic acids with longer chains are demonstrated to adsorb onto the surface of TiO_2 through bridging bidentate modes.¹⁰⁷ The author also demonstrated

that quantum calculation supported both the bridging bidentate and possible monodentate mode is favorable (Figure 1.20). The mechanism of adsorption involves dissociation of the carboxyl group on the surface of TiO₂:



In the bridging bidentate species, two oxygen atoms of the carboxyl group bind to two different Ti⁴⁺ cations, while the proton links to a lattice oxygen atom to form a hydroxyl group. In the monodentate mode, one oxygen atom from the carboxyl group binds to one Ti⁴⁺ cation, whereas the other oxygen atom binds to a lattice oxygen through a hydrogen atom.

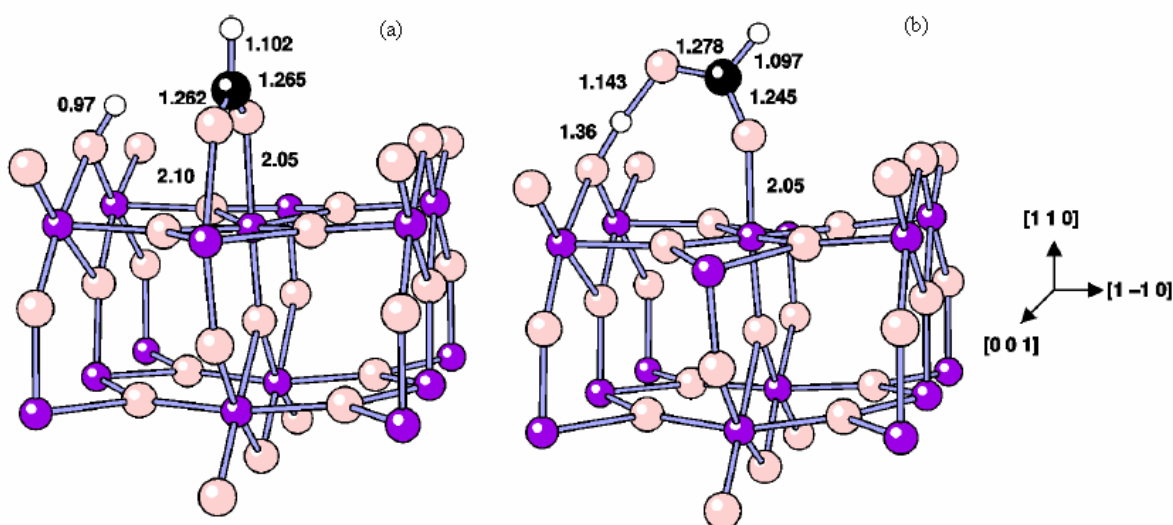


Figure 1.20. Adsorption of acid formic on the (110) surface of rutile. Bridging bidentated mode (a) and monodentate mode (b). White balls represent H atoms, black is used for C atoms, pink for O atoms and violet for Ti atoms. The bond length is expressed in angstroms. Adapted from Ojamae 2006¹⁰⁷

Obviously, the adsorption of carboxylic acids on TiO₂ is dependent on environmental conditions, particularly pH since the dissociation of carboxyl group is controlled by pH. pKa values are highly different from one acid to another (*i.e.* 3.75 for formic acid, 4.8 for acetic acid, and 3.13, 4.76 and 6.4 for citric acid).

1.4.3 Sorption of hydroxyl-containing molecules

Some hydroxyl-containing molecules have potential usage in solar energy conversion, synthesis and material sciences. Therefore interactions between these molecules and TiO₂ have attracted considerable attention.^{49,108} They relate essentially to diols.

1.4.3.1 Catechol-based molecules

In bioadhesion studies, catecholic amino acid 3,4-dihydroxyphenylalanine (DOPA) attracted many studies. The molecular structure of DOPA is reported in Figure 1.21.

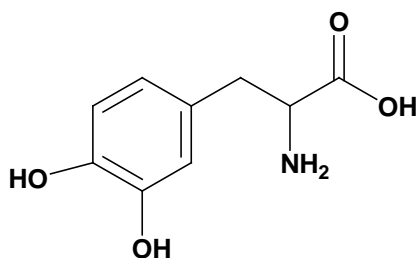
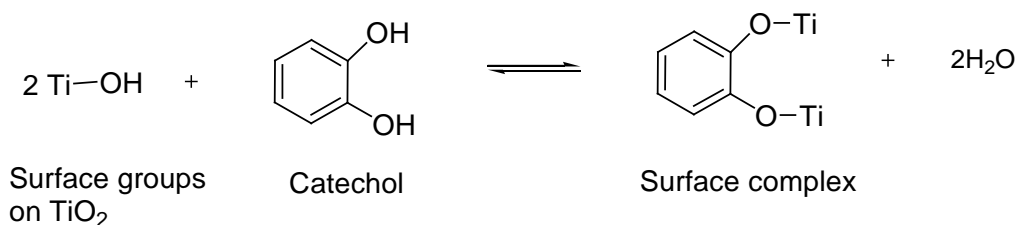


Figure 1.21. Molecular structure of 3,4-dihydroxyphenylalanine (DOPA).

Bahri et al. investigated the adsorption of this molecule on rutile particles in aqueous medium containing NaCl, at different pH.¹⁰⁸ The authors found that DOPA formed surface complexes with TiO₂. Both hydroxyl groups of DOPA were involved into this adsorption, via bidentate binding to two adjacent Ti⁴⁺ sites or monodentate to one Ti⁴⁺ site combining with H-bonds binding to terminal hydroxyl group on TiO₂. Lee et al. did similar work on adsorption of DOPA on rutile particles as a function of pH and surface coverage.¹⁰⁹ Their results are consistent with that reported earlier. In addition, the strong effect of pH and surface coverage on the adsorption was reported. At pH 6, hydroxyl groups of DOPA bind to rutile surface via bidentate mode (two points of attachment), whilst at pH 2, DOPA has three point of attachment to rutile surface: two from hydroxyl groups, and another from carbonate group. Other studies have been conducted with catechol (1,2-dihydroxybenzene) and dopamine (2-(3,4-Dihydroxyphenyl)ethylamine). These molecules with two hydroxyl groups on benzene ring resemble DOPA. Both catechol and dopamine formed chemical bonds with TiO₂ surface.^{49,110,111} Catechol formed surface complexes with Ti⁴⁺ sites on surface of TiO₂ via bidentate binding mode.^{110,111}



Terranova et al. studied charge – transfer mechanism between catechol and TiO₂ by density functional theory calculation.⁴⁹ They proposed four possibilities of binding modes for

catechol adsorbed on rutile (100). The binding modes are through covalent bonds or/and H-bonds. They suggested that monodentate mode is the most probable. Both experimental and theoretical studies converged that hydroxyl groups on benzene ring are responsible for this binding, although pKa values of catechol are 9.25 and 13¹¹² and pKa of carboxylic and amine function are respectively 2.3 and 8.7.

1.4.3.2 Ethylene glycol

Ethylene glycol (EG) is extensively used in synthesis of TiO₂ nanoparticles.¹¹³ In this process, EG easily coordinated to Ti⁴⁺ ions and controls the hydrolysis reaction.¹¹⁴ Eventually, morphologies and faces of TiO₂ nanoparticles can be tuned. EG is suggested to create surface complexes with Ti⁴⁺ on TiO₂ surface via bidentate binding mode.¹¹⁵

1.5 Phospholipids (PLs)

Lipids and proteins are the main components of all cellular membranes.¹¹⁶ 50% in mass of most animal cell membranes is composed of lipids, and almost the remaining are proteins.¹¹⁷ Lipids are very diverse, and whatever they are from eukaryotic, prokaryotic sources or are synthetic lipids, they are categorized in eight types according to their chemical structure, hydrophobic and hydrophilic properties: fatty acyls, glycerolipids, glycerophospholipids, sphingolipids, sterol lipids, prenol lipids, saccharolipids and polyketides.¹¹⁸

Phospholipids are amphiphilic molecules that self-assemble in two apposed layers, usually not symmetrical and called bilayer.¹¹⁶ Phospholipids rapidly rotate around their axis and exchange places with neighboring molecules (10⁷ times per second) within the layer.¹¹⁷ They rarely moved to the other leaflet (so-called flip-flop phenomenon). This helps to keep the membrane asymmetry, which is considered essential for the function of cell. The bilayer constitutes an impermeable barrier between the inner and the outer of the cell. The proteins, embedded in the membrane, ensure the ion exchange between the inner and the outer of the cell.

1.5.1 Structure of phospholipids

The structure of phospholipid molecule consists of two hydrophobic chains and a hydrophilic group also called polar head group. The hydrophobic chains and the polar head

group are linked together by a linker, either glycerol or sphingosine. Phospholipids are divided into two classes: glycerophospholipids with glycerol backbone and phosphosphingolipids with sphingosine rather than glycerol as backbone (figure 1.22). The number of phospholipid molecules is huge because of the variability of substituent and backbone structure, length and saturation of hydrocarbon tails.

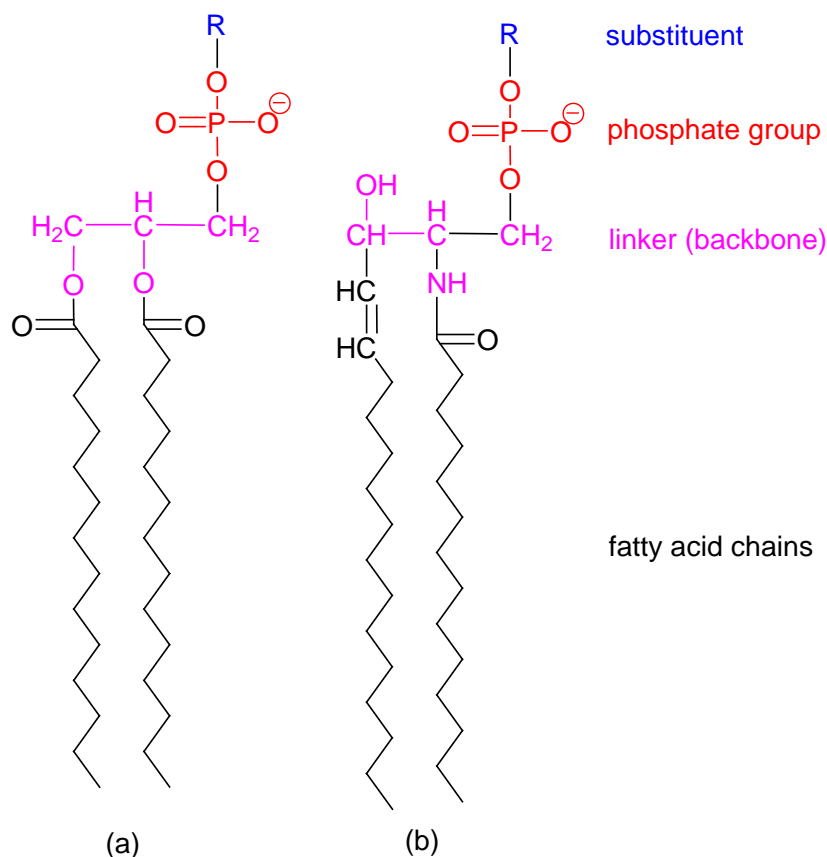


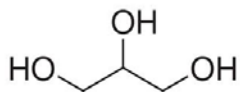
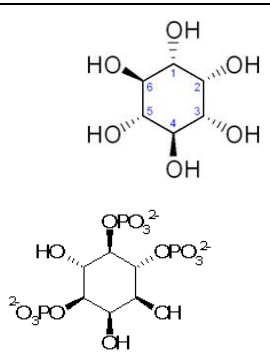
Figure 1.22. General structure of (a) glycerophospholipids (b) phosphosphingolipid. Fatty acid chains shown here are saturated, however they can be unsaturated. The substituents and linkers are listed in table 1.1

Glycerophospholipids are the most common in cell membranes.¹¹⁹ The glycerol backbone of these phospholipids is substituted by a phosphate group (that is usually branched with nitrogen derivatives) and two fatty acid chains (Table 1.1). The most common glycerophospholipids in membranes are respectively phosphatidylcholine (PC), phosphatidylethanolamine (PE) and phosphatidylserine (PS).¹¹⁷ In phosphatidylcholine, that is the key building block in all biological cell membrane found in animal and plant, the phosphate group is substituted by a quaternary amine ($-\text{CH}_2\text{CH}_2\text{N}(\text{CH}_3)_3$). In phosphatidylethanolamine, the phosphate group is substituted by an amine ($-\text{CH}_2\text{CH}_2\text{NH}_3$). The phosphatidylserine looks like a phosphatidylethanolamine substituted on the second

carbon atom by a carboxylic function. For all phospholipids, the length of hydrophobic chains usually varies between 12 and 22 carbon with unsaturation ranging from 0 to 6. The minor phospholipids are phosphatidylglycerol (PG) and cardiolipin (CL). They contain an additional glycerol group branched on phosphate. Moreover, CL possesses 4 hydrophobic chains and resembles two phosphatidylglycerols connected to a glycerol backbone. PG is normally found in pulmonary surfactant¹²⁰ while CL is found in membranes of inner mitochondria and gram-positive bacteria.^{119,121,122} Phosphatidic acid (PA) is the simplest glycerophospholipid (no substituent on the phosphate group) and less abundant in comparison with the others. It is a key intermediate in lipid metabolism and is a signaling molecule.¹²³ Phosphoinositol possesses an inositol group branched on the phosphate. In one, two or three positions of the inositol ring, phosphate groups can be found and are called phosphatidylinositol phosphates. They play an important role in lipid signaling, cell signaling and membrane trafficking since the inositol ring can be phosphorylated then dephosphorylated by enzymes.

Another important class of phospholipids is phosphosphingolipids. Sphingomyelins (SM) are the major phosphosphingolipids of mammalian tissues.^{117,118,124} For example, SM covers 10% lipid in myelin of human brain.¹²⁵

Table 1.1. Names, abbreviations and architectures of the main molecules belonging to the class of phospholipids, according to the nomenclature of biomedical community (LIPID MAPS Lipidomics Gateway) covering eukaryotic, prokaryotic sources and synthetic lipids (<http://www.lipidmaps.org/>).

Name	Linker	Substituents	Common abbreviations
Sphingomyelin	Sphingosine	$-O-CH_2-CH_2-NH_3^+$	SM
Glycerophosphocholine	Glycerol	$O-CH_2-CH_2-NH_3^+$	PC
Glycerophosphoethanolamine	Glycerol	$O-CH_2-CH_2-NH_3^+$	PE
Glycerophosphoserine	Glycerol	$O-CH_2-CHCOOH-NH_3^+$	PS
Glycerophosphoglycerols	Glycerol		PG
Diphosphoglycerols			CL
Glycerophosphoinositols and derivatives	Glycerol		PI PIP ₃
Glycerophosphate	Glycerol	O-H	PA

According to the length of the hydrocarbon chain (including carbonyl) and the head polar groups, the molecules are abbreviated with two first letters (Table 1.1) designing the length of the hydrocarbon chains and the last two for the head polar groups. In nature, the

number of carbon atoms is mainly an even number. A long time before IUPAC nomenclature, the length of the chains were designed as dilauroyl for 2 C12 chains, dimyristoyl for 2 C14, distearoyl for 2 C16 and so on. The common abbreviations take into account this tradition so that a phospholipid with 2 C14 chains and no substituent on the phosphate moiety will be abbreviated as DMPA. The above-presented phospholipids display two identical hydrocarbon chains. In fact, non-symmetrical phospholipids are most common in cells. Typically, the saturated fatty acids are found in the first position on the glycerol backbone and the highly unsaturated fatty acids in the middle.

1.5.2 Characteristics of phospholipids in aqueous medium

1.5.2.1 In bulk phase

Due to the length of the hydrophobic part, phospholipids are poorly soluble in water. For example, the solubility of the compound dimyristoyl phosphatidylcholine (DMPC) is 10^{-8} mol/L (<http://www.avantilipids.com/>). The heteropolar character of phospholipids confers on them an amphiphilic character that helps them to spontaneously self-assemble as bilayers in water. Bilayer is the most favorable arrangement of phospholipids in aqueous medium.¹¹⁷ The bilayer is constituted of two leaflets, in which the polar head groups interact with aqueous environment and the hydrocarbon tails point inwards. This organization is more favorable in terms of energy, and in fact is the most prevailing for diacyl phospholipids.^{126,127} With this structure, the head groups are hydrated and bind to water through H-bonds. The hydrocarbon chains do not have interactions with water and display interactions (van der Waals) between each other.

The assembly of phospholipids in water leads to the formation of several types of organization. At low concentrations, bilayers are in equilibrium with water. Planar bilayers exist but their formation is less favorable in terms of energy than spherical bilayers because of the interaction of hydrocarbon chains with water at edge positions. These spherical assemblies of bilayers are called vesicles or liposomes (Figure 1.23). They naturally consist of multiple bilayers with the same center (multilamellar vesicles). They can be transformed into unilamellar vesicles (each vesicle is formed by a single bilayer) by membrane extrusion and microfluidization methods.¹²⁸ The size of vesicles varies between 25 nm to 1 μ m, depending on the chain length, the head group size of phospholipids and the formation processes (up and down temperature cycling, ultrasound). At higher concentrations, bilayers remain planar for

each bilayer or in average, and form a more or less perfect stacking of bilayers that depends on temperature.

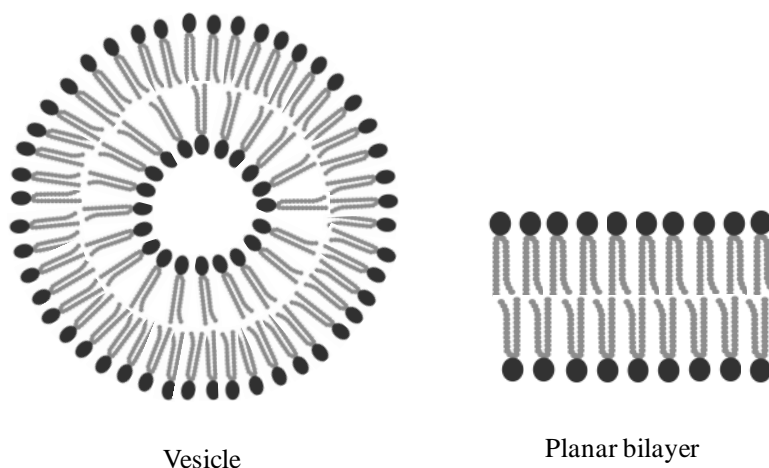


Figure 1.23. Bilayers formed by phospholipids.

At very low temperatures and in the hydrated state, phospholipids are fully crystallized and form lamellar crystals. When the temperature increases, the head polar group gains fluidity. The structure of lamellar crystal is characterized by equidistant bilayers which are parallel to each other and separated by water. Within each bilayer, the phospholipid chains are stiff, essentially fully extended (all-trans conformation), tilted or untilted and packed in a 2D array.¹²⁹ The tilting of chains results from the packing mismatch between the hydrocarbon chains and the large and strongly hydrated head groups. No in-plane diffraction arises from the head groups which are in a disordered state.¹³⁰ When approaching the melting temperature of phospholipids (T_m), the stiffness of the hydrocarbon chains is progressively lost, subsequently the long-order range within a bilayer is lost but the long-range order between bilayers is preserved, even if the bilayer may undulate (rippled phase or phase $P_{\beta'}$). Chains are in a liquid state and the phase is simply called a lamellar phase (Figure 1.24).

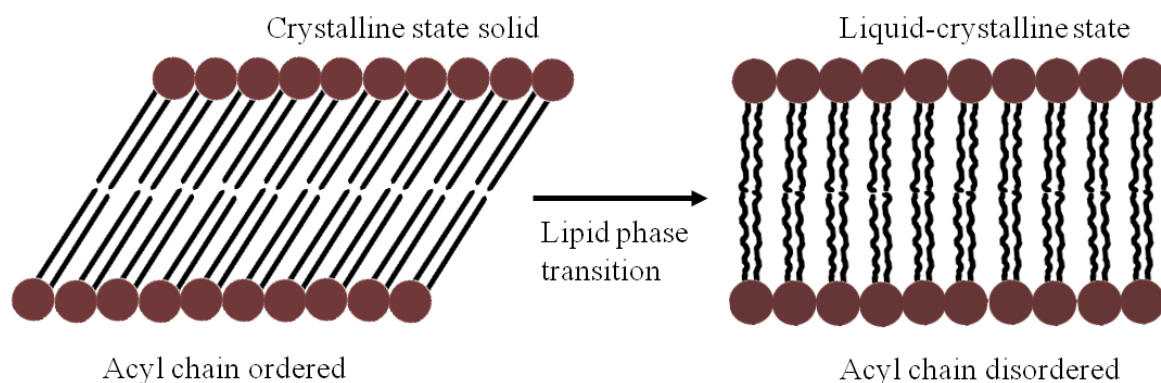


Figure 1.24. Lipid organization in two phases: the liquid crystalline phase and the lamellar phase (adapted from Cullis 1996)¹³¹. In the crystalline state, hydrocarbon chains are in gel state, more stretched, ordered and less flexible. In contrast, in liquid-crystalline state, hydrocarbon chains are disordered and exhibit greater translational diffusion.

The molecular structure of phospholipids strongly affects the phase transition temperature of bilayers. The temperatures are given in Table 1.2 for symmetrical phospholipids. Moreover, for a given phospholipid, the transition temperature may vary with pH and salt,¹³² or with the nature of the counterion if the data were obtained in the dry state.

Table 1.2. Phase transition temperature of lipids T_m (taken from the website of Avanti polar lipid). The abbreviations refer to the traditional classification.

Molecules	DMPA	DMPC	DMPE	DMPG	DMPS	DPPC	DSPC	DOPC	TMCL	SM
Number of carbon in acyl chain:unsaturation	14:0	14:0	14:0	14:0	14:0	16:0	18:0	18:1	14:0	16/18
Phase transition temperature (°C)	50	24	50	24*	35	41	55	-20	39	7

* at pH 7 otherwise 42 °C at pH 2.

As the chain length increases (from DMPC to DPPC and finally DSPC), the melting temperature increases from 24 to 55°C. Phospholipids with long hydrocarbon chains give stiffness in bilayers while phospholipids with shorter chain length contribute to the fluidity of

the bilayers. Phospholipids with more double bonds in hydrocarbon chain reinforce the fluidity of bilayer due to the effect of kinks, which limit the packing of hydrocarbon chains together (DOPC has for example a lower melting temperature than DSPC). Moreover, the location of the unsaturations along the hydrocarbon chain also impacts the melting temperature. Another point is that the nature of the headgroup has a remarkable effect on the transition temperature. For example, in the series with 14 carbon atoms (14:0), the melting temperature varies between 23°C for the phosphatidylglycerol and 50°C for the phosphatidylethanolamine. Due to the high tendency of phospholipids to self-assemble, it is difficult to define a value of pKa in bulk. In fact, the pKa at the bilayer-water interface is better defined. It differs from the intrinsic value by the contribution of the surface polarity and the electrostatic enhancement of the surface H⁺ concentration.¹³² It increases roughly by two units toward higher values for carboxylic and amine functions.

Acyl chains and head groups strongly affect the organization of vesicles.¹²⁸ The lateral interaction between acyl chains and head groups are determining factors. Particularly, the surface charges of head groups, which exhibit lateral repulsion, significantly interact with surrounding aqueous medium. Charges at vesicles surface are dependent on protonation/deprotonation of phospholipid head groups in aqueous solution (Figure 1.25).

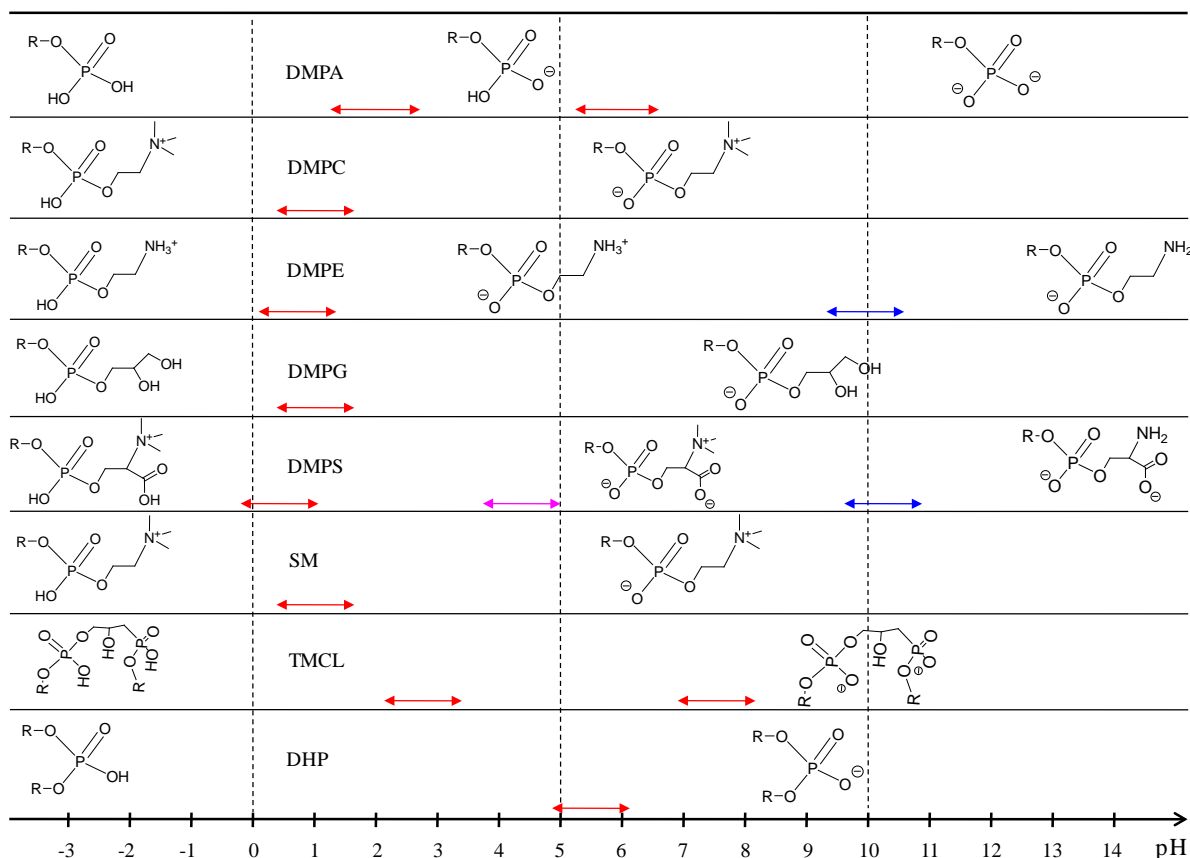


Figure 1.25. Ionization state of phospholipids in aqueous medium. The left right arrow represents the pK_a value of corresponding groups: phosphate (red), amine (blue) and carboxyl (magenta). The dash vertical line is used to facilitate the coordination reading only. The figure was adapted from Tocanne 1989¹³³ and CRC handbook of bilayer (page 81-82)¹³². pK_a of SM was assumed as that of dimyristoylphosphatidylcholine (DMPC) because they bear the same head group. pK_a of TMCL was taken from Mattsson 2012¹³⁴. pK_a of dihexadexyl phosphate (DHP) was taken from Carmena-Ribeiro1990¹³⁵.

Zeta potential measurement is a convenient method to characterize electrostatic properties of vesicles. This measurement not only serves as a basic understanding for biological membrane, but also for the technical application of liposome.¹²⁵ Zeta potential values of phospholipid vesicles are affected by pH and ionic strength. An electrical double layer is formed at the interface vesicles – aqueous medium. In fact, the charges carried on phospholipids head groups can be considered as the inner Helmholtz layer. The counter-ions such as cations and anions, which are present in the aqueous medium, accumulate at the interface and generate Stern layer and diffuse layer.¹³⁶ The thicknesses of these layers are considerably influenced by ionic strength and temperature of surrounding environment. The barrier between diffuse layer and surrounding aqueous medium is termed shear plane, where zeta potential is commonly measured by electrophoretic mobility method.¹³⁶ For example, in a

solution of phosphocholine-containing vesicles, the increasing concentration of KCl and CaCl₂ increases zeta potential values of vesicles from negative values to zero for KCl and to positive values for CaCl₂.¹³⁷ KCl leads only to ionic strength modification, which does not provoke sign change of zeta potential. In contrast, Ca²⁺ ions bind to the head groups of phospholipids in vesicles. This results in the sign change of zeta potential.

1.5.3 Characteristics of phospholipids at the air-water interface

Biological membranes are very complex in structure, composition and behavior. For simplicity, scientists use models to study membranes. The monolayer of phospholipids at the air-water interface is one of them (Figure 1.26).¹³⁸ It constitutes only one layer of the membrane but helps in characterizing the interactions of one sheet with its environment and other molecules¹³⁹ such as proteins^{140,141} and cholesterol^{142,143}.

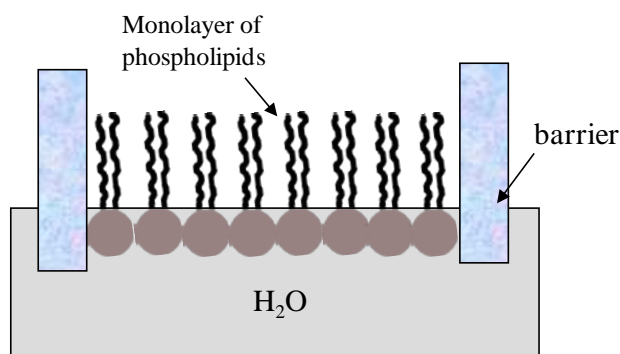


Figure 1.26. Monolayer of phospholipids at the air-water interface compressed between two barriers.

According to the nature of the head polar group, phospholipids can spontaneously form a film at the air-water interface.¹⁴⁴ It is also possible to control the formation of the monomolecular film by spreading a volatile organic solution of the phospholipid on a Langmuir trough. The latter is composed of a rectangular trough controlled in temperature and usually made of Teflon® to prevent any leakage of the subphase over the edges. It is equipped with two movable barriers that can glide on it and a pressure captor that measures the surface tension. The trough is filled with an aqueous solution (water with or without salts, proteins and so on), which is called subphase. On the surface and between the barriers, which determine a surface area, a defined volume of an organic solution of the phospholipid at a known concentration is spread drop by drop to form a monomolecular film. The choice of the

solvent is important as it must solubilize the organic molecule, spread on water and easily evaporate. This helps in stabilizing a monolayer film of molecules.

The surface area of the trough can be varied by sweeping symmetrically the movable barriers over the surface of the subphase. The surface pressure and the molecular area are continuously monitored during the compression. The curve showing the surface pressure as a function of the molecular area is called surface pressure-area isotherm or π -A isotherm of compression.

1.5.3.1 The general phase behavior of lipids at the air-water interface

A typical π -A isotherm of compression is depicted in Figure 1.27.

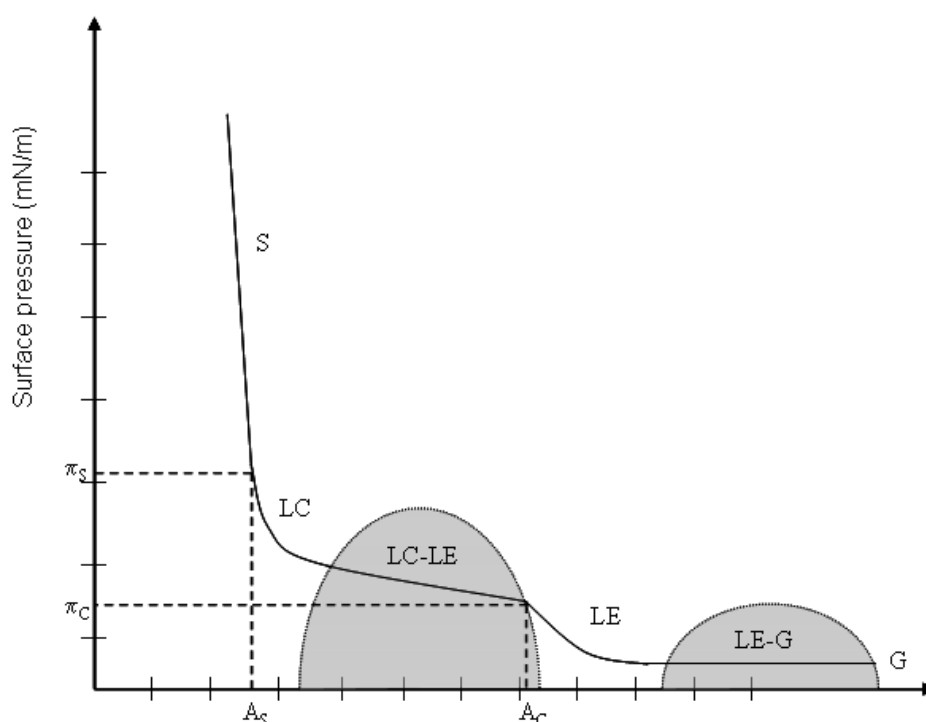


Figure 1.27. Typical surface pressure-area isotherm of phospholipid monolayer resulting from Langmuir trough. S represents solid-like region, LC liquid-condensed region, LE liquid-expanded region; LC-LE & LE-G represent the coexistence regions; G represents the gaseous region; π_S & A_S are the surface pressure and the molecular area at the transition point between LC & S; π_C & A_C are the critical surface pressure and molecular area between LE & LC-LE. (Adapted from Mohwald 1995)¹⁴⁵

The increase of the surface pressure is not monotonous versus the molecular area. The different slopes are interpreted in terms of phase transitions and phase states. At high molecular area (around 150 \AA^2 to 100 \AA^2 , depending on the nature of molecules), molecules

are far from each other, do not interact between them and arrange arbitrarily at the interface, even parallel to the surface. The surface pressure remains almost close to zero. This state is called gaseous (noted G in Figure 1.27). Monolayer in the gaseous state possesses high compressibility in comparison with that in typical liquids and bilayers. By compressing the monolayer, the area available for each molecule decreases. The state of the monolayer transforms progressively from the gaseous phase (G) to the liquid expanded phase (LE) via a phase co-existence. In the LE phase, there are more contacts among headgroups of molecules, whereas the hydrocarbon chains are still far from each other and organize arbitrarily. This phase transition is rarely observed as the change in pressure is usually less than 1 mN/m. In the liquid expanded phase, the compressibility of monolayer is still high. Upon compressing further the monolayer, the surface pressure starts to increase. At the critical area A_C , the hydrocarbon chains enter in contact not very tightly and organize in a long-range order with hydrocarbon chains still tilted from vertical direction (roughly 30°). First, they form some condensed domains developed in the liquid phase (co-existence liquid expanded/liquid condensed phases). As long as there are molecules in the liquid expanded phase, the surface pressure increases hardly. These domains are usually evidenced by grazing incidence X-ray diffraction¹⁴⁶ or by Brewster angle optical microscopy. The surface is fully covered by the condensed domains (liquid condensed phase) when the surface pressure increases again noticeably. Upon compressing further, molecules are less and less tilted. At the critical area A_C , molecules are arranged vertically to the surface (solid phase) and strong interactions exist on one hand between the headgroups, and on the other hand between the hydrocarbon chains. Molecules can hardly be compressed and the surface pressure increases greatly. In fact, the compressibility of monolayer in solid region is 3 times smaller than that of LC region.¹⁴⁵ In this state, if the compression is continued, the monolayer collapses. All along this phase behavior, level of hydration decreases from G phase to S phase because water is squeezed out of the monolayer (see Figure 1.24). However, it is unlikely to remove all water molecules from the monolayer due to the strong binding of water to headgroups. Water interacts with carbonyl groups and especially strongly with phosphate groups.¹⁴⁷

1.5.3.2 Factors affecting the polymorphism of lipids at the air-water interface

The nature of phospholipid molecules (headgroup, chain length, unsaturation, mixtures of phospholipids...) and environment conditions (temperature, pH, ionic strength, and presence of other substances...) significantly influence the phase transitions of monolayers.¹⁴⁸

The transition mechanism is primarily driven by the ordering of hydrocarbon chains and the interaction among headgroup moieties.

For example, dimyristoylphosphatidylcholine, dipalmitoylphosphatidylcholine and distearoylphosphatidylcholine compounds, which differ in the length of the saturated chain, exhibit respectively only a liquid expanded phase, a succession of LE, LE-LC, LC phases, and only a liquid condensed phase.¹⁴⁹ The increase in chain length enhances van der Waals forces between the hydrocarbon chains and favors the condensation of the chains.

The presence of ions in the subphase affects the hydration of headgroups and reduces the repulsive forces between headgroups due to electrostatic screening. Divalent cations such as Mg^{2+} and Ca^{2+} have stronger impact than monovalent ions by binding headgroups together. Ca^{2+} is considered to bind to phosphate headgroup stronger than Na^+ and Cl^- , which are excluded from headgroup regions, especially from phosphate groups. Estimated binding constant of Ca^{2+} to phosphate group is 12 – 37, two times higher than that of Na^+ (0.16 – 0.61).¹⁴⁷

As we see, the monolayer is very sensitive to the nature of molecules and the environmental condition. The two dimensional structure of the monolayer is easily controlled by either changing the composition and molecular area, or the condition of the environment (pH, ionic strength).¹⁵⁰ The ease of tailoring its properties renders monolayer popular for scientific studies.

1.5.3.3 Investigating structure and dynamics of monolayer at the air-water interface

In addition to surface tension measurements, several techniques were developed in the last 30 years to characterize either the structural or dynamical properties of monolayers. They include vibrational spectroscopy, neutron scattering, X-ray diffraction, fluorescence microscopy and many others reviewed by Pichot,¹⁵¹ Mohwald¹⁴⁵ and Dynarowics-Latka¹⁵². For example, the analysis by fluorescence microscopy technique of the lateral distribution of probe dye molecules, which were incorporated into the monolayer, confirmed the coexistence of phases in the monolayer.^{145,153} This result was later approved by newer instruments: Brewster angle microscopy and imaging ellipsometry. Fluorescence technique also provides a way to investigate the dynamics of phospholipid molecules in the monolayer. Fluorescence recovery after photobleaching is able to determine the diffusion coefficient of phospholipids molecules in different crystalline phases, such as of 10^{-8} cm²/sec in liquid-expanded and

below 10^{-10} cm²/sec in liquid condensed phase.¹⁴⁵ This technique has been proved to be very useful because one can probe the diffusion of molecules while modifying molecular area and compressibility of the monolayer.

Some structural parameters like layer thickness, refractive index, lattices can be determined by ellipsometry, X-ray diffraction and X-ray reflectivity. Particularly, X-ray diffraction is very powerful to unravel the arrangement of aliphatic hydrocarbon chains of phospholipids in the monolayer as a function of lateral pressure. It helps to determine the tilt of chains and the lattices in condensed phases like oblique, rectangular or hexagonal lattice.¹⁴⁵ X-ray reflection data also bring information about the thickness of the film through the electron density profiles in the head groups region of phospholipids molecules at air-water interface.

Vibrational spectroscopy like infrared reflection-absorption spectroscopy or sum-frequency generation (SFG) vibrational spectroscopy are used to study structural information of phospholipids layer on air-water interface, in particular via the frequency and intensity of methylene groups vibrations on hydrocarbon chains of phospholipids. It allowed concluding that phase transitions of monolayer are linked to the ordering of hydrocarbon chains.¹⁴⁵

1.6 Literature review on TiO₂-phospholipids interactions

The separation and purification of phosphorylated biomolecules, in particular phospholipids by using TiO₂ micro-column chromatography¹⁰⁴⁻¹⁰⁶ was suggested to be related to the strong interaction between TiO₂ surface and phosphates. However, the results raise several questions. First, the phospholipids identified are only phosphatidylcholine, phosphatidylethanolamine and sphingomyelin whereas the composition of phospholipids in milk is much richer. It includes phosphatidylinositol and phosphatidylserine. It is true that they are less present in milk than the above cited phospholipids but the absence of even any trace in the MS spectra is surprising. Second, the numerous studies on interactions between phosphate and TiO₂ surfaces proved that the bonding was covalent in a large pH range. If phospholipids formed covalent bonds, they would not be released from the column. This raises the question about the interactions between phospholipids and TiO₂. There are not many experimental or theoretical studies related to this question. Although their motivations are fully out the scope of this thesis^{39,154-159} (these studies are mainly relevant to biosensors,

biomaterial applications^{160–164} and suspension stabilization¹⁶⁵), they give some clues about the interactions of phospholipids with TiO₂. They are presented and discussed in this section.

1.6.1 TiO₂-supported phospholipid bilayers

Phospholipids were deposited on TiO₂ surfaces as supported phospholipid bilayers (SPB) through two main routes, by sequential Langmuir-Blodgett deposition of lipid monolayers on a hydrophilic substrate or by fusion of phospholipid vesicles on the substrate (Figure 1.28).¹⁶⁶ The formation of SPB was analyzed as a function of an environmental factor (pH, ionic strength, surface charge . . .) by using different techniques, mainly quartz crystal microbalance dissipation (QCM-D) and atomic force microscope (AFM).^{159,166} Contrary to silica surface, there is no phospholipid vesicle fusion on the surface of TiO₂.¹⁶⁷ The reason behind might come from the different strengths in the interaction between vesicles and surfaces, including related to surface chemistry and surface polarizability.^{168,169}

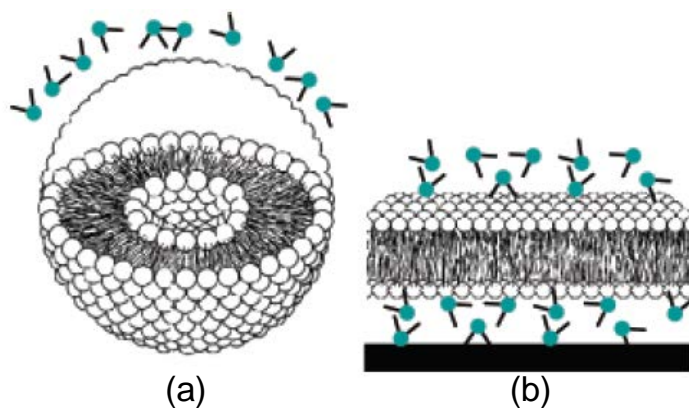


Figure 1.28. Phospholipid vesicle (a) and supported phospholipids bilayer on substrate (b). Adapted from Reimhult 2003¹⁵⁵

1.6.2 Role of divalent cations

The presence of divalent cations such as Ca²⁺ and Mg²⁺ in the environment usually helps to rupture vesicles on the surface of TiO₂ and to wrap it by a bilayer.^{39,170,171} A similar phenomenon was observed with both Ca²⁺ and Mg²⁺ on mica¹⁷² and gold.¹⁷⁰ Only the study of Reviakine et al. reported that calcium cations failed to induce the formation of bilayer.¹⁷³ The mechanism of Ca²⁺-induced phospholipid supported bilayer is still obscure. Reviakine suggested that Ca²⁺ modifies the bending moduli of vesicle bilayers and enhance the fusion. Likewise, Oleson suggested that divalent cations bridge the substrates with vesicles and promote the adsorption.¹⁵⁶

1.6.3 Chemisorption or physisorption?

In this context, molecular dynamic simulation was employed to clarify the adsorption of phospholipids on TiO₂ (110) surface.¹⁷⁴ This study took many parameters into account including hydration state of oxide surface, temperature, pH and ionic strength. The authors predicted that bidentate or monodentate binding mode exists between oxygen-containing moieties (phosphate group and/or carboxyl group) and titanium sites available on the surface of TiO₂. The attachment of those moieties to the surface was not only affected by the environment conditions but also by the nature of phospholipid head groups and substrate surface. This result was experimentally confirmed by the results of Kang et al. that proved by ³¹P NMR the formation of bidentate or monodentate binding mode.⁹⁶ However, several authors confirmed the presence of interfacial water layer thickness of 0.4-1.5 nm between SPB and the solid substrate surface.^{167,171} According to them, chemical bonds between SPB and substrate surface are precluded and hydroxyl groups on the surface of substrates form H-bonds with water and maintain the layer of water.

1.6.4 Role of the surface characteristics

Regarding the nature of TiO₂ (crystallinity, surface charge and so on), the majority of them was not specified, and surface properties were not fully characterized.^{39,163,168,169,173,175} A small change in dimension, or composition of materials can lead to a different reactivity, therefore the materials of interest (TiO₂) should be well characterized for size, crystallinity, chemical composition, surface charge, surface chemistry, purity, swarming, surface area etc.¹⁷⁶

1.6.5 Nature of the head polar group

Although phospholipids are very diverse in structure with various kinds of headgroups, resulting in different properties, glycerophosphatidylcholine was the main phospholipid investigated in studies dealing with interactions between phospholipids and TiO₂. A few of them introduced glycerophosphatidylserine that interestingly helps in forming a phospholipid bilayer on TiO₂ substrate, similarly as on SiO₂ substrate.¹⁷⁵

1.7 Gaps of knowledge and objective of the thesis

Regardless of the extensive effort of scientists to understand the vesicles-substrates interaction, there are open questions regarding the interactions between TiO_2 and phospholipids:

(1) nature of surface

The nature of studied surfaces was not considered until now whereas they differ by the nature of surface functional groups, surface charge, surface polarizability, surface defects and crystallinity. The characteristics of TiO_2 are dependent on crystallinity, faces and defective sites.^{40,177} However, the poor characterization of substrates hampered to relate the whole observations.

(2) nature of phospholipids

The different studies never consider phospholipids other than phosphatidylcholine or a mixture with phosphatidylserine or phosphatidylglycerol. Only Monti's group¹⁷⁴ addressed phosphatidylserine alone by molecular dynamic simulation. The whole class of phospholipids was not fully investigated whereas (i) their different head groups may hinder or facilitate the approach of molecules to the surface by different charge or functional groups, (ii) only some phospholipids from milk were separated on a TiO_2 column chromatography.

(3) Nature of binding

The interactions between phospholipids and TiO_2 surface was often explained according to the interaction between phosphate and TiO_2 . Moreover, all studies are not in agreement as regards the nature of forces involved (van der Waals and/or electrostatics, hydration forces, covalent bonds, H-bonds).

It appears obvious that many questions are still open. Does the nature of TiO_2 surface play a role? Is there any difference between rutile and anatase surfaces? Are the substituents on phosphate important for the interactions between PL and TiO_2 ?

The present study attempts to answer those questions to some extent. Several phospholipids with different head group structures were investigated. The use of a popular sample of TiO_2 (P25 particles) was a first step towards understanding phospholipid adsorption. Then two main crystalline varieties of TiO_2 (anatase and rutile) were employed

for the study taking care of their characterization. The contradictory results about the involved forces make necessary to clarify the problem by alternative approaches, like vibrational spectroscopy. The combination of four techniques (Langmuir film, laser Doppler velocimetry, infrared spectroscopy and ^{31}P NMR spectroscopy) is considered to investigate the nature of the interaction between phospholipids and TiO_2 surfaces.

References

1. Brown, G. E. *et al.* Metal Oxide Surfaces and Their Interactions with Aqueous Solutions and Microbial Organisms. *Chem. Rev.* **99**, 77–174 (1999).
2. Atkins, P. & Paula, J. de. *Physical Chemistry*. (Oxford university Press, 2008).
3. Woodruff, D. P. & Delchar, T. A. *Modern Techniques of Surface Science*. (Cambridge University Press, 1994).
4. Henderson, M. A. The interaction of water with solid surfaces: fundamental aspects revisited. *Surf. Sci. Rep.* **46**, 1–308 (2002).
5. Thiel, P. A. & Madey, T. E. The interaction of water with solid surfaces: fundamental aspects. *Surf. Sci. Rep.* **7**, 211–385 (1987).
6. Diebold, U. The surface science of titanium dioxide. *Surf. Sci. Rep.* **48**, 53–229 (2003).
7. Tero, R., Ujihara, T. & Urisu, T. Lipid bilayer membrane with atomic step structure: supported bilayer on a step-and-terrace TiO₂(100) surface. *Langmuir* **24**, 11567–76 (2008).
8. Gun'ko, V. M., Zarko, V. I., Leboda, R. & Chibowski, E. Aqueous suspension of fumed oxides: particle size distribution and zeta potential. *Adv. Colloid Interface Sci.* **91**, 1–112 (2001).
9. Noh, J. S. & Schwarz, J. a. Estimation of the point of zero charge of simple oxides by mass titration. *J. Colloid Interface Sci.* **130**, 157–164 (1989).
10. Parks, G. The isoelectric points of solid oxides, solid hydroxides, and aqueous hydroxo complex systems. *Chem. Rev.* **65**, 177–198 (1965).
11. Kosmulski, M. pH-dependent surface charging and points of zero charge. III. Update. *J. Colloid Interface Sci.* **298**, 730–41 (2006).
12. Jolivet, J.-P., Henry, M. & Livage, J. *Metal Oxide Chemistry and Synthesis*. 213 (John Wiley & Sons, LTD).
13. Kosmulski, M. pH-dependent surface charging and points of zero charge. IV. Update and new approach. *J. Colloid Interface Sci.* **337**, 439–48 (2009).
14. Kosmulski, M. The pH-dependent surface charging and points of zero charge: V. Update. *J. Colloid Interface Sci.* **353**, 1–15 (2011).
15. Yoon, R. H., Salman, T. & Donnay, G. Predicting points of zero charge of oxides and hydroxides. *J. Colloid Interface Sci.* **70**, 483–493 (1979).

16. Venema, P., Hiemstra, T., Weidler, P. G. & Riemsdijk, W. H. Van. Intrinsic Proton Affinity of Reactive Surface Groups of Metal (Hydr) oxides: Application to Iron (Hydr) oxides. *J. Colloid Interface Sci.* **295**, 282–295 (1998).
17. Barteau, M. A. Organic Reactions at Well-Defined Oxide Surfaces II. What Is Different Between Metals and. *Chem. Rev.* **96**, 1413–1430 (1996).
18. Batzill, M. & Diebold, U. The surface and materials science of tin oxide. *Prog. Surf. Sci.* **79**, 47–154 (2005).
19. Woll, C. The chemistry and physics of zinc oxide surfaces. *Prog. Surf. Sci.* **82**, 55–120 (2007).
20. Fenoglio, I., Fubini, B., Ghibaudi, E. M. & Turci, F. Multiple aspects of the interaction of biomacromolecules with inorganic surfaces. *Adv. Drug Deliv. Rev.* **63**, 1186–209 (2011).
21. Liufu, S.-C., Xiao, H.-N. & Li, Y.-P. Effect of MA-Na copolymer adsorption on the colloidal stability of nano-sized ZnO suspension. *Mater. Lett.* **59**, 3494–3497 (2005).
22. Hanaor, D. A. H., Michelazzi, M., Leonelli, C. & Sorrell, C. C. The Effects of Carboxylic Acids on the Aqueous Dispersion and Electrophoretic Deposition of ZrO₂. **32**, 235–244 (2012).
23. Venkatesha, T. G., Nayaka, Y. A. & Chethana, B. K. Adsorption of Ponceau S from aqueous solution by MgO nanoparticles. *Appl. Surf. Sci.* **276**, 620–627 (2013).
24. Diebold, U., Li, S.-C. & Schmid, M. Oxide surface science. *Annu. Rev. Phys. Chem.* **61**, 129–48 (2010).
25. Tao, J. & Batzill, M. *Metal Oxide Nanomaterials for Chemical Sensors*. 35–68 (Springer New York, 2013). doi:10.1007/978-1-4614-5395-6
26. Pászti, Z., Keszthelyi, T., Hakkel, O. & Guzzi, L. Adsorption of amino acids on hydrophilic surfaces. *J. Phys. Condens. Matter* **20**, 224014 (2008).
27. An, K., Alayoglu, S., Ewers, T. & Somorjai, G. A. Colloid chemistry of nanocatalysts: a molecular view. *J. Colloid Interface Sci.* **373**, 1–13 (2012).
28. Creecy, C. M., Puleo, D. A. & Bizios, R. Biological Interactions on Materials Surfaces. 343–353 (2009). doi:10.1007/978-0-387-98161-1
29. Sugimoto, T. & Wang, Y. Mechanism of the Shape and Structure Control of Monodispersed alpha-Fe₂O₃ Particles by Sulfate Ions. *J. Colloid Interface Sci.* **207**, 137–149 (1998).
30. Nicholas, N. J., Franks, G. V & Ducker, W. a. Selective adsorption to particular crystal faces of ZnO. *Langmuir* **28**, 7189–96 (2012).

31. Paria, S. & Khilar, K. C. A review on experimental studies of surfactant adsorption at the hydrophilic solid-water interface. *Adv. Colloid Interface Sci.* **110**, 75–95 (2004).
32. Cesarano III, J., Aksay, I. A., Bleier, A. Stability of aqueous alpha-Al₂O₃ suspensions with poly(methacrylic acid) Polyelectrolyte. **55**, 250–255 (1988).
33. Fritz, G., Scha, V., Willenbacher, N. & Wagner, N. J. Electrosteric Stabilization of Colloidal Dispersions. *Langmuir* **18**, 6381–6390 (2002).
34. Wang, Y. & Zhitomirsky, I. Bio-inspired catechol chemistry for electrophoretic nanotechnology of oxide films. *J. Colloid Interface Sci.* **380**, 8–15 (2012).
35. Persson, P., Nilsson, N. & Sjöberg, S. Structure and Bonding of Orthophosphate Ions at the Iron Oxide-Aqueous Interface. *J. Colloid Interface Sci.* **177**, 263–275 (1996).
36. Kwon, K. D. & Kubicki, J. D. Molecular orbital theory study on surface complex structures of phosphates to iron hydroxides: calculation of vibrational frequencies and adsorption energies. *Langmuir* **20**, 9249–54 (2004).
37. Jeon, S. J., Sperline, P. R., Raghavan, S., Hiskey, B. J. In situ analysis of alkyl phosphate surfactant adsorption at the alumina/aqueous solution interface. *Colloids Surfaces A Physicochem. Eng. Asp.* **111**, 29–38 (1996).
38. Hiemstra, T., Venema, P. & Riemsdijk, W. Intrinsic Proton Affinity of Reactive Surface Groups of Metal (Hydr)oxides: The Bond Valence Principle. *J. Colloid Interface Sci.* **184**, 680–92 (1996).
39. Rossetti, F. F., Bally, M., Michel, R., Textor, M. & Reviakine, I. Interactions between titanium dioxide and phosphatidyl serine-containing liposomes: Formation and patterning of supported phospholipid bilayers on the surface of a medically relevant material. *Langmuir* **21**, 6443–6450 (2005).
40. Diebold, U. The surface science of titanium dioxide. *Surf. Sci. Rep.* **48**, 53–229 (2003).
41. Fujishima, A., Zhang, X. & Tryk, D. TiO₂ photocatalysis and related surface phenomena. *Surf. Sci. Rep.* **63**, 515–582 (2008).
42. Henderson, M. A. A surface science perspective on TiO₂ photocatalysis. *Surf. Sci. Rep.* **66**, 185–297 (2011).
43. Ruzycski, N., Herman, G. S., Boatner, L. a. & Diebold, U. Scanning tunneling microscopy study of the anatase (100) surface. *Surf. Sci.* **529**, L239–L244 (2003).
44. Reyes-Coronado, D. *et al.* Phase-pure TiO₂ nanoparticles: anatase, brookite and rutile. *Nanotechnology* **19**, 145605 (2008).
45. Rousseau, N. Identification et modélisation de complexes du titane dans des sols gels photosensibles. Université de Nantes, 40 (2013).

46. Baraton, M. Nano-TiO₂ for Solar Cells and Photocatalytic Water Splitting: Scientific and Technological Challenges for Commercialization. *Open Nanosci. J.* **5**, 64–77 (2011).
47. Hengerer, R., Bolliger, B., Erbudak, M. & Gra, M. Structure and stability of the anatase TiO₂ (101) and (001) surfaces. **460**, 162–169 (2000).
48. Barnard, A. S. & Curtiss, L. A. Prediction of TiO₂ nanoparticle phase and shape transitions controlled by surface chemistry. *Nano Lett.* **5**, 1261–6 (2005).
49. Terranova, U. & Bowler, D. R. Adsorption of Catechol on TiO₂ Rutile (100): A Density Functional Theory Investigation. *J. Phys. Chem. C* 6491–6495 (2010).
50. Barnard, A. S., Zapol, P. & Curtiss, L. A. Anatase and rutile surfaces with adsorbates representative of acidic and basic conditions. *Surf. Sci.* **582**, 173–188 (2005).
51. Tian, F. H. *et al.* Adsorption of 2-propanol on anatase TiO₂ (101) and (001) surfaces: A density functional theory study. *Surf. Sci.* **616**, 76–84 (2013).
52. Yang, H. G. *et al.* Anatase TiO₂ single crystals with a large percentage of reactive facets. *Nat. Lett.* **453**, 638–641 (2008).
53. Dozzi, M. & Selli, E. Specific Facets-Dominated Anatase TiO₂: Fluorine-Mediated Synthesis and Photoactivity. *Catalysts* **3**, 455–485 (2013).
54. Henderson, M. A. The interaction of water with solid surfaces: fundamental aspects revisited. *Surf. Sci. Rep.* **46**, 1–308 (2002).
55. Esch, T. R., Gadaczek, I. & Bredow, T. Surface structures and thermodynamics of low-index of rutile, brookite and anatase – A comparative DFT study. *Appl. Surf. Sci.* **288**, 275–287 (2014).
56. Henderson, M. A. Structural Sensitivity in the Dissociation of Water on TiO₂ Single-Crystal Surfaces. *Langmuir* **7463**, 5093–5098 (1996).
57. Lun Pang, C., Lindsay, R. & Thornton, G. Chemical reactions on rutile TiO₂ (110). *Chem. Soc. Rev.* **37**, 2328–53 (2008).
58. Vittadini, A., Selloni, A., Rotzinger, F. P. & Grätzel, M. Structure and Energetics of Water Adsorbed at TiO₂ Anatase (101) Surfaces. *Phys. Rev. Lett.* **81**, 1–4 (1998).
59. Yates, J. T. J. Chemisorption on surfaces — an historical look at a representative adsorbate: carbon monoxide. *Surf. Sci.* **299-300**, 731–741 (1994).
60. Mino, L., Spoto, G., Bordiga, S. & Zecchina, A. Particles Morphology and Surface Properties As Investigated by HRTEM, FTIR, and Periodic DFT Calculations: From Pyrogenic TiO₂ (P25) to Nanoanatase. *J. Phys. Chem. C* **116**, 17008–17018 (2012).

61. Holm, M. S. *et al.* Assessing the acid properties of desilicated ZSM-5 by FTIR using CO and 2,4,6-trimethylpyridine (collidine) as molecular probes. *Appl. Catal. A Gen.* **356**, 23–30 (2009).
62. Coluccia, S., Marchese, L. & Martra, G. Characterisation of microporous and mesoporous materials by the adsorption of molecular probes: FTIR and UV–Vis studies. *Microporous Mesoporous Mater.* **30**, 43–56 (1999).
63. Linsebigler, A. L., Lu, G. & Yates, J. T. Photocatalysis on TiO₂ Surfaces: Principles, Mechanisms, and Selected Results. *Chem. Rev.* **95**, 735–758 (1995).
64. Sorescu, D. C. & Yates, J. T. Adsorption of CO on the TiO₂ (110) Surface: A Theoretical Study. *J. Phys. Chem. B* **2**, 4556–4565 (1998).
65. Spoto, G., Morterra, C., Marchese, L., Orio, L. & Zecchina, A. The morphology of TiO₂ microcrystal and their adsorptive properties towards CO: A HRTEM and FTIR study. *Vacuum* **41**, 39–41 (1990).
66. Martra, G. Lewis acid and base sites at the surface of microcrystalline TiO₂ anatase: relationships between surface morphology and chemical behaviour. *Appl. Catal. A Gen.* **200**, 275–285 (2000).
67. Freund, H. & Roberts, M. W. Surface chemistry of carbon dioxide. *Surf. Sci. Rep.* **25**, 225–273 (1996).
68. Henderson, M. A. Evidence for bicarbonate formation on vacuum annealed TiO₂ (110) resulting from a precursor-mediated interaction. *Surf. Sci.* **400**, 203–219 (1998).
69. Henderson, M. A., Epling, W. S., Perkins, C. L., Peden, C. H. F. & Diebold, U. Interaction of Molecular Oxygen with the Vacuum-Annealed TiO₂ (110) Surface: Molecular and Dissociative Channels. *J. Phys. Chem. B* **2**, 5328–5337 (1999).
70. Henderson, M. A., Epling, W. S., Peden, C. H. F. & Perkins, C. L. Insights into Photoexcited Electron Scavenging Processes on TiO₂ Obtained from Studies of the Reaction of O₂ with OH Groups Adsorbed at Electronic Defects on TiO₂ (110). *J. Phys. Chem. B* **2**, 534–545 (2003).
71. Wendt, S. *et al.* Oxygen vacancies on TiO₂ (110) and their interaction with H₂O and O₂: A combined high-resolution STM and DFT study. *Surf. Sci.* **598**, 226–245 (2005).
72. Diebold, U. *et al.* Intrinsic defects on a TiO₂ (110) (1 × 1) surface and their reaction with oxygen: a scanning tunneling microscopy study. *Surf. Sci.* **411**, 137–153 (1998).
73. Epling, W. S., Peden, C. H. F., Henderson, M. A. & Diebold, U. Evidence for oxygen adatoms on TiO₂ (110) resulting from O dissociation at vacancy sites. *Surf. Sci.* **413**, 333–343 (1998).
74. Thomas, A. G. & Syres, K. L. Adsorption of organic molecules on rutile TiO₂ and anatase TiO₂ single crystal surfaces. *Chem. Soc. Rev.* **41**, 4207–17 (2012).

75. Vittadini, A., Selloni, A., Rotzinger, F. P. & Gra, M. Formic Acid Adsorption on Dry and Hydrated TiO₂ Anatase (101) Surfaces by DFT Calculations. *J. Phys. Chem. B* **104**, 1300–1306 (2000).
76. Martinez, U., Vilhelmsen, L. B., Kristoffersen, H. H., Stausholm-møller, J. & Hammer, B. Steps on Rutile TiO₂ (110): Active Sites for Water and Methanol Dissociation. *Phys. Rev. B* **84**, 1–6 (2011).
77. León, C. P., Sagisaka, K., Fujita, D. & Han, L. Ethanol adsorption on rutile TiO₂ (110). *RSC Adv.* **4**, 8550 (2014).
78. Shi, H., Magaye, R., Castranova, V. & Zhao, J. Titanium dioxide nanoparticles: a review of current toxicological data. *Part. Fibre Toxicol.* **10**, 15 (2013).
79. Hansen, J. Ø. *et al.* Direct Evidence for Ethanol Dissociation on Rutile TiO₂ (110). *Phys. Rev. Lett.* **107**, 136102 (2011).
80. Farfan-Arribas, E. & Madix, R. J. Different binding sites for methanol dehydrogenation and deoxygenation on stoichiometric and defective TiO₂ (110) surfaces. *Surf. Sci.* **544**, 241–260 (2003).
81. Herman, G. S., Dohna, Z., Ruzycki, N. & Diebold, U. Experimental Investigation of the Interaction of Water and Methanol with. *J. Phys. Chem. B* **2**, 2788–2795 (2003).
82. Tilocca, A. & Selloni, A. Methanol Adsorption and Reactivity on Clean and Hydroxylated Anatase(101) Surfaces. *J. Phys. Chem. B* **108**, 19314–19319 (2004).
83. Panagiotou, G. D. *et al.* Mapping the surface (hydr)oxo-groups of titanium oxide and its interface with an aqueous solution: the state of the art and a new approach. *Adv. Colloid Interface Sci.* **142**, 20–42 (2008).
84. Bourikas, K., Hiemstra, T. & Riemsdijk, W. H. van. Ion Pair Formation and Primary Charging Behavior of Titanium Oxide (Anatase and Rutile). *Langmuir* **12**, 749–756 (2001).
85. Panagiotou, G. Mapping the surface (hydr)oxo-groups of titanium oxide and its interface with an aqueous solution: The state of the art and a new approach. *Adv. Colloid Interface Sci.* **142**, 20–42 (2008).
86. Leroy, P., Tournassat, C. & Bizi, M. Influence of surface conductivity on the apparent zeta potential of TiO₂ nanoparticles. *J. Colloid Interface Sci.* **356**, 442–53 (2011).
87. Bouhaik, I. S., Leroy, P., Ollivier, P., Azaroual, M. & Mercury, L. Influence of surface conductivity on the apparent zeta potential of TiO₂ nanoparticles: application to the modeling of their aggregation kinetics. *J. Colloid Interface Sci.* **406**, 75–85 (2013).
88. Connor, P. A. & Mcquillan, A. J. Phosphate Adsorption onto TiO₂ from Aqueous Solutions: An in Situ Internal Reflection Infrared Spectroscopic Study. *Langmuir* **15**, 2916–2921 (1999).

89. Huynh, L., Feiler, A., Michelmore, A., Ralston, J. & Jenkins, P. Control of slime coatings by the use of anionic phosphates: a fundamental study. *Mater. Eng.* **13**, 1059–1069 (2000).
90. Gong, W. A real time in situ ATR-FTIR spectroscopic study of linear phosphate adsorption on titania surfaces. *Int. J. Miner. Process.* **63**, 147–165 (2001).
91. Lefèvre, G. In situ Fourier-transform infrared spectroscopy studies of inorganic ions adsorption on metal oxides and hydroxides. *Adv. Colloid Interface Sci.* **107**, 109–23 (2004).
92. Tosatti, S., Michel, R., Textor, M. & Spencer, N. D. Self-Assembled Monolayers of Dodecyl and Hydroxy-dodecyl Phosphates on Both Smooth and Rough Titanium and Titanium Oxide Surfaces. *Langmuir* **18**, 3537–3548 (2002).
93. Kasemo, B. Biological surface science. *Surf. Sci.* **3**, 451–459 (1998).
94. Zawisza, I. *et al.* Application of thin titanium/titanium oxide layers deposited on gold for infrared reflection absorption spectroscopy: structural studies of lipid bilayers. *Langmuir* **24**, 7378–87 (2008).
95. Carravetta, V. & Monti, A. S. Interaction of biomolecular systems with titanium-based materials: computational investigations. *Theor. Chem. Acc.* **123**, 299–309 (2009).
96. Kang, S. a, Li, W., Lee, H. E., Phillips, B. L. & Lee, Y. J. Phosphate uptake by TiO₂: batch studies and NMR spectroscopic evidence for multisite adsorption. *J. Colloid Interface Sci.* **364**, 455–61 (2011).
97. Murcia, J. J., Hidalgo, M. C., Navío, J. A., Araña, J. & Doña-Rodríguez, J. M. In situ FT-IR study of the adsorption and photocatalytic oxidation of ethanol over sulfated and metallized TiO₂. *Appl. Catal. B Environ.* **142-143**, 205–213 (2013).
98. Spori, D. M. *et al.* Influence of alkyl chain length on phosphate self-assembled monolayers. *Langmuir* **23**, 8053–60 (2007).
99. Gnauck, M. *et al.* Carboxy-terminated oligo(ethylene glycol)-alkane phosphate: synthesis and self-assembly on titanium oxide surfaces. *Langmuir* **23**, 377–81 (2007).
100. Raj, K. J. A., Ramaswamy, a. V. & Viswanathan, B. Surface Area, Pore Size, and Particle Size Engineering of Titania with Seeding Technique and Phosphate Modification. *J. Phys. Chem. C* **113**, 13750–13757 (2009).
101. Raj, K. J. A., Shanmugam, R., Mahalakshmi, R. & Viswanathan, B. XPS and IR spectral studies on the structure of phosphate and sulphate modified titania – A combined DFT and experimental study. *Indian J. Chem.* **49A**, 9–17 (2010).
102. Bachinger, A. & Kickelbick, G. Photocatalytic stability of organic phosphonates and phosphates on TiO₂ nanoparticles. *Appl. Catal. A Gen.* **409-410**, 122–132 (2011).

103. Myller, A. T., Karhe, J. J. & Pakkanen, T. T. Preparation of aminofunctionalized TiO₂ surfaces by binding of organophosphates. *Appl. Surf. Sci.* **257**, 1616–1622 (2010).
104. Engholm-Keller, K. & Larsen, M. R. Titanium dioxide as chemo-affinity chromatographic sorbent of biomolecular compounds--applications in acidic modification-specific proteomics. *J. Proteomics* **75**, 317–28 (2011).
105. Calvano, C. D., Jensen, O. N. & Zambonin, C. G. Selective extraction of phospholipids from dairy products by micro-solid phase extraction based on titanium dioxide microcolumns followed by MALDI-TOF-MS analysis. *Anal. Bioanal. Chem.* **394**, 1453–1461 (2009).
106. Pinkse, M. W. H., Uitto, P. M., Hilhorst, M. J., Ooms, B. & Albert, J. R. Selective enrichment of phosphopeptides from proteolytic digest using 2D-LC-ESI-MS and titanium oxide pre-columns. *Anal. Chem.* **76**, 3935–3943 (2004).
107. Ojamäe, L., Aulin, C., Pedersen, H. & Käll, P.-O. IR and quantum-chemical studies of carboxylic acid and glycine adsorption on rutile TiO₂ nanoparticles. *J. Colloid Interface Sci.* **296**, 71–8 (2006).
108. Bahri, S. *et al.* Adsorption and Surface Complexation Study of L-DOPA on Rutile (alpha-TiO₂) in NaCl Solutions. *Environ. Sci. Technol.* **45**, 3959–3966 (2011).
109. Lee, N. *et al.* Speciation of L-DOPA on nanorutile as a function of pH and surface coverage using surface-enhanced Raman spectroscopy (SERS). *Langmuir* **28**, 17322–30 (2012).
110. Liu, Y., Dadap, J. I., Zimdars, D. & Eisenthal, K. B. Study of Interfacial Charge-Transfer Complex on TiO₂ Particles in Aqueous Suspension by Second-Harmonic Generation. *J. Phys. Chem. B* **103**, 2480–2486 (1999).
111. Syres, K., Thomas, a, Bondino, F., Malvestuto, M. & Grätzel, M. Dopamine adsorption on anatase TiO₂ (101): a photoemission and NEXAFS spectroscopy study. *Langmuir* **26**, 14548–55 (2010).
112. Schweigert, N., Zehnder, A. J. B. & Eggen, R. I. L. Chemical properties of catechols and their molecular modes of toxic action in cells, from microorganisms to mammals. Minireview. *Environ. Microbiol.* **3**, 81–91 (2001).
113. Li, Q. *et al.* Ethylene glycol-mediated synthesis of nanoporous anatase TiO₂ rods and rutile TiO₂ self-assembly chrysanthemums. *J. Alloys Compd.* **471**, 477–480 (2009).
114. Uekawa, N., Endo, N., Ishii, K., Kojima, T. & Kakegawa, K. Characterization of Titanium Oxide Nanoparticles Obtained by Hydrolysis Reaction of Ethylene Glycol Solution of Alkoxide. *J. Nanotechnol.* **2012**, 1–8 (2012).
115. Xiang, G., Wang, Y.-G., Li, J., Zhuang, J. & Wang, X. Surface-specific interaction by structure-match confined pure high-energy facet of unstable TiO₂ (B) polymorph. *Sci. Rep.* **3**, 1411 (2013).

116. Voelker, D. R. in *Biochem. Lipids, Lipoproteins Membr.* 449–450 (Elsevier Science B.V., 2002).
117. Alberts, B. *et al.* *Molecular Biology of the Cell.* (2007).
118. Fahy, E. *et al.* A comprehensive classification system for lipids. *J. Lipid Res.* **46**, 839–61 (2005).
119. Dowhan, W. & Bogdanov, M. in *Biochem. Lipids, Lipoproteins Membr.* 1 (Elsevier B.V., 2002).
120. King, R. J. & Macbeth, M. C. Interaction of the lipid and protein components of pulmonary surfactant. Role of phosphatidylglycerol and calcium. *Biochim. Biophys. Acta* **647**, 159–168 (1981).
121. Barroso, R. P., Perez, K. R., Cuccovia, I. M. & Teresa Lamy, M. Aqueous dispersions of DMPG in low salt contain leaky vesicles. *Chem. Phys. Lipids* **165**, 169–77 (2012).
122. Chicco, A. J. & Sparagna, G. C. Role of cardiolipin alterations in mitochondrial dysfunction and disease. *Am. J. Physiol. -Cell Physiol.* **292**, (2007).
123. Athenstaedt, K. & Daum, G. Phosphatidic acid, a key intermediate in lipid metabolism. *Eur. J. Biochem.* **266**, 1–16 (1999).
124. Alfred H. Merrill, Jr., & Sandhoff, K. Spingolipids: metabolism and cell signaling. In *Biochem. Lipids, Lipoproteins Membr.* 383 (Elsevier B.V., 2002).
125. Yitbarek, E. Characterization and Analytical applications of Dye-encapsulated Zwitterionic liposomes. (2010).
126. Israelachvili, J. N. *Intermolecular and surface forces.* (Academic Press, 2011).
127. Marsh, D. General features of phospholipid phase transitions. *Chem. Phys. Lipids* **57**, 109–20 (1991).
128. Rutherford, H. Structural Investigation of Liposomes: effect of phospholipid hydrocarbon length and incorporation of Sphingomyelin. *MSc thesis*, University of Saskatchewan (2011).
129. Tardieu, A., Luzzati, V. & Reman, F. C. Structure and polymorphism of the hydrocarbon chains of lipids: a study of lecithin-water phases. *J. Mol. Biol.* **75**, 711–33 (1973).
130. Seddon, J. D. & Cerv, G. *Phospholipids Handbook.* 403–454 (Marcel Dekker, 1993).
131. Cullis, P. R., Fenske, D. B. & Hope, M. J. Physical properties and functional roles of lipids in membranes. *Biochem. Lipids, Lipoproteins Membr.* (1996).
132. Marsh, D. in *CRC Handb. lipid bilayers* 81–85 (2013).

133. Tocanne, J. F. & Teissié, J. Ionization of phospholipids and phospholipid-supported interfacial lateral diffusion of protons in membrane model systems. *Biochim. Biophys. Acta* **1031**, 111–42 (1990).
134. Mattsson, M. Cardiolipin in phospholipid bilayers. 2012
135. Carmona-Ribeiro, A. M. Dihexadecylphosphate Bilayers: Interbilayer Interactions and Intrabilayer Structure. *J. Colloid Interface Sci.* **139**, (1990).
136. Disalvo, E. a *et al.* Structural and functional properties of hydration and confined water in membrane interfaces. *Biochim. Biophys. Acta* **1778**, 2655–70 (2008).
137. Yamaguchi, T., Nishizaki, K. & Itai, S. Molecular interactions between phospholipids and electrolytes in a monolayer of parenteral lipid emulsion. *Colloids Surfaces B Biointerfaces* **9**, 275–282 (1997).
138. Mangeney, C., Dupres, V. & Bernard, S. Interfacial assembly of a phospholipid Langmuir monolayer by electrodeposited silver colloids. *J. Colloid Interface Sci.* **305**, 250–5 (2007).
139. Stefaniu, C., Brezesinski, G. & Möhwald, H. Langmuir monolayers as models to study processes at membrane surfaces. *Adv. Colloid Interface Sci.* 1–17 (2014).
doi:10.1016/j.cis.2014.02.013
140. Chazalet, M. S. P. & Fressign, C. Phospholipid-protein interactions at the air-water interface: a monolayer study. *Thin Solid Films* **211**, 743–746 (1992).
141. Serrano, A. G. & Pérez-Gil, J. Protein-lipid interactions and surface activity in the pulmonary surfactant system. *Chem. Phys. Lipids* **141**, 105–18 (2006).
142. Standish, M. M. & Pethica, B. A. Interactions in phospholipid-cholesterol at the air/water interface. *Biochim. Biophys. Acta* **144**, 659–665 (1967).
143. Dynarowicz-Łatka, P. & Hac-Wydro, K. Interactions between phosphatidylcholines and cholesterol in monolayers at the air/water interface. *Colloids Surf. B. Biointerfaces* **37**, 21–5 (2004).
144. Mansour, H., Wang, D.-S., Chen, C.-S. & Zografi, G. Comparison of Bilayer and Monolayer Properties of Phospholipid Systems Containing Dipalmitoylphosphatidylglycerol and Dipalmitoylphosphatidylinositol. *Langmuir* **17**, 6622–6632 (2001).
145. Möhwald, H. Phospholipid Monolayers. in *Handb. Biol. Phys.* (1995).
146. Kaganer, V., Möhwald, H. & Dutta, P. Structure and phase transitions in Langmuir monolayers. *Rev. Mod. Phys.* **71**, 779–819 (1999).

147. Casillas-Ituarte, N. N., Chen, X., Castada, H. & Allen, H. C. Na⁺ and Ca²⁺ effect on the hydration and orientation of the phosphate group of DPPC at air-water and air-hydrated silica interfaces. *J. Phys. Chem. B* **114**, 9485–95 (2010).
148. Pichot, R., Watson, R. L. & Norton, I. T. Phospholipids at the interface: current trends and challenges. *Int. J. Mol. Sci.* **14**, 11767–94 (2013).
149. Mingotaud, A. F., Mingotaud, C. & Patterson, L. K. *Handbook of monolayers, Vol 1.* (Academic Press, 1993).
150. Mohwald, H. Phospholipid and phospholipid-protein monolayer at the air-water interface. *Annu. Rev. Phys. Chem.* **41**, 441–76 (1990).
151. Taylor, D. J. F., Thomas, R. K. & Penfold, J. Polymer/surfactant interactions at the air/water interface. *Adv. Colloid Interface Sci.* **132**, 69–110 (2007).
152. Dynarowicz-Latka, P., Dhanabalan, a & Oliveira, O. N. Modern physicochemical research on Langmuir monolayers. *Adv. Colloid Interface Sci.* **91**, 221–93 (2001).
153. Katherine, M. S. & John, B. O. in *Biochem. Lipids, Lipoproteins Membr.* 172–173 (Elsevier B.V., 2002).
154. Starr, T. E., Thompson, N. L., Hill, C. & Carolina, N. Formation and Characterization of Planar Phospholipid Bilayers Supported on TiO₂ and SrTiO₃ Single Crystals. *Langmuir* **16**, 10301–10308 (2000).
155. Reimhult, E., Hook, F. & Kasemo, B. Intact Vesicle Adsorption and Supported Biomembrane Formation from Vesicles in Solution: Influence of Surface Chemistry, Vesicle Size, Temperature, and Osmotic Pressure. *Langmuir* **19**, 1681–1691 (2003).
156. Oleson, T. A., Sahai, N. Oxide-dependent adsorption of a model membrane phospholipid, dipalmitoylphosphatidylcholine: Bulk adsorption isotherms. *Langmuir* **24**, 4865–4873 (2008).
157. Oleson, T. A. & Sahai, N. Interaction energies between oxide surfaces and multiple phosphatidylcholine bilayers from extended-DLVO theory. *J. Colloid Interface Sci.* **352**, 316–326 (2010).
158. Oleson, T. A., Sahai, N. & Pedersen, J. A. Electrostatic effects on deposition of multiple phospholipid bilayers at oxide surfaces. *J. Colloid Interface Sci.* **352**, 327–336 (2010).
159. Xu, J., Stevens, M. J., Oleson, T. A., Last, J. A. & Sahai, N. Role of Oxide Surface Chemistry and Phospholipid Phase on Adsorption and Self-Assembly: Isotherms and Atomic Force Microscopy. *J. Phys. Chem. C* **113**, 2187–2196 (2009).
160. Keller, C. A & Kasemo, B. Surface specific kinetics of lipid vesicle adsorption measured with a quartz crystal microbalance. *Biophys. J.* **75**, 1397–1402 (1998).

161. Cho, N.-J., Cho, S.-J., Cheong, K. H., Glenn, J. S. & Frank, C. W. Employing an amphipathic viral peptide to create a lipid bilayer on Au and TiO₂. *J. Am. Chem. Soc.* **129**, 10050–1 (2007).
162. Roiter, Y. *et al.* Interaction of nanoparticles with lipid membrane. *Nano Lett.* **8**, 941–4 (2008).
163. Cho, N. J. & Frank, C. W. Fabrication of a Planar Zwitterionic Lipid Bilayer on Titanium Oxide. *Langmuir* **26**, 15706–15710 (2010).
164. Oliver, A. E. & Parikh, A. N. Templating membrane assembly, structure, and dynamics using engineered interfaces. *Biochim. Biophys. Acta* **1798**, 839–50 (2010).
165. Wiącek, A. E., Anitowska, E., Delgado, A. V., Hołysz, L. & Chibowski, E. The electrokinetic and rheological behavior of phosphatidylcholine-treated TiO₂ suspensions. *Colloids Surfaces A Physicochem. Eng. Asp.* **440**, 110–115 (2014).
166. Tero, R. Substrate Effects on the Formation Process, Structure and Physicochemical Properties of Supported Lipid Bilayers. *Materials (Basel)*. **5**, 2658–2680 (2012).
167. Tero, R., Ujihara, T. & Urisut, T. Lipid Bilayer Membrane with Atomic Step Structure: Supported Bilayer on a Step-and-Terrace TiO₂ (100) Surface. *Langmuir* **24**, 11567–11576 (2008).
168. Reimhult, E., Hook, F. & Kasemo, B. Vesicle adsorption on SiO₂ and TiO₂: Dependence on vesicle size. *J. Chem. Phys.* **117**, 7401–7404 (2002).
169. Reimhult, E., Hook, F. & Kasemo, B. Intact vesicle adsorption and supported biomembrane formation from vesicles in solution: Influence of surface chemistry, vesicle size, temperature, and osmotic pressure. *Langmuir* **19**, 1681–1691 (2003).
170. Ekeröth, J., Konradsson, P. & Höök, F. Bivalent-Ion-Mediated Vesicle Adsorption and Controlled Supported Phospholipid Bilayer Formation on Molecular Phosphate and Sulfate Layers on Gold. *Langmuir* **18**, 7923–7929 (2002).
171. Oleson, T. A & Sahai, N. Oxide-dependent adsorption of a model membrane phospholipid, dipalmitoylphosphatidylcholine: bulk adsorption isotherms. *Langmuir* **24**, 4865–73 (2008).
172. Reviakine, I. & Brisson, A. Formation of Supported Phospholipid Bilayers from Unilamellar Vesicles Investigated by Atomic Force Microscopy. *Langmuir* **16**, 1806–1815 (2000).
173. Reviakine, I., Rossetti, F. F., Morozov, A. N. & Textor, M. Investigating the properties of supported vesicular layers on titanium dioxide by quartz crystal microbalance with dissipation measurements. *J. Chem. Phys.* **122**, 204711 (2005).
174. Fortunelli, A. & Monti, S. Simulations of lipid adsorption on TiO₂ surfaces in solution. *Langmuir* **24**, 10145–10154 (2008).

175. Khan, T. R. *et al.* Lipid redistribution in phosphatidylserine-containing vesicles adsorbing on titania. *Biointerphases* **3**, FA90–FA95 (2008).
176. National Science and Technology Council, C. on T.-U. *Strategy for Nanotechnology-Related Environmental, Health and Safety Research*. (2008).
177. Fujishima, A, Zhang, X. & Tryk, D. TiO₂ photocatalysis and related surface phenomena. *Surf. Sci. Rep.* **63**, 515–582 (2008).

Chapter 2

Materials and Methods

Table of Contents

2.	Materials and methods	98
2.1	Materials	98
2.1.1	Titanium dioxide (TiO ₂) samples	98
2.1.2	Phospholipids	98
2.1.3	Other chemicals	100
2.2	Sample preparation	100
2.2.1	Dry powders of TiO ₂	100
2.2.2	Aqueous dispersion of TiO ₂	100
2.2.3	Phospholipid vesicles	101
2.2.4	Mixture of TiO ₂ and phospholipids	102
2.3	Methods	102
2.3.1	X-ray diffraction (XRD)	103
2.3.2	Raman spectrometer	103
2.3.3	Transmission Electron Microscopy (TEM)	104
2.3.4	Nitrogen gas adsorption isotherms	104
2.3.5	X-ray photoelectrons spectroscopy (XPS)	105
2.3.6	Diffuse reflectance Fourier transform infrared spectroscopy (DRIFTS)	106
2.3.7	Nuclear Magnetic Resonance	108
2.3.8	Dynamic light scattering (DLS)	108
2.3.9	Laser Doppler Electrophoresis (LDE)	112
2.3.10	Langmuir films	115
2.3.11	Phosphorus dosage/isotherms of adsorption	117
2.4	Materials characterization	119
2.4.1	TiO ₂	119
2.4.2	Morphology and textural properties of TiO ₂	124

2.4.3 Phospholipids vesicles in aqueous dispersion	139
2.5 Conclusion	140
References.....	142

2. Materials and methods

This section provides detailed information about the materials and methods used for the characterization and for the investigation of the interaction between oxide particles and phospholipids. The materials mainly consist in TiO_2 , and phospholipids (PLs). All of them are commercial products. Methods to characterize the materials are briefly described. Then first characterization results are given and discussed in this chapter.

2.1 Materials

2.1.1 Titanium dioxide (TiO_2) samples

Titanium dioxide dried powders in different crystalline phases at nanometer scale were used as supplied. They consist in TiO_2 -P25 from Degussa (Essen, Germany), Anatase from MTI Corporation (TiO_2 -A, California, USA), TiO_2 -PC, that comprises TiO_2 -PC10, TiO_2 -PC50 and TiO_2 -PC100 from Millenium Inorganic Chemicals (Maryland, USA) and rutile from Sigma-Aldrich (TiO_2 -R, Missouri, USA). Powders in plastic container are kept in the darkness to protect them from the effect of light due to the extreme photosensitivity of TiO_2 .

2.1.2 Phospholipids

Lipids were supplied by Avanti Polar Lipid (Alabaster, Alabama, USA) and Sigma-Aldrich (Saint Quentin-Fallavier, France). The synthetic glycerophospholipids used in our study were 1,2-dimyristoyl-sn-glycero-3-phosphate monosodium salt (DMPA, >99%, from Avanti Polar Lipids), 1,2-dimyristoyl-sn-glycero-3-phosphocholine (DMPC, >99%, from Avanti Polar Lipids), 1,2-dimyristoyl-sn-glycero-3-phosphoethanolamine (DMPE, 99% from Sigma-Aldrich), 1,2-dimyristoyl-sn-glycero-3-phospho-rac-1-glycerol (DMPG, Sodium Salt, 99% Sigma-Aldrich) and 1,2-dimyristoyl-sn-glycero-3-phosphoserine (DMPS, Sodium Salt, >99%, Avanti Polar Lipids), 1,3-bis(sn-3'-phosphatidyl)-sn-glycerol (TMCL, sodium salt, >99%, Avanti Polar Lipids). As sphingolipids, only sphingomyelin from bovine brain (SM, >97%, Sigma-Aldrich) was used. In addition to these phospholipids, a lipid-like molecule called dihexadecyl phosphate (DHP, Sigma-Aldrich) was also used. Molecular structures of all phospholipids and lipid are depicted in Figure 2.1. Molecules of DMPA, DMPC, DMPE, DMPG and DMPS possess the same backbone: two fatty acids branched on a glycerol unit. They differ in the polar headgroups that is fixed at the third position of glycerol. TMCL has got a dimeric structure formed by two molecules of DMPA connected to a glycerine

backbone. DHP is a lipid with two 16 carbon acid chains linked to a phosphate group without glycerol backbone.

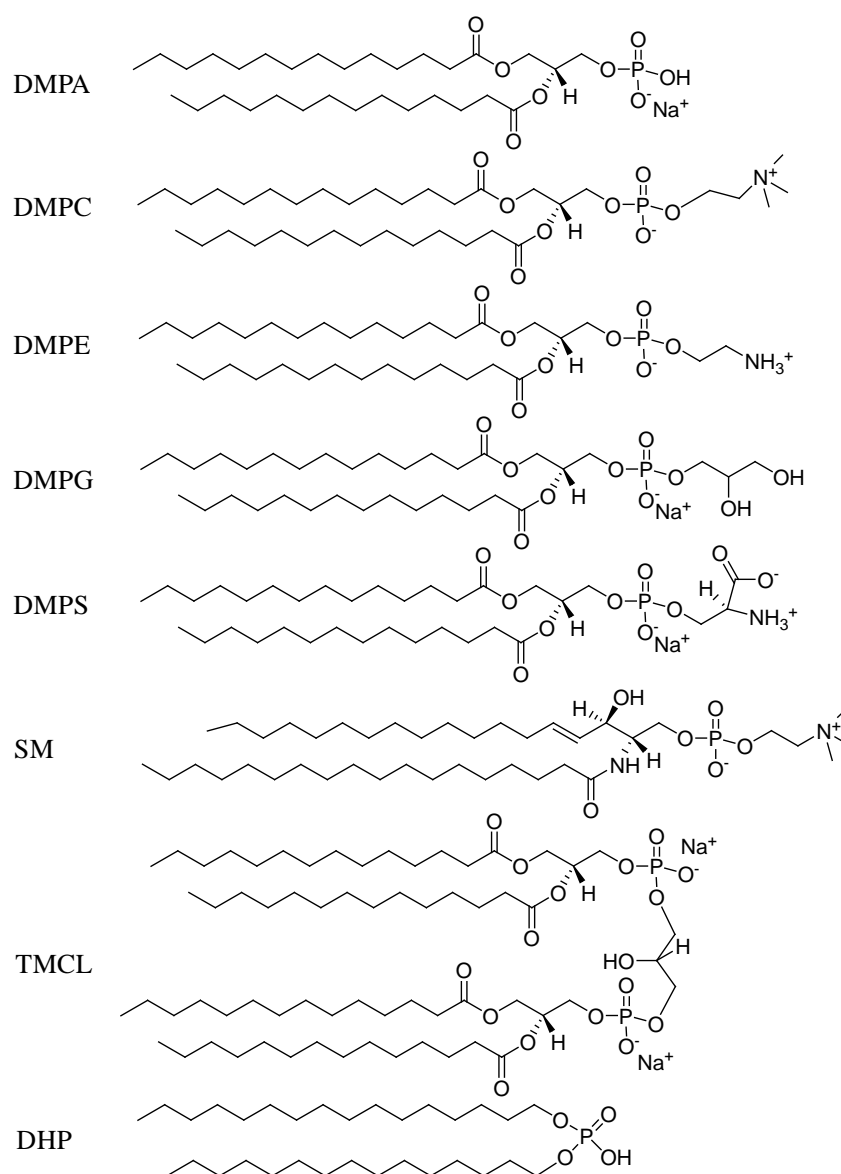


Figure 2.1. Molecular structures of phospholipids and lipid used in this work.

In comparison to glycerophospholipids, SM possesses the same headgroup as DMPC but the anchoring unit is a sphingosine on which a monounsaturated chain and a fatty acid are linked.

As DHP is a lipid-like molecule and other molecules are phospholipids, hereafter we designate as *phospholipids* all these molecules.

2.1.3 Other chemicals

Supplementary chemical substances used for this study comprise NaOH in flake form (99%, Alfa Aesar, MA, USA), HCl solution diluted from HCl solution 37% (Carlo ERBA, Milan, Italy), NaCl solid (Bioextra, $\geq 99.5\%$, Sigma-Aldrich), $\text{Mg}(\text{NO}_3)_2 \cdot 6\text{H}_2\text{O}$ (Fluka), L - ascorbic (analytical grade, Merck, Germany), H_2SO_4 (95%, Fisher Chemical), $\text{NH}_4(\text{MoO}_4 \cdot 4\text{H}_2\text{O})$ (99%, ACROS), Na_2HPO_4 (Merck, Germany) and organic solvents such as chloroform CHCl_3 , methanol CH_3OH and ethanol $\text{C}_2\text{H}_5\text{OH}$ (Carlo ERBA, Milan, Italy). For all experiments, ultra pure water (Milli-Q, resistivity = $18.2 \text{ M}\Omega \cdot \text{cm}$), was freshly used.

2.2 Sample preparation

2.2.1 Dry powders of TiO_2

The different commercial powders of titanium dioxide were used as supplied for the basic characterization. For TiO_2 -A and TiO_2 -R samples, the powders were additionally dispersed in aqueous solutions according to the protocol described in the next section. The suspensions were then centrifuged and dried in a desiccator with silica gel as dehydrating material.

2.2.2 Aqueous dispersion of TiO_2

All preparation steps are sketched in Figure 2.2. The suspensions were prepared by dispersing 100 mg TiO_2 in 500 mL of ultra-pure water and they were vigorously stirred by magnetic stirrer during 2 minutes. Then, this dispersion was bath sonicated for 10 minutes with a bath sonicator at 275 W (Elmasonic S 30 H from Elma, Singen, Germany). The resulting dispersion was diluted to get the final concentration of $0.1 \text{ g}\cdot\text{L}^{-1}$ with ultra-pure water or NaCl solution to control ionic strength. The addition of NaCl to the dispersion was realized after sonication to avoid any possible effects of ions on TiO_2 surfaces during the sonication. Finally, the resulting dispersion was subjected to pH adjustment by addition of HCl or NaOH solutions (0.01 - 0.5 M). During the preparation and experiments, the container of dispersion was covered by aluminum foil to limit the impact of light on TiO_2 . These solutions were freshly used (within 12h).

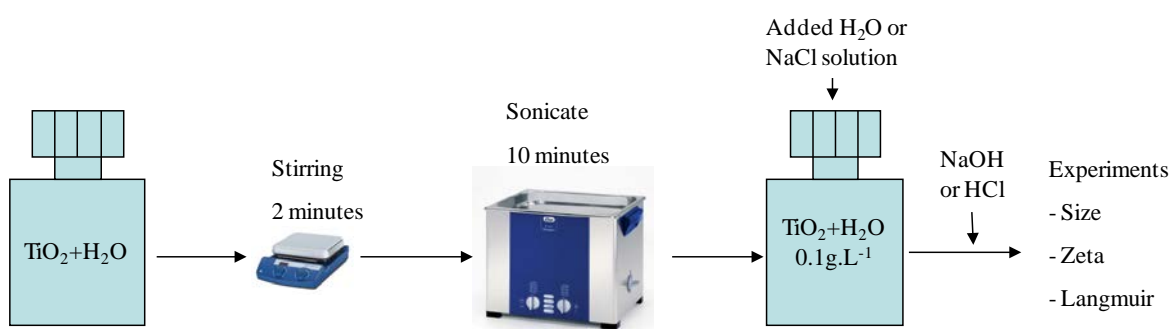


Figure 2.2. Schematic description of the steps to prepare TiO_2 aqueous suspensions

2.2.3 Phospholipid vesicles

Phospholipid powders kept in deep freezer at $-20\text{ }^{\circ}\text{C}$ were left at room condition for ca. 20 minutes to get equilibrium with environment. Phospholipid vesicles were prepared by the protocol described in Figure 2.3. Firstly, a suitable amount of powders was dispersed in ultra-pure H_2O ($0.125\text{ mg}\cdot\text{mL}^{-1}$) by shaking for 2 minutes and bath sonication (10 minutes). Sonication processes were conducted with the same bath sonicator as previously used (Elmasonic S 30 H, 275 W from Elma, Singen, Germany) and at a temperature slightly higher than the transition temperature of each phospholipid (Table 2.1). Secondly, the dispersions were extruded through a polycarbonate membrane on Mini-Extruder (Avanti Polar Lipids, Alabama, USA) by 10 passes on each membrane with pore size of 800 nm, 400 nm, 100 nm, successively. During this step, the temperature of dispersions and extruder was kept at a temperature slightly higher than the transition temperature of phospholipids in order to facilitate the extrusion processes with molecules in the fluid state.

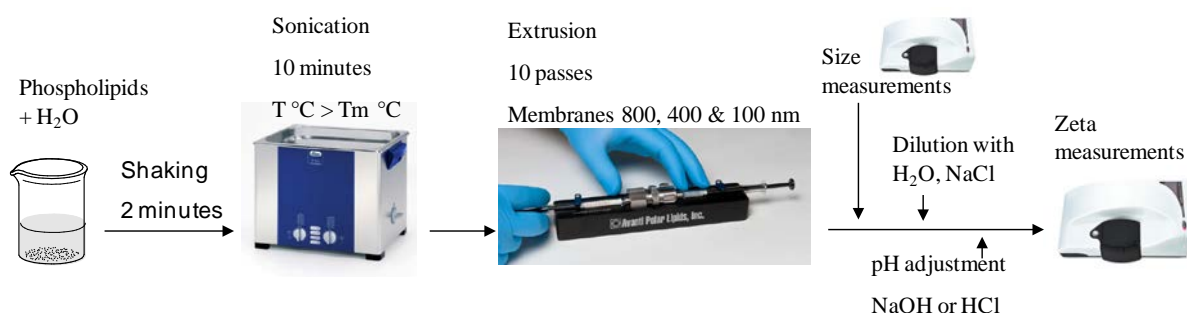


Figure 2.3. Schematic description of the preparation steps of the phospholipid vesicles in aqueous suspensions that were characterized by size and surface charge measurements.

Table 2.1. Phase transition temperature of lipids

Molecules	Number of carbons in acyl chain	Phase transition temperature (°C)	Reference
DMPA	14	50	Avanti Polar lipids
DMPC	14	24	Avanti Polar lipids
DMPE	14	50	Avanti Polar lipids
DMPG	14	23	Avanti Polar lipids
DMPS	14	35	Avanti Polar lipids
SM	16/18	37	Barenholz 1999 ¹
TMCL	14	47	Lewis 2009 ²
DHP	16	75	Sigma-Aldrich

2.2.4 Mixture of TiO₂ and phospholipids

Solid mixtures of TiO₂ (TiO₂-A, TiO₂-R) and phospholipids (DMPA, DMPG, DHP) were prepared in three steps. First, the dispersion of TiO₂ and that of phospholipids were prepared separately. Suspension of TiO₂ was prepared according to the protocol mentioned in section 2.2.2. Separately, a suitable amount of phospholipids (DMPA, DMPG) was dispersed in 10 mL of H₂O. These dispersions were sonicated for 10 minutes at transition temperature to get the quasi-transparent dispersion. Next, the TiO₂ dispersion was mixed with that of phospholipids with loading ratio of 2 molecules of phospholipids over 1 nm² surface of TiO₂. Afterward, the resulting dispersion was adjusted by HCl solution to reach the value of pH desired in the experiments. The obtained samples were vortexed and kept in polypropylene tubes (type 15 ml). These tubes were covered by aluminum foil and left rotating (10 rpm) for 10 hours so that the interaction between phospholipids and TiO₂ particles gets an equilibrium state. These samples were finally centrifuged (20 minutes at 3500 g) to separate the solid from the liquid phases. The solid phases were washed 3 times by the same aqueous solution. At the end, the solid phases were dried by keeping them in desiccators with silica gel connected with vacuum pump for at least 72 hours.

2.3 Methods

All dry powders were characterized by different methods prior to their characterization in aqueous dispersion. The crystallographic structure and phase composition are characterized by X-ray diffraction and Raman Spectroscopy. Specific surface area of TiO₂, is determined by volumetric adsorption isotherms at 77K of N₂ gas. Surface chemistry of TiO₂ powders are

characterized by Infrared spectroscopy and x-ray photoelectron spectroscopy (XPS). Morphology and elemental size of TiO₂ particles were examined by transmission electron microscopy (TEM).

2.3.1 X-ray diffraction (XRD)

Room temperature of XRD data of TiO₂ commercial powders were obtained using a Bruker D8 Advance powder diffractometer, which operated in Bragg-Brentano geometry with a Cu anode sealed X-ray tube and a focusing Ge(111) primary monochromator (selecting the Cu K α_1 radiation; $\lambda = 1.540598 \text{ \AA}$). We used a 1-D silicon-strip position sensitive detector (LynxEye detector) with an active area of $3.7^\circ 2\theta$ (goniometer radius = 217.5 mm). Diffractometer settings were 40 kV, 40 mA, $20 - 100^\circ 2\theta$, step size $0.03^\circ 2\theta$ and 5 s counting per step.

Application of Rietveld refinement method to XRD diffractogram help to identify the homogeneity of crystalline phases in TiO₂-P25 powders. The refinement was carried out on Fullprof software.

2.3.2 Raman spectrometer

The Raman spectroscopy is a non-invasive sensitive technique if the wavelength of the excitation laser is tuned to the optical properties of the studied samples. Therefore in our case, in order to avoid any photo-induced effect of TiO₂, we have chosen to use a near infrared excitation. As the Raman effect is roughly proportional to the power 4 of the frequency, the use of a near infrared excitation forces the use of an optical non-dispersive interferometer to record the inelastic signal in order to keep an exploitable signal/noise ratio. The sample powders can be analyzed quickly without any supplementary preparation step. This study used a FT-Raman set-up (MultiRam Raman Spectrometer from Bruker equipped Nd: YAG crystal) to characterize powder samples kept in small glass bottles (2 ml). The laser beam (1064 nm) was slightly focused on a sample area of about 100 μm diameter with a power varied from 100 mW to 250 mW. The backscattered spectra were recorded with 1000 scans/spectrum with a spectral resolution of 4 cm^{-1} at room condition. Spectral analyses were performed by OPUS software, which was received from Bruker company.

2.3.3 Transmission Electron Microscopy (TEM)

The TEM experiments were performed on an Hitachi HNAR9000 setup. The coherent electron beam is produced by electron gun. This beam is accelerated at 300 kV and the wavelength of electrons is 2 pm. The beam then passes through system of condenser lens and parallel or converging illuminate the specimen in an area of a few nanometers to several micrometers in diameter. Upon impinging on the specimen, there are subsequently diffracted electrons beam and transmitted electrons beam. This thesis considers only the imaging function of TEM. The transmitted electrons beam is magnified and detected by CCD detector. It has been well known that, apart from scanning tunneling microscope, TEM creates very high resolution image, up to angstrom level. Thus, TEM is normally used to determine the inter-atomic distance in crystals.

TiO₂ powders were firstly dispersed in ethanol (at very low concentration) and this suspension was sonicated for 5 minutes. Finally, one drop of dispersion was deposited on copper grids covered by lacey carbon and left at room condition for 15 minutes to evaporate completely ethanol. Once dried, the sample was entered into the analysis chamber for observation.

2.3.4 Nitrogen gas adsorption isotherms

Specific surface areas of TiO₂ samples were is determined from the volumetric adsorption isotherms at 77K of N₂ gas using ASAP 2010 Physisorption Analyzer (Micromeritics, Georgia, USA). The data were treated by the multipoint Brunauer-Emmett-Teller (BET) method in order to able to compare our results with the literature. BET theory usable for multilayer adsorption is based on several assumptions: (i) gas molecules multilayer physically adsorb on surface of solid (ii) there is no interaction among adsorbate molecules (iii) the first layer is Langmuir adsorption (iv) the adsorption enthalpy the first layer is higher than that of the second and that of each layer from the second layer equals to enthalpy of gas condensation (v) at saturation pressure, the number of layer is infinite and (vi) Langmuir theory is applicable for each individual monolayer. In our work, we have not verified that all these assumptions may be adapted for the description of the interaction between N₂ molecules and the different crystalline faces of our TiO₂ samples. Typically in the literature BET model is used to estimate the specific surface area, the average pore size and pore volume of samples. Nitrogen (N₂), Argon (Ar) or Krypton (Kr) gas are widely used as adsorbate in this measurement. The cross-sectional of one adsorbed N₂ molecule is about 0.162 nm², that of Ar

is 0.166 nm^2 and of Kr is about 0.21 nm^2 . According to the number of gas molecules required to cover completely the solid surface with a monolayer, the surface of solid is estimated. Usually, the measurement of specific surface area takes 2 days (for out-gassing and analysis). At first, the sample is outgassed by heating at $90 \text{ }^\circ\text{C}$ under vacuum or with flowing gas to remove adsorbed contaminants acquired from atmosphere exposure (e.g. CO_2 and H_2O). Then, the sample is cooled down to cryogenic temperature (77 K , boiling point of N_2 liquid) under vacuum; adsorptive gas (like N_2) is dosed to the surface of samples with controlled increments. At each dose, the pressure of system is allowed to equilibrate and subsequently the amount of adsorbed gas is calculated. The relationship between quantity of adsorbed gas versus pressure at constant temperature is established (adsorption isotherm). This relationship determines the specific area of samples. As our work was not a chemical-physic study of the adsorption of gas molecules on TiO_2 samples, the obtained results will be qualitatively used to compare our samples with those of the literature however a detailed quantitative comparison between our samples without care could be too speculative.

2.3.5 X-ray photoelectrons spectroscopy (XPS)

XPS known also as Electron spectroscopy for chemical analysis (ESCA) is the most widely used technique in surface analysis for determining the composition and the oxidation state of surface constituents.³ XPS can detect almost every element except H and He. The detection limit of XPS to element is about part per thousand. In XPS measurement, the sample is exposed to X-ray (such as: $\text{Al K}\alpha$) under ultrahigh vacuum and only the first 10 nm of the surface are probed. Kinetic energy (E_k) and the amount of the escaped electrons are measured. Finally, the binding energy (E_b) of electrons in samples is deduced following the equation:

$$E_b = h\nu - E_k - w,$$

where w is the work function and $h\nu$ is the energy of X-ray photon.

Binding energy of electron in materials depends on the surrounding environment; therefore XPS can distinguish the oxidation state of elements at surface of samples.

Surface chemistry composition of TiO_2 samples were analyzed by X-ray photoelectron spectroscopy (XPS) with AXIS Nova model from Kratos Analytical Company. Samples were deposited on a special specimen holder for powders. Survey scan was recorded at pass energy of 160 eV . The final data were treated by Casa XPS software. Samples for this

measurement (pristine TiO₂ commercial powders) were first neutralized and characterized. Calibration was carried out by setting binding energy of Ti (IV) 2p^{3/2} at 458.7 eV.

2.3.6 Diffuse reflectance Fourier transform infrared spectroscopy (DRIFTS)

Wavelength of IR ranges from 0.8 μm to 1000 μm, which is divided in three regions: near, mid and far infrared (Figure 2.4).

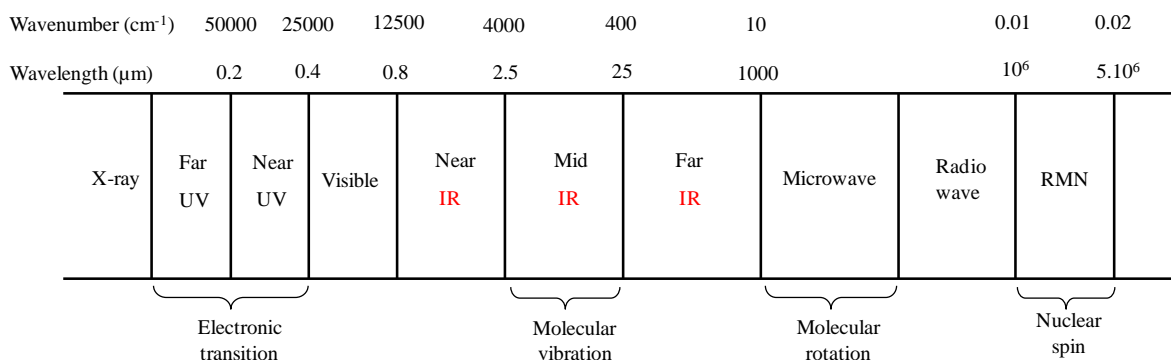


Figure 2.4. Infrared light in spectrum of electromagnetic radiation.

Infrared spectroscopy is a powerful technique for qualitative and quantitative analysis. Fourier Transform Infrared (FTIR) spectrometer uses a simple optical device called interferometer to produce signals (interferogram) that contains all information about frequencies of infrared light sources, resulting in very fast measurement (a few milli-seconds for one spectrum). However, interferogram cannot be interpreted directly for analysis. Mathematical method called Fourier transformation is required to decode interferogram, performing by computer and generate the spectrum which is a plot of intensity versus frequency. There are different modes (Figure 2.5) to record IR spectrum: Transmission, Specular Reflection, Diffuse Reflection and Attenuated Total Reflectance (ATR-FTIR).

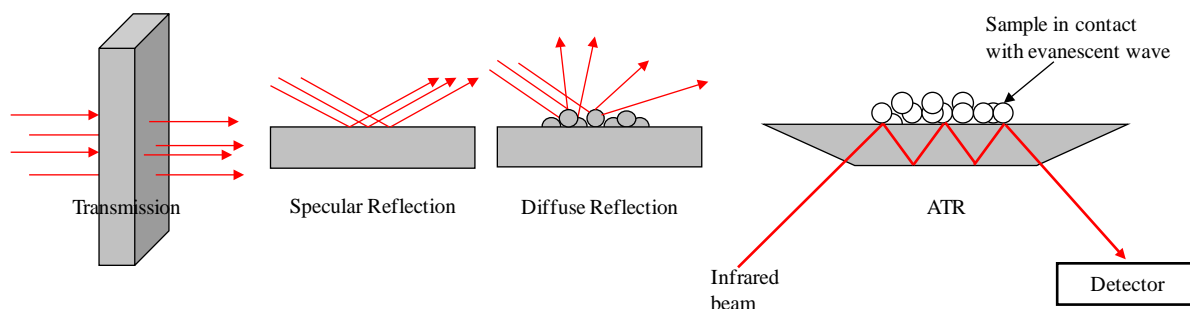


Figure 2.5. Recording spectra modes of IR signals.

Our study used Diffuse reflection (diffuse reflectance) mode. The recorded spectra may be treated by the Kubelka-Munk (KM) theory,⁴ in which absorption properties of samples are extracted from reflected light using equation:

$$F(R) = \frac{K}{S} = \frac{(1 - R_{\infty})^2}{2R_{\infty}}$$

Where

- K is absorption coefficient of medium
- S is scattering coefficient of medium
- R_{∞} is the reflectance of medium at infinite thickness
- F(R) is KM function, which is dependent on ratio K/S but not on the absolute value of K, S.

The experimental definition of the scattering coefficient, acceptable for all the samples, is difficult; therefore the use of the logarithm function of the reflectance, where the reflectance are compared at one specular reflected signal obtained on a mirror, consist in an acceptable method.⁵

This diffuse reflectance method to obtain infrared spectra has been widely used thanks to its simplicity and acceptable prediction accuracy, particularly in paper, paint, colorant industry.⁶ In this thesis, we have chosen this experimental technique at first to avoid the use of the classical pellets of mixture of our samples with another powder as KBr or NaCl ; thus our sample surfaces could be probed with the minimum of physical perturbation. Secondly, this experimental approach allowed us to record simultaneously the spectra in the near and in the middle infrared ranges.

In this thesis, experiments were conducted on FTIR Bruker Vertex 70 spectrometer with diffuse DRIFTS mode. The spectra were recorded at resolution 4 cm^{-1} and 1000 scans in wavenumber range of $400 - 8000 \text{ cm}^{-1}$. Samples for measurement were prepared according the protocol describing in section 2.2.4. All data were treated by using OPUS 5.5 software provided by Bruker company. The resulting spectra was represented in relationship between $\log(\text{reflectance})$ versus wavenumber (cm^{-1}).

Sample powders (TiO_2 , mixture TiO_2 & phospholipids) were not diluted with KBr for the $8000\text{-}2000 \text{ cm}^{-1}$ range recording while they are diluted with KBr (2% in weight) in the range $4000\text{-}400 \text{ cm}^{-1}$ to overcome the highly absorption of TiO_2 . The range $4000\text{-}2000$ consisted then in an overlap range in order to be able to study and compare both the spectral ranges. Samples were investigated at room condition and also at under weak pressure between

300 K and 550K. At room condition, Praying Mantis Diffuse reflection accessory (HARRICK Scientific Product Inc) was used. The special configuration of this accessory eliminates the specular reflectance component away from the ellipsoid and subsequently in order to minimize the distortion of the result spectra (distortion due to the anomalous dispersion phenomena related to the strong absorption). At vacuum (order of 10^{-6} mbar), measurements were conducted with Praying Mantis High Temperature Reaction Chambers (HARRICK Scientific Product Inc). The chamber equipped a dome with two KBr windows and one glass window for observation from outside, was connected to a membrane vacuum pump. Samples at first passed for measurements at room condition, then at vacuum when required. In order to get high vacuum, chamber with sample inside was evacuated by pump for 30 minutes (to get pressure of $\sim 10^{-6}$ mbar), at room temperature. Thus, spectra were recorded soon after.

2.3.7 Nuclear Magnetic Resonance

^{31}P solid-state NMR measurements were performed at ambient temperature on a Bruker AVANCE 500 MHz spectrometer, equipped with a CP-MAS DVT 4 mm probe. $\{^1\text{H}\}$ - ^{31}P Cross-Polarization (CP) spectra of dry powders were recorded with a contact time of 0.75 ms, under Magic Angle Spinning (MAS) of 10 kHz frequency and using a recycle time of 3s. ^{31}P chemical shift data are referenced at 0 ppm against standard of 85% phosphoric acid.

2.3.8 Dynamic light scattering (DLS)

The thesis commits great effort to examine hydrodynamic size and zeta potential of materials in aqueous medium by using Dynamic Light Scattering and Laser Doppler Electrophoresis techniques. Although these techniques are frequently used in research and industry, the related theories are not always familiar to a non specialist reader. For that reason, a brief review about the theories is presented in the following.

DLS is also named photon correlation spectroscopy or quasi-elastic light scattering.⁷ Hydrodynamic size measurement is based on the interaction between light and particles submitted to Brownian motion. The intensity of scattered light from particles fluctuates with time. These fluctuations are recorded, and their mathematical treatment allows determination of the translational diffusion coefficient of the particles. Thanks to Stokes-Einstein equation, hydrodynamic size of particles is calculated:

$$d = \frac{kT}{3\pi\mu D}$$

Where

- d is the hydrodynamic diameter of the particle (m)
- k is the Boltzmann constant (J.K⁻¹)
- T is the absolute temperature at measurement condition (K)
- μ is the dynamic viscosity of the medium (kg.m⁻¹.s⁻¹)
- D is the translational diffusion coefficient (m².s⁻¹)

The hydrodynamic diameter represents the size of particles including their electrical double layer. Therefore, when ionic strength of medium increases, the hydrodynamic diameter will decrease accounting for the reduction of the double layer thickness. The mathematical treatment of the fluctuating scattered intensity leads to an auto-correlation function:

$$G(\tau) = \int_0^{\infty} I(t)I(t + \tau)dt$$

Where

- I(t) is the scattering light intensity at moment t
- I(t + τ) is the scattering light intensity at moment t + τ
- τ is the sampling time

The auto-correlation function represents the probability to find the particle at the same point at two close moments t and t + τ. Depending on the size of particles, either small or large, this probability is high or low, accordingly. Indeed, small particles move quickly under Brownian motion, whereas large particles move slowly. If the correlation is perfect, the probability equals 100 %. When time is running, this probability exponentially decreases until 0 %, the decay ratio being directly linked to the translational diffusion coefficient of the particles, and thus their hydrodynamic diameter.

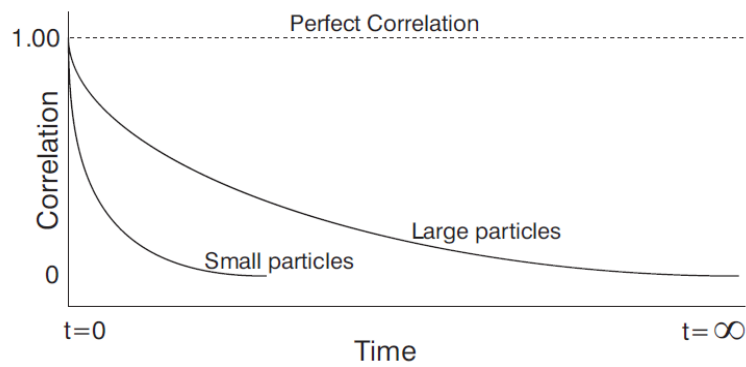


Figure 2.6. The correlation decay of small and large particles with time. Adapted from Zetasizer Nano Series User Manual 2004.

With the help of mathematical algorithms, a raw relation between relative intensity of scattering light with hydrodynamic diameter is established. Depending on the requirement of experimenter, the intensity distribution can be converted to volume-based distribution (by Mie theory) or number-based distribution. This study uses volume-based distribution to show hydrodynamic diameter of TiO₂ particles and phospholipids vesicles. Figure 2.7 displays the configuration of operating system to measure hydrodynamic size of particles, equipped with Zetasizer NS (Malvern).

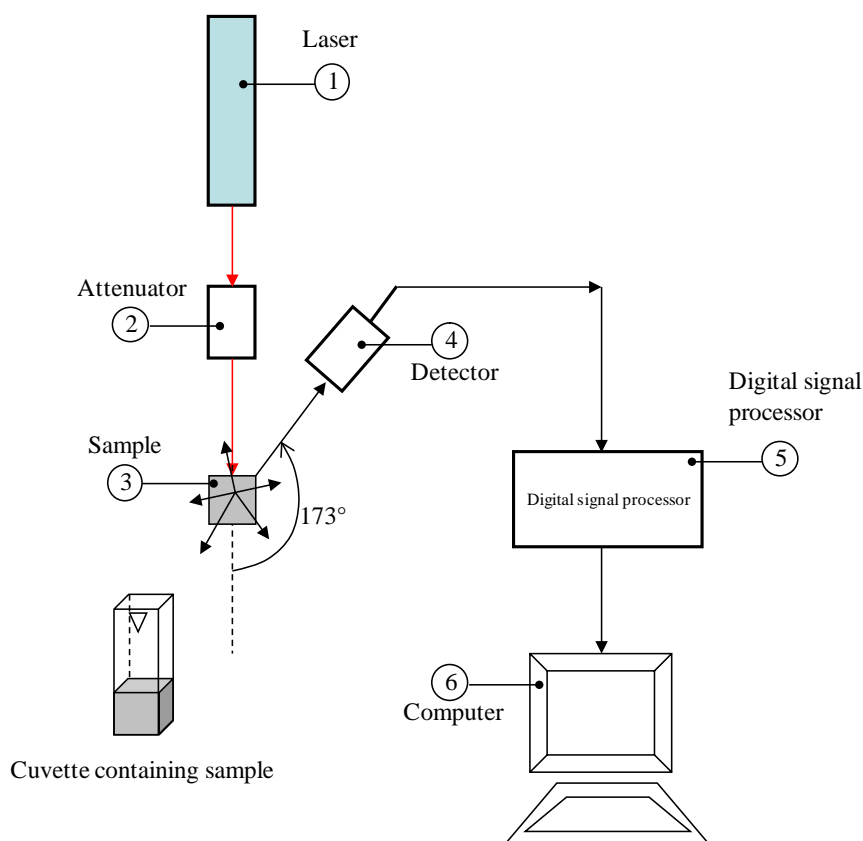


Figure 2.7. Components of Dynamic light scattering instrument in Zetasizer Nano ZS (Malvern instruments Inc., UK). Laser wavelength is of 633 nm. Attenuator (2) reduces the intensity of laser when the detector (4) becomes overloaded. Detector locates at a standard position of 173° from the laser beam. Digital signal processor (5) compares the intensity of scattering light at successive time intervals and deduces the rate at which the intensity varies. Signals will be sent to computer (6), where the data will be treated to give information about hydrodynamic size of particles.

TiO₂ particles measurements

Hydrodynamic size of TiO₂ in aqueous suspension was measured at different pH points (2, 5 and 9) in the presence of NaCl 0.01M. 2 mL of samples were placed in a square disposable polystyrene cuvette and left in sample chamber two minutes for equilibrium at 25°C before running the measurement. Repeatability of results was verified by at least 2 aliquots at each pH point and 3 measurements were carried out for each aliquot. All experiments were conducted at room conditions (25°C and atmospheric pressure). The refractive index of TiO₂ was taken from literature,⁸ that for rutile is 2.9, that of anatase is 2.49. The refractive index value for P25 was set at 2.54, taking into account that P25 consists in a mixture of 86% anatase and 16% rutile). The mathematical algorithm used to convert the autocorrelation function in diameter distribution is the NNLS algorithm available in Malvern software.

Vesicle size measurements

Dynamic light scattering (DLS) and electron microscope are both popular techniques applied to measure size of lipid vesicles.⁹ Nevertheless, DLS is more preferable because it is noninvasive to fragile vesicles and quite easy for implementation.

Phospholipids vesicles size measurements were conducted soon after the extrusion process. The concentration of phospholipids at this stage is about 0.125 mg.mL⁻¹ in the absence of NaCl at pH~6. 2 mL of samples were placed in a square disposable polystyrene cuvette and analyzed at 25 °C. Time for equilibrium in the sample chamber was two minutes. The refractive index was assumed 1.43.¹⁰ As for TiO₂ particles, data were treated with Malvern software.

2.3.9 Laser Doppler Electrophoresis (LDE)

This thesis uses LDE to measure the zeta potential of TiO₂ particles and phospholipids vesicles in aqueous dispersion. Hence, it is useful to remind briefly the theory behind this technique in order to facilitate the interpretation of the obtained results. LDE technique is also named laser Doppler velocimetry. The principle of this technique is based on electrophoresis phenomenon. Charged particles moving in an applied electric field are illuminated by a laser beam which allows the measurement of their velocity. Indeed, the movement of particles causes the shift in frequency of scattering light. A detector measures this shift, and thus calculates the electrophoretic mobility of particles, which is the ratio between their velocity and the intensity of the electrical field. Zeta potential can be deduced from Henry equation using Smoluchowski approximation:

$$\zeta = \frac{\mu U}{\varepsilon}$$

Where

- ζ is the zeta potential (mV)
- μ is the dynamic viscosity of the medium (kg.m⁻¹.s⁻¹)
- U is the electrophoretic mobility of the particles (m².V⁻¹.s⁻¹)
- ε is the electric permittivity of the medium (C².N⁻¹.m⁻²)

It is worth noting that the zeta potential not exactly reflects the surface charge of particles, as it is the electrostatic potential measured at the slipping plane. The slipping plane

is usually considered as the frontier between Stern layer and Gouy layer, according to the electrical double layer model.¹¹

Polycarbonate capillary cells (Figure 2.8) were used for the zeta potential measurements, which were carried out with two aliquots of samples at the same pH point, and 3 measurements for each aliquot, to verify the repeatability. The experiments were conducted at room conditions (25°C and atmospheric pressure). In order to conduct successful zeta potential measurements, there are a few precautions that must be taken into account. Firstly, the capillary of the cells must be rinsed thoroughly with ethanol to wet the inner cell surface, then they must be washed several times with ultra-pure water to remove ethanol. Secondly, it is necessary to rinse the capillary a few times with the sample before filling slowly the cell with 2 mL of sample for measurements (at required pH and ionic strength). Caution must be taken to insure there are no bubbles in the cell and the electrodes are completely immersed in the sample suspension. Finally, the ports of the cell must be closed by two stoppers. Then, the cell was placed in the sample chamber, left two minutes for equilibrium at 25°C before running measurements. Data were treated by software supplied by Malvern Instruments Inc., and the validity of each measurement was verified through the phase plots relative to Doppler Effect.

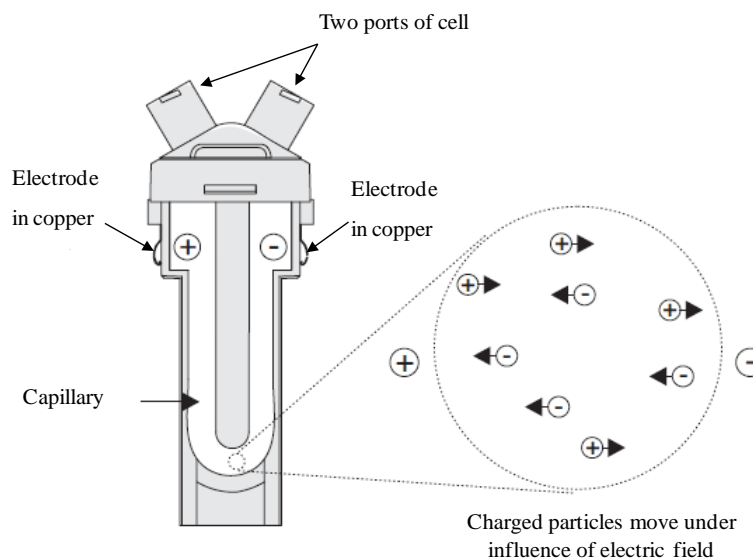


Figure 2.8. Folded capillary cell used for zeta potential measurement.

Zeta potential measurements of TiO₂ suspensions

Zeta potential of TiO₂ in aqueous suspension (0.1 g.L⁻¹) was measured according to pH, for various ionic strengths, fixed by NaCl. The suspension was continuously stirred during these measurements, and protected from light by aluminum foil. Moreover, contact of

the suspension with air was limited by paraffin film deposited on the suspension container, in order to avoid formation of carbonates. As carbonates are mainly present in solution in basic medium, we chose to begin zeta potential measurements at acidic pH. So first, HCl solution (0.25 mol.L^{-1}) was added to reach pH 2. Then NaOH solution (0.25 mol.L^{-1}) was progressively added in order to increase pH until 10. For each pH value, the suspension was let equilibrate for a few minutes, until pH does not vary anymore. Then, an aliquot of the suspension was introduced in the cell for zeta potential measurement.

Zeta potential measurements of phospholipid vesicles

After the size measurement, the phospholipids dispersions were diluted with NaCl solution to control ionic strength. The concentration of phospholipids in the final dispersion was about 0.04 mg.mL^{-1} and that of NaCl was 0.01 M. These suspensions were magnetically stirred for 15 minutes. Similarly to TiO_2 suspension, pH of phospholipids suspensions was adjusted by adding NaOH or HCl solutions. At each pH point, suspensions were left stirring for at least 5 minutes for equilibrium before taking aliquots for measurements.

Zeta potential measurements of TiO_2 particles in contact with phospholipid molecules

Zeta potential measurements for mixtures of TiO_2 with some molecules were also performed to investigate the effect of phospholipid molecules on surface properties of TiO_2 particles through analyzing zeta potential. Samples were prepared by mixing a suspension of TiO_2 with one of phospholipids, so that the density of molecules on the surface of TiO_2 is $0.5 \text{ molecule/nm}^2$. Samples for these measurements were prepared a little differently from those of TiO_2 suspensions or phospholipids. There are three steps to prepare the mixture samples. Firstly, 100 mL of TiO_2 suspension was prepared by the previous method (see 2.2.2) with the same concentration 0.1 g/L . Secondly, a suitable amount of phospholipids was dispersed in 2 mL of ultra pure water to ensure that the number of phospholipid molecules in the mixture is about $0.5 \text{ molecules/nm}^2$ of TiO_2 . The suspension of phospholipids was bath sonicated about 20 minutes at temperature higher than the corresponding transition temperature of phospholipids (see Table 2.1) in order to get a quasi-transparent suspension. Finally, the phospholipid suspension was mixed with the TiO_2 one. Then, the mixture was shaken during 2 minutes and stirred at room condition for two hours to make sure that the adsorption process gets equilibrium state. Zeta potential measurements were carried out at each pH point, from 2 to 10. The pH value of this suspension was adjusted by NaOH or HCl solutions. In this particular case, the glass beakers containing these mixture suspensions were carefully covered by aluminum foil to prohibit the activation of TiO_2 photocatalytic activity, which can potentially decompose phospholipid molecules under ultraviolet radiation.

2.3.10 Langmuir films

Monolayers of phospholipids (so-called Langmuir films) were prepared at the interfaces water/air, and TiO_2 suspension/air on a Langmuir trough (model 302LL, Nima Technology, UK). The Langmuir trough was placed on an anti-vibrating table far from natural light. The trough ($30 \times 10 \text{ cm}^2$) was in polytetrafluoroethylene, a chemically inert and hydrophobic material. The liquid (water or buffer) that fills the trough is called the subphase. The trough was equipped with two movable barriers and a pressure sensor (Figure 2.9).

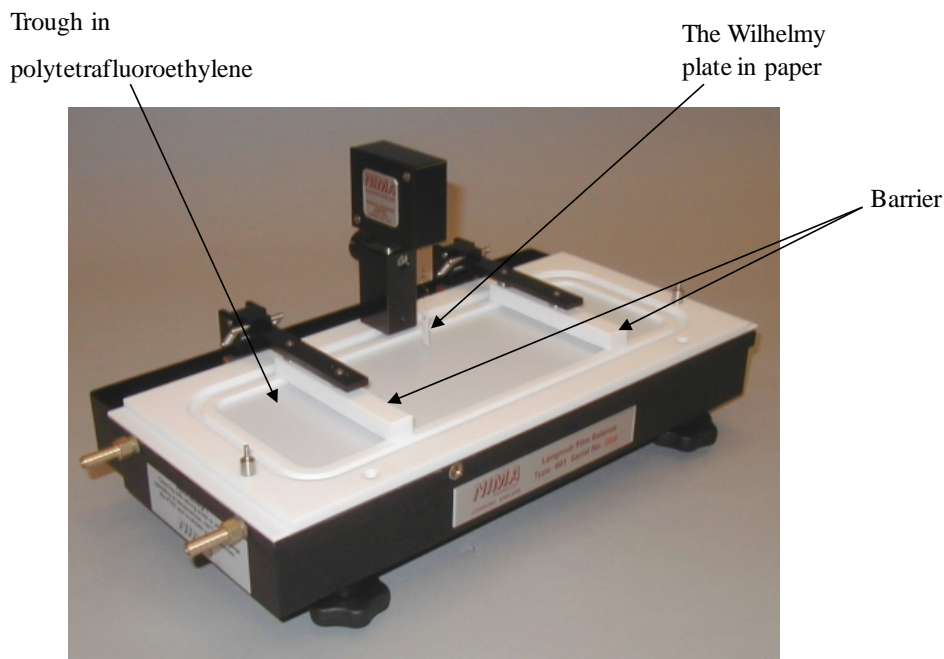


Figure 2.9. Langmuir trough and its components.

A step-by-step motor controls the gliding of the barriers at the top of the subphase. The calibration (linking the steps and the length between barriers) allows defining the area between barriers and later on the area available for spreading molecules. As regards the pressure sensor, it is composed of an electrobalance on which is hanged a filter paper (ashless Whatman chromatography paper from Whatman International Ltd, Maidstone, Kent, UK). Placed at the top of the surface, the wet filter paper works like a Wilhelmy plate that is highly sensitive to the presence of molecules at the surface. The pressure sensor is calibrated with a weight of 100 mg (slope) and the Y-intercept is the value of the surface tension measured on pure water in the operating conditions. This value is named γ_0 and equals 72.0 mN/m at 298 K and 1 atm.¹² In the same conditions, the surface tensions of subphases containing TiO_2 particles were found identical to pure water. The software calculates automatically the film pressure that corresponds to the difference between the surface tension of the interface free of

molecules and the interface covered by the molecule film. Film pressure, defined as $\pi = \gamma_o - \gamma$ was measured with an accuracy of 0.2 mN/m. The plot that describes the relationship between surface pressure and area available per molecule at a given temperature is known as the pressure-area isotherm, or surface pressure-area isotherm or isotherm of compression or π -A isotherm.

The surface tension is measured from the forces acting upon the plate (Figure 2.10). They consist in the gravity downwards and the surface tension downwards and the buoyancy due to displaced water upward. For a rectangular plate of dimensions l , w and t , of density ρ_p , immersed to a depth d in a liquid of density ρ_s , the net downward force (F) is given by the following equation:

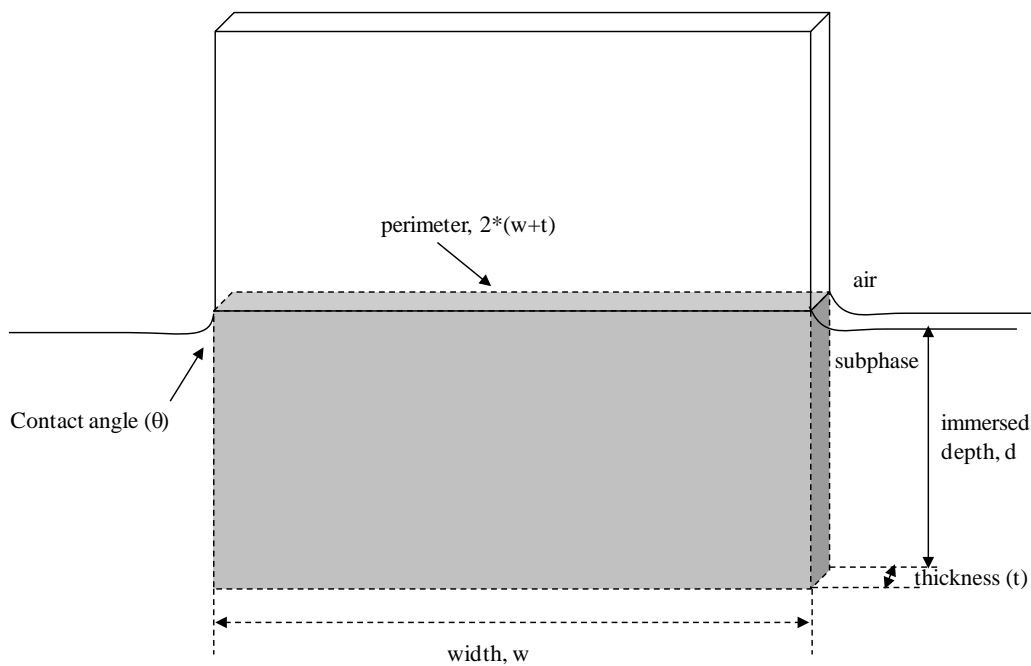


Figure 2.10. A Wilhelmy plate immersed in subphase to measure surface pressure

$$F = (\rho_p l w t) \cdot g - (\rho_s d w t) \cdot g + 2 \cdot (w + t) \cdot \gamma \cdot \cos \theta \quad (1)$$

where g is the gravitational acceleration, θ is the contact angle and γ the surface tension.

During the compression process, surface tension changes but the position of the plate is constant so that the difference between the free surface and the surface covered is given by:

$$\Delta F = 2 \cdot (w + t) \cdot (\gamma_o - \gamma) \cdot \cos \theta \quad (3)$$

Assuming the plate, made of chromatographic paper, is totally wet by the subphase, then $\theta = 0^\circ$.

We have: $\Delta F = 2.(w+t).(\gamma_0 - \gamma)$ (4)

Hence, film pressure deduced by $\pi = \gamma_o - \gamma = \frac{(\Delta F)}{2.(w+t)}$ (mN/m) (6)

As the number of lipid molecules (N) spread at the air-water interface and the surface available (S) between two barriers are known, area per molecule (A) is calculated:

$$A = \frac{N}{S} \text{ (molecule/\AA}^2\text{)} \text{ (7)}$$

Cleanliness is the key to conduct successfully the experiments with Langmuir film balance. The fabrication of a lipid monolayer consists in several steps:

- Careful cleaning of the trough under water and surfactant solution.
- Rinsing under distilled water until observing pearls of water on Teflon.
- Filling the trough with subphase (a volume of about 330 ml of ultra-pure water, or aqueous suspension of TiO₂ particles at a given ionic strength and pH).
- Placing the filter paper at the top of the liquid surface and setting the pressure at zero value.
- Spreading dropwise 22 μ l phospholipids solution in CHCl₃ (0.22 mg/mL) onto the surface of subphase and wait 20 minutes for the full evaporation of CHCl₃.
- Recording the pressure-area isotherm.

The volume was chosen to obtain the full π -A isotherm from zero pressure to the collapse. The temperature room was fixed at 20 °C and the temperature of the Langmuir balance was controlled thermostatically by a circulating water system set at 25°C.

2.3.11 Phosphorus dosage/isotherms of adsorption

In order to determine the amount of phospholipid molecules (DMPA and DMPG) adsorbed on the surface of TiO₂ (anatase or rutile), adsorption isotherms were conducted. A known mass of solid was put in contact with 10 mL of solution containing the phospholipid molecules to adsorb, with a known initial concentration C_i and with pH adjusted at 2 or 9. The suspensions were stirred during one night in order to be sure that equilibrium was reached, at a fixed temperature of 25°C (Memmert oven). Then, solid and liquid phases were separated through centrifugation at 5700 rpm during 20 minutes. At last, the final concentration C_f of phospholipid molecules was measured in the liquid phase. The same

experiment was repeated for several values of C_i . The final concentration of phospholipids was used to calculate the amount of adsorbed molecules, by subtraction from the initial concentration. The evolution of the adsorbed amount versus equilibrium concentration (C_f) is called “adsorption isotherm”. In this work, we chose to draw the adsorbed amount versus initial concentration, in order to depict more easily what occurs at low concentrations.

Phospholipids concentration was determined based on the phosphorus dosage method coupled with the calcination procedure for organic phosphate compounds (Figure 2.11). This protocol was well established in literature,¹³ and was performed in the Chemistry and Interdisciplinary laboratory (CEISAM) of Nantes University. The procedure leading to free phosphate ions in the solution consists in two steps. Firstly, phospholipid samples were mixed with magnesium nitrate solution $Mg(NO_3)_2 \cdot 6H_2O$ in a special glass test tube and heated to dryness under high temperature of flame (fueled by butane). This step takes a few seconds until the disappearance of brown fumes (NO_2). Secondly, the tubes were left to cool down to room temperature. Then they were added with HCl solution, capped and then maintained in a water bath at $90^\circ C$ for 15 minutes in order to hydrolyze any pyrophosphate formed during the calcination step. Finally, the phosphate amount in these tubes can be determined following the inorganic phosphate dosage method. This method lies in the development of blue color of the phosphomolybdate complex $PMo_4^V Mo_8^{VI} O_{40}^{7-}$ in the presence of a reducing agent such as ascorbic acid,¹⁴ which is examined by UV-Vis spectrophotometer. The absorbance, recorded at a wavelength of 820 nm, is proportional to the phosphate concentration up to at least 1.8 according to Beer-Lambert law. A calibration curve is established with phospholipid solutions to determine the concentration of phosphate in the samples. This method can easily determine down to $0.01 \mu mol/L$ of phosphate.¹³

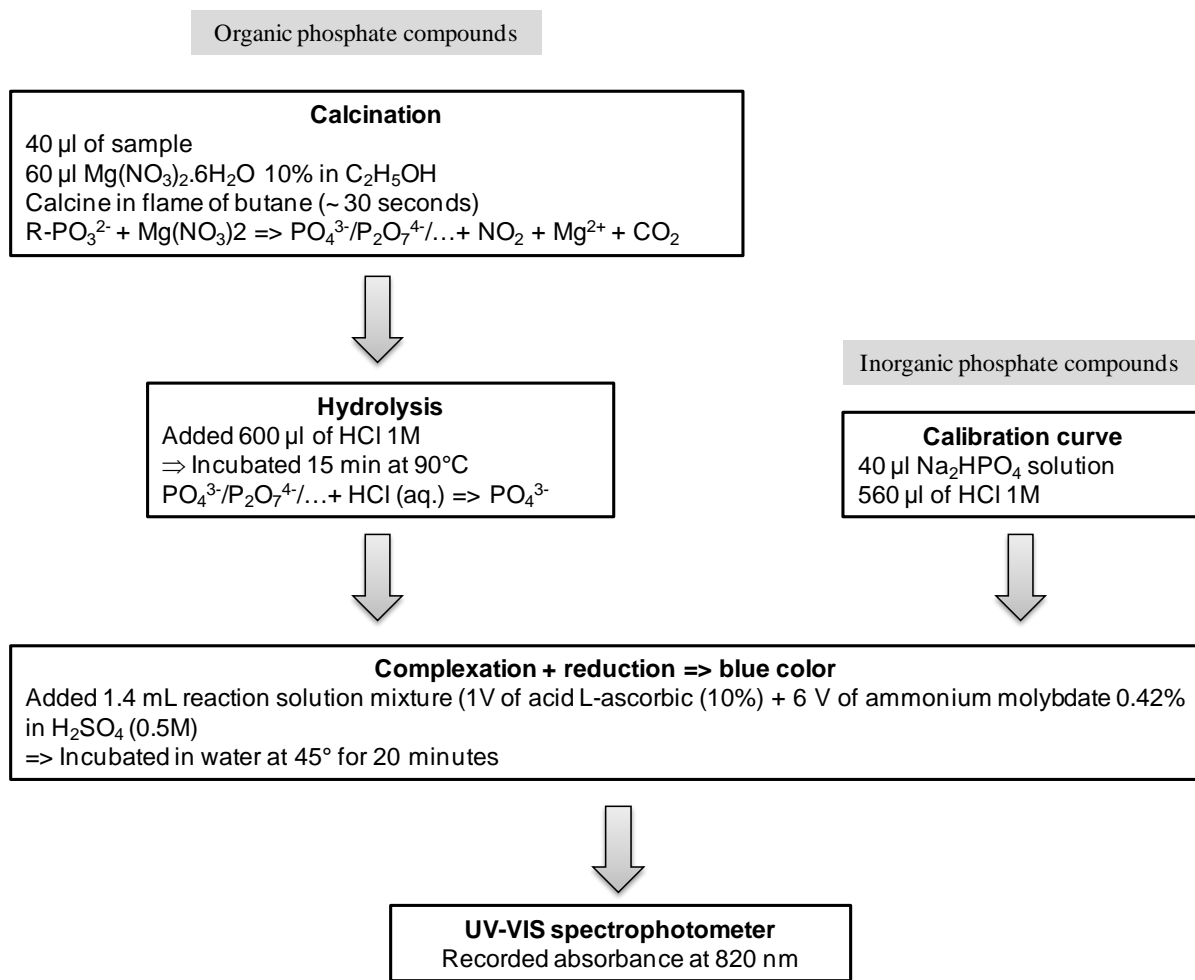


Figure 2.11. Diagram show the procedure to determine concentration of phospholipids samples in suspension

2.4 Materials characterization

2.4.1 TiO₂

2.4.1.1 Crystallinity

The indexation of X-ray diffraction (XRD) patterns (Figure 2.12) indicated that TiO₂-P25 is a mixture of anatase and rutile. The others, TiO₂-A, TiO₂-PC10, TiO₂-PC50 and TiO₂-PC100 are pure anatase, while TiO₂-R is pure rutile.

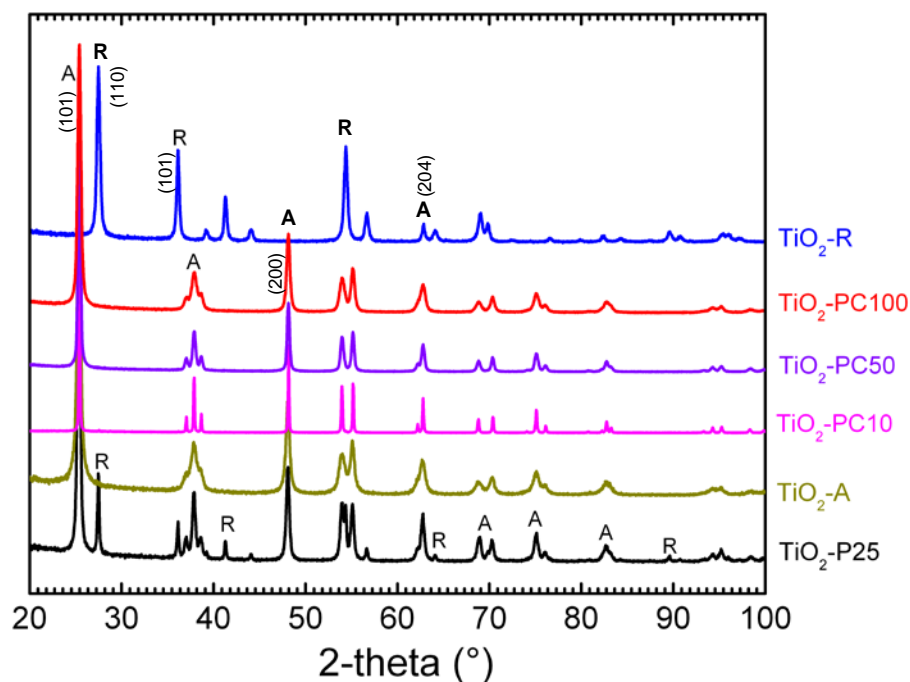


Figure 2.12. Diffractograms of different commercial TiO_2 powders. Values of 2θ are from 20° to 100° , with step angle 0.03° , step time of 5 s at room condition.

The composition of TiO_2 -P25 was determined by Rietveld refinement method. It contains approximately $85 (\pm 6) \%$ of anatase and $15 (\pm 2) \%$ of rutile. These findings are in accordance with literature.¹⁵⁻²⁰ According to literature, TiO_2 -P25 particles also contain a small amount of amorphous phase in variable amounts according to the synthesis process.^{20,21} The presence of amorphous phase was actually observed on TiO_2 -P25 particles under TEM (Figure 2.13). This phase is only present on particle edges. It was difficult to quantify the relative proportion of this phase, but it may intervene in the chemical interfacial process.

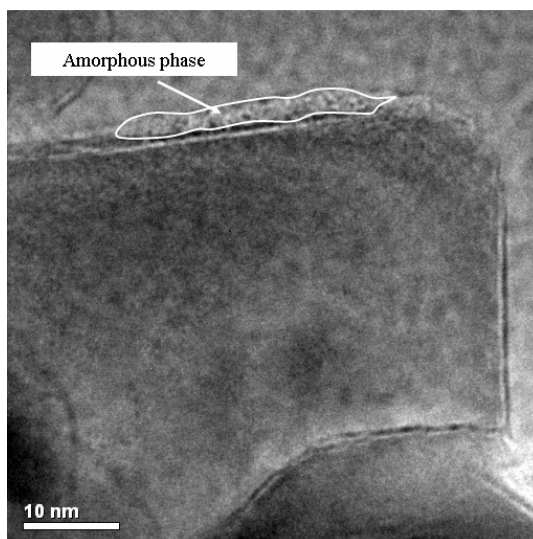


Figure 2.13. TEM image of a TiO₂-P25 particle indicating the presence of amorphous phase in this material.

Raman spectroscopy was another alternative technique to provide a qualitative information on the crystalline phase of TiO₂.²² The spectra of all commercial TiO₂ powders are displayed in Figure 2.14 – 16. The assignments of bands are in agreement with the structure evidenced by XRD.

TiO₂-R is pure rutile phase (Figure 2.14), in agreement with X-ray pattern analyses. Group theoretical analysis indicated that there are four Raman active modes of rutile: A_{1g} (612 cm⁻¹), B_{1g} (144 cm⁻¹), B_{2g} (827 cm⁻¹) and E_g (448 cm⁻¹).²³ In this study, TiO₂-R exhibits the major peaks at 144 cm⁻¹, 235 cm⁻¹, 449 cm⁻¹ and 610 cm⁻¹. Spectra did not show any peak at 827 cm⁻¹, the signal was too weak. The presence of broad peak at 235 cm⁻¹ in accordance with literature²³⁻²⁶ was assigned a two-phonon signal.

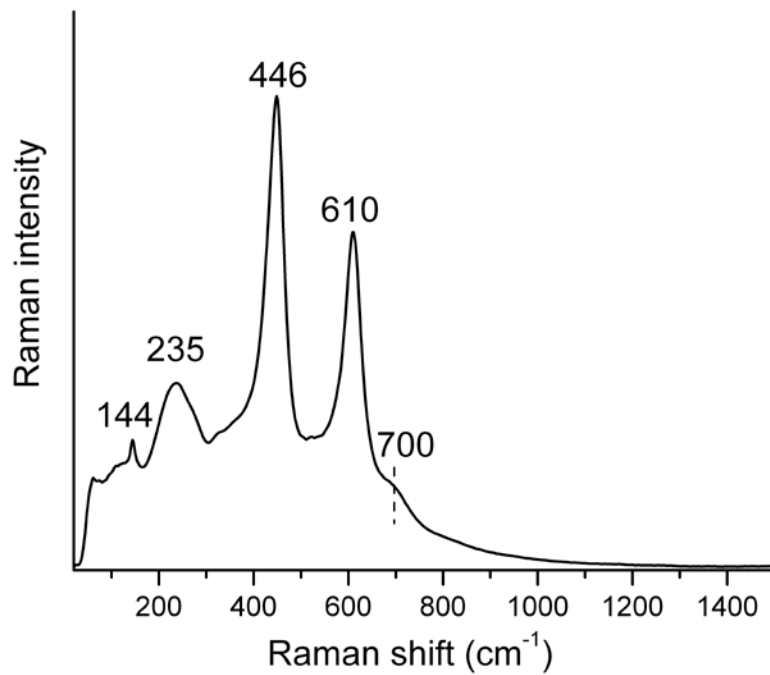


Figure 2.14. Raman spectra of commercial TiO₂-R powder.

The Raman spectra of TiO₂-A and TiO₂-PC revealed that they are pure anatase phase (Figure 2.15). Anatase unit cell displays six modes that are Raman active: A_{1g} (515 cm⁻¹), 2B_{1g} (398 and 515 cm⁻¹), 3E_g (147, 198, and 640 cm⁻¹).²³ Experimentally, they were observed at 144 cm⁻¹, 198 cm⁻¹, 396 cm⁻¹, 516 cm⁻¹ and 640 cm⁻¹. The broad peak with a low intensity at 797 cm⁻¹ corresponds to the overtone of vibration mode B_{1g} (398 cm⁻¹).

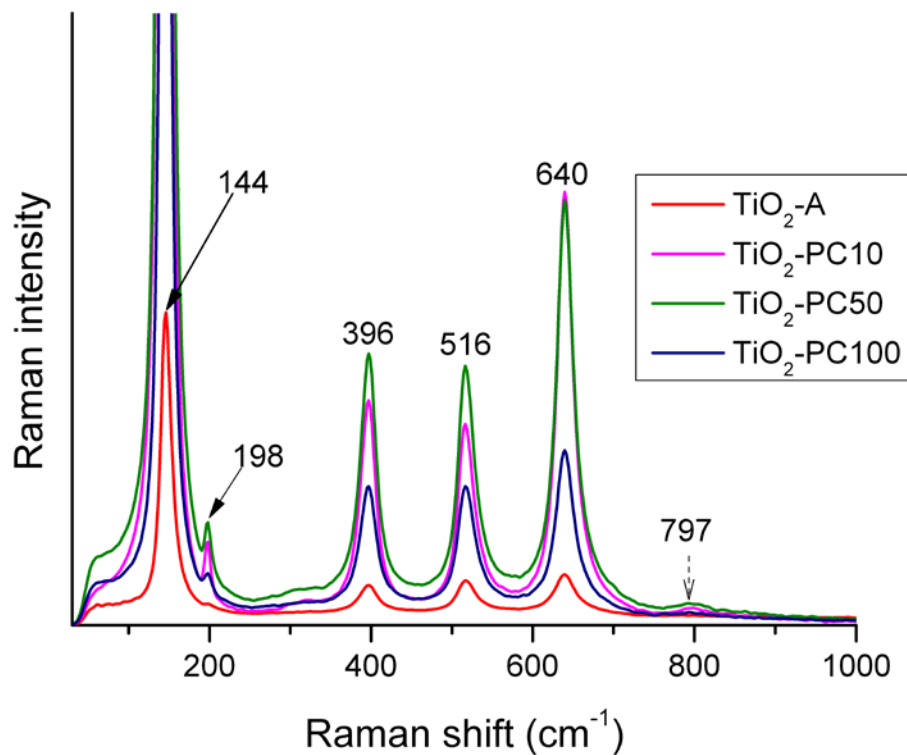


Figure 2.15. Raman spectra of different Anatase commercial powders.

The Raman spectrum of TiO₂-P25 clearly shows the major peaks associated to the anatase and rutile forms (Figure 2.16). Regarding to TiO₂-P25, the bands relative to anatase are clearly seen and only the intense bands relative to rutile can be seen (449 cm⁻¹) as documented in literature.^{27,28} Rutile peak at 610 cm⁻¹ is not clearly identified. It is probably overlapped by the strong peak from anatase (640 cm⁻¹).²⁶

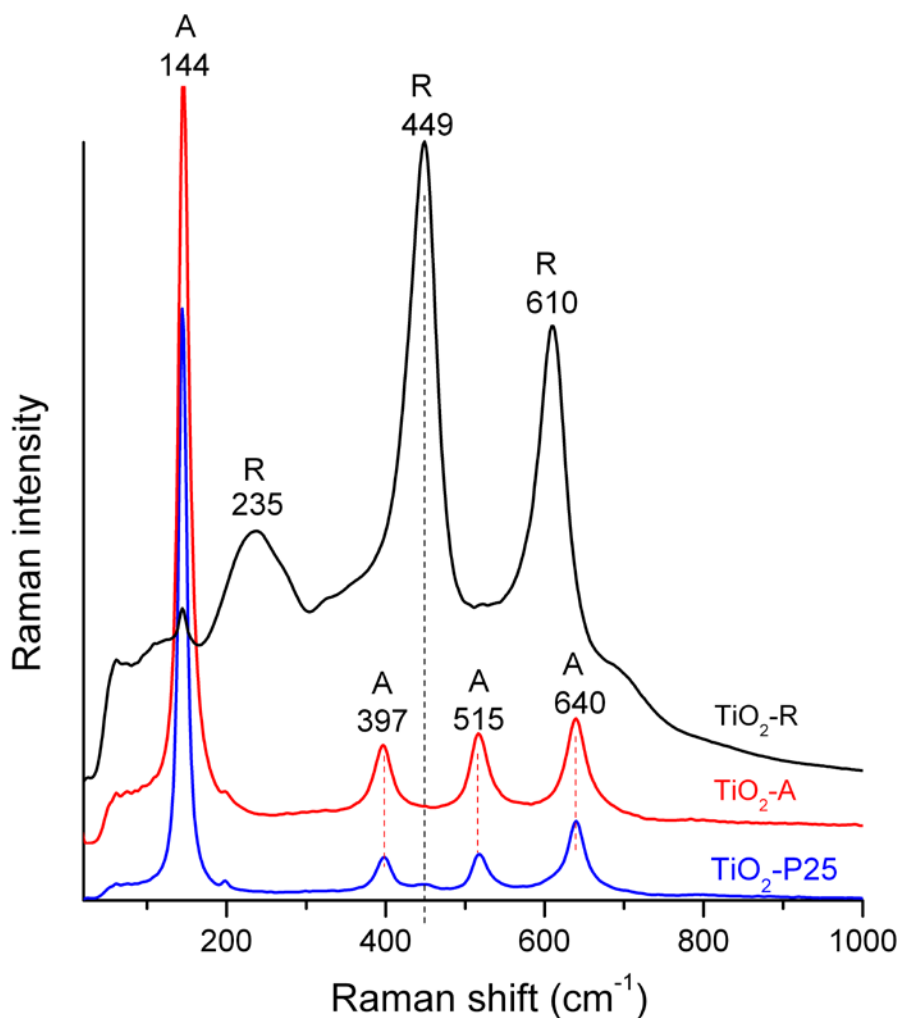


Figure 2.16. Raman spectra of TiO₂-P25 in comparison with that of TiO₂-A and TiO₂-R

2.4.2 Morphology and textural properties of TiO₂

TiO₂-P25

TEM images of TiO₂-P25 were displayed in Figure 2.17 and Figure 2.18. The result shows that anatase and rutile particles in TiO₂-P25 powders exist separately (Figure 2.17a). There are small particles of anatase (from 20 to 30 nm) and the bigger particles of rutile (from 40 to 65 nm). These findings are in agreement with literature data.²⁰ Calculation by Scherrer equation²⁹ executed on EVA software (from Bruker-AXS), indicated that the average size of TiO₂-P25 particles is around 25 nm.

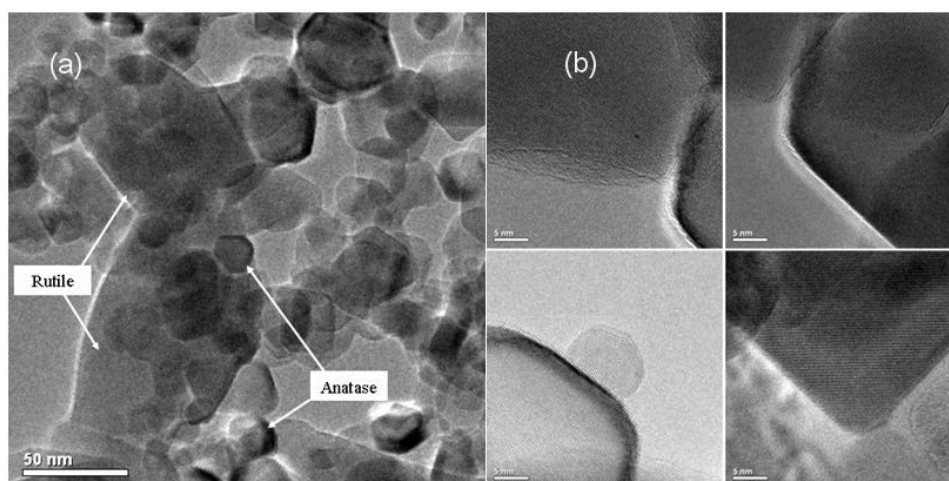


Figure 2.17. TEM images of TiO₂-P25 at (a) low magnification scale where the presence of small particle of anatase and bigger particles of rutile phase are identified and (b) high magnification scale to see highly crystalline particles.

The random orientation of particles in samples makes difficult to confirm the morphology of anatase and rutile in TiO₂-P25. High resolution TEM was performed on anatase and rutile particles contained in TiO₂-P25 (Figure 2.18). The distance of 0.35 nm between parallel fringes corresponds to the interplanar spacing of (101) faces on anatase structure.^{30,31} Besides, the distance of 0.32 nm corresponds to the interplanar spacing of (110) of rutile structure.³² However, this information was not achievable to all particles due to the random orientation of particles relative to the electron beam direction. The dominant face (110) of rutile and (101) of anatase crystal was observed, in accordance with literature.³³

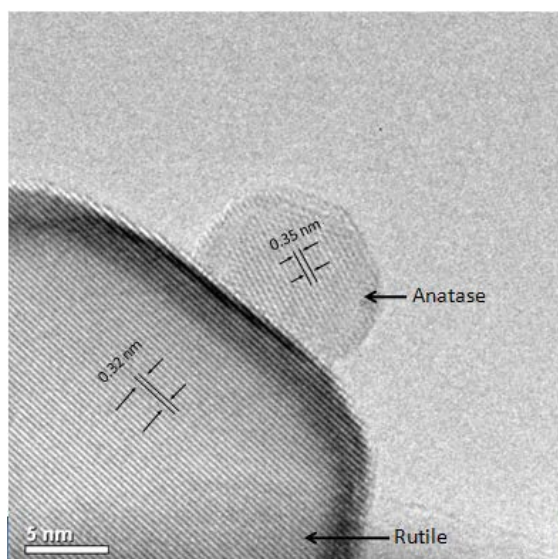


Figure 2.18. TEM image of $\text{TiO}_2\text{-P25}$ at high resolution indicated the presence of anatase and rutile particles. The 0.35 nm distance between parallel fringes corresponds to the interplanar spacing of (101) faces of anatase particles.^{30,31} And the 0.32 nm fringes pattern corresponds to the interplanar spacing of (110) of rutile particles.³²

$\text{TiO}_2\text{-A}$

Particle average diameter of $\text{TiO}_2\text{-A}$ particles ranges from 10 to 20 nm (Figure 2.19). The powder is a mixture of small and big particles. The smaller particles have an average diameter size of around 10 nm, whereas that of the bigger is about 20 nm. Calculation by Scherrer equation results in an average size of $\text{TiO}_2\text{-A}$ crystallites of about 18 nm.

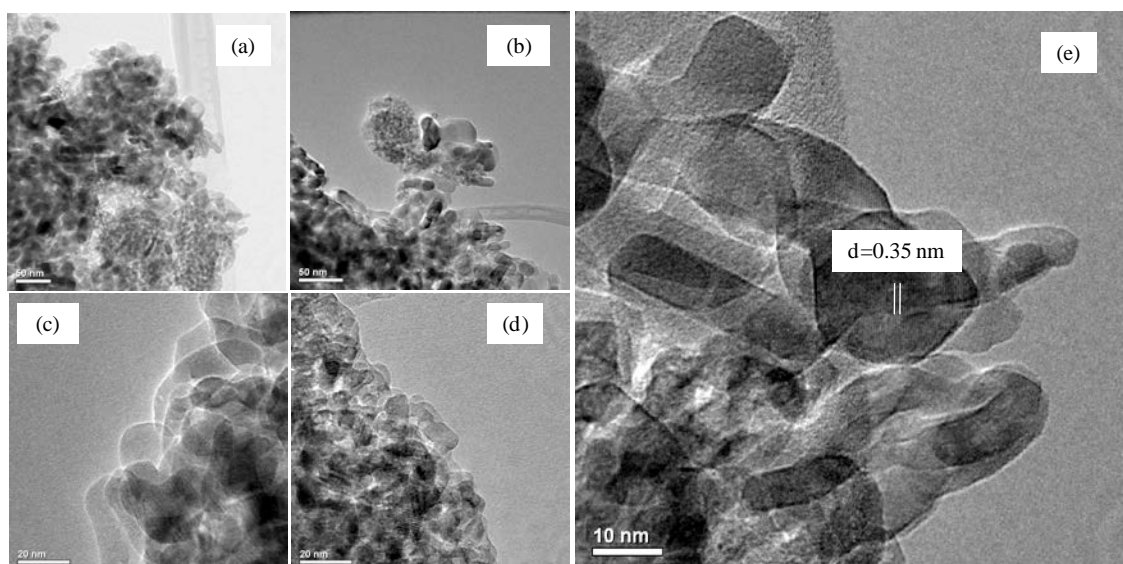


Figure 2.19. TEM images of $\text{TiO}_2\text{-A}$ particles. The lattice fringes distance in (e) is 0.35 nm, corresponding to the distance between (101) planes of anatase.

TiO₂-R

Average diameter size of TiO₂-R particles ranges from 20 to 40 nm (Figure 2.20), which is larger than that of TiO₂-A. Average crystallite size given by Scherrer equation is about 22 nm. Rutile particles with a rod-like shape (average 25 x 60 nm) are observed. They are very highly crystallized, and the distance between two planes on particles is approximately 0.32 nm (Figure 2.20 e), corresponding to distance between planes (110) of rutile crystal. This plane is also present in rutile of TiO₂-P25.

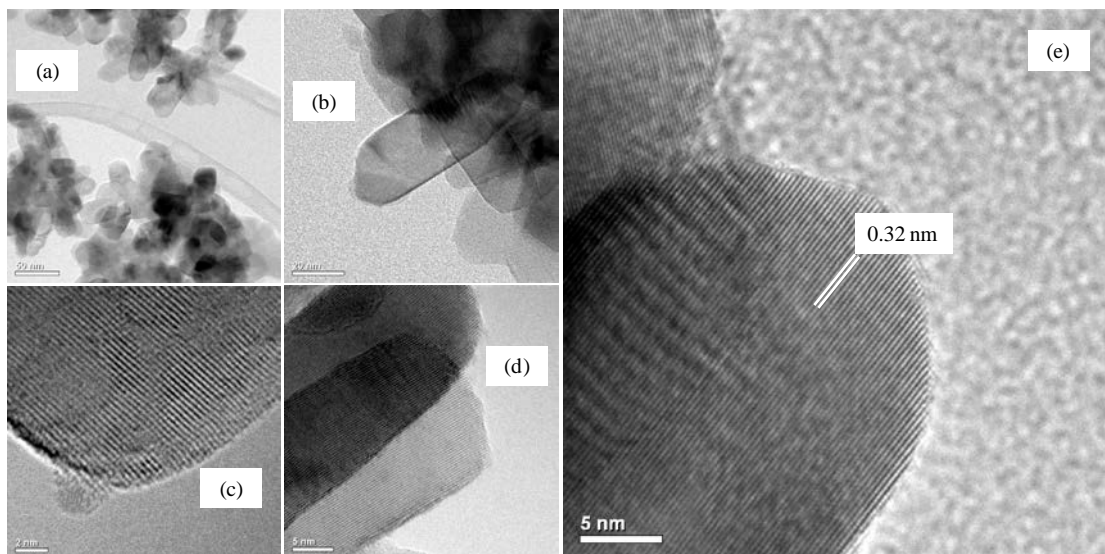


Figure 2.20. TEM images of TiO₂-R particles. The distance between fringes in (e) is 0.32 nm, corresponding to the distance between plane (110) of rutile crystal.

TiO₂-PC

The size of TiO₂-PC10 particles is very heterogeneous (Figure 2.21). The powder consists of small particles (~50 nm) and bigger particles (~100 nm or larger). TiO₂-PC10 particles seem to not contain amorphous phases because the edge of particles is very sharp and clean (Figure 2.21e). Scherrer equation estimated that average size of TiO₂-PC10 is around 72 nm.

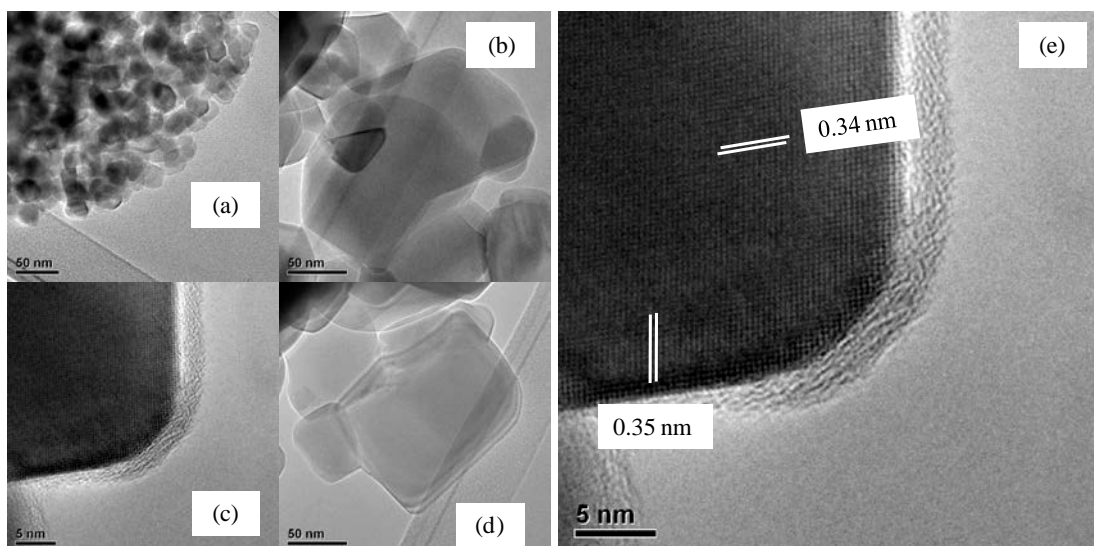


Figure 2.21. TEM images of TiO₂-PC10 particles. The 0.35 nm spacing corresponds to the distance between (101) planes in anatase crystal.

TiO₂-PC50 powder is more homogeneous in particle size than TiO₂-PC10. Indeed the particle diameter ranges from 25 to 35 nm. TiO₂-PC50 particles contain amorphous phase, which appears on the edges of particles (Figure 2.22 c). There are patches on surface of particles (Figure 2.22 b), which are probably amorphous phase formed during the crystallization process. Scherrer equation gave an average size of TiO₂-PC50 around 30 nm.

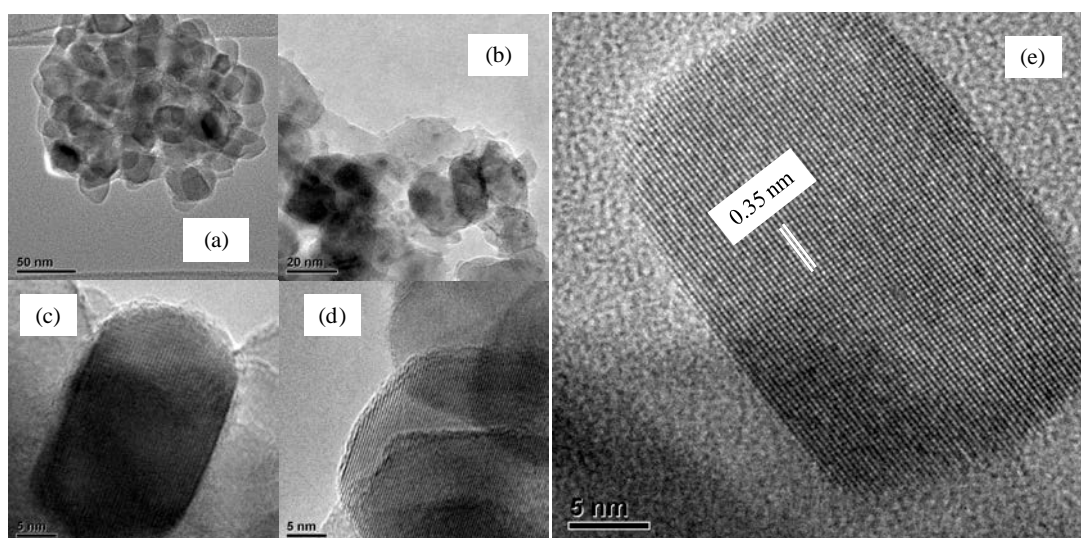


Figure 2.22. TEM images of TiO₂-PC50 particles. The spacing between planes in (e) is 0.35 nm, is the distance between (101) planes in anatase crystal.

TiO₂-PC100 particles have the smallest average size among anatase powders investigated in this work, approximately between 10 to 25 nm (Figure 2.23). The particles are

well crystallized and do not show the presence of amorphous phase. Applying Scherrer equation, the average size of TiO₂-PC100 particles is about 22 nm.

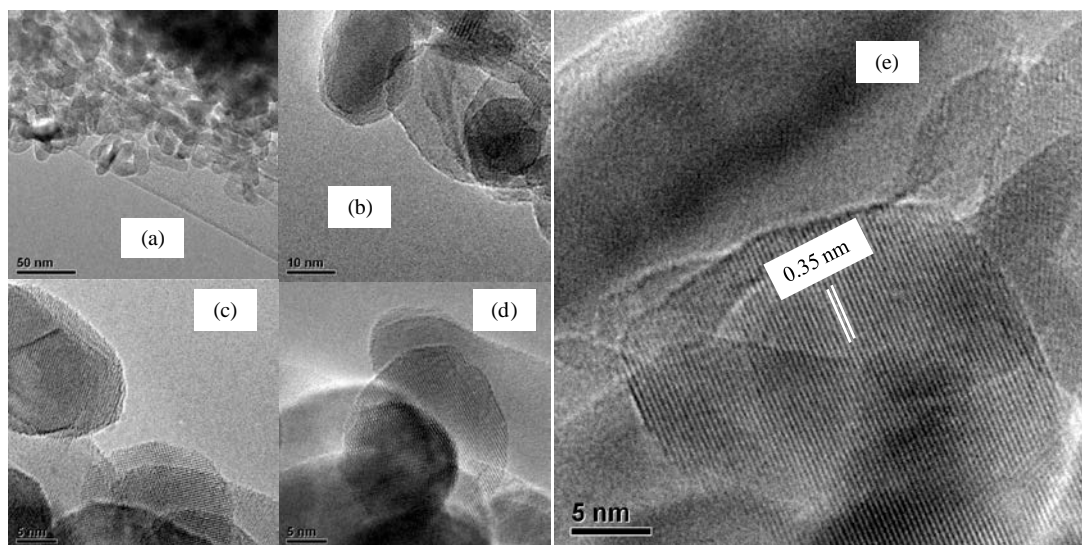


Figure 2.23. TEM images of TiO₂-PC100 particles. The spacing between planes in (e) is 0.35 nm, corresponding to the distance between (101) planes in anatase crystal.

2.4.2.1 Specific surface area

Specific Surface Area (SSA) and porosity of TiO₂ powders were measured and analyzed through gas adsorption experiments. Smaller size particles show higher specific area and vice versa. TiO₂-A particles having the smallest size, they possess the highest specific surface area of 136 m²/g. In contrast, TiO₂-PC10 has the biggest particle size bearing pores with the smallest diameter, thus it presents the lowest specific area of ~10 m²/g. SSA of TiO₂-P25 reported in literature varies from 42 to 60 m²/g.^{20,34-38} This current study found that SSA of TiO₂-P25 has a value of 48 m²/g, which is in agreement with literature. TiO₂-R particles have a SSA value of 26 m²/g. TiO₂-PC50 possesses almost the same SSA of TiO₂-P25, that is 48 m²/g. The agglomeration of particles create the pores between them. A summary related to specific surface area and pore of TiO₂ powders is reported in Table 2.2.

Table 2.2. Specific surface areas, average particle diameter and pore volume of TiO₂ particles as measured by BET with adsorption of N₂ at 77K.

Sample	BET Surface area (m ² /g)	Average pore diameter size (Å)	Pore volume (cm ³ /g)
TiO ₂ -P25	48 ± 0.1	70	0.085
TiO ₂ -A	136 ± 0.5	80	0.264
TiO ₂ -R	26 ± 0.06	10	0.064
TiO ₂ -PC10	9 ± 0.07	23	0.055
TiO ₂ -PC50	48 ± 0.09	20	0.253
TiO ₂ -PC100	75 ± 0.3	13	0.294

2.4.2.2 Surface chemistry by FT-IR

a) Native powders

The IR spectra of the pure TiO₂ powders collected in the diffuse reflectance mode are displayed Figure 2.24 in the spectral range 6000-1500 cm⁻¹. This spectral range is characteristic of three zones involving the O-H bonds:

- at first, the bending mode of adsorbed water molecules around 1600 cm⁻¹,
- secondly, the stretching modes of OH groups of either the Ti_x-O-H surface group or Ti-OH₂^{δ+} at the surface or yet adsorbed water between 2800 and 3800 cm⁻¹
- and at last, the combination modes (angular deformation + stretching) of specific Ti-O-H groups between 4000-4700 cm⁻¹ and of specific H₂O groups between 4800 and 5400 cm⁻¹

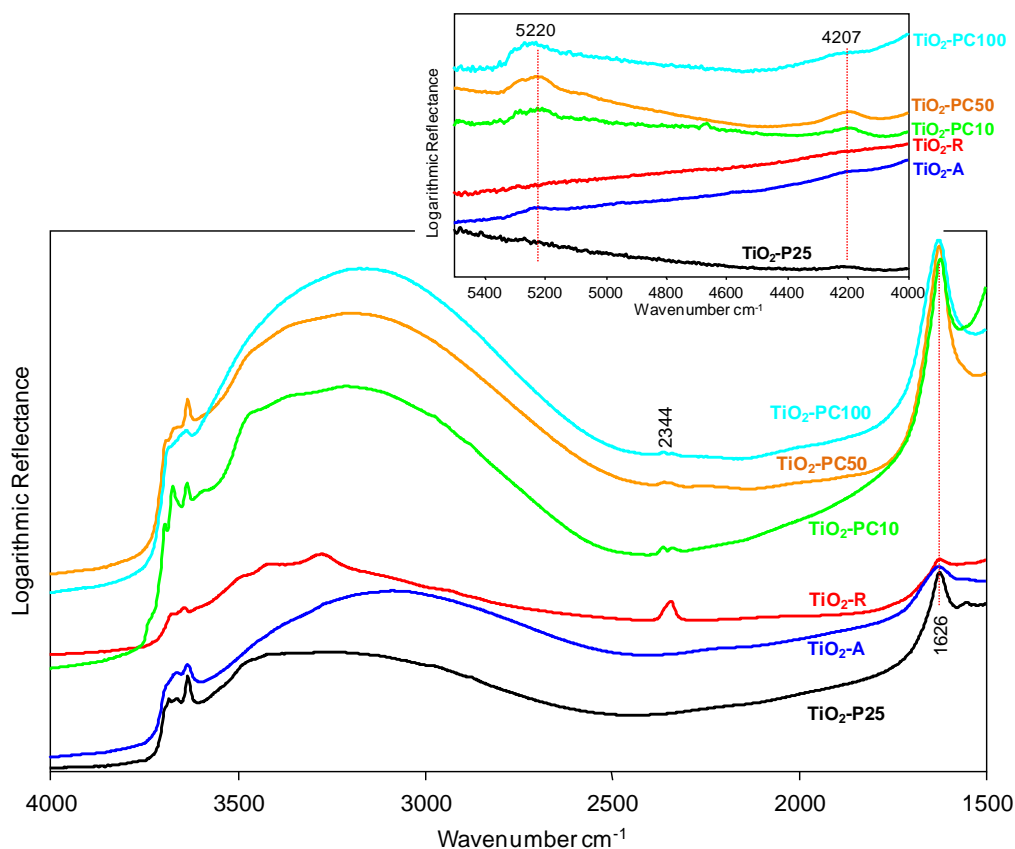


Figure 2.24. DRIFTS spectra of different TiO_2 commercial powders.

According to the literature, H_2O adsorbs onto TiO_2 surface either molecularly or dissociatively^{39,40} in order to obtain respectively the C_{2v} structures of H_2O or $\text{Ti-OH}_2^{\delta+}$ and the surfaces structures as Ti-O-H or Ti-OH-Ti .

Molecular sorption of H_2O is proved by the bending vibration mode of hydroxyl groups (1623 cm^{-1}) of H_2O ^{38,41} and the bands centered at 5220 cm^{-1} . All TiO_2 spectra contain signals characteristic of molecularly adsorbed water. The former band is present in all spectra of our samples (Figure 2.24). The second one is assigned to the combination of the bending of hydroxyl group (δ_{OH}) in molecular adsorbed H_2O and of the stretching of hydroxyl group (ν_{OH}) in H_2O molecules perturbed by H-bonds.⁴² The intensity of this second component shows clearly that $\text{TiO}_2\text{-P25}$, $\text{TiO}_2\text{-R}$ contain less molecularly adsorbed H_2O than the other powders.

Dissociative adsorption is characterized by the presence of OH groups (terminal or bridging OH groups) on the surface of TiO_2 . It is evidenced by bands in region ranging from 2500 cm^{-1} to 3750 cm^{-1} .^{37,43} However, this region is also overlapped with the stretching frequencies of hydroxyl groups of molecularly adsorbed H_2O .^{38,43,44} Our spectra that can be seen in more details in Figure 2.25 are interpreted according to the Minella's paper⁴¹.

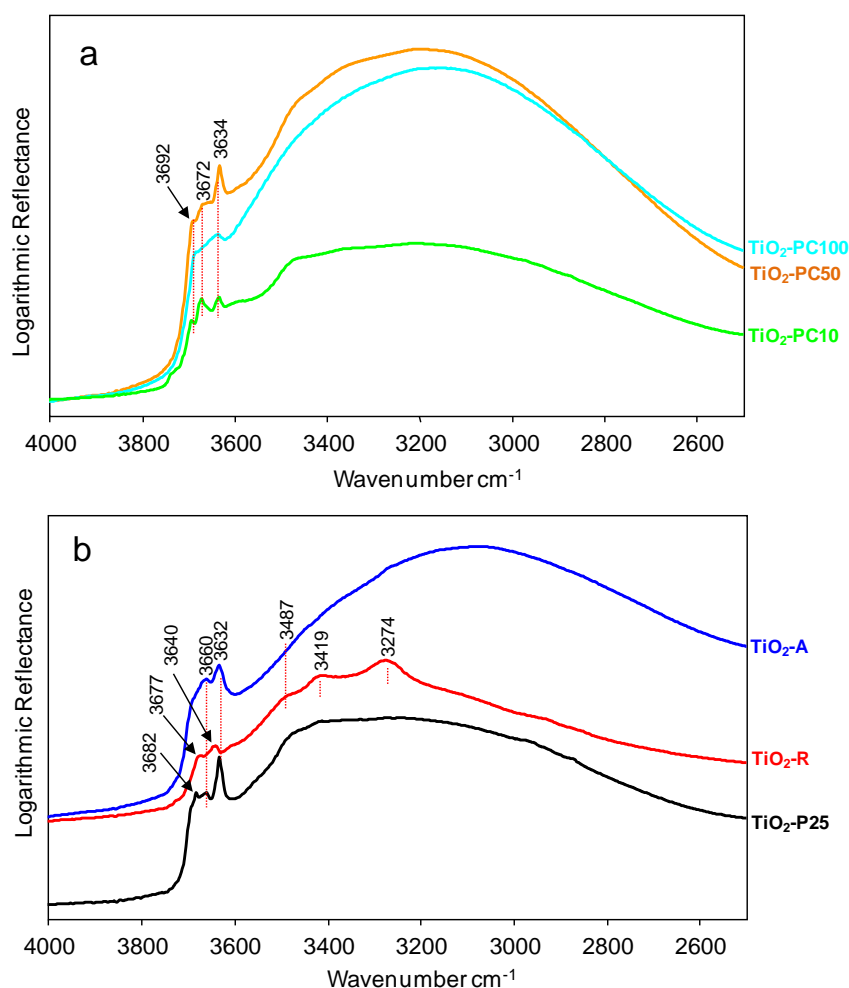


Figure 2.25. Surface state of commercial TiO_2 powders displayed by DRIFTS spectra at room condition.

At high frequency ($3550 - 3750 \text{ cm}^{-1}$) are the stretching modes of different free hydroxyl groups.⁴⁴ The stretching mode of terminal H-bond free OH groups is observed around $3680\text{-}3750 \text{ cm}^{-1}$ and that of bridging OH, H-bond free, is around $3550\text{-}3680 \text{ cm}^{-1}$.^{41,45} Figure 2.26 show spectra of $\text{TiO}_2\text{-R}$, $\text{TiO}_2\text{-A}$ in comparison with $\text{TiO}_2\text{-P25}$. Peaks at 3631 , 3659 and 3682 cm^{-1} are ascribed to terminal OH groups on $\text{TiO}_2\text{-A}$.

In particular, $\text{TiO}_2\text{-R}$ exposes sharp peaks at 3419 and 3487 cm^{-1} ; they are attributed to bridging OH, involved in H-bonds, located on $\text{TiO}_2\text{-R}$.

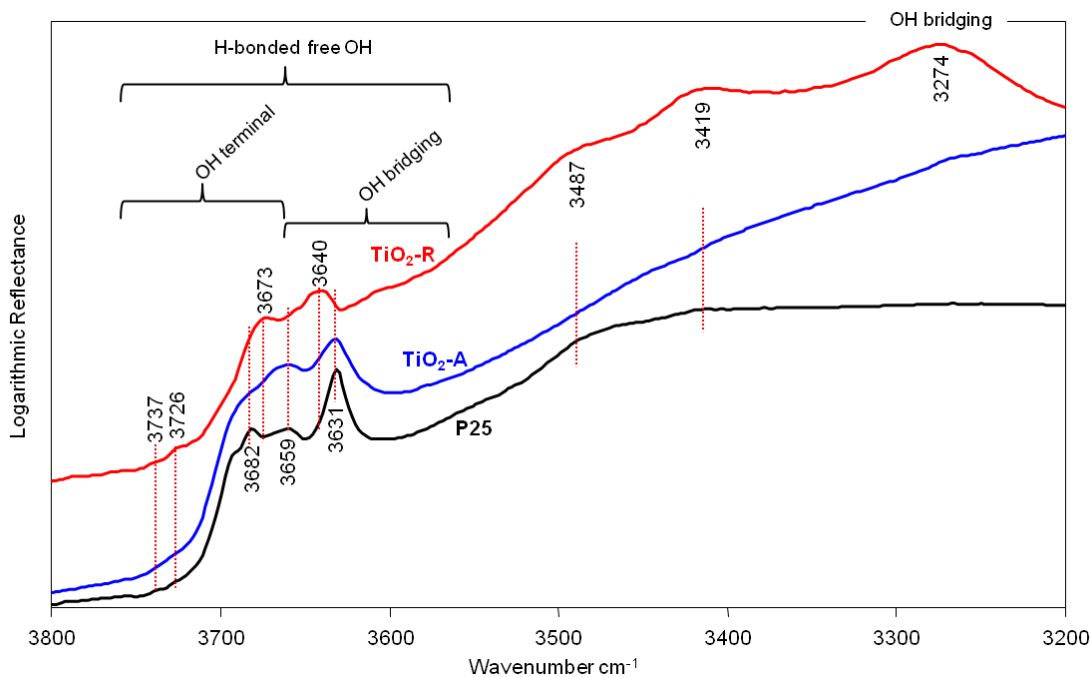


Figure 2.26. IR spectra of $\text{TiO}_2\text{-R}$ (red), $\text{TiO}_2\text{-A}$ (blue) and $\text{TiO}_2\text{-P25}$ (black) in room conditions. Assignment of OH groups adapted from literature^{41,43,46}

b) Spectra of powders dried at defined pH values

The differences between $\text{TiO}_2\text{-R}$ and $\text{TiO}_2\text{-A}$ can be observed through the protonation/deprotonation of hydroxyl groups with respect to pH of surrounding environment. Previous studies proved that the bridging OH groups are more acidic than terminal^{47,48} and Ti-OH_2^+ on anatase and bridging OH groups on rutile vary with pH.

Figure 2.27 shows the DRIFT spectra of $\text{TiO}_2\text{-A}$ powders prepared in aqueous solutions adjusted at pH 5 and 2 (in the follow, we will notice these samples as pH5-A and pH2-A). In the mid-IR range, the broad band centered at 3125 cm^{-1} shifts to 3091 cm^{-1} from pH2-A to pH5-A concomitantly to a decrease of the intensity of the component centered around 3400 cm^{-1} . Inversely, the intensity of the fine components at $3670\text{-}3690\text{ cm}^{-1}$ increases. This slight increase prove the relative increase of the H-bond free Ti-OH groups concentration. In the near IR region, TiOH_2^+ characterized by two components at 5153 and 5272 cm^{-1} (as two shoulders of the principal peak at 5230 cm^{-1}) decreases from pH2-A to pH5-A. At the same time, intensity of characteristic peaks of Ti_xOH groups (at 4196 cm^{-1}) increases slightly.

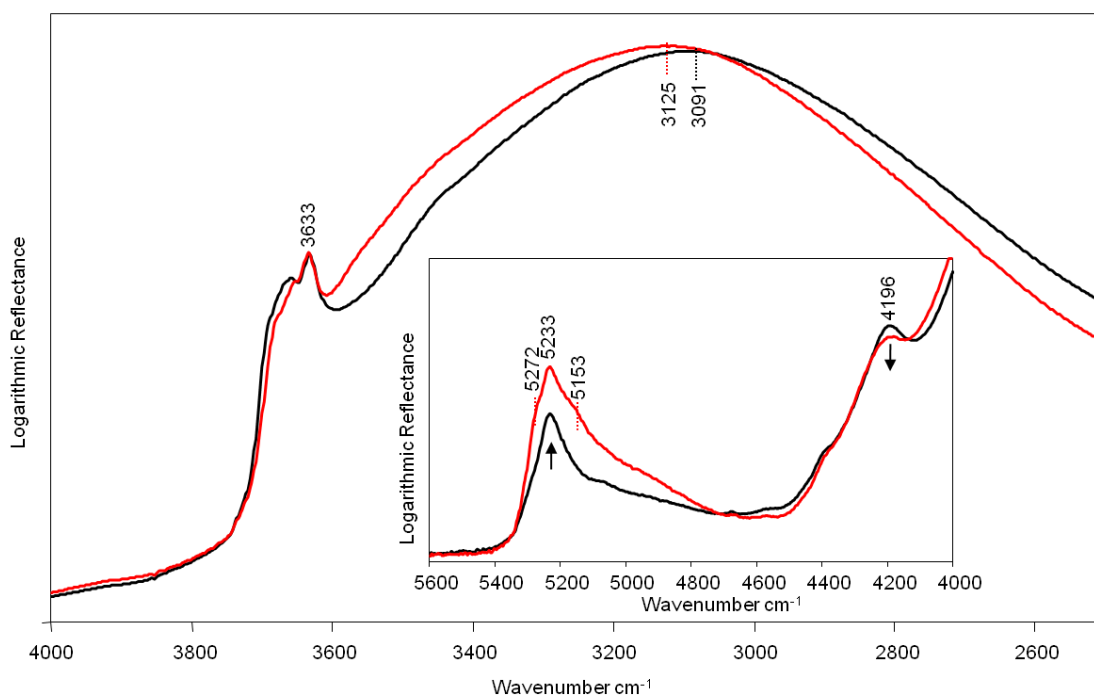


Figure 2.27. DRIFT spectra of TiO₂-A powders filtrated from the aqueous solutions at pH 2 (red) and pH 5 (black) in the mid-IR range and in the far IR range as insert.

The evolution of OH groups on TiO₂-R is more spectacular as demonstrated in Figure 2.28. When pH values of the aqueous solutions increases from 2 to 5 and 10, the intensities of peaks located at 3670-3720, 3607, 3513, 3380 and 4221 cm⁻¹ increase. By contrast, the intensities of peaks at 3416, 3277, and 4105 cm⁻¹ decrease. Since the signal at 3277 cm⁻¹ and its combination with the bending mode of the same OH group at 4105 cm⁻¹ are assigned to OH-bridging involved in H-bond (face (110) and (100) of rutile phase), the H-bonded bridging OH groups are decreased by more than 80% when the pH value is increased from 2 to 5. Concomitantly, the signals at 3520 cm⁻¹ and 3690 cm⁻¹ increased; these signals are assigned to free H-bond bridging OH as proposed by Takahashi et al⁴⁶ on their experiment carried out a rutile single crystal. During the deprotonation, the H-bond network is disrupted, releasing the remaining bridging OH. Consequently, the DRIFT spectrum seems to conserve an “image” of the interface of the suspension in aqueous media at the thermodynamical equilibrium. The component at 3420 cm⁻¹, displayed also on the spectra of degassed anatase at 373K, may be assigned on the base of the Deiana et al⁴³ paper to the symmetric stretching modes of the strongly sorbed molecular water on Ti_{5c} sites. The problem raised by Deiana was to find the asymmetric mode of these molecules. In our case and on the basis of our experiments carried out under weak pressure, we can propose that the wavenumber of this asymmetric mode is displayed around 3600-3620 cm⁻¹. Thus the increasing intensity is related to the deprotonation of TiOH₂⁺. This deprotonation results then in more terminal H-bonded free Ti-OH groups.

On the basis of vibrational infrared spectra, rutile sample surface is more dominated by the OH-bridging than our anatase sample. At pH value of 5, these Ti-OH-Ti bridging are strongly deprotonated, releasing H-bond free OH bridging. For the anatase sample, the infrared spectra are dominated by terminal $\text{Ti}_{5c}\text{-OH}$ or $\text{Ti}_{5c}\text{-OH}_2^{\delta+}$. The surface charge of the anatase will be then more dependent on the balance between both the forms of the terminal groups.

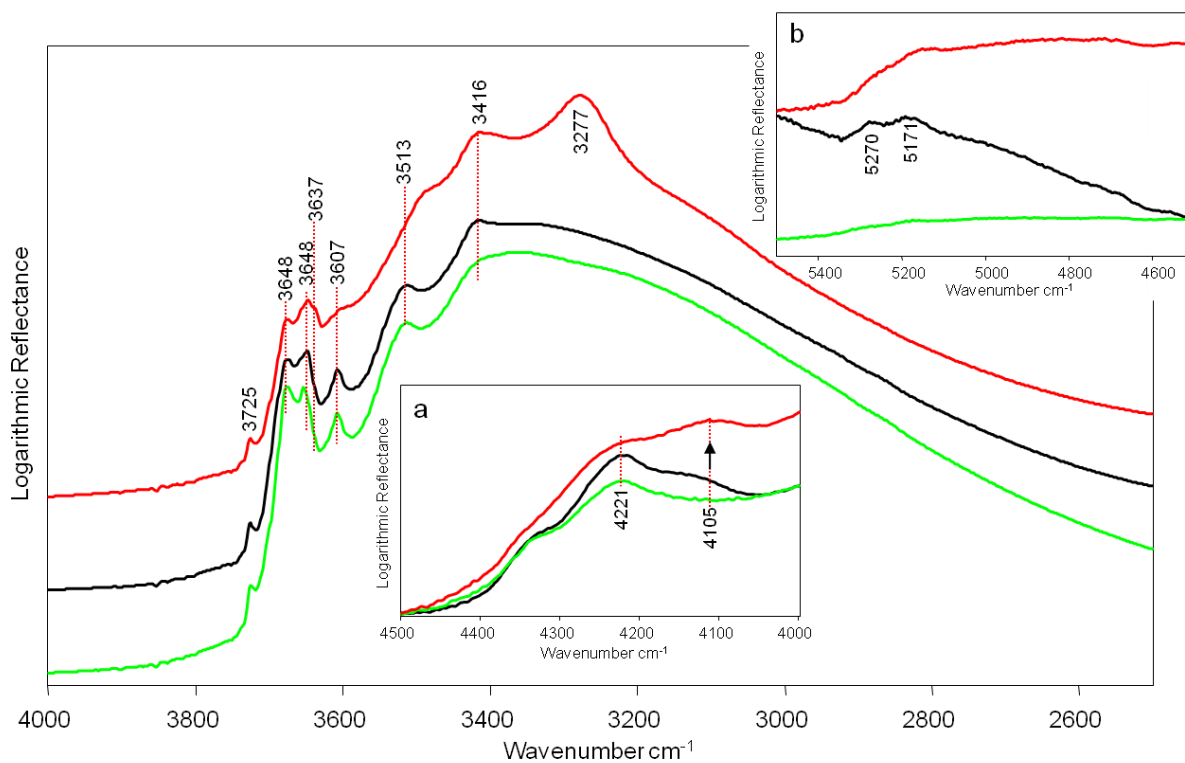


Figure 2.28. DRIFT spectra of $\text{TiO}_2\text{-R}$ powders at pH 2 (red), pH 5 (black) and pH 10 (green). The arrows indicate the evolution of peaks when the pH value increases.

2.4.2.3 Properties of TiO_2 in aqueous dispersion

State of TiO_2 particles in aqueous suspension is very different from the dried particles because of the presence of the electrical double layer and the interaction of particle surface with solvent. TiO_2 suspensions are more or less milky according to the concentration and easily sediment after several hours.

Surface charge

For TiO_2 dispersed in NaCl solution, IEP gets the same value with PZC because there is no specific adsorption for Na^+ or Cl^- to the surface of TiO_2 .^{7,49} IEP of TiO_2 was shown in Figure 2.29 and summarized in Table 2.3.

IEP of TiO_2 -P25 is about 6.5, which is in agreement with data in literature.^{35,49,50} By increasing the concentration of NaCl, the Debye length is reduced due to the contraction of the electrical double layer and this results in a slight decrease of the zeta potentials.

In the literature, IEP (or PZC) of anatase and rutile in aqueous dispersion was reported getting average value of 5.9 and 5.4, respectively.^{51,52} In agreement with literature data, IEP of TiO_2 -A is 6 and that of TiO_2 -R is 5.5. However, IEP of TiO_2 -PC was found to be 7, which is larger than the value of anatase reported in literature. Reason for this is not known, probably associated with the history of powders.

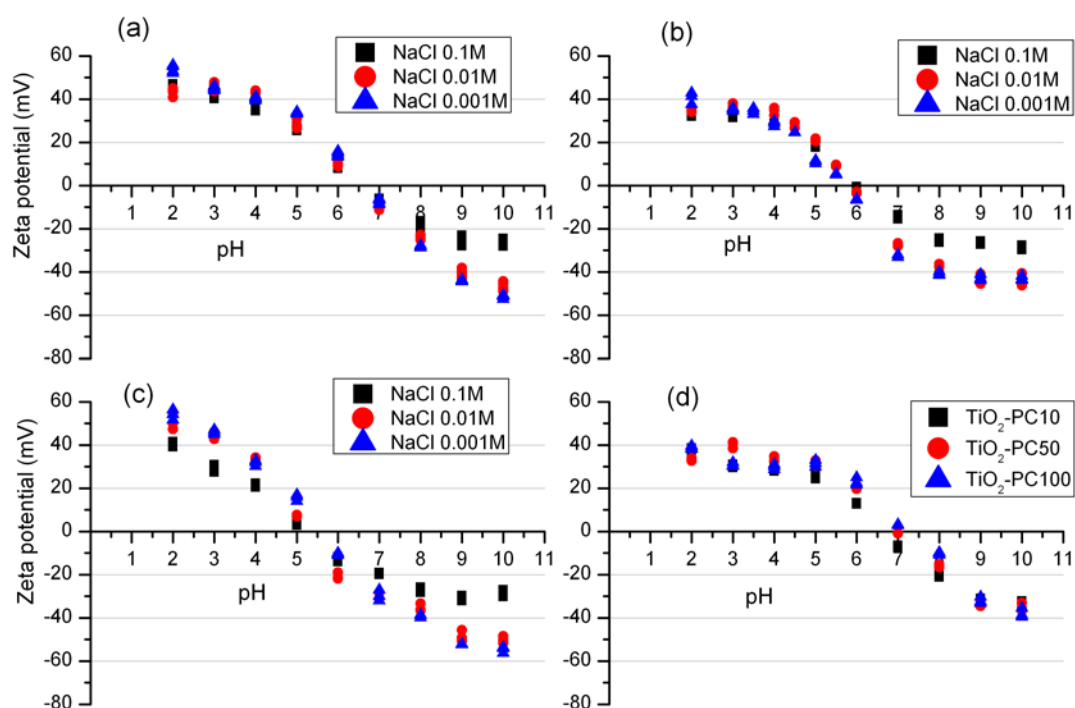


Figure 2.29. Zeta potential values of TiO_2 particles in aqueous suspension. (a) TiO_2 -P25, (b) TiO_2 -A and (c) TiO_2 -R are in aqueous suspension with the presence of NaCl. (d) TiO_2 -PC10, TiO_2 -PC50 and TiO_2 -PC100 are in aqueous suspension without NaCl. Mass concentration of TiO_2 in aqueous suspensions is 0.1 g.L^{-1} .

Size distribution

Hydrodynamic size distribution of pure anatase TiO₂-A and TiO₂-P25 presents a similar span, which depends on pH and ionic strength (Figure 2.30). At pH 2 and 9, the distribution span over a wide range of size, with a large proportion of particles around 100 nm, specially for P25. The distribution is strongly reduced at pH 5, next to IEP, with very large sizes close to 2 μm due to agglomeration of quasi neutral particles. The hydrodynamic size distribution of pure rutile TiO₂-R is hardly dependent on pH, with a small population close to 200 nm, and a larger one around 1 μm. Systems of TiO₂-PC50 and TiO₂-PC100 behave slightly different: hydrodynamic size of particles are more uniform but very large, and ranges from 500 nm to a few μm. Effect of surface charge on the hydrodynamic size is not apparent in this case, even if the peak is thinner at pH 9. For the system consisting of TiO₂-PC10 dispersed in aqueous medium, the suspension was so unstable that it was not possible to obtain a valid fit of the autocorrelation function. Thus, the distribution presented in Figure 2.30 for TiO₂-P10 must be cautiously considered, as it probably does not represent real size of particles in this sample.

With regards to the stabilization of TiO₂ in aqueous suspension, it was observed by naked eye the sedimentation phenomenon over several days. The sedimentation was faster in the order TiO₂-P25 < TiO₂-A ~ TiO₂-R < TiO₂-PC10 ~ TiO₂-PC50 ~ TiO₂-PC100. TiO₂-PC suspensions were subjected to quick sedimentation: a freshly prepared suspension of TiO₂-PC (0.1 g.L⁻¹) in H₂O (without NaCl) becomes transparent just within 24 hours. In contrast, the same suspension of TiO₂-P25 can remain homogeneous for several days. The higher stabilization of TiO₂-P25 may be due to the smaller size of particles in aqueous phase. The finding for TiO₂-P25 is consistent with literature.⁵³ TiO₂-PC dispersions are not stable because particles formed large agglomerates, in which particles are linked to each other by strong bonds, which cannot be broken down by bath sonication.

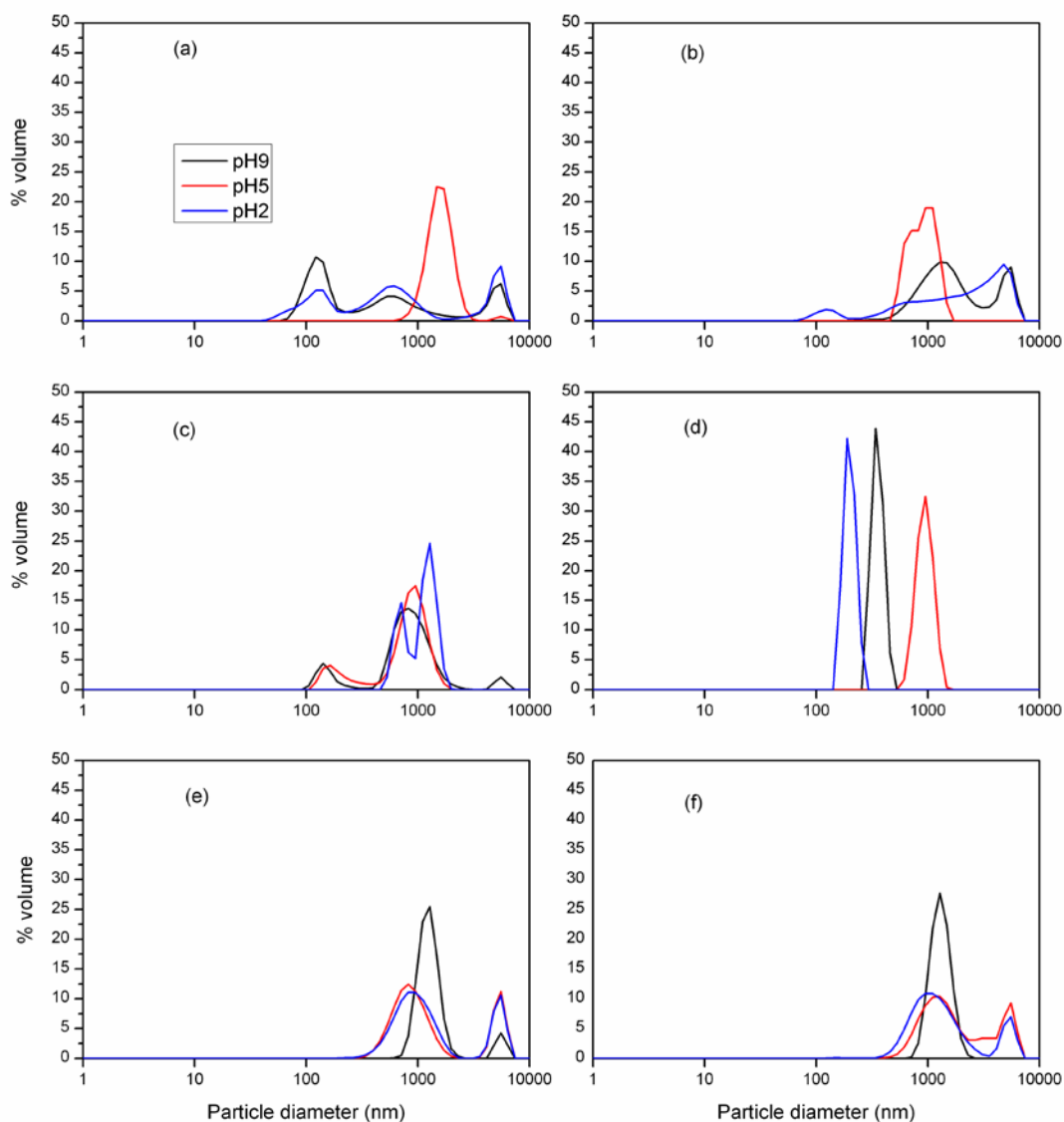


Figure 2.30. Size distribution of TiO_2 particles in aqueous suspension at mass concentration 0.1 g.L^{-1} . (a) for $\text{TiO}_2\text{-P25}$, (b) for $\text{TiO}_2\text{-A}$, (c) for $\text{TiO}_2\text{-R}$, (d) for $\text{TiO}_2\text{-PC10}$, (e) for $\text{TiO}_2\text{-PC50}$ and (f) for $\text{TiO}_2\text{-PC100}$.

For convenience, Table 2.3 summarizes the main properties of TiO_2 particles. Although the particles were observed under TEM, nevertheless to confirm the particle size by this technique for highly heterogeneous powder is difficult. Therefore, the diameter of particles were reported from approximating by Scherrer equation.

Table 2.3. Summary of some physical properties of TiO₂ samples.

Sample	Approximated particle average diameter (nm)	BET Surface area (m ² /g)	IEP
TiO ₂ -P25	25	48	6.5
TiO ₂ -A	18	136	6
TiO ₂ -R	22	26	5.5
TiO ₂ -PC10	72	9	7
TiO ₂ -PC50	30	48	7
TiO ₂ -PC100	22	75	7

2.4.3 Phospholipids vesicles in aqueous dispersion

Hydrodynamic size of phospholipids vesicles

The size distributions of phospholipids are reported in Figure 2.31. For each phospholipid, size distribution of vesicles obtained after extrusion is rather monomodal. The distributions are different and highly dependent on the head polar groups. The presence of large vesicles can be partially explained by the metastability of phospholipids vesicles that may undergo fusion and aggregation after preparation, particularly when stored at a temperature lower than the transition temperature.^{54,55}

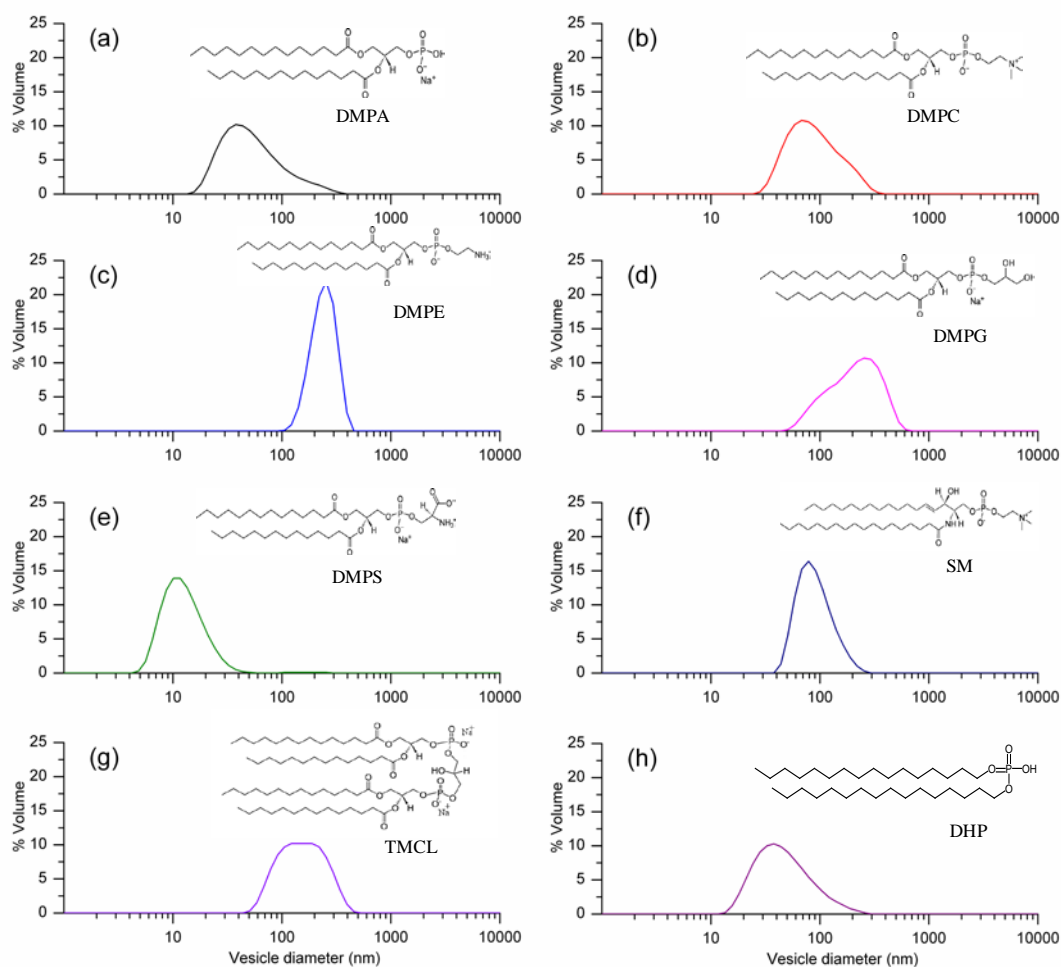


Figure 2.31. Size distribution (expressed as volume distribution) of phospholipids in aqueous suspension. Size distribution of phospholipid vesicles were measured in the absence of NaCl at 25°C.

Hydrodynamic size of DMPA vesicles is centered at 40 - 50 nm, those of DMPC is centered at around 80 – 100 nm, size of DMPE and DMPG is quite similar and centered at 200 - 300 nm. DMPS shows an exception, the vesicles size in majority is less than 20 nm, which is the lower limit for small unilamellar vesicles size.⁵⁴ It is worth noting that typical thickness of lipidic bilayer is approximately from 4 to 5 nm.⁵⁶ Probably, the existing forms of DMPS in dispersion were not vesicles but they were micelles or planar lamellar which have much smaller size than vesicles,⁵⁷ presumably in the range of 10 - 20 nm. Size of SM vesicles is slightly similar to that of DMPC, around 90-100 nm. TMCL vesicles (100-200 nm) have size smaller than that of DMPE and DMPG. Size of DHP vesicles resembles with that of DMPA, at around 40-50 nm.

2.5 Conclusion

The characterization of TiO₂ in the solid state and in aqueous medium has shown that TiO₂ powders are free from contaminants and well crystallized. Elementary size of TiO₂

particles is at the nanoscale. In spite of our efforts, there are some limits regarding to the morphology of TiO₂ particles, which could be determined by neither high resolution TEM nor XRD. These small particles strongly aggregate in aqueous medium and their hydrodynamic size depends on pH. Infrared spectroscopy revealed how the surface of TiO₂ samples is charged according to pH and dependent on the surface structure.

Concerning phospholipids, the vesicles were fabricated by extrusion through a 100 nm membrane. However, sizes of vesicles range from 10 nm to 600 nm, depending on the head polar group of phospholipid.

References

1. Barenholz, Y. & Thompson, T. E. Sphingomyelin: biophysical aspects. *Chem. Phys. Lipids* **102**, 29–34 (1999).
2. Lewis, R. N. A. H. & McElhaney, R. N. The physicochemical properties of cardiolipin bilayers and cardiolipin-containing lipid membranes. *Biochim. Biophys. Acta* **1788**, 2069–79 (2009).
3. Turner, N. & Schreifels, J. Surface analysis: X-ray photoelectron spectroscopy and Auger electron spectroscopy. *Anal. Chem.* **72**, 99R–110R (2000).
4. Hair, M. *Infrared spectroscopy in surface chemistry*. (Marcel Dekker, 1967).
5. Humbert, B. Developpements experimentaux et theoriques en spectrometries infrarouge et raman. Application à l'étude des silices divisisées. (1991).
6. Džimbeg-malčić, V., Barbarić-mikočević, Ž. & Itrić, K. Kubelka-Munk theory in describing optical properties of paper (I). *Tech. Gaz.* **18**, 117–124 (2011).
7. Jiang, J., Oberdörster, G. & Biswas, P. Characterization of size, surface charge, and agglomeration state of nanoparticle dispersions for toxicological studies. *J. Nanoparticle Res.* **11**, 77–89 (2009).
8. Rampaul, A., Parkin, I. P. & Cramer, L. P. Damaging and protective properties of inorganic components of sunscreens applied to cultured human skin cells. *J. Photochem. Photobiol. A Chem.* **191**, 138–148 (2007).
9. Pitcher III, W. H. & Huestis, W. H. Vesicles of a uniform size. *Biochem. Biophys. Res. Commun.* **296**, 1352–1355 (2002).
10. Strawbridge K. B. and Hallett F. R. Size Distributions Obtained from the Inversion of. **24126**, 2283–2290 (1994).
11. Hunter, J. R. *Foundations of Colloid Science. J. Psychother. Pract. Res.* **5**, (Oxford university Press, 2001).
12. *CRC Handbook of Chemistry and Physics*. (CRC Press, 2004).
13. Ames, B. N. in *Methods Enzymol. Vol 8* 115–118 (Elsevier, 1966). doi:10.1016/0076-6879(66)08014-5
14. Eibl, H. & Lands, W. E. A new, sensitive determination of phosphate. *Anal. Biochem.* **30**, 51–7 (1969).
15. Mano, S. S., Kanehira, K., Sonezaki, S. & Taniguchi, A. Effect of Polyethylene Glycol Modification of TiO₂ Nanoparticles on Cytotoxicity and Gene Expressions in Human Cell Lines. *Int. J. Mol. Sci.* **13**, 3703–17 (2012).
16. Pagnout, C. *et al.* Role of electrostatic interactions in the toxicity of titanium dioxide nanoparticles toward Escherichia coli. *Colloids Surf. B. Biointerfaces* **92**, 315–21 (2012).

17. Weir, A., Westerhoff, P., Fabricius, L., Hristovski, K. & von Goetz, N. Titanium dioxide nanoparticles in food and personal care products. *Environ. Sci. Technol.* **46**, 2242–50 (2012).
18. Suttiponpanit, K. *et al.* Role of Surface Area, Primary Particle Size, and Crystal Phase on Titanium Dioxide Nanoparticle Dispersion Properties. *Nanoscale Res. Lett.* **6**, 27 (2011).
19. Gustafsson, Å., Lindstedt, E., Elfsmark, L. S. & Bucht, A. Lung exposure of titanium dioxide nanoparticles induces innate immune activation and long-lasting lymphocyte response in the Dark Agouti rat. *J. Immunotoxicol.* **8**, 111–21 (2011).
20. Ohno, T., Sarukawa, K., Tokieda, K. & Matsumura, M. Morphology of a TiO₂ Photocatalyst (Degussa, P-25) Consisting of Anatase and Rutile Crystalline Phases. *J. Catal.* **203**, 82–86 (2001).
21. Ohtani, B., Prieto-Mahaney, O. O., Li, D. & Abe, R. What is Degussa (Evonik) P25? Crystalline composition analysis, reconstruction from isolated pure particles and photocatalytic activity test. *J. Photochem. Photobiol. A Chem.* **216**, 179–182 (2010).
22. Bertoni, G. *et al.* Quantification of crystalline and amorphous content in porous samples from electron energy loss spectroscopy. *Ultramicroscopy* **106**, 630–635 (2006).
23. Balachandran, U. & Eror, N. . Raman Spectra of Titanium Dioxide. *J. Solid State Chem.* **282**, 276–282 (1982).
24. Felske, A. & Plieth, W. J. Raman spectroscopy of titanium dioxide layers. *Electrochim. Acta* **34**, 75–77 (1989).
25. Bezrodna, T., Gavrilko, T., Puchkovska, G., Shimanovska, V. & Baran, J. Spectroscopic study of TiO₂ (rutile) – benzophenone heterogeneous systems. *J. Mol. Struct.* **614**, 315–324 (2002).
26. Hardcastle, F. D. Raman Spectroscopy of Titania (TiO₂) Nanotubular Water-Splitting Catalysts. *J. Ark. Acad. Sci.* **65**, 43–48 (2011).
27. Surmacki, J., Wroński, P., Szadkowska-Nicze, M. & Abramczyk, H. Raman spectroscopy of visible-light photocatalyst – Nitrogen-doped titanium dioxide generated by irradiation with electron beam. *Chem. Phys. Lett.* **566**, 54–59 (2013).
28. Nam, C. T., Falconer, J. L., Duc, L. M. & Yang, W.-D. Morphology, structure and adsorption of titanate nanotubes prepared using a solvothermal method. *Mater. Res. Bull.* **51**, 49–55 (2014).
29. Langford, J. & Wilson, A. J. Seherrer after Sixty Years: A Survey and Some New Results in the Determination of Crystallite Size. *J. Appl. Crystallogr.* **11**, 102–113 (1978).
30. Database. Powder diffraction file JCPDS 021-1272.
31. Spoto, G., Morterra, C., Marchese, L., Orio, L. & Zecchina, A. The morphology of TiO₂ microcrystal and their adsorptive properties towards CO: A HRTEM and FTIR study. *Vacuum* **41**, 39–41 (1990).

32. Database. Powder diffraction file JCPDS 021-1276.
33. Diebold, U. The surface science of titanium dioxide. *Surf. Sci. Rep.* **48**, 53–229 (2003).
34. Dutta, P. K., Ray, A. K., Sharma, V. K. & Millero, F. J. Adsorption of arsenate and arsenite on titanium dioxide suspensions. *J. Colloid Interface Sci.* **278**, 270–5 (2004).
35. Ferguson, M. a, Hoffmann, M. R. & Hering, J. G. TiO₂-photocatalyzed As(II) oxidation in aqueous suspensions: reaction kinetics and effects of adsorption. *Environ. Sci. Technol.* **39**, 1880–6 (2005).
36. Rashidzadeh, M. Synthesis of High-Thermal Stable Titanium Dioxide Nanoparticles. *Int. J. Photoenergy* **2008**, 1–4 (2008).
37. Baraton, M. Nano-TiO₂ for Solar Cells and Photocatalytic Water Splitting: Scientific and Technological Challenges for Commercialization. *Open Nanosci. J.* **5**, 64–77 (2011).
38. Mino, L., Spoto, G., Bordiga, S. & Zecchina, A. Particles Morphology and Surface Properties As Investigated by HRTEM, FTIR, and Periodic DFT Calculations: From Pyrogenic TiO₂ (P25) to Nanoanatase. *J. Phys. Chem. C* **116**, 17008–17018 (2012).
39. Herman, G. S., Dohna, Z., Ruzycki, N. & Diebold, U. Experimental Investigation of the Interaction of Water and Methanol with. *J. Phys. Chem. B* **2**, 2788–2795 (2003).
40. Arrouvel, C., Digne, M., Breyse, M., Toulhoat, H. & Raybaud, P. Effects of morphology on surface hydroxyl concentration: a DFT comparison of anatase–TiO₂ and γ -alumina catalytic supports. *J. Catal.* **222**, 152–166 (2004).
41. Minella, M. *et al.* Effect of fluorination on the surface properties of titania P25 powder: an FTIR study. *Langmuir* **26**, 2521–7 (2010).
42. Rinnert, E. *et al.* Hydration of a synthetic clay with tetrahedral charges: a multidisciplinary experimental and numerical study. *J. Phys. Chem. B* **109**, 23745–59 (2005).
43. Deiana, C., Fois, E., Coluccia, S. & Martra, G. Surface Structure of TiO₂-P25 Nanoparticles: Infrared Study of Hydroxy Groups on Coordinative Defect Sites. *J. Phys. Chem. C* **114**, 21531–21538 (2010).
44. Martra, G. Lewis acid and base sites at the surface of microcrystalline TiO₂ anatase: relationships between surface morphology and chemical behaviour. *Appl. Catal. A Gen.* **200**, 275–285 (2000).
45. Deiana, C., Fois, E., Coluccia, S. & Martra, G. Surface Structure of TiO₂-P25 Nanoparticles: Infrared Study of Hydroxy Groups on Coordinative Defect Sites. *J. Phys. Chem. C* **114**, 21531–21538 (2010).
46. Takahashi, K. & Yui, H. Analysis of Surface OH Groups on TiO₂ Single Crystal with Polarization Modulation Infrared external Reflection Spectroscopy. *J. Phys. Chem. C* **113**, 20322–20327 (2009).

47. Hiemstra, T., Venema, P. & Riemsdijk, W. Intrinsic Proton Affinity of Reactive Surface Groups of Metal (Hydr)oxides: The Bond Valence Principle. *J. Colloid Interface Sci.* **184**, 680–92 (1996).
48. Panagiotou, G. Mapping the surface (hydr)oxo-groups of titanium oxide and its interface with an aqueous solution: The state of the art and a new approach. *Adv. Colloid Interface Sci.* **142**, 20–42 (2008).
49. Suttiponparnit, K. *et al.* Role of Surface Area, Primary Particle Size, and Crystal Phase on Titanium Dioxide Nanoparticle Dispersion Properties. *Nanoscale Res. Lett.* **6**, 27 (2011).
50. Kang, S. a, Li, W., Lee, H. E., Phillips, B. L. & Lee, Y. J. Phosphate uptake by TiO₂: batch studies and NMR spectroscopic evidence for multisite adsorption. *J. Colloid Interface Sci.* **364**, 455–61 (2011).
51. Kosmulski, M. The significance of the difference in the point of zero charge between rutile and anatase. *Adv. Colloid Interface Sci.* **99**, 255–64 (2002).
52. Chadwick, M. ., Goodwin, J. ., Lawson, E., Mills, P. D. & Vincent, B. Surface charge properties of colloidal titanium dioxide in ethylene glycol and water. *Colloids Surfaces A Physicochem. Eng. Asp.* **203**, 229–236 (2002).
53. Liu, X., Chen, G. & Su, C. Effects of material properties on sedimentation and aggregation of titanium dioxide nanoparticles of anatase and rutile in the aqueous phase. *J. Colloid Interface Sci.* **363**, 84–91 (2011).
54. Chang, E. L., Gaber, B. P. & Sheridan, J. P. Photon correlation spectroscopy study on the stability of small unilamellar DPPC vesicles. *Biophys. J.* **39**, 197–201 (1982).
55. Patty, P. J. & Frisken, B. J. The pressure-dependence of the size of extruded vesicles. *Biophys. J.* **85**, 996–1004 (2003).
56. Di Biasio, A. & Cametti, C. Dielectric properties of aqueous zwitterionic liposome suspensions. *Bioelectrochemistry* **70**, 328–34 (2007).
57. Glover, K. J. *et al.* Structural evaluation of phospholipid bicelles for solution-state studies of membrane-associated biomolecules. *Biophys. J.* **81**, 2163–71 (2001).

Chapter 3

Probing the interactions between phospholipids and TiO₂ particles through surface tension measurements

Table of content

3. Probing the interactions between phospholipids and TiO ₂ particles through surface tension measurements	149
3.1 Introduction	151
3.2 Experimental section	152
3.2.1 Materials	152
3.2.2 Characterization of TiO ₂ -P25 particles	152
3.2.3 TiO ₂ -P25 suspension : preparation and characterization	153
3.2.4 Surface pressure-area isotherms of lipid films	154
3.2.5 Lipid dispersions: preparation and characterisation	155
3.3 Results	155
3.3.1 Surface properties of lipids in the presence of TiO ₂ -P25.....	155
3.3.2 Surface charge of TiO ₂ -P25 and lipids.	159
3.4 Discussion	162
3.4.1 pH-dependent partitioning of lipids and TiO ₂ at the interface and in the subphase	162
3.4.2 Evidence for electrostatic interactions between TiO ₂ -P25 particles and phospholipids.....	163
3.4.3 Significance of the molecular structure in the adsorption of lipids onto TiO ₂	165
3.5 Conclusion.....	166
Supporting information (Chapter 3).....	168
References	177

3. Probing the interactions between phospholipids and TiO₂ particles through surface tension measurements

Interactions between phospholipids and titanium dioxide particles (Article)

Quoc-Chon Le¹, Marie-Hélène Ropers², Hélène Terrisse¹, Bernard Humbert¹

Accepted for publication in Journal of Colloids and Surfaces B: Biointerfaces

¹ Institut Matériaux Jean Rouxel IMN, UMR 6502 Univ Nantes - CNRS, 44322 Nantes

3

² INRA, UR1268 Biopolymères Interactions Assemblages, F-44300 Nantes, France

Corresponding author: M.-H. Ropers

Full postal address: INRA, Rue de la Géraudière, BP 71627, 44322 Nantes Cedex 3

E-mail: marie-helene.ropers@nantes.inra.fr

Phone: 0033 240675189

Fax: 0033 240675084

Abstract

A systematic study was carried out on monolayer films and lipid vesicles to elucidate the interactions between membrane lipids and commercial particles of titanium dioxide TiO_2 (TiO_2 -P25). Pressure-area isotherms of lipids at various pH values were recorded on a Langmuir trough with or without TiO_2 -P25 and NaCl in the subphase. Electrophoretic mobilities of lipid vesicles and TiO_2 -P25 particles were measured to identify the pH range where attractive electrostatic interactions between lipids and TiO_2 -P25 could take place. The results show that i) the surface of TiO_2 -P25 particles interacts only with some phospholipids, ii) the driving forces are electrostatic and iii) non-electrostatic interactions were also observed, depending on the molecular structure. More precisely, the phospholipids 1,2-dimyristoyl-*sn*-glycero-3-phosphate monosodium salt (DMPA), 1,2-dimyristoyl-*sn*-glycero-3-phospho-*rac*-1-glycerol (DMPG) and 1',3'-bis[1,2-dimyristoyl-*sn*-glycero-3-phospho]-*sn*-glycerol (TMCL) interacted strongly with the TiO_2 -P25 surface through electrostatic interactions, providing they were oppositely charged, *i.e.* for pH between 2 and 6.6. For TMCL and DMPG, interactions with the surface of TiO_2 -P25 in non-favourable electrostatic conditions, suggested another kind of binding, probably through the hydroxyl groups of the terminal glycerol. Weaker attractive interactions were demonstrated for 1,2-dimyristoyl-*sn*-glycero-3-phospho-L-serine (DMPS) and the synthetic lipid dihexadecyl phosphate (DHP). For DMPS, the carboxylate group is involved in the adsorption onto TiO_2 . The other membrane lipids such as 1,2-dimyristoyl-*sn*-glycero-3-phosphocholine (DMPC), 1,2-dimyristoyl-*sn*-glycero-3-phosphoethanolamine (DMPE) and sphingomyelin (SM) did not interact with TiO_2 -P25 regardless of pH.

Keywords

Titanium dioxide, phospholipid, surface charge, zeta potential, Langmuir film, pressure-area isotherm

3.1 Introduction

Titanium dioxide (TiO_2) particles are widely used in consumer products such as coloring agents in food¹ and UV filters in sunscreens². As some of these particles were reported to have adverse effects on mammalian cells³, understanding the interaction of titanium dioxide with cell membranes is an important step toward understanding the biological effects. Besides the role of proteins,⁴ lipids were rarely studied and deserve consideration. TiO_2 has been shown to exhibit some lipid affinity in some cases.^{5–14} The main method consisted in observing the rupture or the adsorption of the phospholipid vesicle on the surface of TiO_2 . It was shown that glycerophosphatidylcholine has a lower affinity for titanium dioxide than glycerophosphatidylserine.^{7,9,11,14} Changing pH and introducing calcium ions improved the adsorption. Consequently, the energetic barriers preventing or permitting adsorption were assumed to be primarily electrostatic in origin, at least for the investigated lipid glycerophosphatidylcholine, and its mixtures with glycerophosphatidylserine, glycerophosphatidylglycerol, and glycerophosphatidylethanolamine.^{6,10,13,15,16} However, van der Waals forces were also shown to be involved in the adsorption mechanisms.¹⁰ Moreover, several studies suggested that phosphate groups can form covalent bonds with the surface hydroxyl groups of TiO_2 .^{17–20} Hence, from these studies, it is difficult to have a global view of the interactions between phospholipids and TiO_2 and to predict subsequent biological effects, since the interactions were studied with only four systems (glycerophosphatidylcholine alone and in mixture with glycerophosphatidylserine, glycerophosphatidylglycerol or glycerophosphatidylethanolamine), and they were investigated under varying experimental conditions and TiO_2 supports (primarily amorphous and rutile), that are not fully relevant with respect to the above-mentioned applications.

The aim of the present paper is to identify the target lipids when TiO_2 particles are in contact with membranes, and as much as possible to determine the nature of forces involved in the adsorption of these lipids on TiO_2 particles in aqueous solutions. For this study, we selected commercial particles of titanium dioxide from Evoniks Industries AG (AEROXIDE® TiO_2 -P25, hereafter called TiO_2 -P25), due to its wide industrial application and abundant literature data concerning the potential toxicity of this compound.^{3,21–23} The main membrane components, namely glycerophosphocholine, glycerophosphoethanolamine, glycerophosphoserine, glycerophosphoglycerol and glycerophosphates, sphingomyelin, as well as a synthetic lipid, dihexadecyl phosphate, were considered separately (molecular structures shown in Figure S1). Our approach combined compression isotherms of Langmuir films with Laser Doppler electrophoresis.

3.2 Experimental section

3.2.1 Materials

The titanium (IV) dioxide powder used was AEROXIDE® TiO₂-P25 from Evonik Industries (Essen, Germany). It was used as received and hereafter is referred as TiO₂-P25. Lipids included 1,2-dimyristoyl-*sn*-glycero-3-phosphate monosodium salt (DMPA (Figure S1a), Monosodium salt, >99%, from Avanti Polar Lipids), 1,2-dimyristoyl-*sn*-glycero-3-phosphocholine (DMPC (Fig. S1h), >99% Avanti Polar Lipids), 1,2-dimyristoyl-*sn*-glycero-3-phospho-L-serine (DMPS (Fig. S1e), Sodium salt, >99%, Avanti Polar Lipids), 1,2-dimyristoyl-*sn*-glycero-3-phosphoethanolamine (DMPE (Fig. S1f), 99%, Sigma Aldrich), 1,2-dimyristoyl-*sn*-glycero-3-phospho-*rac*-1-glycerol (DMPG (Fig. S1b), Sodium salt, 99%, Sigma Aldrich), dihexadecyl phosphate (DHP (Figure S1d), Sigma Aldrich), sphingomyelin (SM (Figure S1g) from bovine brain, >97%, Sigma Aldrich) and 1',3'-bis[1,2-dimyristoyl-*sn*-glycero-3-phospho]-*sn*-glycerol (cardiolipin TMCL (Figure S1c), sodium salt, >99%, Avanti Polar Lipids). NaOH solutions were prepared from NaOH solid state in flake form (99%, Alfa Aesar, MA, USA). HCl solutions were prepared from HCl solution 37% (Carlo ERBA, Milan, Italy). NaCl solutions were prepared from solid NaCl (Bioextra ≥99.5%, Sigma Aldrich). Chloroform CHCl₃, methanol CH₃OH, ethanol C₂H₅OH were obtained from Carlo ERBA (Milan, Italy).

3.2.2 Characterization of TiO₂-P25 particles

The crystallographic structure and composition of TiO₂-P25 was characterized by X-ray diffraction (Bruker AXS D8 Advance, equipped with Cu K α 1). The integrated intensities of the peaks deduced from Rietveld analysis gave the relative proportions between anatase and rutile, which were 85 (\pm 6)% for anatase and 15 (\pm 2)% for rutile, in agreement with the literature.^{1,24} The specific surface area of TiO₂-P25, determined by multipoint Brunauer-Emmett-Teller treatment (BET method) from the volumetric adsorption isotherms at 77K of nitrogen gas (instrument ASAP 2010 Physisorption Analyzer) was 48.1 ± 0.4 m²/g, consistent with the literature data.²⁵ Particle morphology of TiO₂-P25 was examined by Scanning Electron Microscopy (SEM) (JEOL JSM-7600F) and Transmission Electron Microscopy (TEM) (Hitachi HNAR9000). TiO₂-P25 powders were deposited directly on the copper support for SEM experiments. The SEM images (Figure S2a) display particles with great size heterogeneity and forming large aggregates. For TEM, a suspension of TiO₂-P25 in ethanol at a concentration of approximately 0.01 mg/mL was prepared and sonicated for 2 minutes at

power 300 W then a few drops of this suspension were deposited on a carbon film coated on copper grids for the measurements. TEM images (Figure S2b) show that anatase particle sizes were in the range 25-30 nm, compared to 50-80 nm for rutile particles, as mentioned in the literature.^{25,26} XPS and IR spectra demonstrate that the powder was pure and not contaminated by inorganic or organic matter (Figure S3).

3.2.3 TiO₂-P25 suspension : preparation and characterization

The suspensions of TiO₂-P25 were prepared in two steps. First, TiO₂-P25 was dispersed in ultra-pure water (Milli-Q-water, resistivity = 18.2 MΩ.cm). The suspension was magnetically stirred (300 rpm) for 10 minutes, then bath-sonicated (Elmasonic S 30 H from Elma, Singen, Germany with a power of 275 W) for 10 minutes. The concentrations of the suspensions were 0.125 g L⁻¹, for electrophoretic mobility measurements, and 0.25 g L⁻¹, for surface pressure-area isotherms and size measurements. In the second step, the suspension was diluted with either ultra-pure water or NaCl solution, in order to get a final suspension at 0.1 g L⁻¹ of TiO₂-P25 with different concentrations in salt ranging from 0 to 10⁻¹ mol L⁻¹. Then pH was adjusted to the desired value by adding a few drops of either NaOH 0.2 mol L⁻¹ or HCl 1 mol L⁻¹. The flasks containing the as-prepared suspensions were covered by an aluminium foil during stirring and measurement process, to prevent the influence of light. The suspensions were always freshly prepared before use.

The particle size distribution of TiO₂-P25 suspensions was determined for three pH values (2, 5, and 9) by Dynamic Light Scattering using a Zetasizer Nano ZS instrument equipped with a 633 nm He-Ne laser (Malvern Instruments Ltd, Malvern, Worcestershire, UK), which measured the scattered light at an angle of 173° and at a temperature of 25°C. The samples were left 2 minutes in the sample-holder chamber to reach an equilibrium state inside the Zetasizer. For the treatment of the data, the refractive index of TiO₂-P25 was set at 2.58 (intermediate between those of rutile and anatase, taking into account their proportions in the mixture). The size distribution was measured three times (each record accumulating at least 12 scans of 10 s) on two aliquots of the same suspension to assess the repeatability of the measurements. The suspensions of TiO₂-P25 particles at pH 2 and 9 contained small particles with a diameter of 140-150 nm (Figure S4) that represented between 80 and 90% of the total surface area of the material, and also larger aggregates that scatter light. At pH 5, the suspensions contained a large proportion of agglomerated particles (around 800 nm to 2µm) whatever the salt concentrations (Figure S4).

Electrophoretic mobility measurements were performed on the TiO₂-P25 suspensions using the same Zetasizer instrument. For each suspension at a given ionic strength, the pH value was adjusted to the desired value, from pH 10 to pH 2, by adding first a few drops of NaOH 0.2 mol L⁻¹ then HCl 1 mol L⁻¹ in the total volume of suspension (500 mL). The measurement of electrophoretic mobility was carried out by taking an aliquot of 2 mL after 3 to 5 minutes of equilibrium. Each point was obtained after six repetitions, resulting from three successive measurements on two aliquots of the same suspension at the same pH value. For easier comparison with other published data, our measurements were converted into zeta potential values only for presentation, using Henry's equation and applying the Smoluchowski approximation, even if this conversion probably underestimates zeta potential values, since it does not take into account the surface conductivity of TiO₂ particles.^{27,28} The electrophoretic mobility evolution of TiO₂-P25 particles, according to pH and ionic strength, is presented in Figure S5. The isoelectric point of TiO₂-P25 particles was identified at pH 6.6 (at null zeta potential), in accordance with the values reported in the literature.^{29,30}

3.2.4 Surface pressure-area isotherms of lipid films

The compression isotherms of lipids were obtained on a Langmuir Trough (NIMA 516, Nima Technology, UK) filled with a subphase of either water or TiO₂-P25 suspension, both at the desired pH (adjusted as previously described) and salt concentration. The Langmuir trough was placed in a room without sunlight. The temperature was set at 25°C with a circulation bath. The solutions of lipids (concentration around 1mg/mL) were prepared by dissolving DMPA, DMPC, DMPE, DMPS, SM, TMCL, and DHP powders into a mixture of chloroform and methanol, with proportions ranging between 80% and 100% for CHCl₃, and between 20% and 0% for CH₃OH. Methanol was added to increase the solubility of lipids in CHCl₃ when it was required. Surface pressure-area isotherms of lipids versus different subphases were measured with the following protocol. The trough and barriers were carefully cleaned with ethanol and rinsed with ultra-pure water. The pressure sensor was calibrated according to the standard method recommended by the provider. The trough was filled with the subphase and the surface was compressed to check the cleanliness of the surface (variation of surface pressure lower than 0.2 mN/m is considered to be clean). Then the lipid solution was spread drop by drop just on the top of the subphase surface (total volume of 22 µL) with a microsyringe (Hamilton, Switzerland). After 10 minutes to evaporate the solvent, the films were compressed. Each experiment was conducted at least twice, for two different films of the same molecules, to assess the repeatability of the results.

3.2.5 Lipid dispersions: preparation and characterisation

Lipid powders, stored at -20°C , were left at room temperature for 20 minutes before use. The powders of lipid were dispersed in ultra-pure water at a concentration around 0.25 mg mL^{-1} . The dispersions were bath-sonicated for 10 minutes (Elmasonic S 30 H from Elma, Singen, Germany with a power of 275 W) at a few degrees above the transition temperature of the phospholipid, namely, 55°C for DMPA and 30°C for DMPG. Then, these suspensions were extruded progressively through polycarbonate membranes (10 passes) with nominal pore size of successively 800 nm, 400 nm and 100 nm, using the Mini extruder from Avanti Polar Lipids (Alabaster, Alabama, USA). The obtained vesicle suspensions were used within 15h.

The stock suspensions of vesicles were diluted in a NaCl solution so that the final concentration of lipid molecules was around 0.04 mg mL^{-1} and the concentration of NaCl was 0.01 mol L^{-1} . The pH values of the as-prepared suspensions were in the range between 5.5 and 6.5. Electrophoretic mobility measurements were then performed on the vesicle suspensions, after adjustment of the pH value with solutions of NaOH 0.2 mol L^{-1} and HCl 1 mol L^{-1} , from pH 10 to pH 2. The suspension was left 3 to 5 minutes at each pH point to reach equilibrium before taking aliquots for measurement, and Smoluchowski's equation was used to convert the electrophoretic mobility into zeta potential, for an easier comparison with the literature data. Both the electrophoretic mobility and the zeta potential values versus pH are given in the results section.

3.3 Results

3.3.1 Surface properties of lipids in the presence of TiO_2 -P25

The surface properties of each lipid were analysed in acidic (pH 2) and basic (pH 9) media and at intermediate pH values (5 and 5.8) depending on the head polar group. The π -A isotherms of each lipid spread on several subphases (water or TiO_2 -P25 dispersions, with or without NaCl) are presented in Figures 3.1-2 and S5 to S9 in the following conditions: at pH 2 without salt (Figures 3.1 and S5), at pH 2 in the presence of NaCl (Figure S7), at pH 9 without salt (Figure S8) and at an intermediate pH value between 5 and 6 (Figures 3.2 and S9 without NaCl, Figure S10 with NaCl). As a control, the π -A isotherms of the free interface were recorded. They remained flat whatever pH and the composition of the subphase.

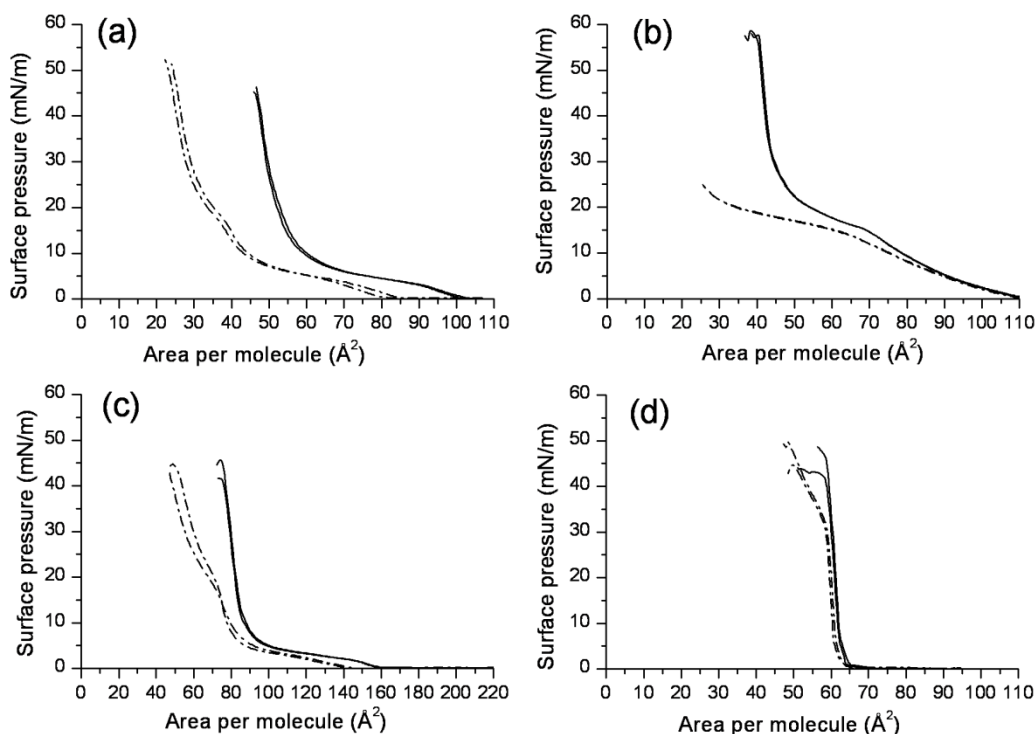


Figure 3.1. π -A isotherm curves of lipid monolayers ($n=2$) at the interface air-subphases of (solid line) pure water at pH 2 and of (dash dotted line) aqueous dispersions of TiO_2 -P25 particles at 0.1 g L^{-1} and pH 2, at $25 \text{ }^\circ\text{C}$. Lipids refer to (a) DMPA, (b) DMPG, (c) TMCL and (d) DHP.

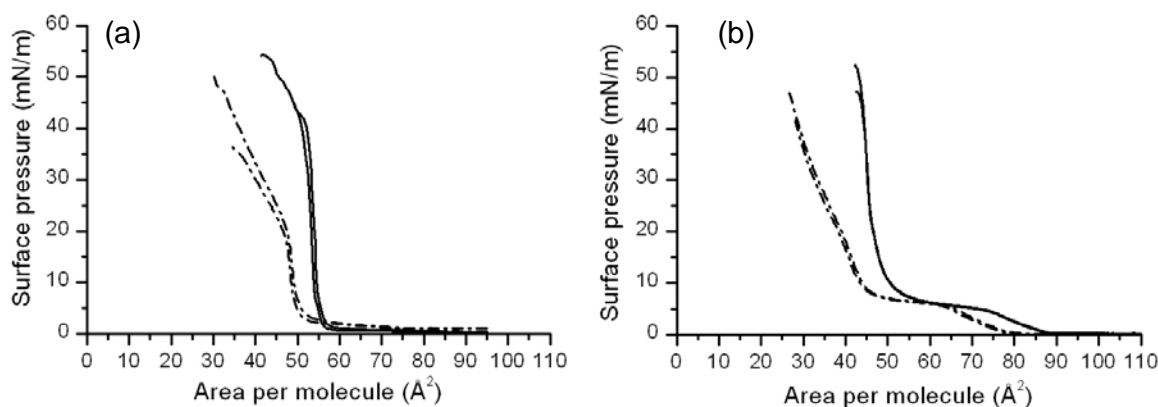


Figure 3.2. π -A isotherm curves ($n=2$) of (a) DHP and (b) DMPS lipid monolayers on subphases of pure water (solid line) and of aqueous dispersions of TiO_2 -P25 particles at 0.1 g L^{-1} (dash dotted line) adjusted at pH 5 at a temperature of $25 \text{ }^\circ\text{C}$.

At pH 2 and 5, the π -A isotherms of DMPA, DMPG, TMCL and DHP monolayers (Figures 1 and S8, panels a-d) differed in the presence of TiO_2 -P25 particles in the subphase,

whereas the π -A isotherms of DMPE, SM, and DMPC monolayers overlapped on both the water and TiO₂-P25 suspension subphases (Figure S6). The π -A isotherms of DMPS monolayers (Figure 3.2, panel b) differed also in the presence of TiO₂-P25 particles in the subphase only at pH 5. For DHP, the effect of TiO₂-P25 is more obvious at pH 5 (Figure 3.2) than at pH 2 (Figure 3.1). In contrast, most π -A isotherms with TiO₂-P25 particles in the subphase at pH 9 overlap those performed on pure water (Figure S8), except those for DMPG, TMCL and DMPS layers. For these molecules, the compression isotherms curves obtained on the TiO₂-P25-charged subphase were not exactly similar to those obtained at pH 9 without TiO₂-P25. A small shift toward larger areas was observed for DMPG and a more pronounced phase transition was observed for TMCL and DMPS monolayers. Depending on the head polar groups, the effect of TiO₂-P25 particles were suppressed at low NaCl concentrations (10⁻² mol/L) (Figure S10) or at high concentrations (10⁻¹ mol/L) (Figure S7). In the following, the modifications are detailed case by case.

3.3.1.1 DMPA monolayer

The π -A isotherm of DMPA recorded at pH 2 (Figure 3.1a) exhibits a liquid expanded phase at low film pressure (0-3 mN/m), followed by a plateau, and finally a liquid condensed phase from 10 mN/m until the collapse of the monolayer over 45 mN/m.³¹ In the presence of TiO₂-P25 particles, the global shape of the curve was found again. However, the whole curve was shifted to smaller areas and, over the plateau of transition, the film pressure increases sharply in two steps: from 10 to 20 mN/m, and from 20 to the collapse at 52 mN/m. This transition almost disappeared at pH 5 (Figure S9). The shift of the π -A isotherms of DMPA at the interface air-aqueous suspension of TiO₂-P25, toward areas that are lower than twice the cross-sectional area of an alkyl chain,³² hints that DMPA partially solubilized in the subphase containing TiO₂-P25 particles. The amount of phospholipid molecules solubilized into the subphase could be estimated from the control isotherm (without TiO₂ in the subphase) at 20 mN/m. The estimated amount of lipid solubilized into the subphase was 35% at pH 2 and 45% at pH 5. When NaCl was added to the subphase at pH 2 with a relatively low concentration, such as 10⁻² mol L⁻¹ (Figure S7, panel a), the shift of the π -A isotherms of DMPA in the presence of TiO₂-P25 was similar as that observed without salt. However, for a higher NaCl concentration (10⁻¹ mol L⁻¹, Figure S7, panel b), the π -A isotherms of DMPA spread on TiO₂-P25 -free and -charged subphases nearly overlap on a large area range. Thus, in these conditions of high ionic strength, the presence of TiO₂-P25 particles had no effect on the DMPA organization.

3.3.1.2 DMPG monolayer

The π - A isotherms of DMPG exhibited, at pH 2 and 5 on the water subphase, a similar behaviour as those obtained with DMPA (Figure 3.1, panel b and Figure S9, panel b): a liquid expanded phase at low and medium film pressures (0-15 mN/m), then a plateau and finally one liquid condensed phase at pH 2 and two liquid condensed phases at pH 5 from 20 mN/m until the collapse of the monolayer at around 55 mN/m. The main modification induced by TiO₂-P25 particles was the partial solubilization of the phospholipid molecules (37% at pH 2, 24% at pH 5, both at 20 mN/m). Additionally at pH 2, the plateau extended over a larger molecular area range and the formation of the liquid condensed phase could not be longer observed in the area range covered by the trough. As the effect of TiO₂-P25 particles was stronger at pH 2, the impact of NaCl was investigated at this pH value. At a concentration of 10⁻² mol L⁻¹, the global shape of the curve was not modified (Figure S7, panel c). At higher salt concentration (10⁻¹ mol L⁻¹), the shift of the compression isotherm obtained on TiO₂-P25 suspension was fully suppressed along the liquid-expanded phase and the plateau (Figure S7, panel d) but the liquid condensed phase was still affected. At pH 9, the compression isotherm of DMPG exhibits only a liquid expanded phase. Surprisingly, the presence of TiO₂-P25 particles shifts the isotherm toward higher areas (Figure S8, panel b).

3.3.1.3 Cardiolipin monolayer

For cardiolipin (TMCL) at pH 2 (Figure 3.1, panel c), the π - A isotherm curve shows a similar shape as that of DMPA but at higher areas, due to the presence of 4 alkyl chains in this molecule. In the presence of TiO₂-P25, the isotherm curve was shifted to lower areas and exhibited an additional phase transition at 17 mN/m, similarly to that of DMPA. The amount of TMCL solubilized in the subphase was estimated to 16% at 20 mN/m. When the ionic strength reaches 10⁻¹ mol L⁻¹ (Figure S7, panel f), this shift (and thus the solubilisation) was fully suppressed and the π - A isotherm curve of TMCL without TiO₂-P25 in the sub-phase was recovered. At pH 9 (Figure S8, panel c), the compression isotherm shifts to higher areas at pressures lower than 20 mN/m (zone where the liquid expanded phase forms) and shifts slightly to lower areas over 20 mN/m where the liquid condensed phase predominates.

3.3.1.4 DHP monolayer

The π - A isotherm curve of DHP at pH 2 is characterized by a vertical slope typical of a liquid condensed state (Figure 3.1, panel d). The π - A isotherm curves with or without TiO₂-P25 in the subphase overlapped until a film pressure of 30 mN/m. Then the slope of the curve

in the presence of TiO₂-P25 is gentler and smaller molecular areas than physically acceptable were recorded. This behaviour corresponds to a partial squeezing out of DHP lipids from the interface in the presence of TiO₂-P25 particles. At pH 5 (Figure 3.2, panel a), a significant shift of the isotherm was observed corresponding to 13% of solubilisation at 20 mN/m. The rupture in the slope was still observed but at 18 mN/m at pH 5 instead of 30 mN/m at pH 2. When the π -A isotherms were recorded at pH 5 in the presence of NaCl 10⁻² mol L⁻¹ (Figure S10, panel a), the typical shape of DHP isotherms was recovered, even though TiO₂-P25 particles were present in the subphase.

3.3.1.5 DMPS monolayer

In the presence of TiO₂-P25 particles at pH 5 (Figure 3.2, panel b), the curve was simply shifted to lower areas until 15 mN/m, suggesting a partial solubilisation of DMPS. The proportion of DMPS solubilized in the subphase is 17% at 20 mN/m. Above 15 mN/m, the slope is smoother than that performed on water, suggesting a less dense phase for the remaining DMPS molecules at the interface. When the π -A isotherms were recorded at pH 5 in the presence of NaCl 10⁻² mol L⁻¹ (Figure S10, panel b), the typical shapes of DMPS isotherms were recovered, even though TiO₂-P25 particles were present in the subphase. At pH 9, a more pronounced phase transition was observed when TiO₂-P25 was present in the subphase (Figure S8).

3.3.2 Surface charge of TiO₂-P25 and lipids.

In order to interpret the results obtained by Langmuir trough experiments, we measured the zeta potential of all studied phospholipids versus pH. The zeta potential values of the vesicles are displayed as a function of pH for each lipid in Figure 3.3, where the data for TiO₂-P25 particles are recalled. The values for lipid vesicles are coherent with the literature data,³³ taking into account salt concentrations³⁴⁻³⁶ and temperature^{37,38}. In acidic solutions (pH < 6.6), TiO₂-P25 particles are positively charged, whereas their surface charge becomes negative in basic solutions (pH > 6.6). In contrast, DMPA, DMPG, DMPS, DHP and TMCL carry negative charges all over the pH range from 2 to 10 ($\mu_E < 0$). DMPA, DMPG, and TMCL are highly charged over the whole pH range from 2 to 10, leading to high negative zeta potentials (ranging between - 60 and - 80 mV) (Figure 3.3, panels a, b, c). On the contrary, DMPS and DHP are less charged, in particular at pH 2 (- 20 mV and - 15 mV respectively) (Figure 3.3, panels d and e). Thus, TiO₂-P25 particles and lipid vesicles of DMPA, DMPG, TMCL, DMPS and DHP are oppositely charged in the pH range 2 to 6.6. On

the contrary, above pH 6.6, the phospholipids and TiO₂-P25 carry negative charges. Figure 3.3f shows that DMPE vesicles carry a positive surface charge at pH values lower than 5. Above pH 5, the mobility of DMPE vesicle is negative, reaching very high values above pH 8. Thus TiO₂-P25 particles and DMPE vesicles are oppositely charged only in a small pH range, between 5 and 6.6. The behaviour of SM vesicles (Figure 3.3, panel g) is close to that of DMPE vesicles. The null zeta potential is obtained around pH 5. Below this pH, SM vesicles carry a positive charge as TiO₂-P25 particles. Above pH 6.6, both of them carry negative surface charges. Consequently, TiO₂ and any of the lipid DMPE or SM carry opposite charges only between pH 5 and 6.6. Finally, the curve of the electrophoretic mobility of DMPC vesicles versus pH (Figure 3.3h) presents a slight variation around the null point of zeta potential from + 20 mV at pH 2 to – 10 mV at pH 10. Between pH 2 and 5, DMPC vesicles are positively charged like TiO₂-P25 particles and are negatively charged like TiO₂-P25 particles above pH 6.6. Consequently, they are oppositely charged between pH 5 and 6.6.

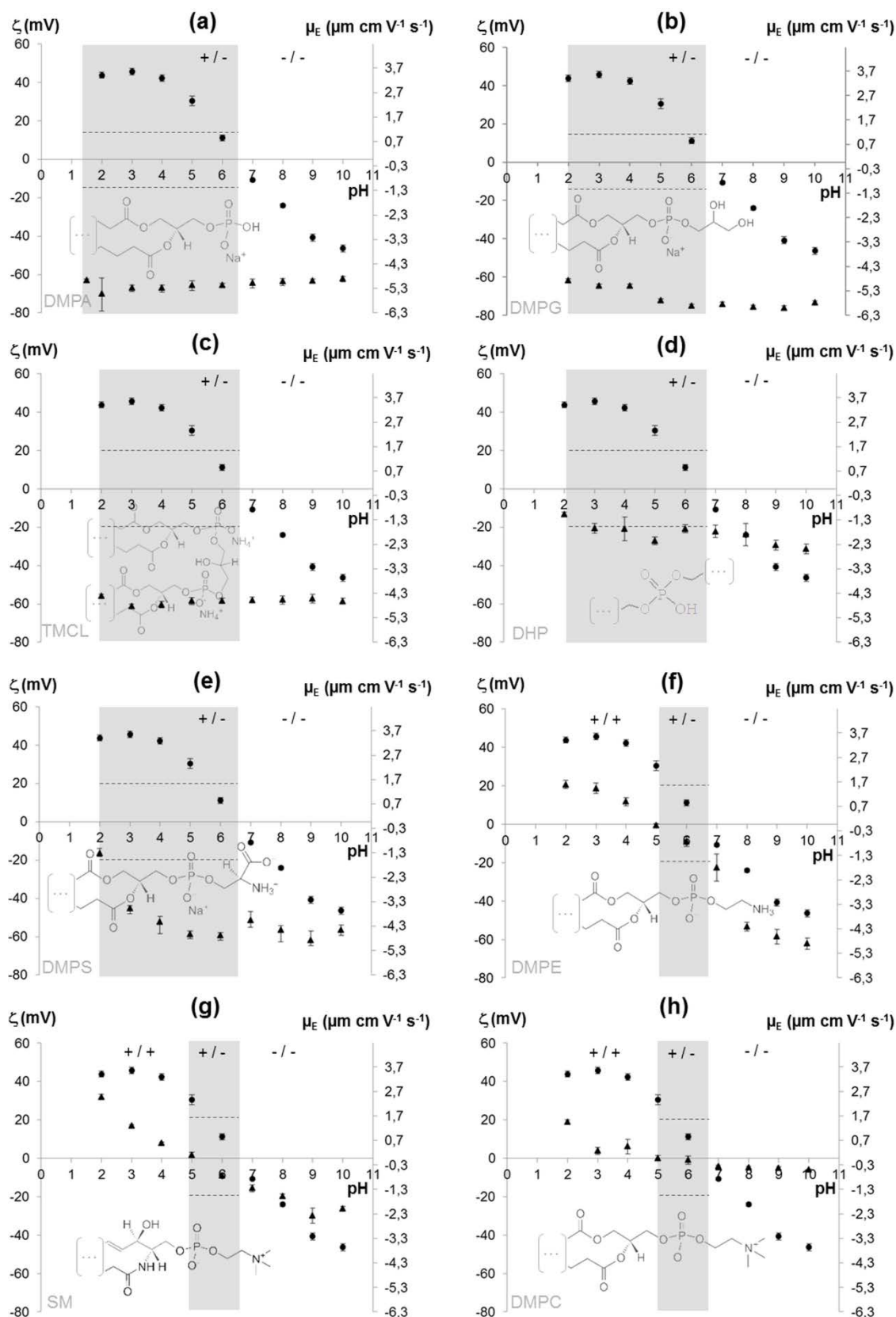


Figure 3.3. Zeta potential and electrophoretic mobility ($n = 3$, six measurements for each) of (●) $\text{TiO}_2\text{-P25}$ particles and (▲) lipids for (a) DMPA, (b) DMPG, (c) TMCL, (d) DHP, (e) DMPS, (f) DMPE, (g) SM and (h) DMPC, versus pH in $\text{NaCl } 10^{-2} \text{ mol.L}^{-1}$ solutions. The grey zones highlight the pH conditions where $\text{TiO}_2\text{-P25}$ particles and vesicles carry surface charges of opposite sign. The dotted lines mark the absolute values of zeta potential equal to 20 mV.

3.4 Discussion

3.4.1 pH-dependent partitioning of lipids and TiO₂ at the interface and in the subphase

The fact that the π -A isotherms of the free interface on TiO₂ dispersions remain flat means that TiO₂ particles do not adsorb spontaneously from bulk at the air-water interface. The presence of such particles at the air-water interface was observed only with particles of large primary size ($> 0.3 \mu\text{m}$) spread from an ethanol solution on pH 2 subphases.³⁹

The removal of DMPG, TMCL and DMPA from the monolayer (at pH 2 and 5) could be assigned to a partial pseudo-solubilisation of lipids to the subphase via an adsorption on TiO₂-P25 particles. This suggests that the energy of interaction between TiO₂-P25 and lipids and the sedimentation forces counterbalanced the potential barrier to desorb lipids from the interface. The very low ratio between the amount of lipids solubilized and TiO₂-P25 surface (about 1 molecule for 1000 nm² of TiO₂) indicates that the molecular coverage of oxide particle is small. The molecules are either highly dispersed at the whole of oxide surface or heterogeneously adsorbed on the crystalline phase of TiO₂ or on the crystal faces.

For the remaining molecules of DMPA and TMCL at the interface, the appearance of a new transition point on the isotherm curves when the subphase contains TiO₂-P25 (Figure 3.1a, 1c), the longer plateau of coexistence, and the smoother slopes of the curves in liquid condensed phases of DMPG (Figure 3.1b), are the signs of the presence of TiO₂-P25 particles still anchored at the interface. Considering the large tendency of TiO₂-P25 particles to settle, these remaining TiO₂-P25 particles are probably not large (they could correspond to the 140-150 nm particles observed by DLS, see Figure S4 in Supporting Material).

The new transition point on the isotherm curves of DMPA and TMCL in the presence of TiO₂-P25 particles occurs at 17 mN/m, after the plateau of transition from the liquid expanded to liquid condensed state. The similar behaviour of DMPA and TMCL is certainly a fingerprint of the interactions between the lipids and the particles at the interface air-water. The transition point is related to a change in lipid organisation at the interface. As the slopes before and after this point are similar and relatively straight, both states correspond probably to two liquid condensed states. It could result from a change in orientation of the lipid chains, resulting for example from the stress induced by the particles of titania.

It is worth noting that for DMPG, TMCL and DMPS at pH 9, a shift toward higher areas was observed on the compression isotherms, contrary to observations at pH 2 or 5. Thus, in these conditions, solubilisation of the lipid layer did not occur. This suggests that the

potential barrier needed to desorb the hydrophobic phospholipids from the interface was not overcome and that some TiO₂-P25 particles remain at the interface.

3.4.2 Evidence for electrostatic interactions between TiO₂-P25 particles and phospholipids

A comparison of the curves of electrophoretic mobilities *vs* pH (Figure 3.3) with the π -A isotherm curves at pH 2 (Figures 3.1 and S5), pH 5 (Figures 3.2 and S8), and pH 9 (Figure S8) demonstrates that the lipids DMPA, DMPG, DMPS, DHP and TMCL interact with TiO₂-P25 particles when the oxide and the lipids carry opposite charges. Table 3.1 summarizes the results with the expected pH range of opposite charges between each lipid and TiO₂-P25, and the pH values at which the interactions were actually observed. In contrast, interaction effects are weak or absent at pH 2 between DHP or DMPS and TiO₂-P25, but become stronger at pH 5. Since the zeta potential value of DMPS vesicles is approximately – 17 mV at pH 2 and – 60 mV at pH 5, we assume that the lipid is not charged enough at pH 2 to allow attractive interaction with dispersed TiO₂-P25 particles. Similarly to DMPS, the surface charge of DHP vesicles is lower at pH 2 (zeta potential – 15 mV) than at pH 5 (zeta potential – 30 mV). These two cases reveal that both the sign and magnitude of the charges control whether interactions occur or not between the lipids and TiO₂-P25. This threshold of charge (corresponding to a minimum zeta potential of 20 mV) can be applied with DMPE, SM, and DMPC lipids. The low absolute values of zeta potential of DMPE, SM (close to – 10 mV) and DMPC (close to 0) at pH 5.8 indicate that the vesicles are too weakly charged and consequently no interaction was observed in these conditions. Our results are not in contradiction with the recent claim that egg lecithin adsorbs to TiO₂ surface by hydrophobic and electrostatic interactions.¹³ Indeed, egg lecithin (mainly composed of PC and PE) contains also minor amounts of cholesterol (highly hydrophobic) and plasmalogen⁴⁰ which could favour the adsorption and moreover, the deposition was performed in chloroform before drying and dispersion¹³.

Table 3.1. Conditions of interactions between lipids and TiO₂-P25 particles: the first column is the pH range of opposite charge between the two species, as deduced by electrophoretic mobility measurements, the second one presents the effective interactions observed at the air-water interface on monolayer Langmuir films. The letters S (for strong), w (for weak) and vw (very weak) are used to indicate the magnitude of the perturbation of the π -A isotherm curves by TiO₂-P25 particles. The last column indicates the salt concentration that suppressed the interaction.

Lipids	pH range of opposite charge	Effective interactions	Salt concentration screening (mol L ⁻¹)
DMPA	2 – 6.6	S (pH 2, 5)	10 ⁻¹
DMPG	2 – 6.6	S (pH 2, 5)	10 ⁻¹
TMCL	2 – 6.6	S (pH 2)	10 ⁻¹
DHP	2 – 6.6	vw (pH 2) w (pH 5)	10 ⁻²
DMPS	2 – 6.6	w (pH 5)	10 ⁻²
DMPE	5 – 6.6	–	–
SM	5 – 6.6	–	–
DMPC ^(a)	5 – 6.6	–	–

^(a) a previous study carried out at pH 6 ± 1 with dipalmitoylphosphatidylcholine (DPPC) observed a slight effect of DPPC on the surface charge of TiO₂-P25.⁴¹

To confirm that electrostatic forces govern the initial interactions between TiO₂-P25 and phosphated molecules, we repeated the measurements with various concentrations of NaCl in the subphase. At low concentration of NaCl (10⁻² mol L⁻¹), no significant effect of ionic strength could be found on the interactions between DMPA, DMPG or TMCL and TiO₂-P25 at pH 2 (Figure S7 on the left). However, at higher concentration of NaCl (10⁻¹ mol L⁻¹), a greater effect of ionic strength could be seen (Figure S7 on the right). The shift of the π -A isotherm curves is greatly reduced and the isotherm of compressions recorded in the presence and in the absence of TiO₂-P25 overlap. The interactions are thus considerably lowered due to the screening of the surface charge by counterions (Na⁺ and Cl⁻). In the case of DMPS and DHP at pH 5, a concentration of 10⁻² mol L⁻¹ in NaCl in the subphase (Figure S10, panels a and b, respectively) is sufficient to suppress the weaker interactions of DMPS and DHP with TiO₂-P25 particles. Thus, the disappearance of interactions by salting demonstrates the role of long-range electrostatic interactions in the approach of TiO₂-P25 particles onto phosphorylated lipid monolayers.

To conclude, the experiments clearly demonstrate that an effective interaction between lipids and TiO₂-P25 can take place when two conditions are fulfilled: both must be oppositely and sufficiently charged. This minimum charge can be related to an absolute value of the zeta potential close to 20 mV, considering the approximation applied for its calculation. However, in the case of DMPG, TMCL and DMPS, other strong interactions exist between the surface of TiO₂-P25 and the phospholipids and we cannot exclude that they also occur via electrostatic interactions.

3.4.3 Significance of the molecular structure in the adsorption of lipids onto TiO₂

In the literature, the binding of phosphate species (PO₄³⁻) on titania surfaces is often described as a chemisorption process with the formation of bridging bidentate surface complexes such as TiO-P(O₂)-OTi. However the infrared spectra have not allowed bridging bidentate and chelate species to be distinguished^{17,18,20} and the occurrence of both monodentate and chelating bidentate species was not excluded⁴². Gong et al. also detected the electrostatically adsorbed PO₄³⁻ ion that attained equilibrium slower than the chemisorbed phosphate species.¹⁸ The number of substituents on the phosphate group plays a large role. When phosphate was substituted with an alkane chain (n-butyl or longer), the compound still adsorbed on titania at pH 6 whereas the substitution with two methyl groups prevented the adsorption.¹⁷ The authors concluded that monodentate binding of phosphate species to oxides is not viable in aqueous solution. Our results suggest that dimethyl phosphate was most probably not charged enough at pH 6 to interact with titania (weaker Lewis acid) and consequently this does not exclude the formation of monodentate binding.

DMPA with only one substituent and DHP with two substituents resemble n-butyl phosphate and dimethyl phosphate respectively (Figure S1). DMPA possesses the three oxygen atoms available for bridging similarly to the monocatenar alkyl phosphate. Due to its long chain, the bridging of the latter is a mixture between mono- and bidentate species.⁴³ For DHP (Figure S1d), weaker interactions with TiO₂-P25 particles were observed at pH 2 (Table 3.1) than those observed for DMPA. The low electrophoretic mobility indicates that the head polar group is not deprotonated at pH 2. This may hamper good electronic delocalization on both free oxygen atoms that are involved in the adsorption of phosphate groups onto the surface of TiO₂.^{17,18,20,42} At pH 5, the two oxygen atoms are deprotonated allowing a stronger interaction than at pH 2.

For the other phospholipids DMPG, TMCL and DMPS, where the phosphorus atoms are also linked to two substituents, the interactions were similar or even stronger than for

DHP. The formation of a bridging bidentate surface complex between DMPG, TMCL or DMPS and TiO₂-P25 particles might occur providing there is a good electronic delocalisation on both free oxygen atoms linked to P. However, this hypothesis is not sufficient to explain the stronger interactions than for DHP, nor the weak interactions observed at pH 9 for these molecules. To explain such a difference, we have to consider the presence of hydroxyl and carboxylate groups in the polar substituent of phosphorus. The hydroxyl groups of the terminal glycerol could interact with the surface of TiO₂, as mentioned in the literature, where adsorption of molecules onto TiO₂ through hydroxyl groups was reported⁴⁴. This would also explain the remaining interactions at pH 9 or at pH 2 with NaCl 0.1 mol L⁻¹ for TMCL and DMPG. Similarly, the adsorption of carboxylate was also reported onto TiO₂ with a monodentate anchoring.^{45,46} This could facilitate the interactions of DMPS with titania surface, as the phosphate group is more embedded in the molecular structure. The involvement of the carboxylate groups in the interactions of DMPS with TiO₂-P25 particles can also be understood from the results of DMPE. The molecular structure of DMPS derives from DMPE by the substitution of a hydrogen atom by a carboxyl group -COOH. Whereas DMPE has no interaction with TiO₂-P25, the introduction of a negatively charged group -COO⁻ creates a favourable environment for adsorption on the inorganic surface. The changes in interfacial properties of DMPS at pH 5 and not at pH 2 confirm that the interactions of DMPS with titania are mediated by the carboxylate group providing the pH is high enough to deprotonate the carboxyl group (pH > 4). It suggests that the phosphate in DMPS is not involved in the interaction with titania. The screening of interaction between DMPS and titania at lower NaCl concentrations than for phosphate can then be explained by the weaker adsorption of carboxylates onto TiO₂ surfaces than that of phosphate species.⁴⁷

3.5 Conclusion

Surface tension measurements combined with laser Doppler electrophoresis can be used to determine the nature of forces mediating the adsorption of different classes of phospholipids onto titanium dioxide. Previously, the interaction for PC, PC+PG and PC+PS mixtures was assumed electrostatic in origin^{10,13,15,16,48} with Van der Waals interactions¹⁰. Our results show that the driving forces are electrostatic but not sufficient: hydrogen bonds are also involved depending on the head polar group. In fact, the phospholipids 1,2-dimyristoyl-*sn*-glycero-3-phosphate monosodium salt (DMPA), 1,2-dimyristoyl-*sn*-glycero-3-phospho-*rac*-1-glycerol (DMPG), 1',3'-bis[1,2-dimyristoyl-*sn*-glycero-3-phospho]-*sn*-glycerol (TMCL), 1,2-dimyristoyl-*sn*-glycero-3-phospho-L-serine (DMPS) and the synthetic lipid

dihexadecyl phosphate (DHP) actually interact with the TiO₂-P25 surface via electrostatic interactions, *i.e.* under pH conditions where TiO₂-P25 and the phospholipid are oppositely charged (between 2 and 6.6). We note that the electrostatic interactions identified between DMPS, DHP and TiO₂ were more easily screened by NaCl than the electrostatic interactions between DMPA, DMPG, TMCL and TiO₂. The involvement of the phosphate group from lipids in the interaction with titania is assumed for DMPA and DHP while the carboxylate group is involved in the interaction between DMPS and TiO₂. However, another kind of binding was demonstrated for DMPG and TMCL in conditions of repulsive electrostatic interactions. We assume this involves the hydroxyl groups of the terminal glycerol. The other membrane lipids such as 1,2-dimyristoyl-*sn*-glycero-3-phosphocholine (DMPC), 1,2-dimyristoyl-*sn*-glycero-3-phosphoethanolamine (DMPE) and sphingomyelin (SM) are not able to interact with TiO₂-P25 regardless of pH, probably due to their zwitterionic nature. This result is not in contradiction with previous studies as divalent cations mediated the adsorption of phospholipids onto TiO₂.^{15,49,50} Finally, the different pH- and salt-dependence of the affinities of phospholipids to titanium dioxide may help in understanding or improving the chromatographic process using titanium dioxide as a stationary phase.^{5,8,51} This work is also expected to serve as a basis for in-depth understanding of particle interactions with biological membranes.

Aknowledgments

Eric Gautron and Florin Popa are acknowledged for the characterization of TiO₂-P25 particles by TEM and XRD respectively, as well as Chris Ewels for revision of the manuscript and English corrections.

Supporting information (Chapter 3)

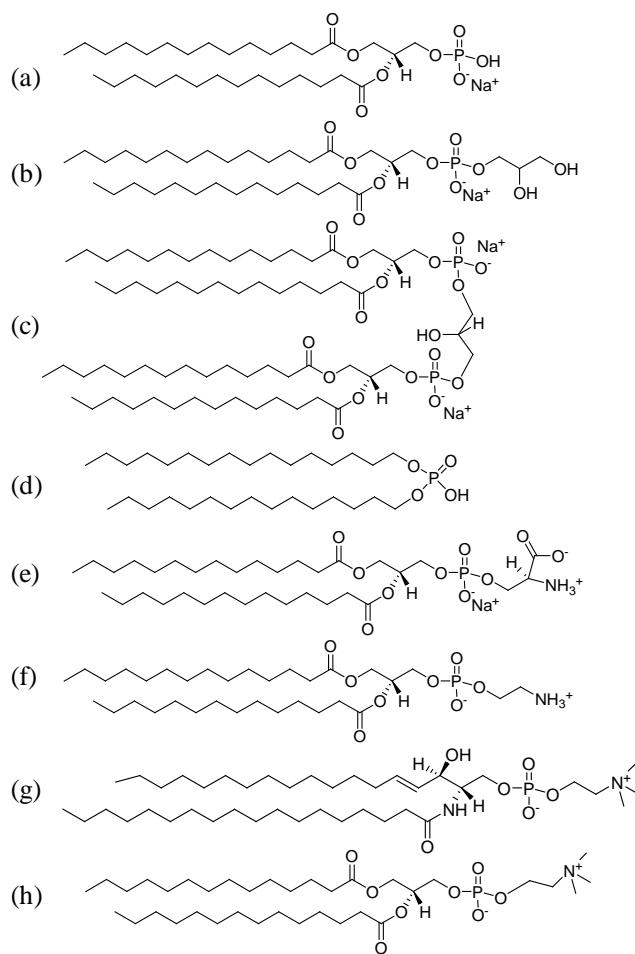


Figure S1. Molecular structures of lipids carrying two C16 chains (except sphingomyelin) or four C16 chains (cardiolipin) and different polar head groups: (a) glycerophosphate, (b) glycerophosphoglycerol, (c) cardiolipin, (d) dihexadecyl phosphate, (e) glycerophosphoserine, (f) glycerophosphoethanolamine, (g) sphingomyelin, and (h) glycerophosphocholine.

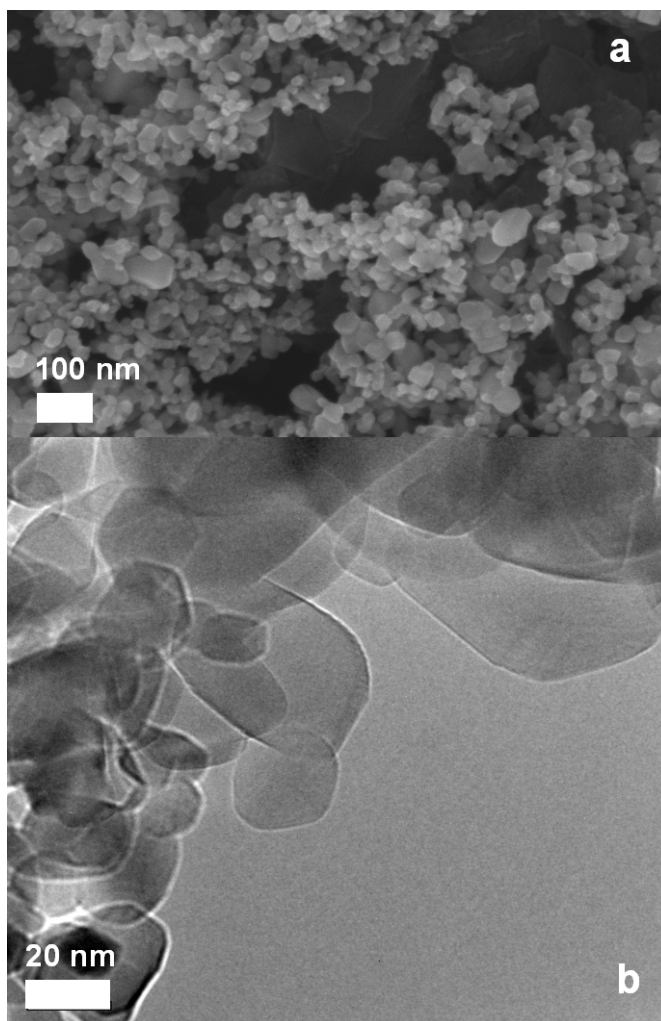


Figure S2. Morphology and size of TiO₂-P25 particles observed by Scanning Electron Microscopy (a) and Transmission Electron Microscopy (b).

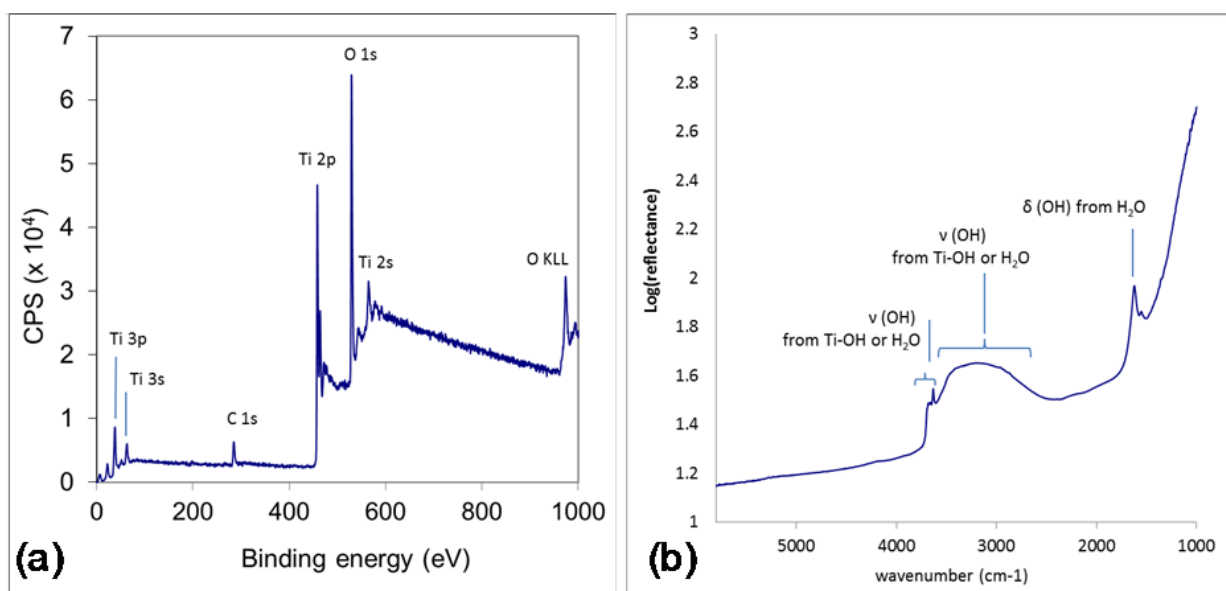


Figure S3. (a) XPS profile of TiO_2 -P25 particles recorded with AXIS Nova model from Kratos Analytical (Manchester, UK) and treated by Casa XPS software. The assignment is in agreement with the data of Diebold and Madey (Surface Science Spectra, Vol. 4, No. 3, 227-231). No contaminants like sodium or calcium ions are present. Carbon comes from the sample cup as proved by the infrared spectra without organic contamination. (b) Infrared spectra of TiO_2 -P25 powder (2% humidity, 30 °C) recorded without diluting material with FTIR Bruker Vertex 70 spectrometer (Bruker, Ettlingen, Germany) in a diffuse reflectance mode (DRIFT). The spectrum was recorded at a resolution of 4 cm^{-1} with 1000 scans in the wavenumber range of $400 - 8000 \text{ cm}^{-1}$ and treated by using OPUS 5.5 software provided by Bruker company. No contamination (carbonate at 1200 cm^{-1} or organic matter at 2800 cm^{-1}) is present in the sample.

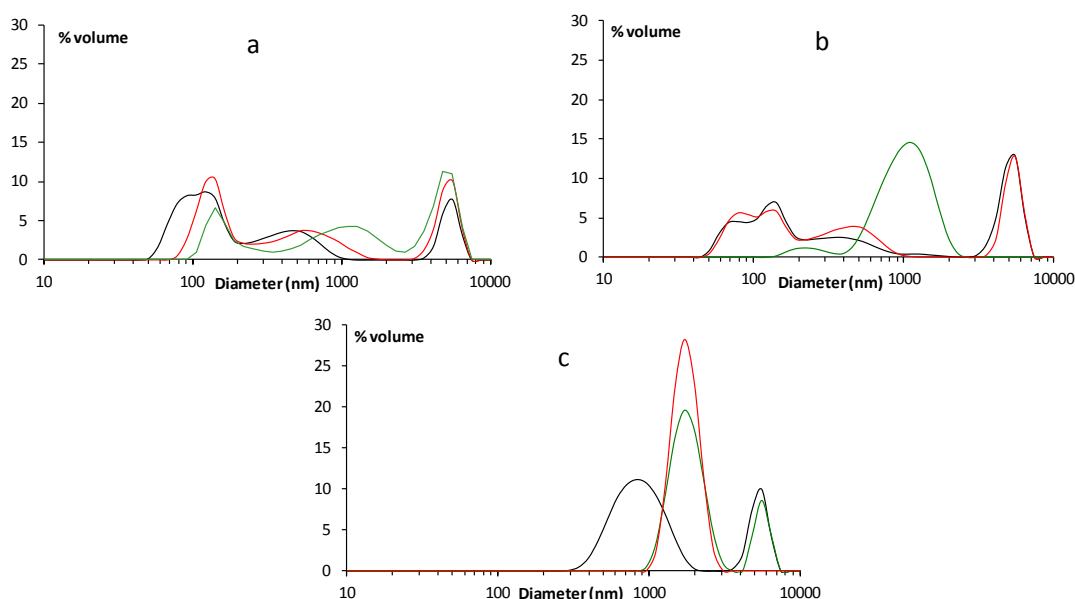


Figure S4. Size distribution in volume of $\text{TiO}_2\text{.P25}$ suspensions (0.1 g/L) according to pH and NaCl concentration. Black lines refer to pH 2; green lines to pH 5 and red lines to pH 9. The concentration in NaCl was (a) $10^{-3} \text{ mol.L}^{-1}$, (b) $10^{-2} \text{ mol.L}^{-1}$ and (c) $10^{-1} \text{ mol.L}^{-1}$. Data were accumulated 3 times with 12 scans of 10s. At pH 2 and 9, and for $\text{NaCl} < 10^{-1} \text{ mol.L}^{-1}$, the suspensions were composed of three populations ranging from 50 nm to 1 μm . Under the assumption that particles are spherical and homogeneous, a simple calculation allowed us to estimate the surface contribution of each population. The smallest particles, with a diameter of 140-150 nm, develop a surface 5 to 10 times higher than the ones developed by the particles of about 700 nm. Thus, the contribution of these small particles represents between 80 and 90% of the total surface area of the solid. If very large aggregates (diameter $> 6 \mu\text{m}$) appear, their number is however negligible in the suspension, and they only contribute to 1% of the total surface area of the solid. At high ionic strength ($\text{NaCl } 10^{-1} \text{ mol.L}^{-1}$), the suspension contained larger particles in particular at pH 9, meaning that the particles remain agglomerated. At pH 5, the suspension was mainly composed of one population of large size (around 1.5 μm).

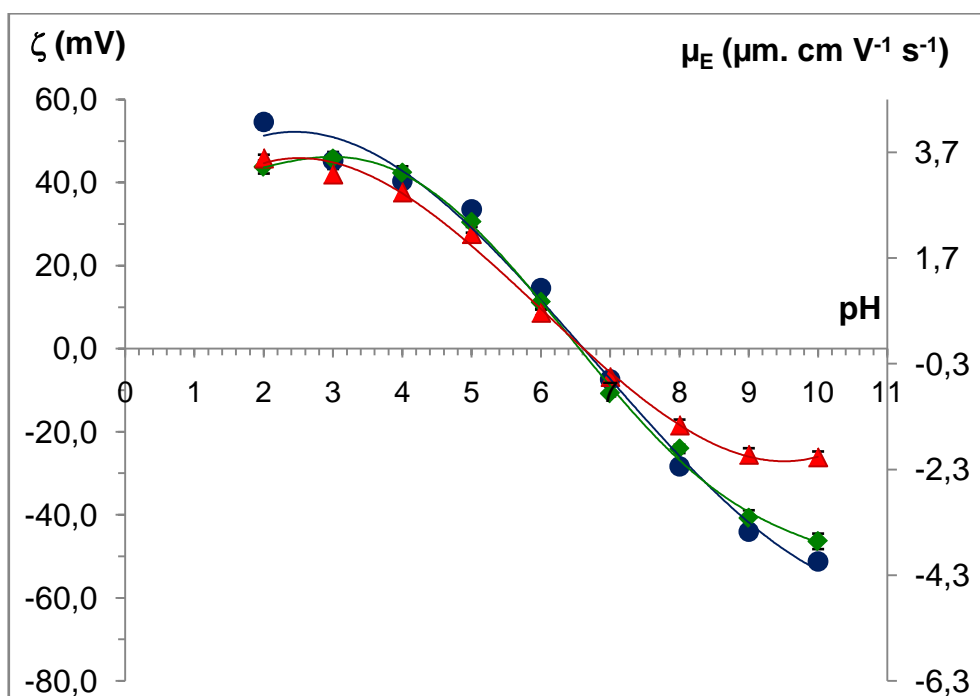


Figure S5. Electrophoretic mobility (on the right axis) converted in zeta potential (on the left axis) of $\text{TiO}_2\text{.P25}$ suspensions (0.1 g/L) according to pH for various ionic strengths: (●) $\text{NaCl } 10^{-3} \text{ mol L}^{-1}$, (◆) $\text{NaCl } 10^{-2} \text{ mol L}^{-1}$ and (▲) $\text{NaCl } 10^{-1} \text{ mol L}^{-1}$. The lines are a guide to the eye to visualize the evolution of electrophoretic mobility (or zeta potential) versus pH and have no physical meaning. The standard deviation is hidden behind points ($n = 3$, six measures for each).

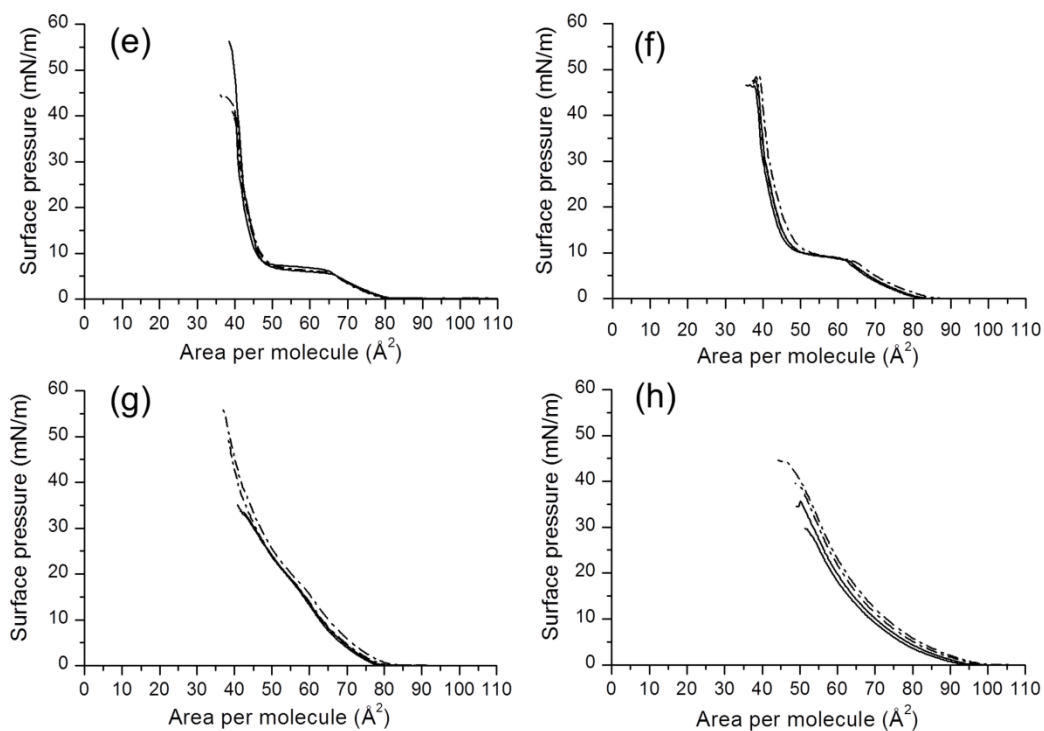


Figure S6. π -A isotherm curves of lipid monolayers ($n=2$) at the interface air-subphases of pure water at pH 2 (solid line) and of aqueous dispersions of TiO₂-P25 particles at 0.1 g L⁻¹ and pH 2 (dash dotted line), at 25 °C. Lipids refer to (e) DMPS, (f) DMPE, (g) SM and (h) DMPC.

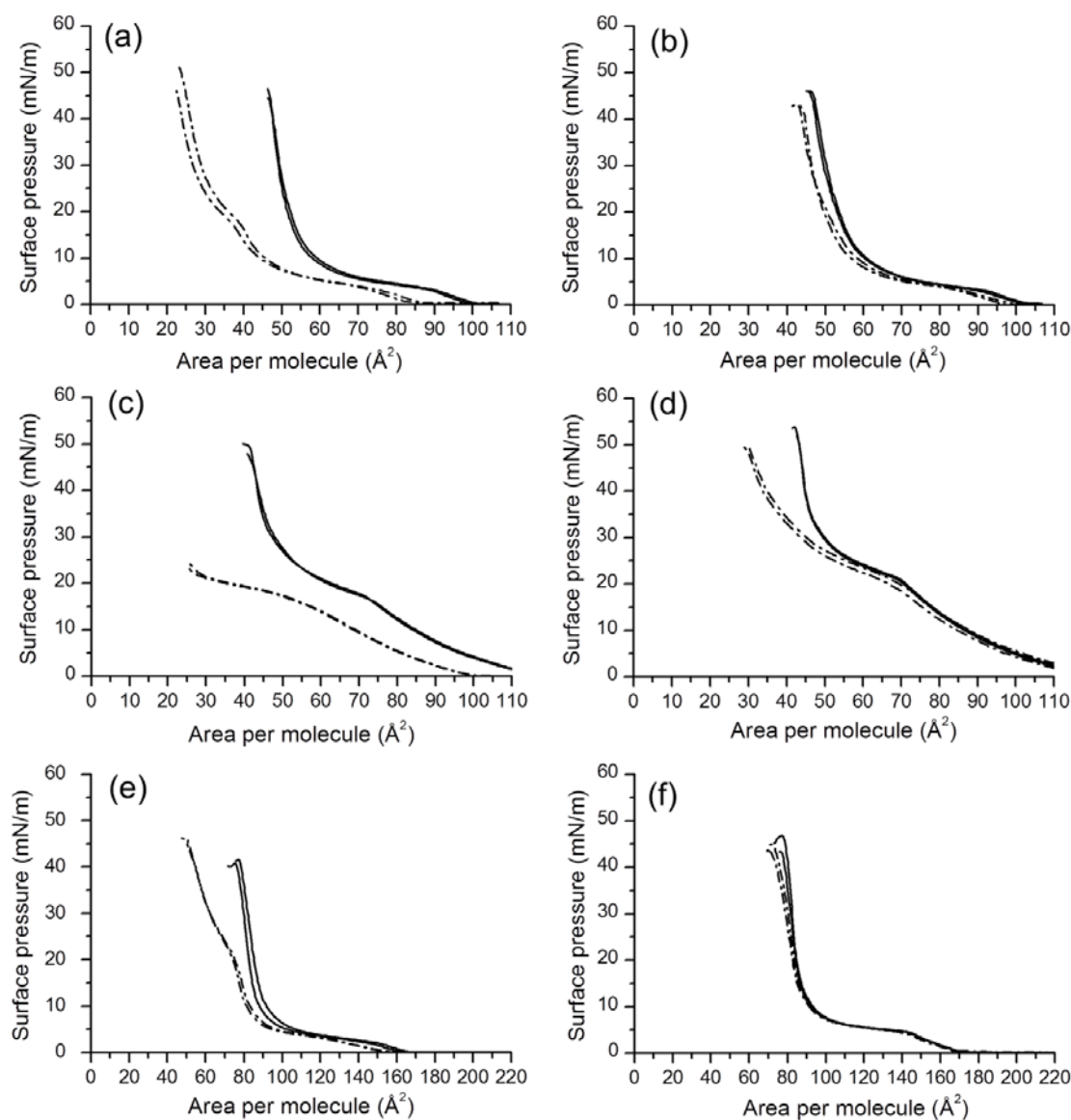


Figure S7. π -A isotherms of monolayers ($n=2$) made of (a, b) DMPA, (c,d) DMPG, and (e, f) TMCL lipids at the interface air- aqueous saline solution (NaCl in solid line) or aqueous dispersions of TiO_2 -P25 particles at 0.1 g L^{-1} with NaCl (dash dotted line). pH was fixed at 2 and temperature was 25°C for all panels. The concentrations in salt were $10^{-2} \text{ mol L}^{-1}$ for panels a, c and e; $10^{-1} \text{ mol L}^{-1}$ for panels b, d and f.

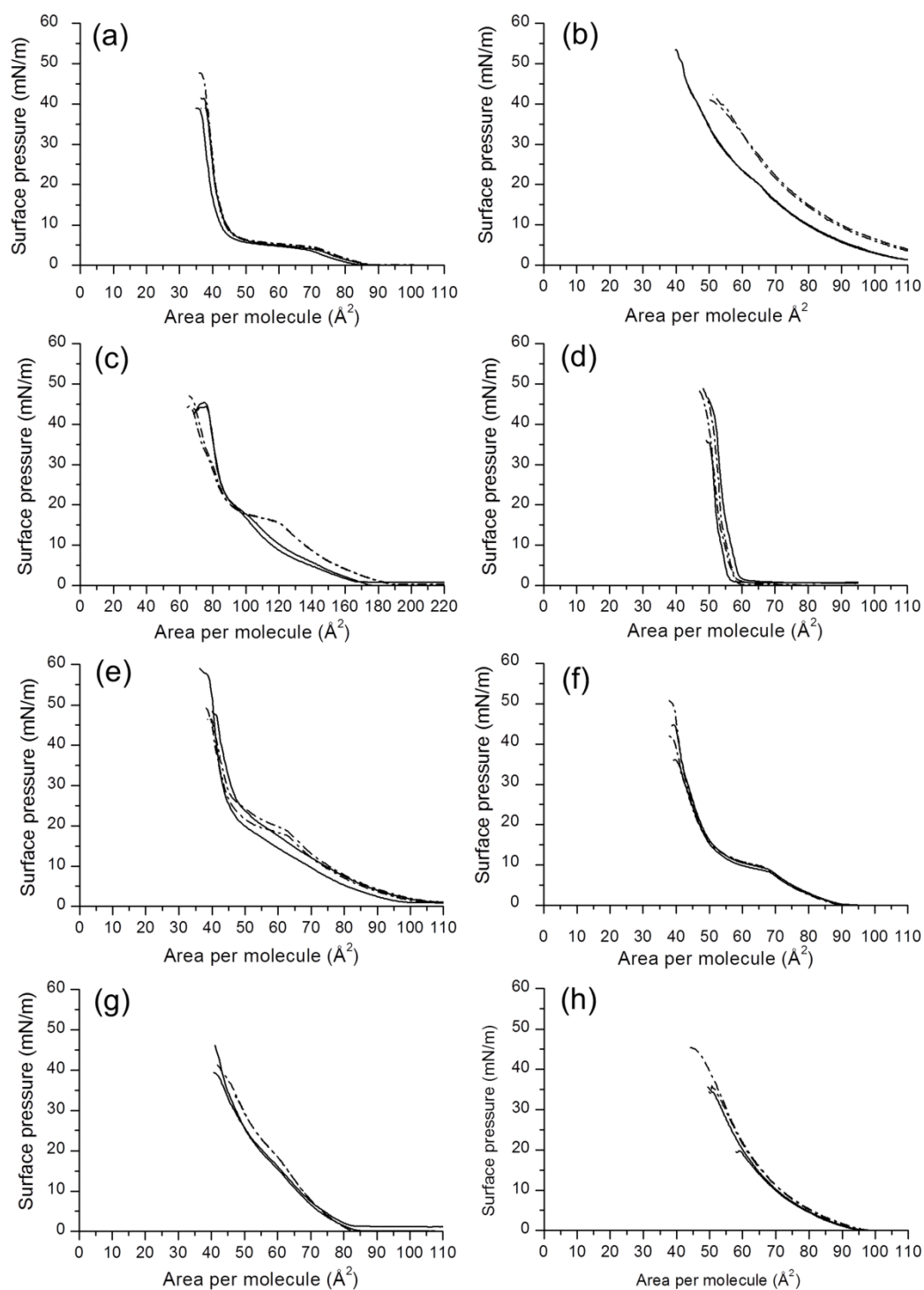


Figure S8. π -A isotherm curves of lipid monolayers ($n=2$) on subphases of pure water at pH 9 (solid line) and aqueous dispersions of TiO_2 -P25 particles at 0.1 g L^{-1} and pH 9 (dash dotted line), at $25 \text{ }^\circ\text{C}$. Lipids refer to (a) DMPA, (b) DMPG, (c) TMCL, (d) DHP, (e) DMPS, (f) DMPE, (g) SM, and (h) DMPC.

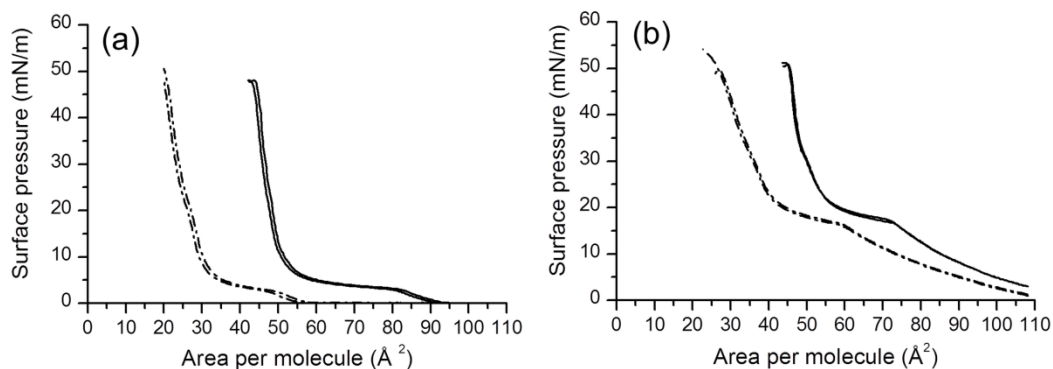


Figure S9. π -A isotherm curves of lipid monolayers ($n=2$) on subphases of pure water (solid line) and of aqueous dispersions of TiO_2 -P25 particles at 0.1 g L^{-1} (dash dotted line). The pH value of the subphase was 5 at a temperature of $25 \text{ }^\circ\text{C}$ for all panels: (a) DMPA and (b) DMPG.

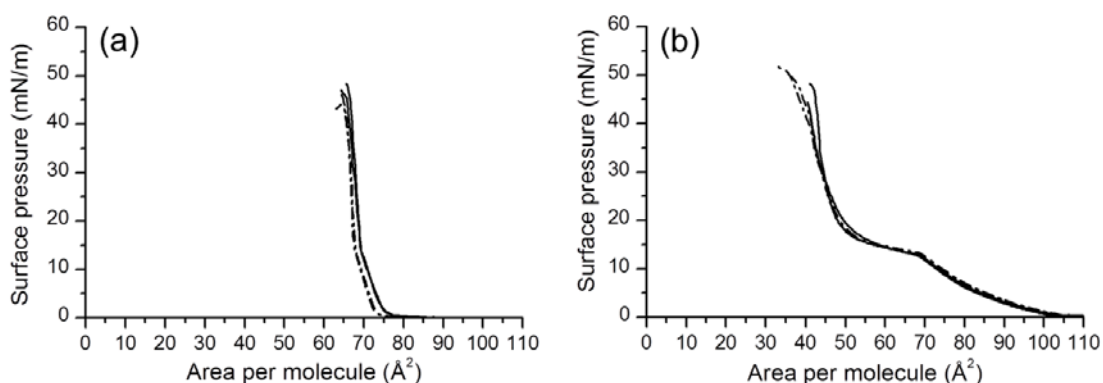


Figure S10. π -A isotherm curves of (a) DHP and (b) DMPS monolayers ($n=2$) at $25 \text{ }^\circ\text{C}$ on subphases of pure water (solid line) and aqueous dispersions of TiO_2 -P25 particles at 0.1 g L^{-1} (dash dotted line). Both subphases were adjusted at pH 5 and contained $10^{-2} \text{ mol L}^{-1}$ NaCl.

References

1. Weir, A., Westerhoff, P., Fabricius, L., Hristovski, K. & von Goetz, N. Titanium dioxide nanoparticles in food and personal care products. *Environ. Sci. Technol.* **46**, 2242–50 (2012).
2. Lin, C. C. & Lin, W. J. Sun protection factor analysis of sunscreens containing titanium dioxide nanoparticles. *J. Food Drug Anal.* **19**, 1–8 (2011).
3. Iavicoli, I., Leso, V., Fontana, L. & Bergamaschi, A. Toxicological effects of Titanium nanoparticles: a review of in vitro mammalian studies. *Eur. Rev. Med. Pharmacol. Sci.* **15**, 481–508 (2011).
4. Fenoglio, I., Fubini, B., Ghibaudi, E. M. & Turci, F. Multiple aspects of the interaction of biomacromolecules with inorganic surfaces. *Adv. Drug Deliv. Rev.* **63**, 1186–209 (2011).
5. Calvano, C. D., Jensen, O. N. & Zambonin, C. G. Selective extraction of phospholipids from dairy products by micro-solid phase extraction based on titanium dioxide microcolumns followed by MALDI-TOF-MS analysis. *Anal. Bioanal. Chem.* **394**, 1453–1461 (2009).
6. Cho, N. J. & Frank, C. W. Fabrication of a Planar Zwitterionic Lipid Bilayer on Titanium Oxide. *Langmuir* **26**, 15706–15710 (2010).
7. Fortunelli, A. & Monti, S. Simulations of lipid adsorption on TiO₂ surfaces in solution. *Langmuir* **24**, 10145–10154 (2008).
8. Hsu, S.-H., Lin, Y.-F. & Chung, T.-W. Potential of metal oxides on the removal of phospholipids in crude *Jatropha curcas* oil. *J. Taiwan Inst. Chem. Eng.* **43**, 659–662 (2012).
9. Khan, T. R. *et al.* Lipid redistribution in phosphatidylserine-containing vesicles adsorbing on titania. *Biointerphases* **3**, FA90–FA95 (2008).
10. Oleson, T. A., Sahai, N. Oxide-dependent adsorption of a model membrane phospholipid, dipalmitoylphosphatidylcholine: Bulk adsorption isotherms. *Langmuir* **24**, 4865–4873 (2008).
11. Tero, R. Substrate Effects on the Formation Process, Structure and Physicochemical Properties of Supported Lipid Bilayers. *Materials (Basel)*. **5**, 2658–2680 (2012).
12. Tero, R., Ujihara, T. & Urisut, T. Lipid Bilayer Membrane with Atomic Step Structure: Supported Bilayer on a Step-and-Terrace TiO₂(100) Surface. *Langmuir* **24**, 11567–11576 (2008).
13. Wiącek, A. E., Anitowska, E., Delgado, A. V., Hołysz, L. & Chibowski, E. The electrokinetic and rheological behavior of phosphatidylcholine-treated TiO₂ suspensions. *Colloids Surfaces A Physicochem. Eng. Asp.* **440**, 110–115 (2014).

14. Xu, J., Stevens, M. J., Oleson, T. A., Last, J. A. & Sahai, N. Role of Oxide Surface Chemistry and Phospholipid Phase on Adsorption and Self-Assembly: Isotherms and Atomic Force Microscopy. *J. Phys. Chem. C* **113**, 2187–2196 (2009).
15. Csucs, G. & Ramsden, J. J. Solubilization of planar bilayers with detergent. *Biochim. Biophys. Acta* **1369**, 304–308 (1998).
16. Ohlsson, G., Tigerström, A., Höök, F. & Kasemo, B. Phase transitions in adsorbed lipid vesicles measured using a quartz crystal microbalance with dissipation monitoring. *Soft Matter* **7**, 10749 (2011).
17. Connor, P. A. & Mcquillan, A. J. Phosphate Adsorption onto TiO₂ from Aqueous Solutions: An in Situ Internal Reflection Infrared Spectroscopic Study. *Langmuir* **15**, 2916–2921 (1999).
18. Gong, W. A real time in situ ATR-FTIR spectroscopic study of linear phosphate adsorption on titania surfaces. *Int. J. Miner. Process.* **63**, 147–165 (2001).
19. Hadjiivanov, K. I., Klissurski, D. G. & Davydov, A. A. Study of Phosphate-Modified TiO₂ (Anatase). *J. Catal.* **116**, 498–505 (1989).
20. Myller, A. T., Karhe, J. J. & Pakkanen, T. T. Preparation of aminofunctionalized TiO₂ surfaces by binding of organophosphates. *Appl. Surf. Sci.* **257**, 1616–1622 (2010).
21. Chang, X., Zhang, Y., Tang, M. & Wang, B. Health effects of exposure to nano-TiO₂: a meta-analysis of experimental studies. *Nanoscale Res. Lett.* **8**, 51 (2013).
22. Iavicoli, I., Leso, V. & Bergamaschi, A. Toxicological Effects of Titanium Dioxide Nanoparticles: A Review of In Vivo Studies. *J. Nanomater.* **2012**, 1–36 (2012).
23. Suh, W. H., Suslick, K. S., Stucky, G. D. & Suh, Y.-H. Nanotechnology, nanotoxicology, and neuroscience. *Prog. Neurobiol.* **87**, 133–70 (2009).
24. Henderson, M. A. A surface science perspective on TiO₂ photocatalysis. *Surf. Sci. Rep.* **66**, 185–297 (2011).
25. Ohno, T., Sarukawa, K., Tokieda, K. & Matsumura, M. Morphology of a TiO₂ Photocatalyst (Degussa, P25) Consisting of Anatase and Rutile Crystalline Phases. *J. Catal.* **203**, 82–86 (2001).
26. Ohtani, B., Prieto-Mahaney, O. O., Li, D. & Abe, R. What is Degussa (Evonik) P25? Crystalline composition analysis, reconstruction from isolated pure particles and photocatalytic activity test. *J. Photochem. Photobiol. A Chem.* **216**, 179–182 (2010).
27. Hunter, J. R. *Foundations of Colloid Science. J. Psychother. Pract. Res.* **5**, (Oxford university Press, 2001).
28. Leroy, P., Tournassat, C. & Bizzi, M. Influence of surface conductivity on the apparent zeta potential of TiO₂ nanoparticles. *J. Colloid Interface Sci.* **356**, 442–53 (2011).

29. Pagnout, C. *et al.* Role of electrostatic interactions in the toxicity of titanium dioxide nanoparticles toward *Escherichia coli*. *Colloids Surf. B. Biointerfaces* **92**, 315–21 (2012).
30. Suttiponparnit, K. *et al.* Role of Surface Area, Primary Particle Size, and Crystal Phase on Titanium Dioxide Nanoparticle Dispersion Properties. *Nanoscale Res. Lett.* **6**, 27 (2011).
31. Mingotaud, A. F., Mingotaud, C. & Patterson, L. K. *Handbook of monolayers, Vol 1.* (Academic Press, 1993).
32. Israelachvili, J. N. *Intermolecular and surface forces.* (Academic Press, 2011).
33. Sabín, J., Vázquez-Vázquez, C., Prieto, G., Bordi, F. & Sarmiento, F. Double charge inversion in polyethylenimine-decorated liposomes. *Langmuir* **28**, 10534–42 (2012).
34. Galera-Cortés, E., Solier, J. D. D., Estelrich, J. & Hidalgo-Alvarez, R. Study on the correlation between lateral diffusion effect and effective charge in neutral liposomes. *Langmuir* **26**, 2665–70 (2012).
35. Garcia-Manyes, S. & Sanz, F. Nanomechanics of lipid bilayers by force spectroscopy with AFM: a perspective. *Biochim. Biophys. Acta* **1798**, 741–9 (2010).
36. Lairion, F. & Disalvo, E. A. Effect of dipole potential variations on the surface charge potential of lipid membranes. *J. Phys. Chem. B* **113**, 1607–14 (2009).
37. Makino, K. *et al.* Temperature- and ionic strength-induced conformational changes in the lipid head group region of liposomes as suggested by zeta potential data. *Biophys. Chem.* **41**, 175–83 (1991).
38. Ramos, A. P., Pavani, C., Yamamoto, Y. & Zaniquelli, M. E. D. Porphyrin-phospholipid interaction and ring metallation depending on the phospholipid polar head type. *J. Colloid Interface Sci.* **350**, 148–54 (2010).
39. McNamee, C. E., Yamamoto, S., Butt, H.-J. & Higashitani, K. A straightforward way to form close-packed TiO₂ particle monolayers at an air/water interface. *Langmuir* **27**, 887–94 (2011).
40. Palacios, L. E. & Wang, T. Egg-yolk lipid fractionation and lecithin characterization. *J. Am. Oil Chem. Soc.* **82**, 571–578 (2005).
41. Chibowski, E., Holysz, L., Terpilowski, K. & Wiacek, A. E. Influence of Ionic Surfactants and Lecithin on Stability of Titanium Dioxide in Aqueous Electrolyte Solution. *Croat. Chem. Acta* **80**, 395–403 (2007).
42. Raj, K. J. A., Shanmugam, R., Mahalakshmi, R. & Viswanathan, B. XPS and IR spectral studies on the structure of phosphate and sulphate modified titania – A combined DFT and experimental study. *Indian J. Chem.* **49A**, 9–17 (2010).
43. Spori, D. M. *et al.* Influence of alkyl chain length on phosphate self-assembled monolayers. *Langmuir* **23**, 8053–60 (2007).

44. Zhou, C.-H. *et al.* Effect of poly (ethylene glycol) on coarsening dynamics of titanium dioxide nanocrystallites in hydrothermal reaction and the application in dye sensitized solar cells. *J. Colloid Interface Sci.* **374**, 9–17 (2012).
45. Thomas, A. G. & Syres, K. L. Adsorption of organic molecules on rutile TiO₂ and anatase TiO₂ single crystal surfaces. *Chem. Soc. Rev.* **41**, 4207–17 (2012).
46. Mpandou, A. & Siffert, B. Sodium Carboxylate Adsorption onto TiO₂: Shortest Chain Length Allowing Hemimicelle Formation and Shear Plane Position in the Electric Double Layer. *J. Colloid Interface Sci.* **102**, 138–145 (1984).
47. Luschtinetz, R., Gemming, S. & Seifert, G. Anchoring functional molecules on TiO₂ surfaces: A comparison between the carboxylic and the phosphonic acid group. *Eur. Phys. J. Plus* **126**, 98 (2011).
48. Cho, N.-J., Jackman, J. a, Liu, M. & Frank, C. W. pH-driven assembly of various supported lipid platforms: a comparative study on silicon oxide and titanium oxide. *Langmuir* **27**, 3739–48 (2011).
49. Rossetti, F. F., Bally, M., Michel, R., Textor, M. & Reviakine, I. Interactions between titanium dioxide and phosphatidyl serine-containing liposomes: Formation and patterning of supported phospholipid bilayers on the surface of a medically relevant material. *Langmuir* **21**, 6443–6450 (2005).
50. Rossetti, F. F., Textor, M. & Reviakine, I. Asymmetric distribution of phosphatidyl serine in supported phospholipid bilayers on titanium dioxide. *Langmuir* **22**, 3467–3473 (2006).
51. Ikeguchi, Y. & Nakamura, H. Selective enrichment of phospholipids by titania. *Anal. Sci.* **16**, 541–543 (2000).

Chapter 4

Effect of the phase crystallinity of TiO₂ on the interaction with phospholipids

Table of Contents

4. Effect of the phase crystallinity of TiO ₂ on the interaction with phospholipids	183
4.1 Introduction	183
4.2 Materials and methods.....	183
4.3 Results	187
4.3.1 Surface pressure-area isotherms of phospholipids on anatase and rutile suspensions.....	187
4.3.2 Amount of phospholipids adsorbed on anatase and rutile.....	193
4.3.3 Surface charge of TiO ₂ particles after adsorption of phospholipids	196
4.3.4 Effect of surface chemistry of various anatase phases on the interactions between TiO ₂ and phospholipids.....	198
4.4 Discussion	200
4.5 Conclusion.....	201
References	202

4. Effect of the phase crystallinity of TiO₂ on the interaction with phospholipids

4.1 Introduction

TiO₂-P25 particles were proven to have strong interaction with several phospholipids, particularly DMPA and DMPG (see chapter 3). The chemical structure of both phospholipids differs by the head groups (figure 4.1). DMPA interacts mainly with TiO₂-P25 particles by electrostatic interactions in the pH range 2-6.6 whereas both electrostatic and non-electrostatic interactions are involved in the adsorption of DMPG with TiO₂-P25 particles, the electrostatic interactions being predominant in the pH range 2-6.6 and the non-electrostatic interactions over 6.6. In fact, TiO₂-P25 particles are constituted of two kinds of crystals, anatase (84 wt%) and rutile (16 wt%). Moreover, anatase particles are smaller than rutile particles. It is currently not known whether anatase or rutile plays a role in the interaction with phospholipids. Since the formation of support lipid bilayer is significantly influenced by physical properties and chemical composition of substrate,¹ the adsorption on rutile and anatase might be different.

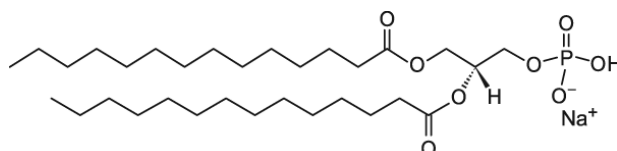
In this chapter, the objective is to determine whether DMPA and DMPG, the main adsorbing phospholipid on TiO₂-P25 particles, adsorb preferentially on a crystal structure or not. To differentiate the effect of each polymorph crystallite in TiO₂-P25 we need to isolate the phases of anatase and rutile. However, these isolation processes with very active chemical substances such as HF and H₂O₂ can alter surface chemistry of the separated particles.^{2,3} Therefore, we used commercial nanopowders. Four anatase powders and one rutile powder were selected for their various specific areas and size of the primary particles, provided in Table 4.1. The interaction of anatase and rutile particles with DMPA and DMPG was detected by surface pressure-area isotherms and zeta potentials, while the adsorbed amount was quantified by batch adsorption experiments.

4.2 Materials and methods

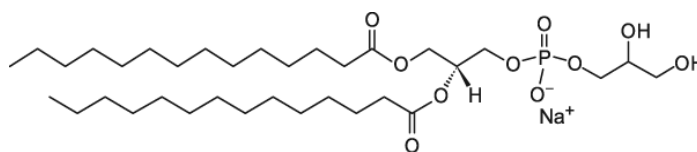
Materials

A pure crystalline phase of anatase (IEP 6) with a high specific area (136 m²/g) was obtained from MTI corporation (TiO₂-A). Pure crystalline phases of anatase with a higher isoelectric point and various specific areas (TiO₂-PC10, TiO₂-PC50 and TiO₂-PC100) were obtained from Millenium company (Hunt Valley, Maryland, USA). Rutile

phase (TiO₂-R) was purchased from Sigma-Aldrich (Missouri, USA). The characterization of these powders is reported in chapter 2. Lipids are 1,2-dimyristoyl-*sn*-glycero-3-phosphate monosodium salt (DMPA, monosodium salt, >99%, from Avanti Polar Lipids) and 1,2-dimyristoyl-*sn*-glycero-3-phospho-*rac*-1-glycerol (DMPG, sodium salt, 99%, Sigma Aldrich) (see Figure 4.1). The pH values of suspensions were adjusted with NaOH solutions prepared from NaOH solid state in flake form (99%, Alfa Aesar, MA, USA) and HCl solutions prepared from HCl solution 37% (Carlo ERBA, Milan, Italy). NaCl solutions for controlling ionic strength were prepared from solid NaCl (Bioextra, 99.5%, Sigma Aldrich). Chloroform CHCl₃, methanol CH₃OH, ethanol C₂H₅OH were obtained from Carlo ERBA (Milan, Italy). Water was ultrapure H₂O and came from Milli-Q purification system (Millipore Corporation), with resistivity of 18 MΩ.cm.



1,2-dimyristoyl-*sn*-glycero-3-phosphate monosodium salt (DMPA)



1,2-dimyristoyl-*sn*-glycero-3-phospho-*rac*-1-glycerol monosodium salt (DMPG)

Figure 4.1. Chemical structure of DMPA and DMPG

For convenience, the main properties of TiO₂ powders are reported again in table 4.1.

Table 4.1. Some properties of TiO₂ powders.

Sample	Approximate particle average diameter (nm)	BET Surface area (m ² /g)	IEP
TiO ₂ -P25	25	48 ± 0.1	6.5
TiO ₂ -A	18	136 ± 0.5	6
TiO ₂ -R	22	26 ± 0.06	5.5
TiO ₂ -PC10	72	9 ± 0.07	7
TiO ₂ -PC50	30	48 ± 0.09	7
TiO ₂ -PC100	22	75 ± 0.3	7

Sample preparation

All steps to prepare suspensions of TiO₂ particles and phospholipid vesicles were similar to those described in chapter 2. However, the initial amounts of TiO₂ were adapted to get final concentrations of TiO₂ ranging between 20 and 500 mg/L. For phospholipids, the suspensions with different concentrations were obtained by dilution from the stock suspension at 0.4 g/L.

Surface pressure-area isotherms from Langmuir trough

The protocol to prepare phospholipid monolayers and acquire surface pressure-area isotherms was identical to that described in chapter 2 and chapter 3. Briefly, the suspension of TiO₂ particles was introduced in the trough and the monolayer of phospholipid was formed on the top of the subphase. After 10 minutes, the pressure-area was recorded. The temperature of the trough was controlled at 25 °C with a water-circulation system. Each isotherm was recorded at least two times to guarantee the reproducibility of the results.

Batch adsorption experiments

The adsorption experiments were carried out for each couple (TiO₂/phospholipid). The stock suspensions of DMPA and DMPG were mixed with TiO₂ suspensions in polypropylene tubes. The final volume was adjusted to 10 mL by adding H₂O then pH was adjusted at 2 or 9. These tubes were covered by aluminum foil and left rotating in thermostat at 25 °C for 12 hours. Afterwards, these tubes were centrifuged for 20 minutes at 5700 rpm at room temperature to separate the supernatants from the solid phases. The supernatant containing all non-adsorbed phospholipid molecules was removed from each tube (1 mL) for quantitative analysis. The concentration in phospholipid was determined by a phosphorus dosage, according to a routine method⁴ based on the formation of a blue phosphomolybdate complex, which is analyzed through UV spectrometry. The steps for dosing phosphorus are shown in Figure 4.2. In our case, instead of using inorganic phosphate compounds for establishing calibration curves, we used phospholipid suspensions.

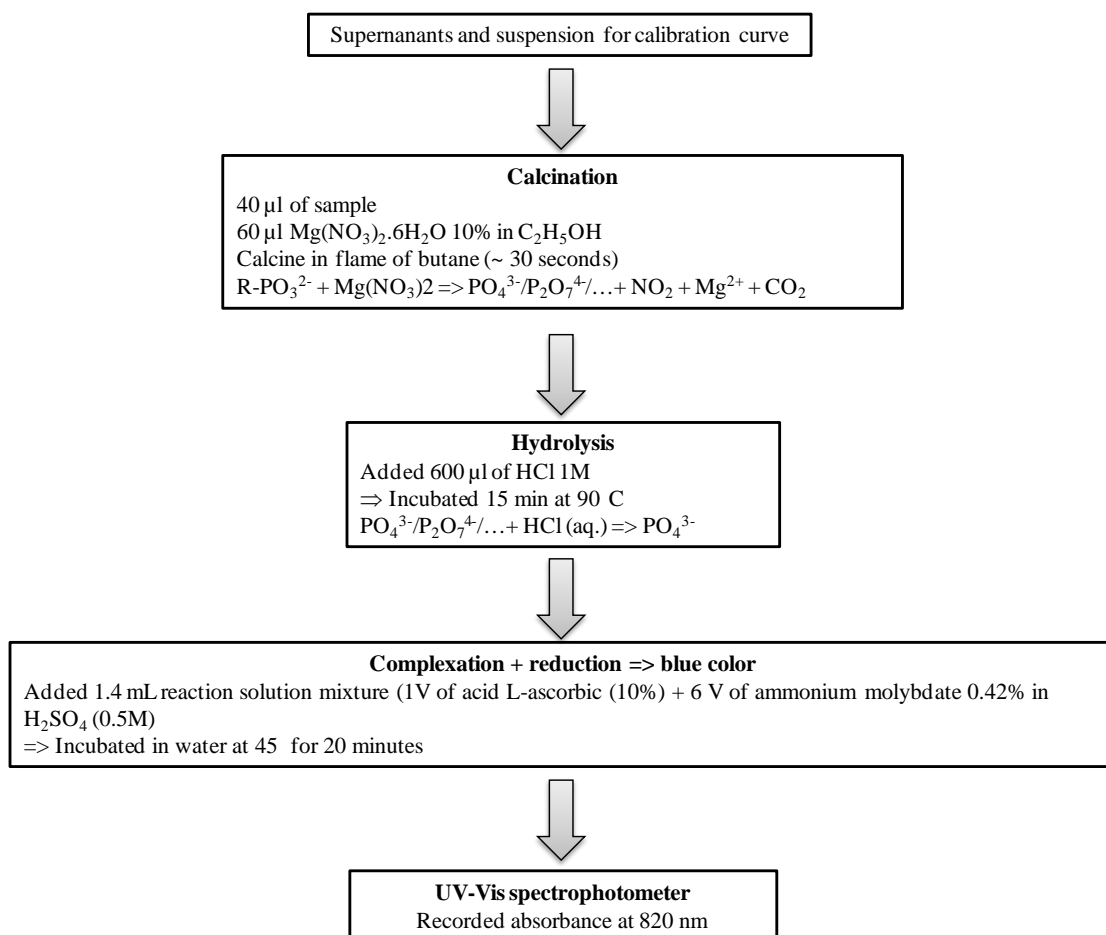


Figure 4.2. Procedure to determine the concentration of phospholipids in supernatants of TiO₂/phospholipid mixtures.

The concentration of the phosphomolybdate complex was finally determined through UV-Visible spectroscopy at a wavelength of 820 nm in the order of low to high concentration. Quartz cuvette with a path length of 1 cm was used. To ensure the reproducibility of the results, two dosages were conducted for each supernatant. The amount of adsorbed phospholipids was calculated from the difference between (1) the equilibrium concentration of phospholipid after centrifugation in tubes without TiO₂ and (2) the remaining amount of phospholipids in the supernatant after adsorption on TiO₂ in tubes containing TiO₂. This calculation method has previously been reported in literature.⁵ The adsorption isotherms showing the amount of adsorbed phospholipids versus initial loading ratio (the number of phospholipids molecules over a unit surface of TiO₂) were built.

Zeta potential experiments

Electrophoretic mobility measurements were performed on TiO₂/phospholipid mixtures using a Zetasizer Nano ZS instrument equipped with a 633 nm He-Ne laser

(Malvern Instruments Ltd, Malvern, Worcestershire, UK). The measurement of electrophoretic mobility was carried out by taking an aliquot of 2 mL of the suspension. Value at each pH point was obtained after six repetitions, resulting from three successive measurements on two aliquots of the same suspension. Data were converted into zeta potential values, using Henry's equation and applying Smoluchowski approximation.

4.3 Results

4.3.1 Surface pressure-area isotherms of phospholipids on anatase and rutile suspensions

4.3.1.1 Experiments without added salt

Surface pressure-area isotherms of DMPA, DMPG on TiO₂-A and TiO₂-R suspensions are shown in Figure 4.3 - 4, compared to those of DMPA, DMPG on pure water. The surface pressure-area isotherms of DMPA and DMPG on H₂O are the same as those described in the previous chapter. Briefly, the curves exhibit three regions identified by 3 ruptures of slopes. These regions are characterized by different arrangements of molecules. For DMPA, the succession of phases by compression is in the following order: a gas phase at high area per molecule ($> 85 \text{ \AA}^2$), a liquid-expanded phase (LE) between $85 - 75 \text{ \AA}^2/\text{molecule}$, coexistence of a liquid-expanded and a liquid-condensed (LC) phase characterized by a plateau ($75 - 50 \text{ \AA}^2/\text{molecule}$) and a liquid-condensed phase that collapses at a pressure of about 40 mN/m. DMPG on H₂O presents a similar succession of phases as DMPA, from the gas phase until the collapse of the liquid condensed phase. The lowest area per molecule of DMPG and DMPA gets similar value at around 40 \AA^2 .

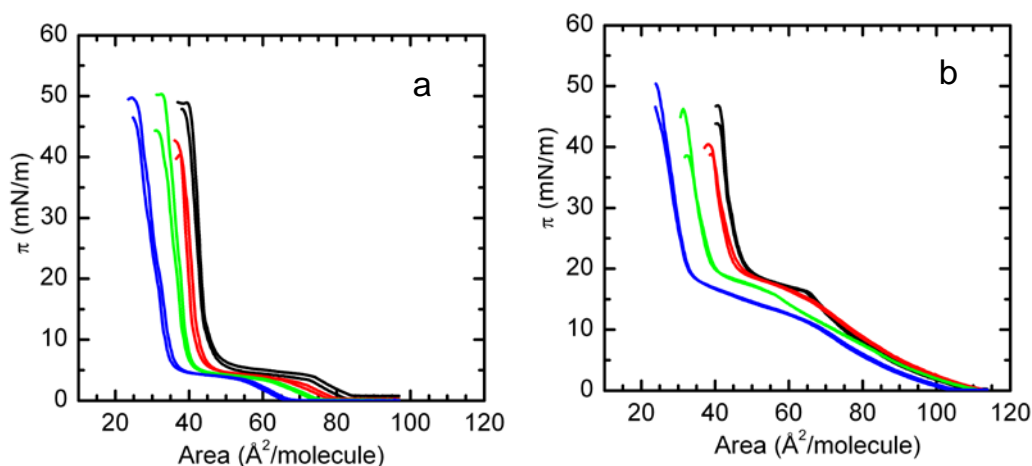


Figure 4.3. Pressure-area isotherms at pH 2 of (a) DMPA and (b) DMPG on (black) H_2O and on TiO_2 -A suspensions at different concentrations (red) 20 mg/L, (green) 50 mg/L and (blue) 100 mg/L. Subphases contain no added salt.

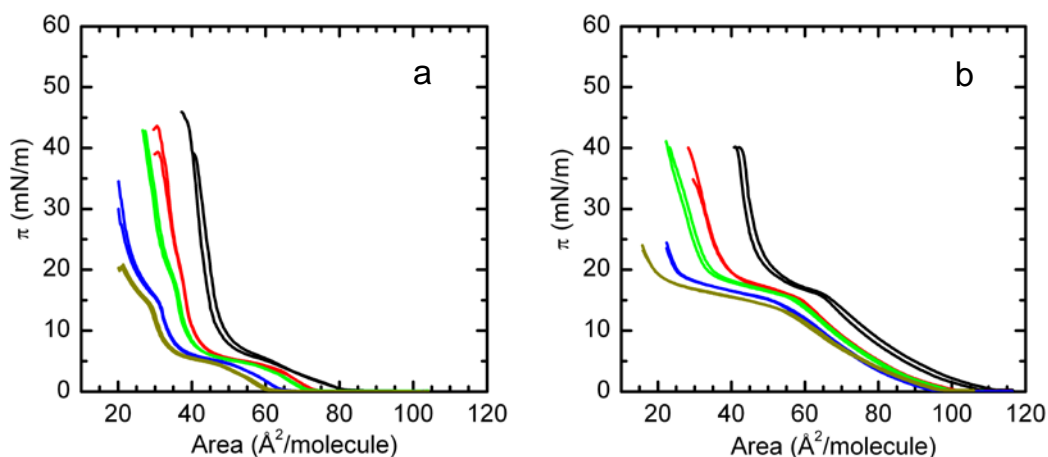


Figure 4.4. Pressure-area isotherms of (a) DMPA and (b) DMPG at pH 2 on (black) H_2O , (red) TiO_2 -R suspension 100 mg/L, (green) 200 mg/L, (blue) 400 mg/L and (dark yellow) 500 mg/L.

When the subphases are TiO_2 suspensions, the surface pressure-area isotherms of both DMPA and DMPG monolayers are shifted to lower areas in respect to that on H_2O subphase. The isotherms are as much shifted as the concentration of TiO_2 is high and this shift is well marked in the liquid condensed phases of DMPA and DMPG. The loss of phospholipids can be calculated as follows, from the shift of the π -area curves:

$$X(\%) = \frac{A_{\pi-w} - A_{\pi-TiO_2}}{A_{\pi-w}} \times 100$$

Where $A_{\pi-w}$ is the molecular area of phospholipids at π mN/m when TiO_2 is absent in subphase and $A_{\pi-\text{TiO}_2}$ is the molecular area of phospholipids at π mN/m when TiO_2 is present in subphase. The loss of phospholipid molecules is reported for each phospholipid in Figures 4.5-6 as a function of mass concentration of TiO_2 in the suspensions and at two film pressures, one in the LE phase (phase with high compressibility) and one in the LC phase (condensed phase with low compressibility).

It appears obvious that the loss in phospholipid is highly dependent on phospholipid, phospholipid assembly and crystalline phase of TiO_2 . The loss in phospholipid is generally lower in the LE phase than in the LC phase, irrespective of phospholipid or crystalline phase of TiO_2 . The fact that phospholipid molecules are close to each other seems thus to be favorable for interactions. The comparison of Figure 4.5 with Figure 4.6 shows that each crystalline phase of TiO_2 induces quite similar loss in phospholipid in the LC phase. In contrast, the loss in DMPG in the LE phase is smaller than that in DMPA in the LE phase, irrespective of crystalline phase. The relationship between the loss of phospholipid and the concentration of TiO_2 in subphase could be adjusted by a linear function in most cases, except for DMPG adsorbed on TiO_2 -R. It is worthy to note that TiO_2 -R induces almost no displacement of DMPG from the interface in the LE phase, in comparison to DMPA. This is additional evidence that the interaction mechanism between DMPA with TiO_2 is distinctive from that of DMPG with TiO_2 .

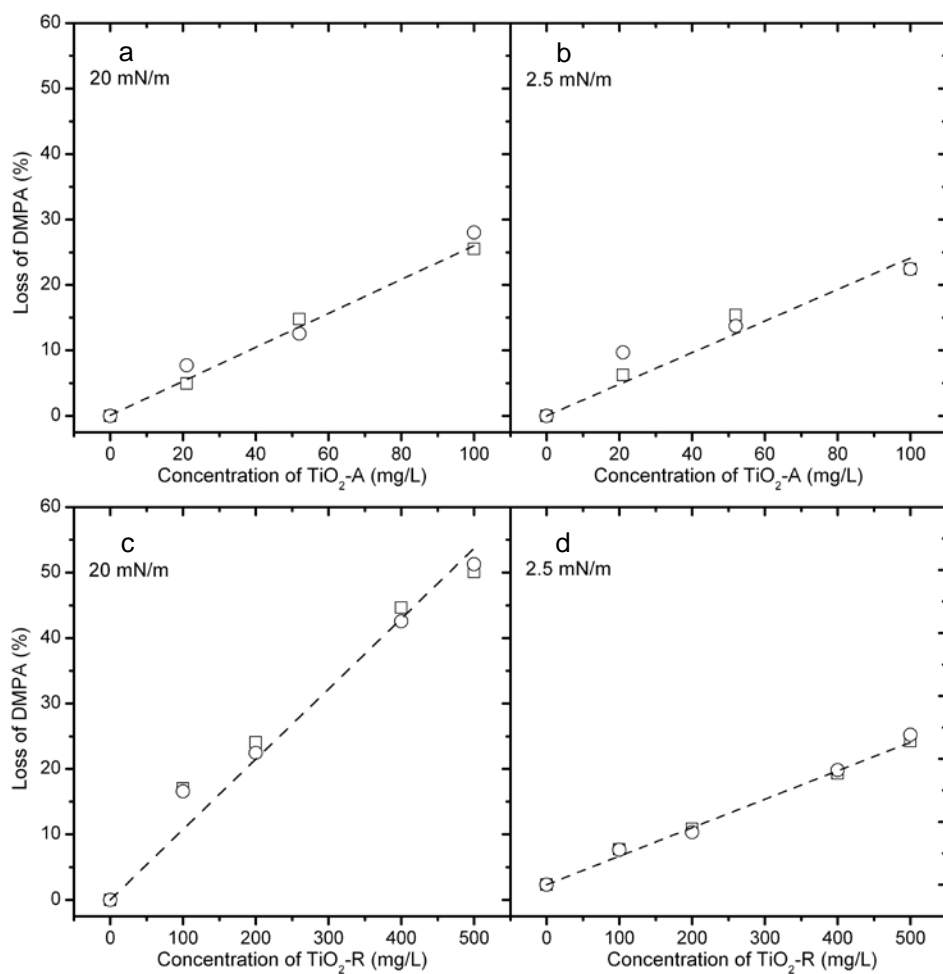


Figure 4.5. Relationship between the amount of DMPA lost from the interface at surface pressure of 20 mN/m and 2.5 mN/m at pH 2 and the mass concentration of (a, b) $\text{TiO}_2\text{-A}$ and (c, d) $\text{TiO}_2\text{-R}$ in subphases.

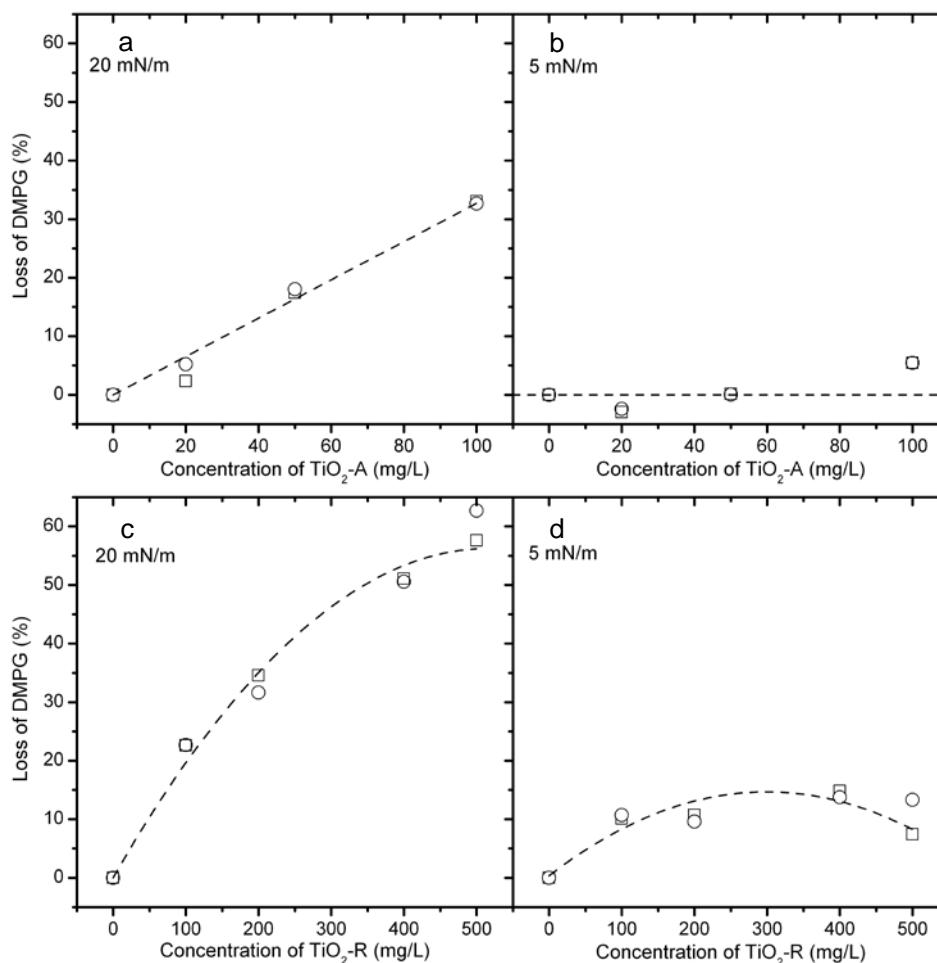


Figure 4.6. Relationship between the amount of DMPG lost from the interface at surface pressure of 20 mN/m and 5 mN/m and the mass concentration of (a, b) TiO₂-A and (c, d) TiO₂-R in subphases at pH 2.

As the specific surface area of TiO₂-A (136 m²/g) is five times higher than that of TiO₂-R (26 m²/g), a defined amount of TiO₂-A powder has a higher total surface area than that of the same amount of TiO₂-R. Therefore anatase exposes more active sites than TiO₂-R and this results in a higher possibility to interact with phospholipids. To mask the effect of surface area, the comparison is now done at a mass ratio TiO₂-A/TiO₂-R 1:5. At the same total specific surface area, the loss in phospholipid is higher with subphases filled with rutile particles than with anatase particles, especially in the LC phase. Some isotherms recorded in these conditions are presented in Figure 4.7. The entire isotherm of DMPA is shifted to lower areas on the subphase of TiO₂-A. This suggests that TiO₂-A particles do not seem to stay anchored at the interface. In contrast, at the same total specific surface area, the compression isotherm of DMPA on TiO₂-R suspensions presents a transition point at 14 mN/m. The remaining molecules of DMPA at the interface are thus not alone. Some TiO₂-R particles are thus probably still anchored at the monolayer. In the

case of DMPG, the plateau of transition from the LE to the LC phases extends on a larger area range. It means that DMPG molecules are more difficult to pack. The presence of TiO_2 particles and especially TiO_2 -R particles at the interface might be the reason.

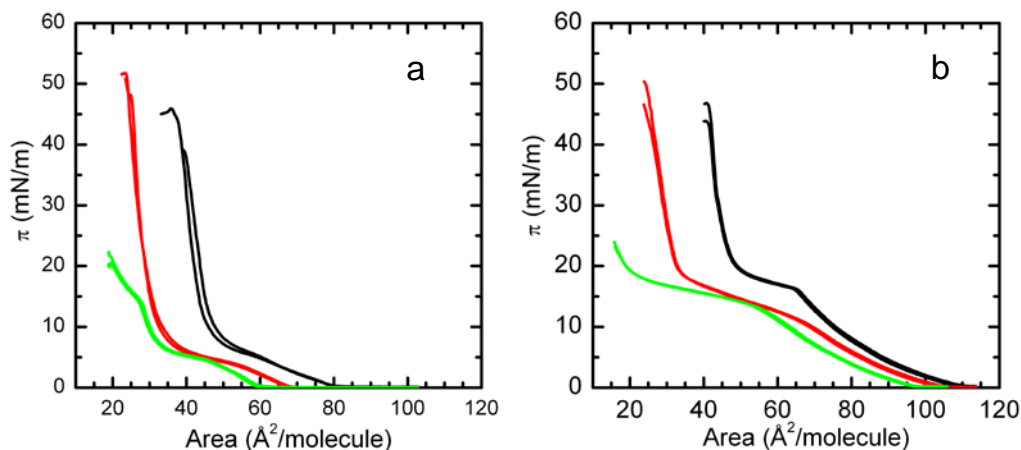


Figure 4.7. Compression isotherms of (a) DMPA and (b) DMPG at pH 2 on (black) H_2O , (red) TiO_2 -A suspension 100 mg/L and (green) TiO_2 -R suspension 500 mg/L. At this concentration, total surface of TiO_2 -A in subphase is equal to that of TiO_2 -R.

4.3.1.2 Screening effect of salt

Until now, the concentration in ions was solely resulting from the adjustment of pH. In the following, salt was incorporated in TiO_2 suspensions. The surface pressure-area isotherms, recorded in the presence of NaCl at 10^{-2} mol/L are plotted in Figure 4.8. In the presence of NaCl, the isotherms of DMPA obtained on TiO_2 subphases overlap with that on water. This suggests that interactions between TiO_2 -A or TiO_2 -R and DMPA were completely screened and are governed by electrostatic interactions. In contrast, the isotherms of DMPG on TiO_2 -A and TiO_2 -R subphases are still strongly shifted, suggesting that interactions between TiO_2 -A or TiO_2 -R and DMPG still exist in the presence of salt. It is worthy to note that the isotherm of DMPG on water is modified by the presence of salt. In fact the isotherms of DMPG on TiO_2 -A and TiO_2 -R subphases with salt are hardly different from that without salt. This result suggests that DMPG interacts with anatase and TiO_2 -R particles mainly through non-electrostatic interactions and NaCl ions do not intervene in the interactions.

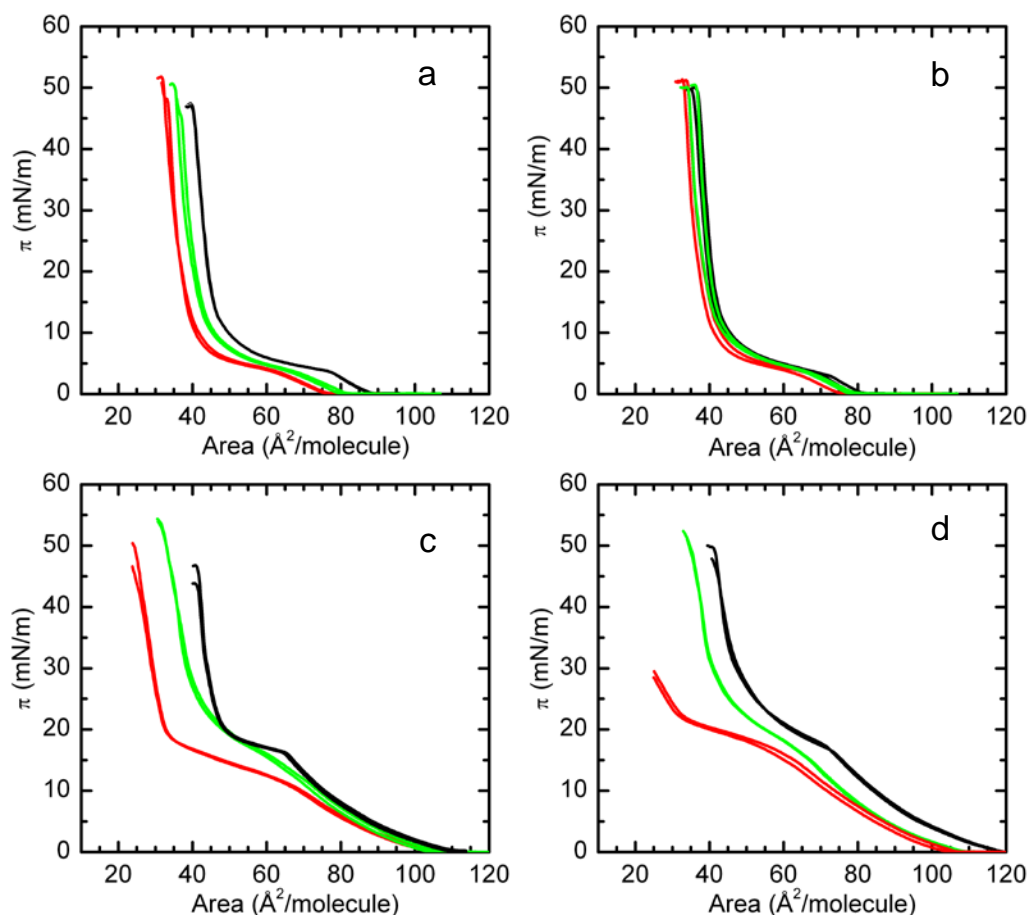


Figure 4.8. Pressure-area isotherms of (a, b) DMPA and (c, d) DMPG on subphase at pH2: (black) H_2O , (red) TiO_2 -A suspension 100 mg/L and (green) TiO_2 -R suspension 100 mg/L. Subphases in panels b and d contain $NaCl$ $10^{-2}M$.

4.3.2 Amount of phospholipids adsorbed on anatase and rutile

Surface pressure-area isotherms of DMPA and DMPG clearly showed the occurrence of interactions between DMPA and DMPG with TiO_2 -A and TiO_2 -R. To estimate the amount of phospholipid molecules adsorbed on TiO_2 , the amount of molecules not adsorbed was quantified in the supernatant of centrifuged phospholipid/ TiO_2 mixtures. The amount of adsorbed molecules was then deduced from the initial amount introduced with TiO_2 . From these experiments, adsorption isotherms of DMPA and DMPG on TiO_2 -A and TiO_2 -R were built at pH 2 and pH 9 (Figures 4.9). The different panels allow us to observe the effects of pH, phospholipid, phospholipid-to- TiO_2 ratio and crystalline phase on the adsorbed amounts on TiO_2 .

a) pH-dependent adsorption for DMPA

The amount of DMPA adsorbed on TiO₂-A or TiO₂-R is strongly dependent on pH. For example, TiO₂-A and TiO₂-R adsorbed more than 2 molecules of DMPA per 1 nm² surface at pH 2, and less than 0.5 molecule at pH 9. These results are in agreement with the previous conclusions that DMPA interacts with TiO₂ by electrostatic interactions. In contrast, the amount of DMPG adsorbed on TiO₂-A or TiO₂-R particles is hardly sensitive to pH. The difference between pH 2 and pH 9 is less than 0.5 molecule/nm², irrespective of the crystalline phase. Again, this corroborates the results given by the surface pressure-area isotherm experiments. It is worthy to note that DMPA is significantly adsorbed at pH 2 but in a higher amount than DMPG, which is adsorbed on a large pH range. This cannot be related to a higher charge density on DMPA than on DMPG, as both present similar zeta potential values in acidic medium (chapter 2). This result suggests that the adsorption mode might be different for DMPA and DMPG molecules.

b) Affinity of phospholipid for TiO₂

The difference of affinity of phospholipid for TiO₂ cannot be decoupled from pH. In acidic media, DMPG is less adsorbed than DMPA and reversely in basic media.

c) Impact of phospholipid-to-TiO₂ ratio

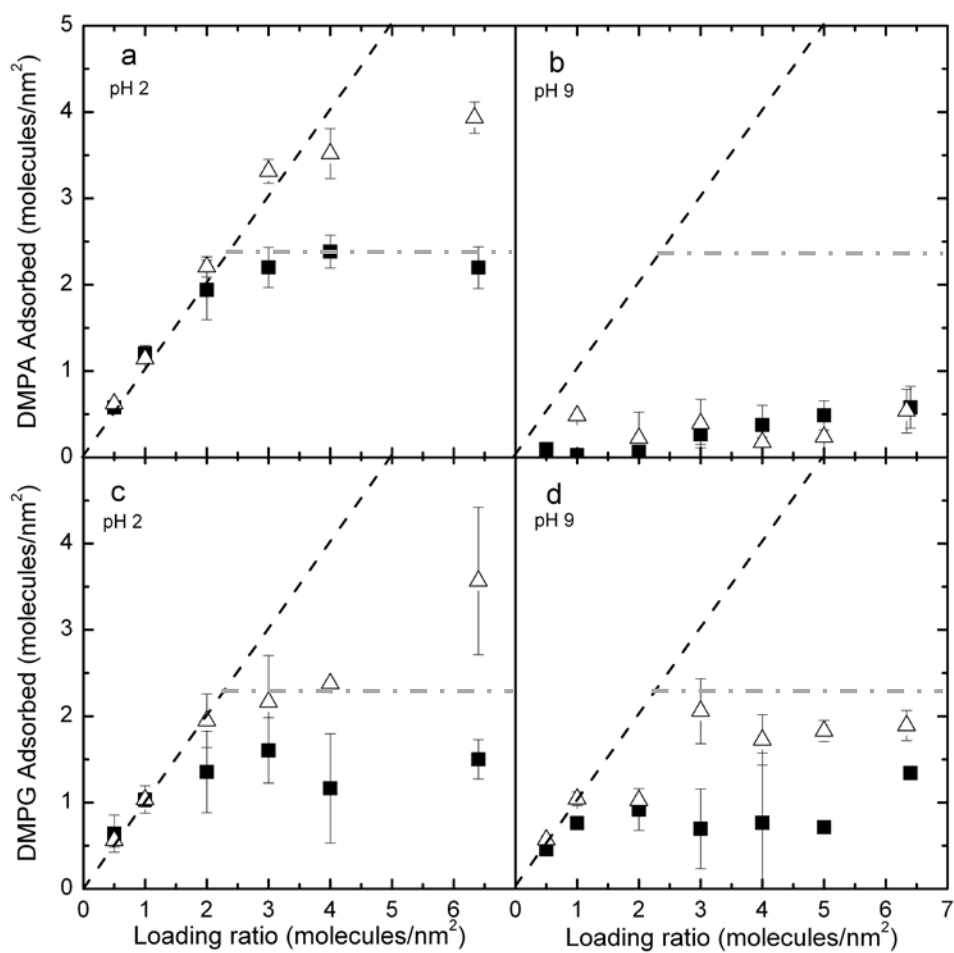


Figure 4.9. Adsorption isotherms of (a, b) DMPA and (c, d) DMPG on $\text{TiO}_2\text{-A}$ (■) and $\text{TiO}_2\text{-R}$ (Δ) at pH 2 and pH 9 (no added NaCl). Error bars represent the standard deviation from duplicate measurements.

When adsorption occurs (DMPA at pH 2, and DMPG at pH 2 and 9), the amount of phospholipids adsorbed on TiO_2 increases with the loading concentration, i.e. the increase of the chemical potential of the PL. At low loading concentrations, the variations are linear and follow the straight line that corresponds to the full adsorption ($y = x$). Over a threshold value, the adsorption is no longer complete and reaches a maximum. Both the threshold value and the maximum are dependent on pH, phospholipid and crystalline phase. For example, the adsorption of DMPG at pH 9 is complete at a loading ratio of 2 molecule/ nm^2 for $\text{TiO}_2\text{-R}$ and at a lower ratio of 1 molecule/ nm^2 for $\text{TiO}_2\text{-A}$. These values increase at pH 2.

The dependence of the adsorbed amount with concentration is analogous to the adsorption of dipalmitoylphosphatidylcholine on rutile particles or the adsorption of phospholipid vesicles on rutile TiO_2 (100) wafer.^{5,6} In the first case, it was even showed that at low concentration (0.013 mg/mL), phospholipid vesicles did not transform to planar

bilayer on rutile (100), whereas at higher concentration (0.025 mg/mL) the bilayer was created. Literature data⁵ reported that adsorption of dipalmitoylphosphatidylcholine on rutile saturated at a coverage density of 3 molecules/nm² and this corresponded to a monolayer. A higher coverage density would evidence multilayer formation. Typically, the minimum molecular area for lipids with two hydrocarbon chains should be approximately in 42 – 45 Å² range.⁷ Taking the smallest area achievable by DMPA and DMPG on water in a monolayer (43 and 42 Å²/molecule at the collapse), the highest density of DMPA and DMPG in a monolayer is 2.3 and 2.4 molecules/nm² respectively. Applying this threshold in Figure 4.9 suggests that DMPG is adsorbed on TiO₂-R and TiO₂-A as a monolayer at pH 2 and 9 (the point at 6 molecules/nm² is excluded due to the large uncertainty on it) whereas DMPA is adsorbed as a monolayer on TiO₂-A and as a multilayer on TiO₂-R at pH 2.

d) Impact of crystalline phase

When adsorption is significant enough (DMPA at pH 9 not considered), the maximal amount adsorbed on anatase is always smaller than that on TiO₂-R, irrespective of the phospholipid and pH. For example, at pH 2, TiO₂-A is saturated by DMPA for a coverage of approximately 2.3 molecules/nm² whereas TiO₂-R can adsorb up to around 4 molecules/nm².

4.3.3 Surface charge of TiO₂ particles after adsorption of phospholipids

Phospholipids were loaded on TiO₂ at low concentration (0.5 molecules per 1 nm²) at pH 2. According to Figure 4.9, phospholipids are fully adsorbed on TiO₂ and no vesicle is free in the suspension. Therefore, the measure of the surface charge is relative to the particles of TiO₂ coated by phospholipids. The surface charge of these modified particles was recorded at pH 2 and followed versus pH. The results are reported in Figure 4.10.

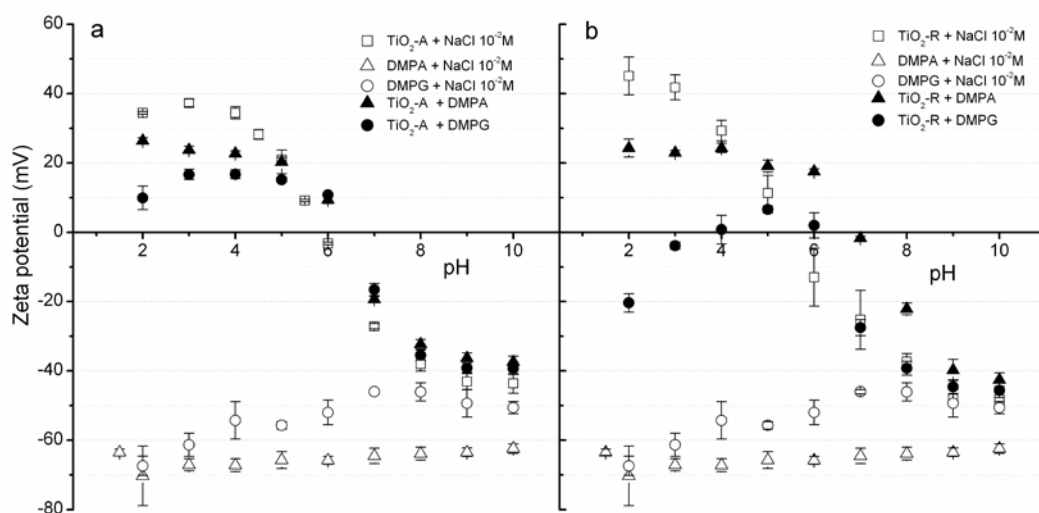


Figure 4.10. Zeta potentials of (a) $\text{TiO}_2\text{-A}$ covered by phospholipids (PLs) and (b) of $\text{TiO}_2\text{-R}$ covered by PLs as a function of pH. PLs were loaded with ratio 0.5 molecules per 1 nm^2 surface of TiO_2 . Zeta potentials of pure TiO_2 , DMPA and DMPG are shown for comparison. Error bars represent the standard deviation. Measurements were conducted at 25°C .

DMPA and DMPG vesicles are negatively charged on the whole pH range whereas $\text{TiO}_2\text{-A}$ and $\text{TiO}_2\text{-R}$ particles are positively charged at low pH (up to 6 for $\text{TiO}_2\text{-A}$ and 5.5 for $\text{TiO}_2\text{-R}$) and negative at basic pH values. At pH 2, the surface charge of TiO_2 was modified after adsorption. Zeta potentials of PLs-adsorbed TiO_2 (coated TiO_2) were less positive than pure TiO_2 (uncoated TiO_2). The decrease enlarges in the order $\text{DMPA}/\text{TiO}_2\text{-A} < \text{DMPA}/\text{TiO}_2\text{-R} \sim \text{DMPG}/\text{TiO}_2\text{-A} < \text{DMPG}/\text{TiO}_2\text{-R}$. It became even negative for DMPG adsorbed on $\text{TiO}_2\text{-R}$ (a decrease of 65 mV). When pH increases from 2 to 5, the surface charges of $\text{TiO}_2\text{-A}$ and $\text{TiO}_2\text{-R}$ are weakly affected by the coating of DMPA, whereas the surface charges of $\text{TiO}_2\text{-A}$ and $\text{TiO}_2\text{-R}$ are more strongly modified by DMPG, in particular that of $\text{TiO}_2\text{-R}$. Zeta potential values of DMPG-coated TiO_2 increase and at pH 5 -6, they reach the values of uncoated TiO_2 . If there are no covalent bonds, this could be the sign of a desorption. At higher pH, DMPA and DMPG did no longer alter the zeta potentials of TiO_2 . The surprising values for DMPA on $\text{TiO}_2\text{-R}$ around pH 5 and 8 must be checked with a second assay; the uncertainty is indeed larger around the IEP. Finally, DMPA exhibits weaker effect on zeta potentials of TiO_2 than DMPG, and this effect is reduced as pH is increased.

4.3.4 Effect of surface chemistry of various anatase phases on the interactions between TiO₂ and phospholipids

The characterization in chapter 2 highlighted various surface properties of anatase samples. In this section, the interactions between several TiO₂ anatase forms and phospholipids were investigated. Figure 4.11 shows the surface pressure-area isotherms of DMPA and DMPG monolayers on several subphases, containing various anatase particles. For recall, the isotherms obtained on the previous anatase suspensions are presented.

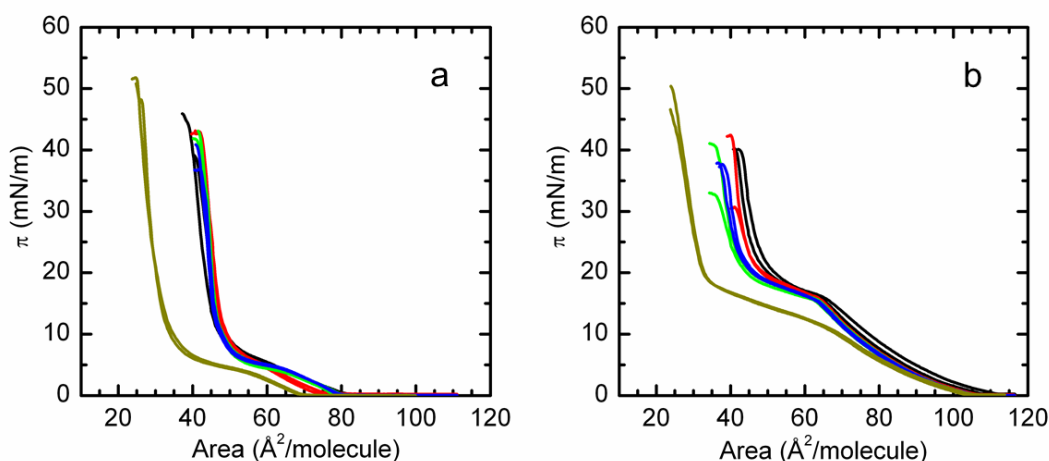


Figure 4.11. Pressure-area isotherms at pH 2 of (a) DMPA and (b) DMPG on (black) H₂O, (red) TiO₂-PC10 suspension, (green) TiO₂-PC50, (blue) TiO₂-PC100 and (dark yellow) TiO₂-A. The mass concentration of TiO₂ in subphases is 0.1g/L (no added NaCl).

Panels a & b indicate that DMPA and DMPG interact much more weakly with TiO₂-PC10, TiO₂-PC50 and TiO₂-PC100 anatase samples than with TiO₂-A. While 25% of DMPA was removed from the interface due to TiO₂-A at 20 mN/m, subphases containing TiO₂-PC10, TiO₂-PC50 and TiO₂-PC100 anatase particles induce no loss of DMPA. Similarly, 33% of DMPG was removed from the interface due to TiO₂-A particles whereas TiO₂-PC10, TiO₂-PC50 and TiO₂-PC100 anatase particles induce a much smaller shift. TiO₂-PC10 induces almost no shift of the isotherm of DMPG, while TiO₂-PC50 and TiO₂-PC100 cause a modest shift of the isotherm.

To remove any surface area effect, the effect of TiO₂ concentration on the interaction with DMPA was investigated. The results are shown in Figure 4.12 (panel a for TiO₂-PC10, panel b for TiO₂-PC50 and panel c for TiO₂-PC100) with concentrations between 100 and 400 mg/L for all anatase TiO₂-PC samples. Surprisingly, all isotherms of compression overlap. Thus, TiO₂-PC samples have almost no interaction with DMPA.

Therefore, although all subphases contain the same crystalline phase at the same mass or total surface specific area concentration and pH, it appears that anatase powders behave differently. Preliminary observation indicated that the suspensions of TiO₂-PC10, TiO₂-PC50 and TiO₂-PC100 tended to settle more quickly than that of TiO₂-A, even though the distribution of hydrodynamic size of these particles in aqueous suspension at pH 2 was below or at the same size ranges as that of TiO₂-A particles (Figure 2.20 chapter 2). However, the time required to record the isotherms was shorter than the time of sedimentation. This suggests that surface chemistry plays a large role. TiO₂-PC10, TiO₂-PC50 and TiO₂-PC100 were free from organic contaminants (chapter 2) but X-ray photoelectron spectroscopy showed a very small sulfur contamination in TiO₂-PC50 and TiO₂-PC100 powders.

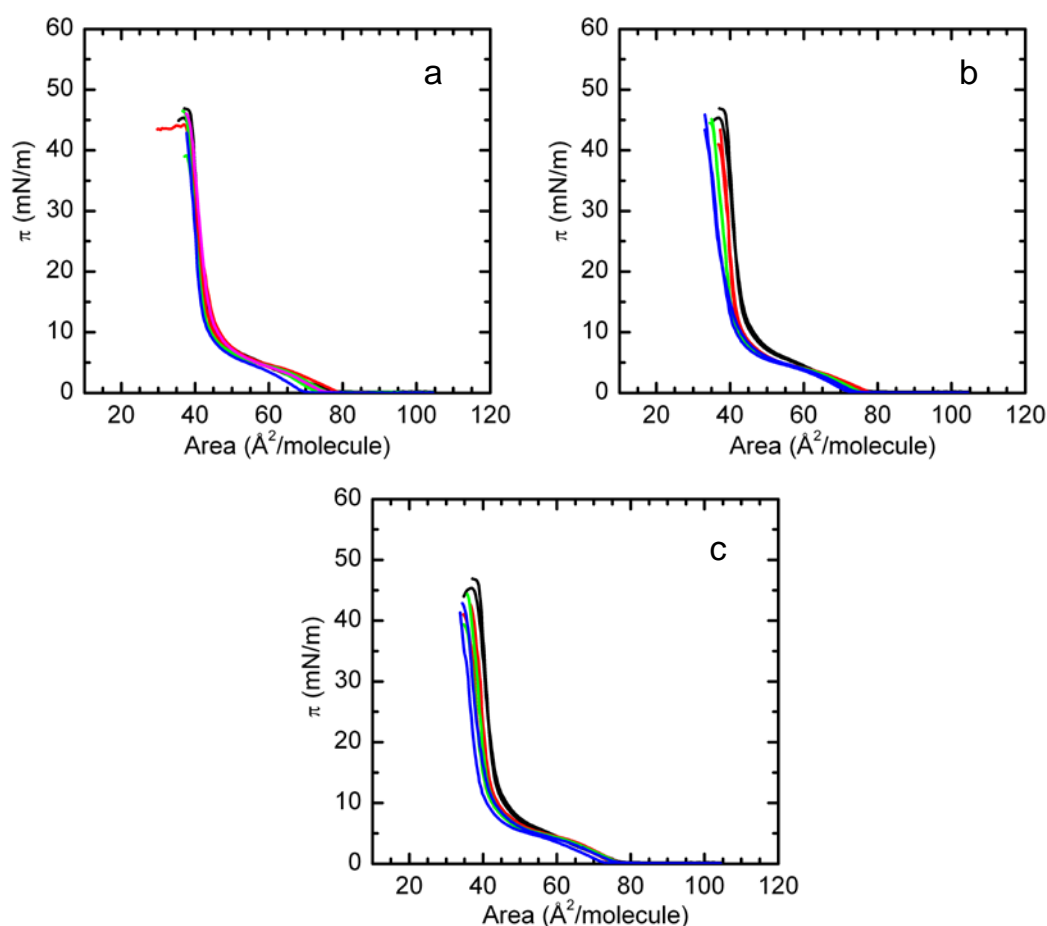


Figure 4.12. Pressure-area isotherms at pH 2 of DMPA on suspension of (a) TiO₂-PC10, (b) TiO₂-PC50 and (c) TiO₂-PC100. Concentration of TiO₂ in subphase is varied from (black) 0 mg/L, (red) 100 mg/L, (green) 200 mg/L and (blue) 400 mg/L.

4.4 Discussion

All measurements (isotherms of compression, batch adsorption and electrophoretic mobility) are in agreement and draw the same conclusion that DMPA and DMPG interact with anatase and rutile.

At the same total specific surface area and at pH 2, TiO₂-R exhibits stronger interactions with phospholipids than TiO₂-A. DMPA interacts mainly through electrostatic interactions, while DMPG adsorbs on TiO₂ by non-electrostatic ones. This finding is consistent with the strong interactions between TiO₂-P25 and DMPA or DMPG at pH 2, and the remaining interactions observed between DMPG and TiO₂-P25 at pH 9 and at pH 2 in the presence of salt (chapter 3).

It is worth noting that the compression isotherms of DMPA on TiO₂-R subphases exhibit an additional transition phase in the liquid condensed region (around 15 mN/m in Figure 4.7a) that is well marked when the concentration in TiO₂-R in the subphase is high. In this case, there is not only a loss of DMPA but also a change in organization at the interface. As particles of TiO₂ have no affinity for the liquid surface (flat isotherms of compression when the interface is free of phospholipid molecules), it is excluded that they insert within the monolayer. This transition reflects thus the adsorption of TiO₂-R particles under the monolayer, modifying the arrangement of DMPA molecules. This may be surprising as the hydrodynamic size of TiO₂-R particles (as agglomerated) is quite large (from 500 nm to 2 μm, see chapter 2). This phenomenon was not observed for the suspensions of anatase that induced simply a shift to lower areas. Yet, this transition was observed with TiO₂-P25 and DMPA (chapter 2) and considering the results with TiO₂-R, it can be therefore attributed to rutile particles anchored under the monolayer of DMPA.

As the remaining DMPA molecules on TiO₂-A subphase exhibit the same behavior as DMPA on water, one can reasonably think that there is no anatase particle at the interface anchored to DMPA monolayer. In the case of DMPG, the transition plateau from the LE phase to the LC phase is smoother in the presence of TiO₂-A in the subphase. The distinction between the LE phase and the plateau of coexistence between the LE and LC phase is less obvious. The longer plateau of coexistence in the presence of TiO₂-R reflects the presence of TiO₂-R particles at the interface and the difficulty for phospholipid molecules to pack densely.

The different behavior of DMPA and DMPG towards TiO₂-A or TiO₂-R may be related to the chemical structure of DMPG head group, which is different from that of

DMPA. The phosphate moiety must be the primary group to take part in the interaction, as studies have found that phosphate moieties are implicated into the direct interaction with TiO_2 surface.^{8,9} For DMPG, the interactions occurring in basic conditions, as well as the equivalent adsorbed amount at acidic and basic pH, suggest that the terminal glycerol of DMPG can be involved. This is in agreement with the fact that glycerol molecule forms, in bulk water, a bridging alkoxy bond through one primary alcohol group to two coordinatively unsaturated metal atoms of anatase, and participates to a Lewis acid/base interaction between the oxygen atom of the other primary alcohol group and a coordinatively unsaturated metal atom that is also involved in the alkoxy bond.¹⁰

4.5 Conclusion

Surface pressure-area isotherm and batch adsorption experiments performed at pH 2 and pH 9 in aqueous medium showed that DMPA and DMPG, the main adsorbing phospholipids on TiO_2 -P25 particles, adsorb on both anatase and rutile surfaces. DMPA adsorbs solely at acidic pH on anatase and rutile, probably through electrostatic interactions implying the phosphate moiety. DMPG adsorbs on TiO_2 in similar amounts at both acidic and basic pH through non-electrostatic interactions, probably involving the glycerol moiety. For any phospholipid, the adsorption is enhanced in the presence of rutile. The geometry of the surface must match better with the geometrical constraints of DMPG molecule. The strong interactions between TiO_2 -P25 (85% anatase + 15% rutile) and DMPA or DMPG at pH 2, as well as the remaining interactions observed between DMPG and TiO_2 -P25 at pH 9 or at pH 2 in the presence of salt (chapter 3), can thus be understood by the interactions of DMPA and DMPG at pH 2 with both anatase and rutile, and with rutile at pH 9. Our study, however, cannot be applied to any kind of anatase and, a deeper understanding of the surface properties of TiO_2 -PC would be necessary to interpret our observations.

At this stage of our study, the nature of bonds formed between DMPG or DMPA and the surface of TiO_2 must be elucidated. Inspection by various spectroscopic methods is necessary to answer this question, and this investigation at molecular level will be developed in the next chapter.

References

1. Tero, R. Substrate Effects on the Formation Process, Structure and Physicochemical Properties of Supported Lipid Bilayers. *Materials (Basel)*. **5**, 2658–2680 (2012).
2. Ohno, T., Sarukawa, K., Tokieda, K. & Matsumura, M. Morphology of a TiO₂ Photocatalyst (Degussa, P25) Consisting of Anatase and Rutile Crystalline Phases. *J. Catal.* **203**, 82–86 (2001).
3. Ohtani, B., Prieto-Mahaney, O. O., Li, D. & Abe, R. What is Degussa (Evonik) P25? Crystalline composition analysis, reconstruction from isolated pure particles and photocatalytic activity test. *J. Photochem. Photobiol. A Chem.* **216**, 179–182 (2010).
4. Ames, B. N. in *Methods Enzymol.* (Elsevier Inc., 1966). doi:10.1016/0076-6879(66)08014-5
5. Oleson, T. a & Sahai, N. Oxide-dependent adsorption of a model membrane phospholipid, dipalmitoylphosphatidylcholine: bulk adsorption isotherms. *Langmuir* **24**, 4865–73 (2008).
6. Tero, R., Ujihara, T. & Urisu, T. Lipid bilayer membrane with atomic step structure: supported bilayer on a step-and-terrace TiO₂ (100) surface. *Langmuir* **24**, 11567–76 (2008).
7. Israelachvili, J. N. *Intermolecular and surface forces*. 550 (Academic Press (Elsevier), 2011).
8. Connor, P. A. & Mcquillan, A. J. Phosphate Adsorption onto TiO₂ from Aqueous Solutions: An in Situ Internal Reflection Infrared Spectroscopic Study. *Langmuir* **15**, 2916–2921 (1999).
9. Myller, A. T., Karhe, J. J. & Pakkanen, T. T. Preparation of aminofunctionalized TiO₂ surfaces by binding of organophosphates. *Appl. Surf. Sci.* **257**, 1616–1622 (2010).
10. Copeland, J. R., Santillan, I. a., Schimming, S. M., Ewbank, J. L. & Sievers, C. Surface Interactions of Glycerol with Acidic and Basic Metal Oxides. *J. Phys. Chem. C* **117**, 21413–21425 (2013).

Chapter 5

Spectroscopic studies of the interaction between phospholipids and TiO₂ surfaces

Table of contents

5. Spectroscopic studies of the interaction between phospholipids and TiO ₂ surfaces.....	205
5.1 Introduction.....	205
5.2 Bibliographic survey of the contribution of the spectroscopy in the characterization of the formation of the chemical bond Ti-O-P.....	205
5.3 Materials and methods	210
5.3.1 Diffuse reflectance infrared Fourier transform spectroscopy (DRIFTS)	210
5.3.2 Raman spectroscopy.....	212
5.3.3 Nuclear Magnetic resonance spectrometry.	212
5.3.4 Material	212
5.3.5 Sample preparations to study the interaction.	219
5.4 Results on the spectroscopic study of the interaction between phospholipids with anatase and rutile	220
5.4.1 Effect of environmental condition on phosphate moiety in head group of phospholipids.....	220
5.4.2 Evolution of surface groups on TiO ₂ upon phospholipids adsorption.....	222
5.4.3 Effect of pH on the adsorbed species	225
5.5 Discussion	227
5.5.1 Existence of Ti-O-P bond?.....	227
5.5.2 Role of glycerol in the adsorption.....	228
5.5.3 Interaction model.....	230
5.6 Perspective	233
References	235

5. Spectroscopic studies of the interaction between phospholipids and TiO₂ surfaces

5.1 Introduction

Although phosphates have been widely used in the various stages of mineral processing for many years, the mechanism of interaction between the phosphate species and mineral surfaces, like those of anatase and rutile, has been investigated and discussed at the molecular scale by spectroscopy only for about fifteen years.¹⁻³ The Infrared spectroscopy yielded information regarding the nature of the bonding between reagents and mineral surfaces, the conformation of the adsorbed species on surfaces and the *in situ* change of the surfaces during the various processes of mineral processing. The chapter 2 has also clearly demonstrated the interest of near-combined middle infrared spectroscopy to monitor the changes of the hydroxyl groups versus the chemical-physical parameters of the aqueous solutions (like pH and ionic strength). In chapters 3 and 4, the chemical conditions to induce strong interactions between a few phospholipids and surfaces of different titanium oxide samples (inner sphere structures) were determined at the macroscopic scale by the compression or adsorption isotherms. However, there is still no proof of the creation of a chemical bond at the molecular scale even if, as noticed in the chapter 1, titanium dioxide surfaces have several reactive surface groups as strong Lewis-type acid sites, weak Brønsted-type acid sites, and basic O²⁻ sites.⁴ This chapter 5 is devoted to this problematic: highlighting or not the existence of chemical bonds in the “inner sphere” adsorbed structures. We have used the near- and middle infrared absorption spectroscopy, Raman inelastic scattering spectroscopy and NMR spectroscopy in order to have concomitantly and respectively data on the environment of the surface hydroxyl groups, on the symmetry of the head phosphate groups and on the electronic clouds around ³¹P atoms.

5.2 Bibliographic survey of the contribution of the spectroscopy in the characterization of the formation of the chemical bond Ti-O-P.

The adsorption of phosphate species has been described to correspond to a chemisorption on the Lewis acidic Ti⁴⁺ groups on the TiO₂ surface leaving the less acidic hydroxyl Brønsted acid sites free.³ Others studies confirm that Lewis acidity on anatase disappears after phosphate modification,⁵ while Brønsted acid sites remain on the phosphate-loaded surfaces⁶. The anatase form would favor the formation of stable bonds with organic

esters of phosphoric acid (organic phosphates). (ATR)-IR studies on linear polyphosphates have been interpreted as the formation of bidentate phosphate species through P–O groups, forming Ti–O–P bonds with the exposed charged titanium atoms (Ti_{5c}).¹ Although the spectra of the adsorbed anions gave clear information on the change of symmetry of the anion structure, no direct information on the possible Ti–O–P chemical bond between oxygen atoms of phosphate anions and titanium atoms could be demonstrated. Connor and McQuillan in 1999 conducted an *in situ* internal reflection infrared spectroscopic study on the adsorption of only the orthophosphate species onto “amorphous” TiO_2 films from aqueous solution.² They indicated that phosphate species bind strongly to the TiO_2 surface, forming bidentate surface species with two kinds of structures. However, their infrared spectra had not allowed bridging bidentate and chelate species to be distinguished. Infrared spectroscopic studies about the adsorption of phosphate anions on iron oxide nanoparticles have been also conducted using an *ex situ* or *in situ* technique.^{7,8} Bidentate and monodentate attachments were both suggested but not proved. Indeed, the structure as chelate or bridged bidentate cannot be distinguished since the point groups for both structures are C_{2v} . Another example deals with the preparation of titania support catalysts by impregnations with phosphate anions. The infrared spectra of solid samples obtained from the calcination at $450^\circ C$ of anatase dispersed with phosphoric acid displayed no absorption peaks in the $900\text{--}1300\text{ cm}^{-1}$ region for pure TiO_2 , while a new IR band appeared at around 1049 cm^{-1} , assigned to the characteristic frequency of PO_4^{3-} , but without the presence of the other characteristic frequency of PO_4^{3-} at $1300\text{--}1450\text{ cm}^{-1}$.⁹ The authors claimed the formation of a Ti–O–P bond on the basis of the previous works of Bhaumik et al¹⁰ or of Lin et al¹¹. However their argumentation is weak, since the signal around 1400 cm^{-1} has been clearly assigned to the P–O–H vibrational mode that is present in the phase $c\text{-}Na_3PO_4$ (hydrated) and absent in the $\alpha\text{-}Na_3PO_4$ phase.¹² Therefore, the conclusion based on the assignment of the peak at $1300\text{--}1450\text{ cm}^{-1}$ to phosphoryl group (with P=O) is clearly questionable and it is hazardous to prove a chemical bond between Ti, O and P solely on the absence of the signal at $1300\text{--}1450\text{ cm}^{-1}$ on the IR spectra.

Consequently, the use of only infrared spectra in the spectral range of vibrational modes of phosphate groups seems to be not sufficient to prove Ti–O–P bonds. DFT computations coupled with experimental diffuse reflectance infrared experiments between 1200 and 600 cm^{-1} could confirm that a combination of monodentate and chelating bidentate complex named as μ -phosphato-bis dioxotitanium complex is the most probable in phosphate modified titania gel samples.¹³ This study eliminated the possibility of monodentate or bridged bidentate complex for these samples. The complexes retained in their work were all

based on O-P-(O-Ti)₃ structures. However this last work is hardly comparable to the other previous works, because of the different nature of titania phases. Similarly, the combination of XPS studies with the vibrational spectroscopy has often resolved some adsorbed structures between phospholipids and metal oxides but in vacuum conditions, that are far from our experimental conditions. NMR has been used as well to study phosphate environment in phases involving TiO_x groups. In 2002, Takahashi et al. summarized from literature the ³¹P NMR chemical shifts of the H₃PO₄ family in solid titanium phosphates.¹⁴ They are given in Table 1 with chemical formulae of the phosphate species (Table 5.1).

Table 5.1. ³¹P NMR chemical shifts of phosphorus atoms in titanium phosphate compounds (in ppm) compiled by Takahashi et al. 2002¹⁴

Titanium phosphate	H ₂ PO ₄	HPO ₄	PO ₄
Ti(HPO ₄) ₂ ·H ₂ O (α-TiP)	—	-18.1	—
Ti(H ₂ PO ₄)(PO ₄)·2H ₂ O (γ-TiP)	-10.6	—	-32.5
TiO(OH)(H ₂ PO ₄)·2H ₂ O	-6.5, -8.4	—	—
Ti ₂ O ₃ (H ₂ PO ₄) ₂ ·2H ₂ O (TiOP)	-5.3, -7.6	—	—

However, they noted small discrepancies in the ³¹P NMR chemical shifts for the H₂PO₄ groups observed among their semi-crystalline synthesized layered titanium phosphate, and titanium phosphates described in literature. These discrepancies could be probably due to the slight difference in hydrogen bonding, in connection with the difference in crystallinity. A larger study including mesoporous titanium phosphate compounds was published in 2000. Using the ³¹P NMR data of various titanium phosphates and oxophosphates then available in literature, including their own work on mesoporous titanium phosphate, Jones et al. discussed a correlation between connectivity and ³¹P NMR shifts.¹⁵ They summarized that, as connectivity increases, an upfield shift is observed from -5.3 to -10.6 ppm for H₂PO₄ (connected to 2 Ti atoms) to -18.1 ppm for HPO₄ (connected to 3 Ti atoms) and finally to -19 to -32.5 ppm for PO₄ (connected to 4 Ti atoms). In addition, deprotonation and/or hydrogen bond donation causes a downfield shift of 1 to 10 ppm. Hydrogen bonding also leads to broadening of the signal. Kovalchuk et al. published in 2005 a work concerning the synthesis and characterization of MCM-41 functionalized with phosphate and titanium phosphate groups, where they analyzed the chemical environment of phosphorus atoms through ³¹P NMR measurements.¹⁶ Their assignment was based on the assumption that the replacement of the protons in phosphoric acid by the more electropositive titanium atoms induces an upfield shift of the corresponding peak, in agreement with the previous analyses of phosphorus environments. Based on the fact that this upfield shift depends on the number of Ti atoms

bonded to one phosphorus atom in the corresponding species, they assigned the observed peaks at -5.4 and -14.7 ppm to the $-\text{TiO}-\text{PO}(\text{OH})_2$ (dihydrophosphate) and $(-\text{TiO})_2=\text{PO}(\text{OH})$ (hydrophosphate) surface species, respectively (figure 5.1). We can notice that this assignment was not in agreement with that proposed by Jones or Takahashi, who assigned H_2PO_4 environments (^{31}P connected to 2 Ti atoms) to resonances around -5 to -10 ppm.



Figure 5.1. Phosphorus environments in MCM-41 functionalized with titanium phosphate groups (Kovalchuk et al. 2005)¹⁶. On the left, monodentate complex ($\delta = -5.4$ ppm), on the right, bidentate complex ($\delta = -14.7$ ppm).

From this work and that of Ren et al. who characterized titanium phosphate compounds, Fei et al. assigned the -8.6 and -12.1 ppm ^{31}P NMR signal of their synthesized mesoporous titanium phosphates to PO_4 units with one or two Ti atoms as neighbors $[\text{P}(\text{OTi})_x(\text{OH})_{4-x}]$ ($x = 1$ or 2) and tetrahedral phosphorus environments connected with three O-Ti bonds $[\text{P}(\text{OTi})_3\text{OH}]$, respectively.^{17,18} However, no clear distinction between monodentate and bidentate species was established.

^{31}P NMR was used as a method of characterization of the local phosphorus environment in amorphous materials that cannot be analyzed through crystallographic studies. In glasses, the phosphate bonding arrangements are described by their Q_n speciation, where n in Q_n refers to the number of bridging oxygen atoms in the phosphate structural unit. As detailed in the work of Brow et al. (2000)¹⁹, the connectivity of Q species decreases from cross-linked Q_3 units to chain-like Q_2 units and finally to Q_1 and Q_0 units. From low to high magnetic field, ^{31}P resonances can be assigned to Q_0 to Q_3 species, as previously described for titanium phosphate compounds. ^{31}P NMR spectra could be thus analyzed by associating each ^{31}P signal with a different connectivity of the phosphate ions towards Ti. However, the relative position of cations as well as the change of the O-P-O angles may have similar effects on the chemical shift. Therefore, this kind of correlation would be valid if it is assumed that the PO_4 groups are almost identical (bond angles, P-O distances) except for the distance of Ti atoms to the bridging oxygens. Based on these kind of assumptions, Schmutz et al. defined in 1994²⁰ a range of chemical shifts for each connectivity of phosphate ions with titanium ones. The proposed range of chemical shifts was then in agreement with the values proposed in Table 5.1. Several papers studied glasses containing TiO_2 and phosphate groups.²¹⁻²⁷ It

appears very difficult to use chemical shifts of ^{31}P in glasses, and a fine analysis of the phosphorus environment is quite complicated in these amorphous materials. The use of this kind of results to our samples dominated by the aqueous medium-oxide interface appears not easy and slightly hazardous. Therefore it is important to investigate the literature with results more representative of our research context.

In 2004, Rice et al. studied the binding of lipoteichoic acid (LTA) that is a long chain (40-50 repeat units) of phosphodiester (anionic) with glucosamine (neutral), hydroxyl (anionic), and D-alanine branches (cationic), to the surface of titanium dioxide through ^{31}P solid-state NMR spectroscopy.²⁸ It is interesting to note that a resonance at -6 ppm appeared on their spectra when the molecule interacts with TiO_2 . In this first publication, they did not interpret precisely this resonance. In 2008, the same group published new NMR results, where a ^{31}P CP-MAS spectrum was collected for pure LTA, characterized by a δ_{iso} of 0 ppm, and a series of spinning sidebands that map out $\Delta(\text{CSA})$ (99 ppm) and η (0.7) of pure LTA.²⁹ When adsorbed on TiO_2 , LTA ^{31}P NMR spectra showed two resonances, at 0 and -6 ppm. The isotropic signal that has shifted upfield (-6 ppm) experiences the largest structural change; thus, it was assigned to the portion of teichoic acid chain that is closest to the TiO_2 surface. The downfield species (0 ppm) was assigned to the portion of teichoic acid further away from the TiO_2 surface, as the chemical shift is unchanged. Adsorption of LTA onto TiO_2 was also indicated by the change in the rotating frame spin-lattice relaxation ($T_{1\rho}$) rate. LTA has a $T_{1\rho}$ of ≈ 3.5 ms while LTA on TiO_2 has a $T_{1\rho}$ of ≈ 30 ms: this drastic change in $T_{1\rho}$ rates indicates that adhesion has occurred. Each isotropic signal has a unique $\Delta(\text{CSA})$ value indicating a different structural conformation of the LTA backbone. However, the upfield signal (-6 ppm) has a η value of 0.8; this large η value indicates that there is a higher degree of axial asymmetry, which also can indicate that this species is closer to the TiO_2 surface. In 2008, another group, Brodard-Severac et al. published a solid-state NMR study on self-assembled monolayers of phosphonic acids ($\text{R-PO}_3\text{H}_2$) deposited on titania anatase substrates.³⁰ In agreement with the previous analyses, they reported that ^{31}P chemical shifts in titanium phosphonates are sensitive to the number of titanium second neighbors, and that each condensation between P-OH and Ti-OH groups should lead to an upfield shift. Conversely, the interactions of the P-O groups with surface Lewis or Bronsted acidic sites should lead to a downfield shift. In addition, ^{31}P chemical shifts are also sensitive to variations in the O-P-O bond angles. Thus, the chemical shifts of $\text{RP}(\text{OTi})_3$ sites in bulk titanium phosphonates and molecular titanium phosphonates could differ by more than 10 ppm. Accordingly, it was not possible to unambiguously ascribe the different components they observed on their ^{31}P spectra

(where they observed three peaks with positive chemical shifts comprised between 11 and 32 ppm), and therefore to quantify the amount of interfacial Ti-O-P bonds. However, they could evidence by ^{17}O NMR the presence of Ti-O-P bonds. Unfortunately, no correlation could be found between the ^{31}P and the ^{17}O MAS NMR spectra.

This non exhaustive bibliographic survey on the use of NMR to describe interaction between molecules and Ti atoms reveals that the ^{31}P NMR is one of the pertinent local probes to understand the mechanism at the molecular scale. However the samples studied in the literature were far from the samples studied in this thesis, because at first they rarely concerned adsorption processes in aqueous media, and secondly phospholipids adsorbed on TiO_2 surfaces have never been investigated. Consequently the spectroscopic characteristics evidenced in the literature would help us to base our interpretations.

Apart the study of Raj et al.,¹³ there is no study combining several methods to get information at the same time about the evolution of the vibrational spectrum of phosphate, the spectral changes of the TiO_2 surface groups, and the evolution of the near environment of the ^{31}P atoms on the same sample at ambient conditions. Therefore our approach proposes to study at the molecular scale the adsorption of DMPA and DMPG phospholipids on rutile and anatase samples by a combination of diffuse reflectance infrared Fourier-transform spectroscopy (middle and near infrared), Raman and NMR spectroscopy:

- Raman spectroscopy to characterize the symmetry of phosphate heads,
- diffuse reflectance Fourier-transform spectroscopy: first in the middle infrared to follow the evolution of the alkyl chains of the PL molecules, and also that of the phosphate heads, complementary to the Raman signals; secondly in the near infrared to elucidate and separate the signal characteristics of H_2O from the surface OH groups, and determine the involvement of Ti-O-H, $\text{Ti-OH}_2^{\delta+}$ and Ti-(OH)-Ti bridges in the interactions displayed in the previous chapters,
- solid-state ^{31}P NMR spectroscopy to establish the possibilities to form chemical bond as Ti-O-P.

5.3 Materials and methods

5.3.1 Diffuse reflectance infrared Fourier transform spectroscopy (DRIFTS)

Infrared spectra of samples were recorded on FTIR Bruker Vertex 70 spectrometer in DRIFTS mode using Praying Mantis Diffuse reflection accessory (HARRICK Scientific Product Inc). The optical configuration of the ellipsoidal mirrors used in the diffuse

reflectance accessory allows separating the optical specular reflectance component away from the diffuse signals, and subsequently minimizing the consequences of the anomalous dispersion on the resulting spectra, displayed as strong shape distortions of the absorption profiles.³¹ The sample chamber was equipped with a dome bearing two KBr windows and one glass window for visual observations from outside (Figure 5.2). It was purged continuously with dried air flow at ambient conditions. Spectra were mostly recorded in this condition. This setup was also connected to a vacuum pump device (composed by two stages: at first a membrane pump to obtain a primary vacuum followed by a second stage constituted by a turbo-pump) enabling to obtain values of pressure of about 10^{-6} mbar, in dynamical conditions and about 10^{-4} mbar in static conditions after 30 minutes. Some spectra were recorded in this condition. All spectra displayed in this chapter were recorded at the temperature imposed by the radiation of the infrared beam focused on the samples, about 30-40°C.

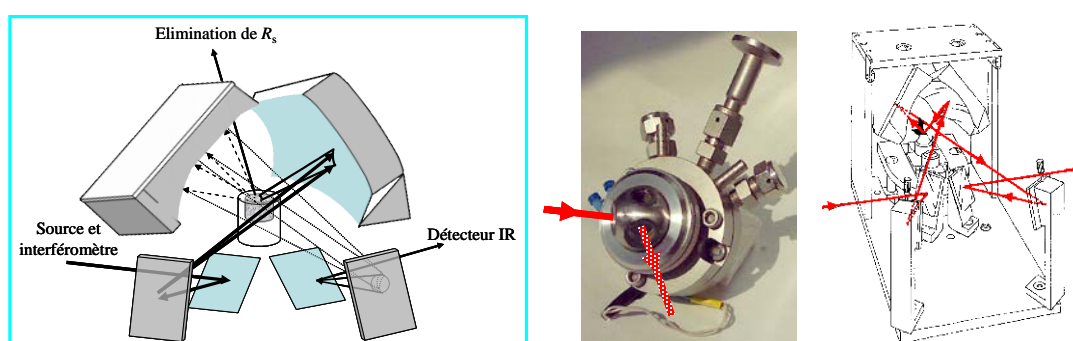


Figure 5.2. From left to right –Principle of the collection of the diffuse part and the elimination of the specular reflection³² - the high-vacuum chamber with the infrared ways and – the scheme of the Harrick setup

In the near- and middle-infrared spectral range ($4000 - 2000 \text{ cm}^{-1}$), the solid powder samples were analyzed pure, *i.e.* without mixing with a dilute optical transparent powder, in order to have a weakly deformed picture of the interface. On the contrary, in the middle IR spectral range ($2000 - 400 \text{ cm}^{-1}$), the absorptions were too strong and solid samples were gently mixed at 2% in weight with finely powdered KBr (Specac, Buckingham, England) using an agate mortar. This sample-to-KBr proportion typically gives good spectra for solid samples.³³ All spectra were recorded with an average of 1000 scans in the wavenumber range of $400 - 8000 \text{ cm}^{-1}$ at resolution 4 cm^{-1} . Spectra were treated by using OPUS 5.5 software provided with the spectrometer. They are displayed as the $\log(\text{reflectance})$ versus wavenumber (cm^{-1}), where the reflectance is the ratio between the recorded reflected intensity

by the sample and the intensity reflected either by an aluminum mirror or by a reference powder.

The sample container at the center of the chamber was equipped with a small heating cartridge in order to cover the temperature range (40°C-600°C) under these low pressures. The setup allowed us to collect infrared spectra at high temperature or after cooling.

5.3.2 Raman spectroscopy.

Raman spectra of the different powders were recorded with a Fourier Transform set-up (Bruker) equipped with a YAG laser emitting at 1064 nm to avoid the visible spectral range and then any photonic degradation of our samples. The near infrared beam at 1064 nm with a power of about 400 mW was focused on the powder on an area of $100 \times 100 \mu\text{m}^2$ and the back-scattered Raman inelastic signals were recorded with a spectral resolution of 2 cm^{-1} and after the average of 1000 scans. The Raman analyses were obtained directly on the powders described in the 5.3.5 section.

5.3.3 Nuclear Magnetic resonance spectrometry.

The interactions of DMPA and DMPG with TiO_2 were analyzed through ^{31}P solid-state NMR measurements, since ^{31}P chemical shifts are very sensitive to the chemical environment of phosphorus atoms. ^{31}P chemical shift data are referenced at 0 ppm against standard of 85% phosphoric acid. Phospholipid powders were analyzed first as commercially received, *i.e.* predominantly deprotonated with sodium counter-ions and then after centrifugation and drying of their suspensions adjusted at pH values of 2 and 9. The solid part of the samples obtained after adsorption of PL on TiO_2 was isolated through the protocol described in section 5.3.5. This powder was then analyzed by $^{31}\text{P} \{^1\text{H}\}$ CP-MAS NMR spectroscopy.

5.3.4 Material

Titanium dioxide (TiO_2) nanoparticles were commercial powders of pure anatase phase (MTI corporation, USA) and pure rutile phase (Sigma-Aldrich), hereafter called TiO_2 -A and TiO_2 -R, respectively. The properties of these powders were given in chapter 2. Briefly, they are recalled here. TiO_2 -A and TiO_2 -R are pure crystalline phases with a high crystallinity. The average particle size of anatase is about 18 nm, and that of rutile is 22 nm. The crystalline faces most viewed in transmission electron microscopy images are (101) of

anatase and (110) of rutile. The specific surface area of these powders was measured by volumetric N₂ gas adsorption at 77K treated by the Brunauer-Emmett-Teller (BET) method: it is around 140 m²/g for anatase, whereas that of rutile is almost five time smaller (around 25 m²/g). DRIFTS and X-ray photoelectron spectroscopy spectra of TiO₂-A and TiO₂-R powders revealed that these powders are not contaminated (chapter 2). Chapter 2 also showed that the surface of TiO₂-A is more covered by molecularly adsorbed H₂O than the surface of TiO₂-R. Both surfaces exhibit free surface hydroxyls. Additionally, TiO₂-R contains relatively more bridging OH groups than TiO₂-A, involved in H-bonds. The concentration of these H-bonded surface bridging OH groups decreases as pH increases from 2 to 5.

The phospholipids retained for this study are the same as previously: 1,2-dimyristoyl-sn-glycero-3-phosphate monosodium salt (DMPA, >99%, from Avanti Polar Lipids) and 1,2-dimyristoyl-sn-glycero-3 phospho-rac-1-glycerol (DMPG, Sodium Salt, 99% Sigma-Aldrich) (Figure 5.3).

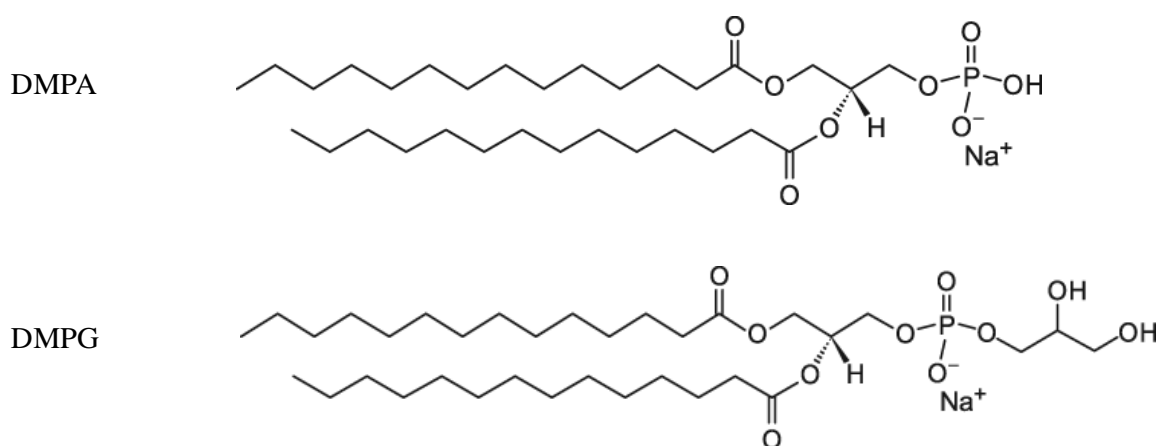


Figure 5.3. Molecular structures of phospholipids DMPA and DMPG

The commercial powders were used directly. These powders were stored in deep-freezer at -20 °C and were left at room condition to get equilibrium state for at least 20 minutes before use. Electrophoretic mobility measurements (chapter 3) showed that DMPA and DMPG in aqueous dispersion were negatively charged from pH 2 to pH 10. Figure 5.4 shows the IR spectra of phospholipids as powders. The major assignments of the peaks are reported in Figures 5.5 and 5.6. They are based on literature data³⁴⁻³⁶ and on the spectra of dehydrated powders and of pH-treated powders (spectra not shown here in order to avoid dull considerations). The most complex vibrational bands originate from the head group of phospholipids approximately in the region 1300 – 900 cm⁻¹ (Figure 5.6.).

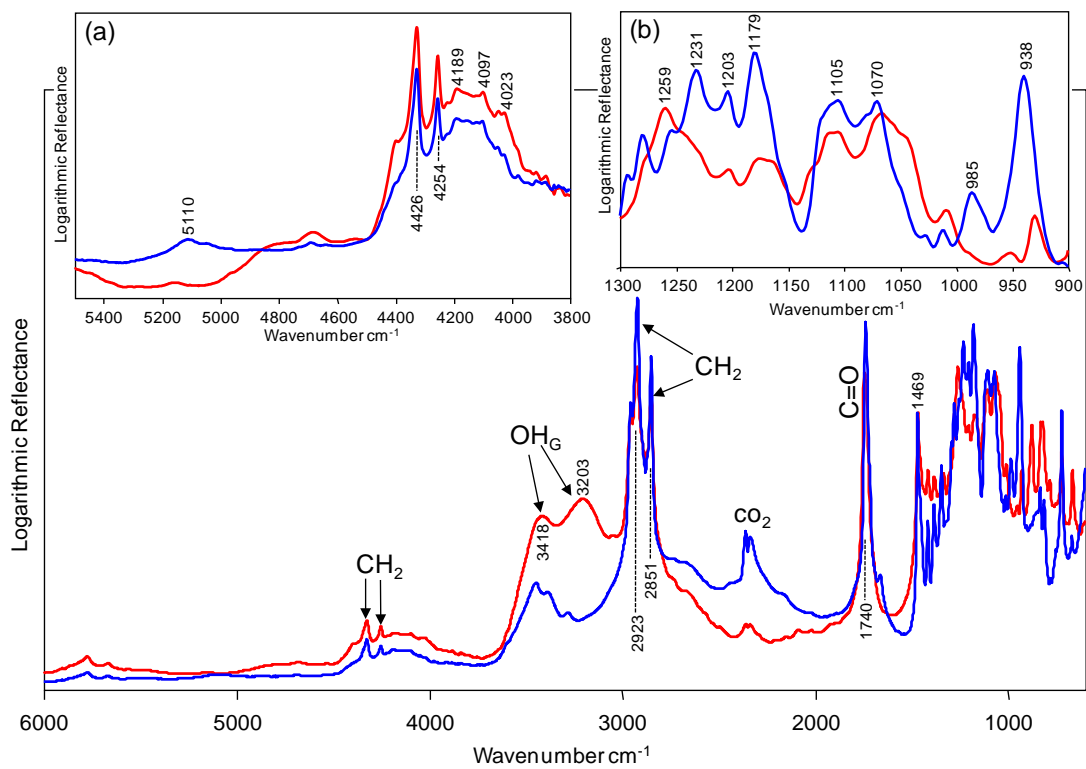
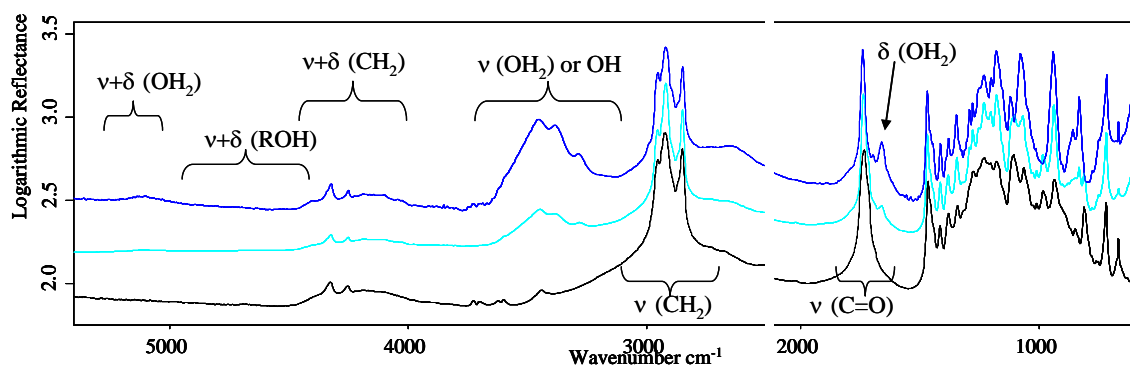
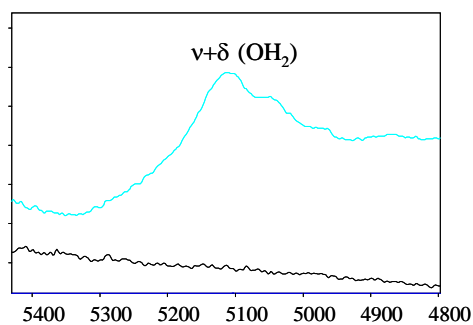


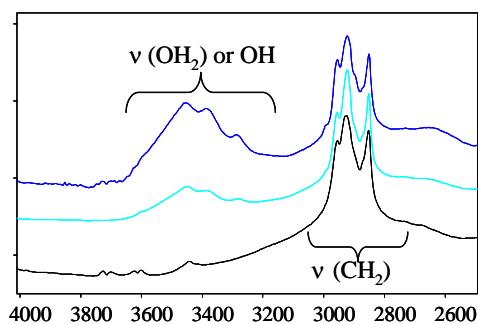
Figure 5.4. IR spectra of commercial powders of (blue) DMPA and (red) DMPG at room conditions.



(A)



(B)



(C)

Figure 5.5. (A) Infrared (Near and middle) spectra of DMPA powders as received (blue), under 2% humidity at room temperature (cyan) and under a weak pressure (black). The assignments are displayed between 5600 and 1500 cm^{-1} . The assignment for the range 1500-700 is detailed in figure 5.6. (B) and (C) spectra are respectively the zooms of the characteristic range of the combination of water modes and of the fundamental stretching modes of hydroxyl groups.

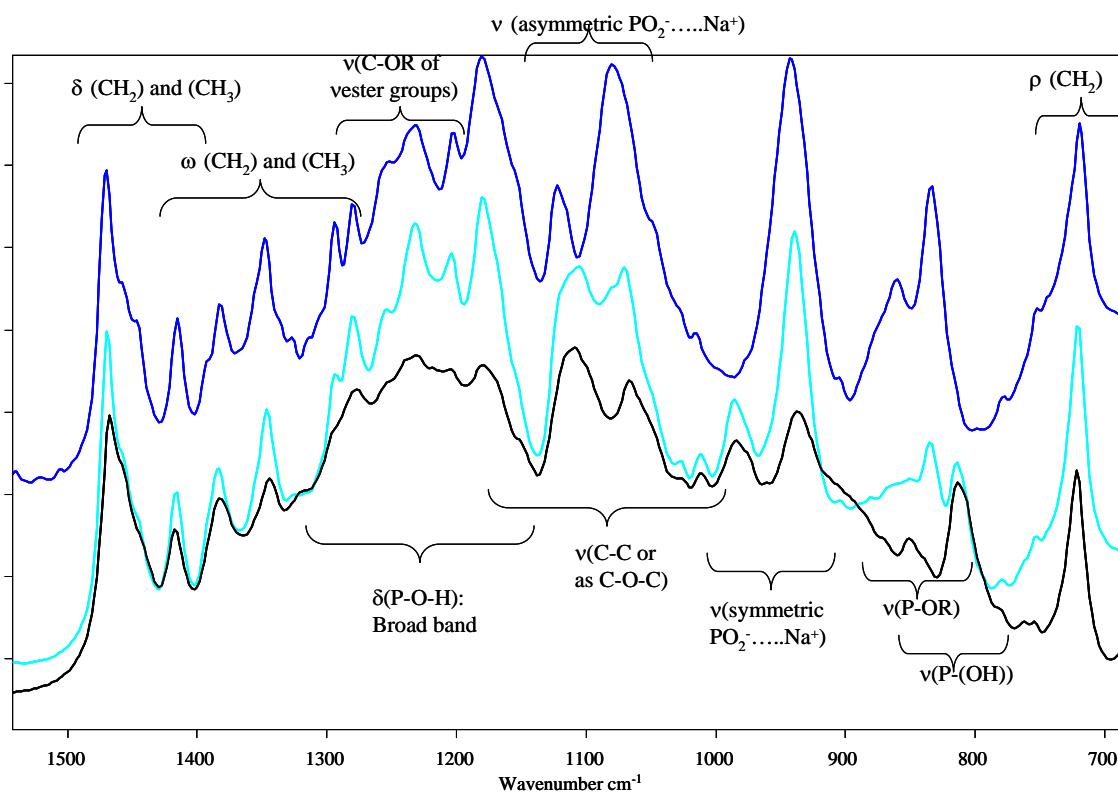


Figure 5.6. Infrared spectra of DMPA powders in the range 700-1550 cm^{-1} of three hydration states.

Commercial powders of phospholipids may be more or less hydrated. The Infrared spectroscopy is the tool of choice to monitor the hydration state. For instance, Figure 5.5 shows the dehydration of DMPA when the powder was submitted to a low pressure. Water was almost removed from the powders as evidenced by i) the disappearance of peaks at 1660 cm^{-1} , characteristic of the bending mode, ii) the disappearance of the three components between 5250 and 4950 cm^{-1} , near IR range specific to the water mode combination, and iii) the strong reduction of the broad structured band between 3000 and 3750 cm^{-1} . In particular, the three bands at 3293, 3390 and 3460 cm^{-1} decrease. The small peak visible at 3459 cm^{-1} after a strong dehydration corresponds to the harmonic of the C=O stretching mode (fundamental at 1720 cm^{-1}). Since at the three components at 3293, 3390 and 3460 correspond three combination components 4976, 5052 and 5110 cm^{-1} , the range from 3100 to 3600 cm^{-1} is dominated by the absorption signals of water molecules. The stretching of the hydroxyl group, POH, that is an acid group and then involved in strong H-bonds, is displayed as a very broad band, appearing as a background between 3200 and 2500 cm^{-1} . The dehydration process modifies the vibration of phosphate group as well (Figure 5.6). A peak at around 984 cm^{-1} appears and increases while the peak at 942 cm^{-1} decreases and shifts to 936 cm^{-1} . Concomitantly the 1080 cm^{-1} band decreases strongly to the benefit of the 1110 cm^{-1}

component that increases in the asymmetric phosphate stretching range. By comparison with the infrared and Raman studies published about the behavior of the phosphate anions in aqueous solution versus pH values and cation natures, the evolution of the vibration of phosphate head of DMPA may be due to interactions with either water by H-bonds or sodium cations by electrostatic attractions. The sensitivity of the head anion phosphate groups with its environment is also displayed by NMR spectroscopy (Figure 5.7). When the content of water of the DMPA is low, the averaged isotropic shift is centered around 2.5 ppm with two closed components (3 and 2.4 ppm). In contrast, when the water content is higher, the anion-cation interaction changes, giving in this example two components much more separated with a negative shift for one component (-0.7 ppm), and a higher positive chemical shift for the other (3.8 ppm).

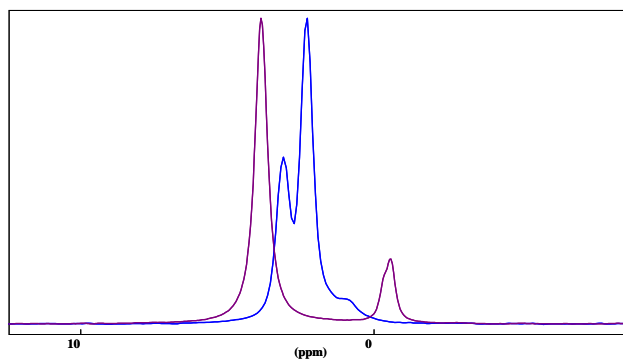


Figure 5.7. ^{31}P $\{^1\text{H}\}$ CP-MAS NMR spectra of DMPA, in blue as received, in purple after contact with a solution at pH value of 2 (with a high hydration rate verified by near IR).

The environment of the head phosphate of DMPG molecule is clearly different from that of DMPA. Infrared spectra (insert in fig 5.4 in the range 5000-5400) do not displayed adsorbed water. This weak physisorption of water on DMPG powders has been verified at different conditions (pH of aqueous solution, and vacuum conditions in DRIFT experiments). Therefore, the figure 5.8 is displayed in order to compare dehydrated DMPA to DMPG spectra in the infrared range between 1500 and 700 cm^{-1} . The essential differences between DMPA and DMPG come from the presence of the glycerol group on the head of DMPG, either by the vibrational modes of C-C-OH of the glycerol or by the $^-\text{O}_2\text{P}(-\text{O}-\text{R})_2$ local structure of DMPG against the $^-\text{O}_2\text{P}(\text{OH})(-\text{O}-\text{R})$ of DMPA. This last difference is underlined by the comparison of the local structure with the DHP signals (in green in fig. 5.8).

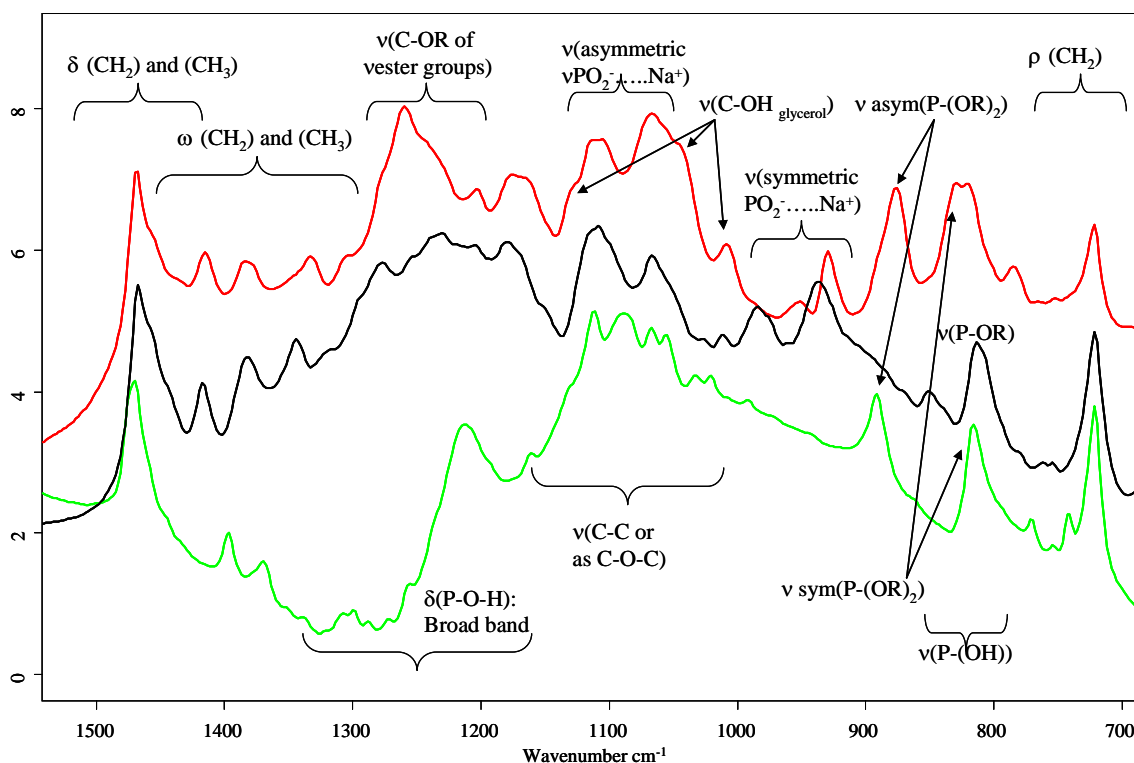


Figure 5.8. Comparison of the DRIFT spectra of dehydrated DMPA powder (black) and DMPG powder (red). The spectrum (green) of DHP powder is added to help the visual interpretation between 780 and 930 cm^{-1} of the asymmetric and symmetric of the local structures $\text{O}_2\text{P}(-\text{O}-\text{R})_2$ characteristic of DMPG and DHP but not of DMPA.

Raman spectra of DMPA and DMPG powders are displayed in figure 5.9. The assignment proposed in this figure are based on the literature.³⁷⁻⁴⁰ The spectra are dominated by the vibrational modes of the alkyl chains. In the spectral region of the head phosphate modes, the modes involving movement of the CC skeleton possess strong Raman activities in opposition of their weak infrared activities. Consequently, the Raman profiles look very different from the infrared absorption profiles. Notice here that the selection rules are different between the infrared absorption involving electric dipolar variations and the inelastic Raman scattering involving the polarisability variations. Thus, often, the more intense the absorption of a vibrational mode is, the weaker its Raman scattering is and vice-versa.

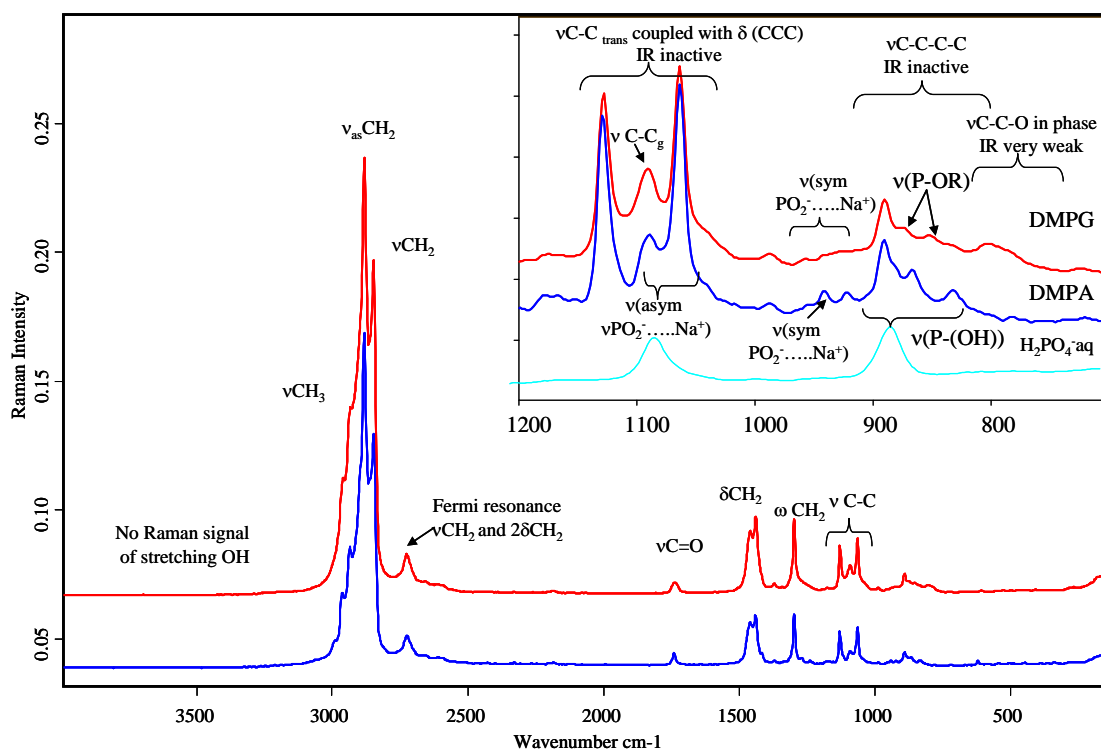


Figure 5.9. Raman spectra of DMPG (red) and DMPA (blue) powders. The insert displayed a zoom of the 700-1300 region and a comparison with the Raman spectrum of the $H_2PO_4^-$ anion in aqueous solution at pH=5. This comparison helps to locate the spectral ranges where the more intense Raman stretching modes are expected.

5.3.5 Preparation of phospholipid-covered TiO_2

Phospholipids/ TiO_2 samples were prepared in accordance with the protocol described in chapter 2 (section 2.2.4). Powders of phospholipids and TiO_2 were prepared separately at pH 2 and 9 in aqueous medium and mixed in the ratio of 2 molecules/ nm^2 defined as the number of phospholipid molecules per surface unit of TiO_2 . At this ratio, the adsorption sites on TiO_2 may be assumed to be saturated by di-hydrocarbon chain phosphate.⁴¹ According to the results of chapter 4, this value is actually the saturation ratio or a little bit above, depending on aqueous acidic conditions. pH values of the aqueous solution in equilibrium with the solid phases were adjusted by adding NaOH and HCl solution. The samples in suspension were left for adsorption under rotation for 48 hours at room temperature in order to reach the equilibrium state. During the preparation process, samples containers were covered with aluminum foils to avoid the effect of light. Solid phases in the aqueous suspension were separated from unadsorbed phospholipids by alternating centrifugation and washing. Solid phases were washed three times by H_2O in the same condition (pH) as the supernatant. Consequently, these samples are not completely comparable with those used in chapter 4 for the establishment of adsorption isotherms. In particular, the quantity of PL in

contact with TiO₂ in the solid-state is evidently higher than those used in chapter 4. Indeed, we speculate that, during this multiple centrifugation and washing process, phospholipid vesicles dispersed in the aqueous medium might have ruptured and precipitated in the solid phase, thus enhancing the apparent adsorbed amount of phospholipids on TiO₂ surface. However, we have first preferred this preparation in order to favor the recording of the potential signals of adsorbed PL. The solid phases were finally dried in desiccators filled with silica-gel. To accelerate the drying process, the desiccators were connected with a membrane vacuum pump for 20 minutes. In addition, the desiccators were also covered by aluminum foil to prevent possible effects of ultraviolet light. When necessary for the middle infrared range analysis, the solid phases were manually crushed and ground in an agate mortar then homogeneously mixed with KBr matrix (2% in weight of sample).

5.4 Results on the spectroscopic study of the interaction between phospholipids with anatase and rutile

5.4.1 Interaction between phospholipids and TiO₂ surface viewed from phosphate group

Figure 5.10 displays the Raman spectra of the phospholipid-covered TiO₂ samples at pH 2. The displayed spectral range corresponds to the vibrational modes of bending CH₂ (1500-1350), vibrational modes involving C-C stretching and CH₂ wagging movements (1350-1200), stretching modes of C-C bonds along the long alkyl chain (1200-900 cm⁻¹) and stretching modes of the phosphate groups between 1200 and 900 cm⁻¹ (Figure 5.9). The difficulty to interpret the Raman data comes from the overlap of the signals coming from the phosphate head group by those of the alkyl chains. The most important changes in the Raman signals of phospholipids were obtained after adsorption on anatase sample. In comparison with the PL spectra before adsorption at the same pH value, two main changes were noticed: (i) a new broad component appears at 1083 cm⁻¹ accompanied by a strong widening of the signal centered at 900 cm⁻¹ and (ii) the ratio between the relative intensities of the signals at 1063 and 1120 cm⁻¹ decreases. The former indicates that the phosphate groups are disturbed by the surface of anatase while the latter indicates an increase of the gauche structure in the C-C arrangement at the expense of the trans form (Figure 5.10). The impact of TiO₂-R on the Raman signals of the PL moiety is much weaker in these conditions. Only the intensity of peak at 1089 cm⁻¹ increases relatively to that of peak at 1063 cm⁻¹, whilst the position of peaks does not change.

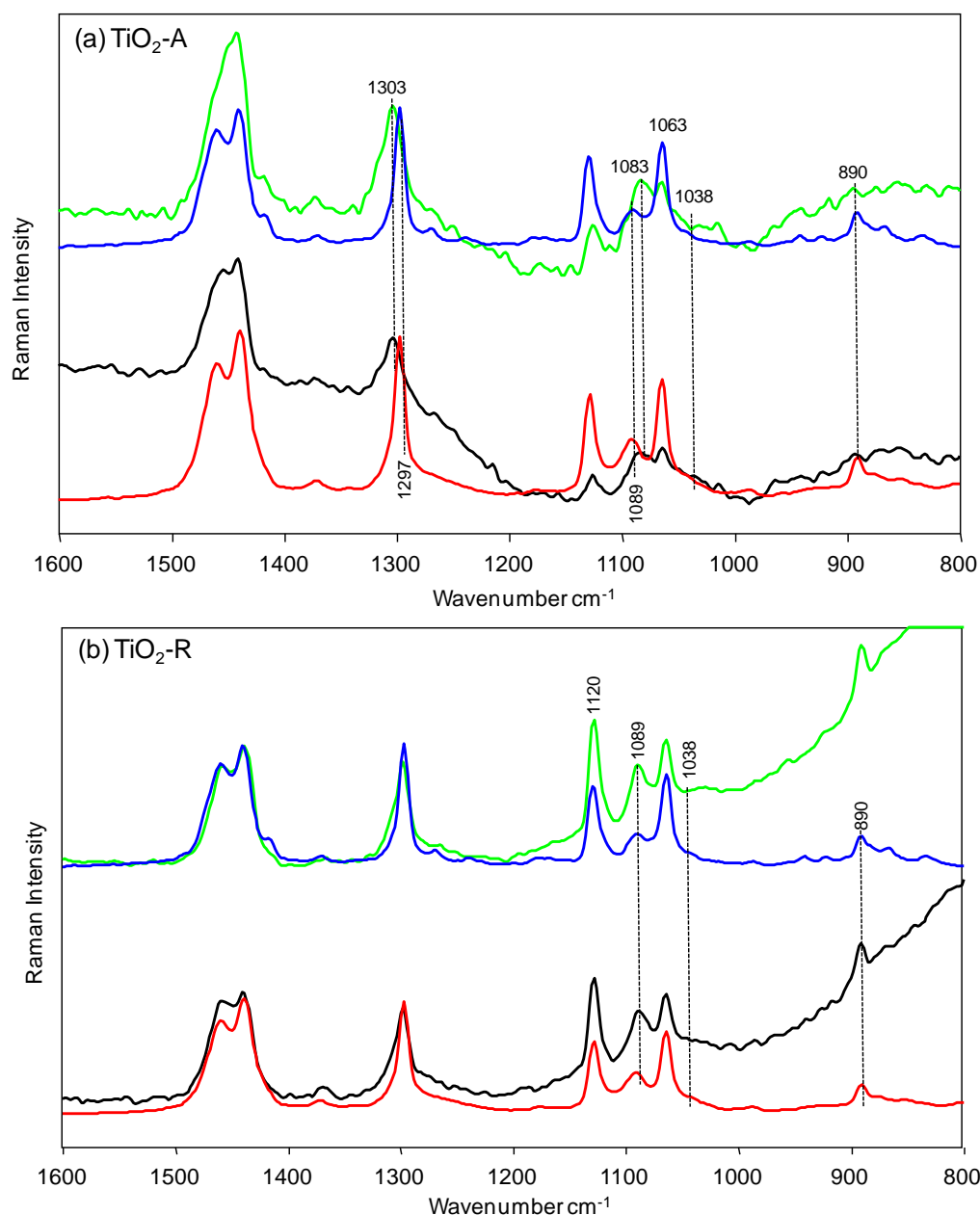


Figure 5.10. Raman spectra of adsorbed (green spectrum) DMPA and (black spectrum) DMPG on (a) $\text{TiO}_2\text{-A}$ and (b) $\text{TiO}_2\text{-R}$. Spectra of pure (blue) DMPA and (red) DMPG are shown for reference. All these sample spectra were recorded at pH 2.

This trend was confirmed by NMR experiments. Figure 5.11 shows the chemical shift of phosphorus atoms of adsorbed DMPG molecules on TiO_2 powders in comparison with that in pure DMPG at pH 2. The chemical shifts are different from one substrate to another. The chemical shift is observed in the negative range on $\text{TiO}_2\text{-A}$ whereas the shift is positive on $\text{TiO}_2\text{-R}$. This illustrates that (i) TiO_2 surfaces remarkably influences the electron density distribution in phosphate moiety and (ii) DMPG adsorbs on $\text{TiO}_2\text{-A}$ and $\text{TiO}_2\text{-R}$ via dissimilar interactions. The negative shifts of the ^{31}P NMR were also reported in the literature

about the synthesis of phosphate-titanate or the adsorption of orthophosphates on TiO_2 samples¹⁴ when Ti-O-P were formed.

Thus NMR and Raman show at first that the adsorption on our anatase sample of the DMPA or DMPG molecules at pH 2 involves strong interactions with the surface groups. The ^{31}P NMR signal might even suggest the formation of Ti-O-P bonds, even if this point has to be confirmed by further work. Secondly, for our rutile sample, the effect is clearly different, underlined by positive chemical shifts of the NMR signals and weak changes of the Raman signals. In order to go deeper into the description of the interaction between the polar head group of PL molecules and the surface, we had to investigate the response of the TiO_2 surface groups after the interaction. Therefore in the next section, the infrared spectra were studied to follow the hydroxyl groups.

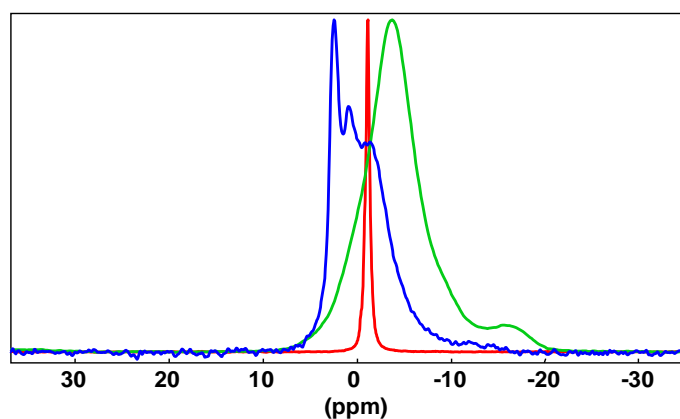


Figure 5.11. DMPG in contact with anatase (green spectrum) and rutile (blue spectrum) at pH2. Comparison with pure DMPG dispersed in water at pH2 and dried (red spectrum).

5.4.2 Interaction between phospholipids and TiO_2 viewed from surface OH groups.

Infrared spectra displayed in Figure 5.12 show the impact of phospholipids on surface functional groups of TiO_2 . The adsorption of phospholipids leads to the decrease in intensity of the peak at 1623 cm^{-1} and the disappearance of the peak at 5236 cm^{-1} . As these peaks are assigned specifically to molecular adsorbed H_2O , we can conclude at this stage that phospholipids adsorb by displacing adsorbed H_2O .

The adsorption also leads to a global shift, towards low wavenumbers, of the massif in the middle infrared, characteristic of the stretching O-H bonds involved in H-bonds (Figure

5.12). Consequently, H-bonds are formed between phospholipids and surface functional groups.

Strikingly, characteristic bands of surface terminal OH groups in the region 3600 – 3750 cm^{-1} disappeared upon adsorption of phospholipids. The $\text{Ti-OH}_2^{\delta+}$ groups characterized by the peak at 5271 cm^{-1} (figure 5.12) are either eliminated or strongly disturbed during the interactions with PL molecules. Moreover since this evolution concerns the whole of H-bond free OH groups, then it is indicative of the full coverage of TiO_2 surface by phospholipids. This behavior was also observed in the literature for the adsorption of phosphate species on thin TiO_2 film.² Accordingly, the adsorption of phospholipids results from interactions either via H-bonds between Ti-OH_2^+ and negatively charged head polar groups, or via a direct bond between phospholipids and Ti_{5c}^+ sites. The effect caused by adsorbed DMPG molecules on $\text{TiO}_2\text{-A}$ is stronger than that induced by DMPA molecules (figure 5.12.). This is evidenced in the range from 3600 to 3700 cm^{-1} (insert c), where the surface hydroxyl groups on $\text{TiO}_2\text{-A}$ are almost completely removed by DMPG. In contrast, some surface functional groups are still observable when DMPA was adsorbed. Since the DMPG has two hydroxyl groups carried on the glycerol function, the different interaction of DMPG on $\text{TiO}_2\text{-A}$ in comparison with DMPA suggests that OH on glycerol could be involved into the interaction.

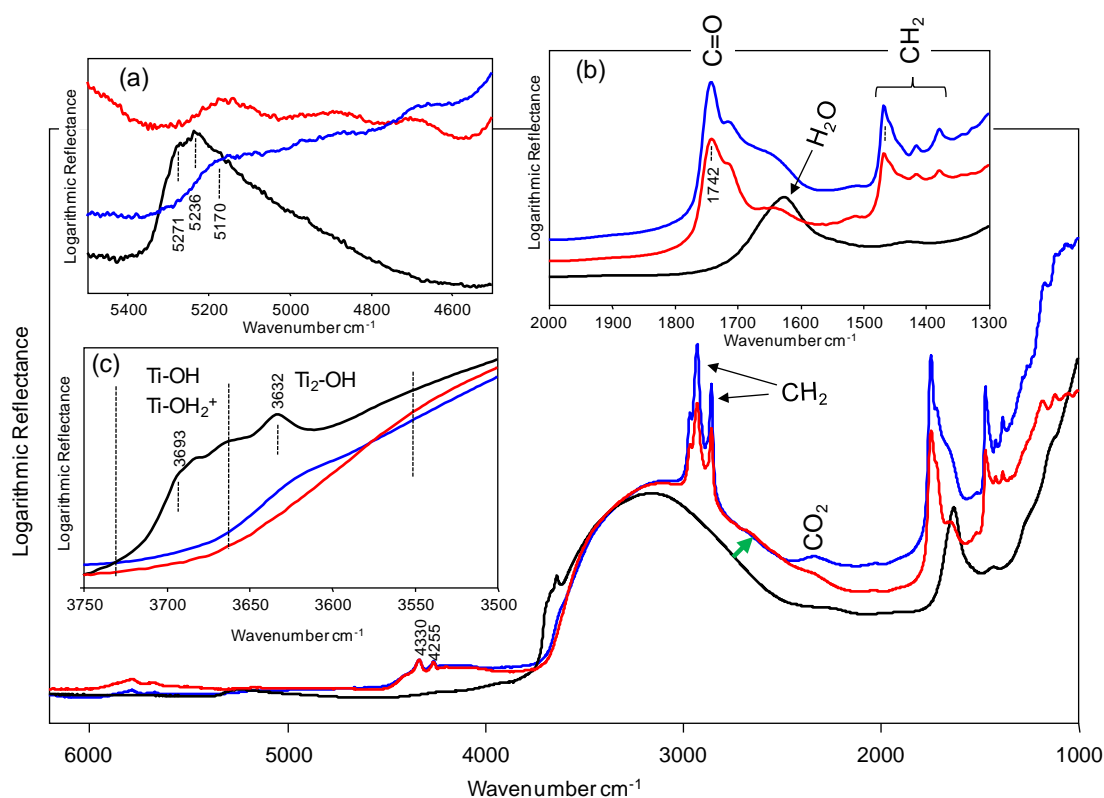


Figure 5.12. IR spectra of (blue) DMPA and (red) DMPG adsorbed on $\text{TiO}_2\text{-A}$ at pH 2. The black spectrum is recorded on pure $\text{TiO}_2\text{-A}$ at pH 2 for comparison. The green arrow indicates the shift of the H-bonded OH signal towards low wavenumbers after the adsorption.

Figure 5.13 displays the infrared spectra after the phospholipid adsorption on $\text{TiO}_2\text{-R}$. Pure $\text{TiO}_2\text{-R}$ exposes before adsorption sharp bands in the region $3200 - 3500 \text{ cm}^{-1}$, that are assigned to vibration of surface OH groups, which can have H-bonds between each other or with adsorbed H_2O (chapter 2). The adsorption of phospholipids led to the disappearance of the band at 3490 cm^{-1} (assigned to weak H-bonded TiOH_2^+),⁴² and either the removal of the band centered at 3275 cm^{-1} (H bonded Ti-OH-Ti bridging OH) or a red shift to 3191 cm^{-1} . On the contrary, the band at 3417 cm^{-1} was not altered by the adsorption.

Moreover we can notice that, the well overlapping of bands in region $2800 - 3000 \text{ cm}^{-1}$ demonstrates the similar density of adsorbed DMPA and DMPG on $\text{TiO}_2\text{-R}$.

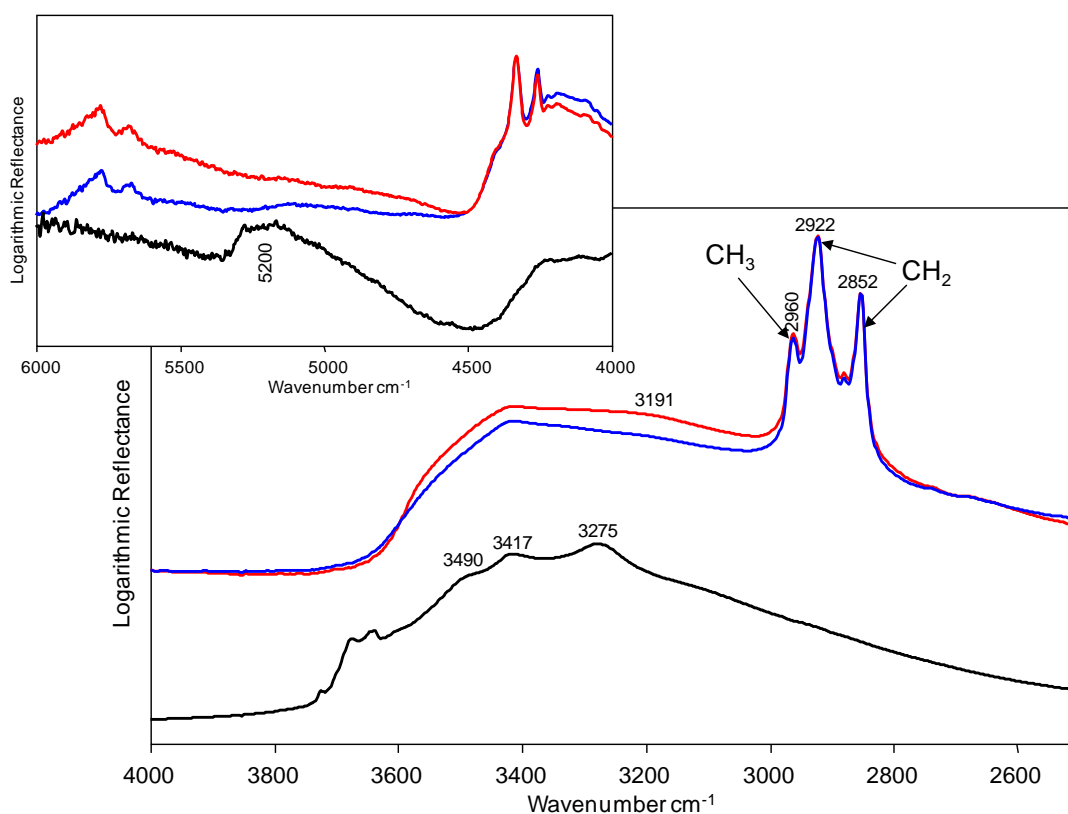


Figure 5.13. IR spectra of (blue) DMPA and (red) DMPG adsorbed on TiO₂-R at pH 2. The black spectrum is recorded on pure TiO₂-R at pH 2 for comparison.

5.4.3 Effect of pH on the adsorbed species

Vibration modes of adsorbed phospholipids are dependent on pH of preparation (Figures 5.14 and 5.15). The difference spectra displayed in Figure 5.14 are obtained by subtraction of the sample spectrum with the spectrum of the TiO₂ powder treated in the same conditions, to eliminate the signals of TiO₂ at low wavenumbers. As the signals of TiO₂ phases are too intense in the spectra recorded without dilution with KBr, we had to use the spectra of mixed powders at 2% in weight with KBr. The absorption bands of the phosphate group of DMPA are noticeably disturbed at pH 2, evidenced by the appearance of a new peak at 1106 cm⁻¹ and the decrease of the peak intensity at 1075 cm⁻¹. These observations are in agreement with the Raman results of the 5.4.1 section. Furthermore, the displacement, already discussed in the previous section 5.4.2, of surface hydroxyl groups and physisorbed H₂O from TiO₂-A at pH 2 by DMPA is illustrated by the strong broad negative band centered at 3457 cm⁻¹. On the contrary, the effect of adsorbed DMPA at pH 9 is weak as shown by the small negative bands at 3400 cm⁻¹. Figure 5.14 also shows that at pH 9 the changes of the IR absorption of phosphate group vibration are weak or negligible. Thus the spectrum of the powder obtained at pH 9 is approximately the spectrum of a mixture between both the TiO₂

and DMPA powders without new interactions. This is in agreement with adsorption isotherm data presented in chapter 4, where we have shown that DMPA molecules do not adsorb on TiO_2 surfaces at pH 9.

Consequently, at pH 2, the positively charged surface, essentially due to the presence of $-\text{OH}_2^+$ groups, proved by IR spectra and Zeta potential measurements, interacts with the negative DMPA head groups, and in a second step these positive charged groups are displaced to allow a stronger interaction between Ti_{5c}^+ with the phosphate head. In contrast at pH 9, this kind of process is not observed because both the surface and the molecules are negatively charged.

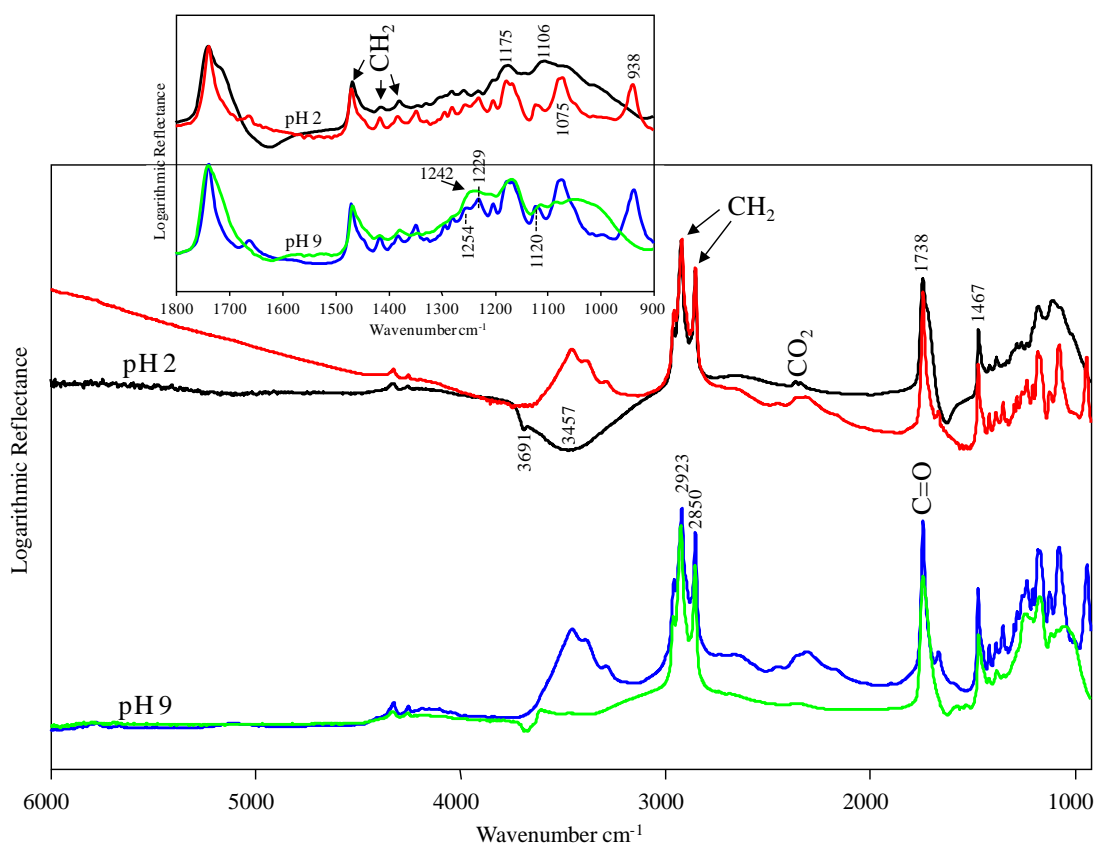


Figure 5.14. Difference IR spectra of (DMPA adsorbed on $\text{TiO}_2\text{-A}$) - ($\text{TiO}_2\text{-A}$) at pH 2 (black) and pH 9 (green). Spectra of pure DMPA at pH 2 (red) and pH 9 (blue) are presented for comparison.

Figure 5.15 displays the IR spectra recorded for the adsorption of DMPG on rutile and anatase powders at pH 2 and pH 9. In addition to the elimination of OH signals from the TiO_2 surfaces (section 5.4.2), the spectra of the adsorbed DMPG exhibit a different profile between 1300 and 1100 cm^{-1} , in comparison with pure DMPG. A new thin component around 1090 cm^{-1} , associated to another one at 1150 cm^{-1} , increases while the component at 1228 cm^{-1} is fully suppressed. As this infrared region is a fingerprint of vibrations arising from both the

glycerol and PO_4 , it should be difficult to interpret these changes. However, one must note that i) the variations look stronger on rutile than on anatase while the reverse was observed in Raman spectra and ii) these spectral features were not observed for DMPA. This means that the changes in Figure 5.15 are essentially due to signals from glycerol. The wavenumbers of 1090 cm^{-1} and 1150 cm^{-1} can be associated to the vibration of an ether bond⁴⁰ and that at 1228 cm^{-1} to the complex vibration modes of an alcohol. Therefore, the adsorption of DMPG on TiO_2 surfaces can be viewed as the formation of an ether bond between surface sites and glycerol. This is particularly obvious for rutile (the effect being stronger at pH 2 than at pH 9) but less clear for anatase. Thus we can speculate that the Ti-OH-Ti bridges, characterized by an intrinsic pKa around 5 (chapter 2) could be involved in the interaction with the glycerol moiety of DMPG head to form $(\text{Ti})_2\text{-O-glycerol}$ bonds as evoked by Copeland et al (2013)⁴³. As the surface concentration of this kind of bridge is relatively higher for our rutile sample than our anatase sample, this effect is more important. To confirm this assumption, isotopic molecules should be used.

5.5 Discussion

5.5.1 Existence of Ti-O-P bond?

Phosphate species have been known to bind strongly to TiO_2 surfaces.^{1,2} Gong indicated that P-O^- groups of phosphate species from aqueous solution can directly bind to exposed Ti sites on TiO_2 through bridging bidentate mode. From mathematical spectral deconvolution treatments, the author claimed that the frequencies of asymmetric and symmetric stretching of Ti-O-P bond are 972 and 915 cm^{-1} , respectively.¹ Our study found that TiO_2 significantly absorbs IR photons at wavenumbers lower than 1000 cm^{-1} . This remarkably masks the absorption bands of adsorbed phospholipids in this region. Therefore in our study, we cannot bring similar evidences to clearly conclude on the formation of Ti-O-P bonds. However, the spectra of adsorbed species were found to be distorted in comparison with that of pure phospholipids. This was supported by both Raman and NMR spectra (Figure 5.10-11). The disturbance of phosphate moiety in phospholipids upon adsorption demonstrates the strong adsorption of phospholipids on TiO_2 . The evolution of surface hydroxyl groups on TiO_2 upon adsorption of phospholipids is also obvious evidence to support the strong interaction of phospholipids with TiO_2 .

5.5.2 Role of glycerol in the adsorption

Copeland et al. illustrated that glycerol readily binds to unsaturated Al atoms on γ - Al_2O_3 in spite of the presence of physisorbed H_2O .⁴⁴ This chemical binding occurs via the primary OH of glycerol, whereas H-bonding with surface metal oxide is involved through the secondary OH group (the primary OH is more acidic than the secondary one). The interaction of glycerol with the surface occurred regardless of the presence of coadsorbed H_2O , which demonstrated that the interaction is strong. Several metal oxides including TiO_2 exhibit Lewis acid sites, and strong interaction of glycerol with these oxides has been recently observed.⁴³ In this work, it was observed that glycerol displaced the hydroxyl groups and directly bound to the surface Ti^{4+} on anatase. Furthermore, the authors claimed that hydrogen bonds were also formed between glycerol and surface hydroxyl groups or surface negative oxygen atoms.

The presence of substituted glycerol on DMPG thus increases the probability of these molecules to adsorb on TiO_2 surface. This has been supported by the adsorption isotherm of DMPG on TiO_2 (chapter 4). The isotherm shows that the adsorption takes place even at pH 9, where electrostatic interaction between TiO_2 and DMPG is repulsive.

The sole difference between DMPA and DMPG is the presence of glycerol substitution in the headgroup of DMPG. As a result, phosphate moiety in DMPA exposes three free oxygen atoms, whereas DMPG has only two oxygen atoms available for interaction. This leads to differences in protonation/deprotonation and hydration behavior. The striking distinction is the presence of two OH groups carried on the terminal glycerol in DMPG. They induce a distinctive adsorption mechanism of DMPG from that of DMPA on TiO_2 . Raman and NMR spectra indicated that the phosphate moiety of DMPG was less sensitive to the adsorption. It is therefore suggested that the phosphate moiety is unlikely involved in the interaction of DMPG with TiO_2 . Glycerol is expected to play a more prominent role in the interaction. For illustration, figure 5.15 shows the IR spectra of adsorbed DMPG on TiO_2 .

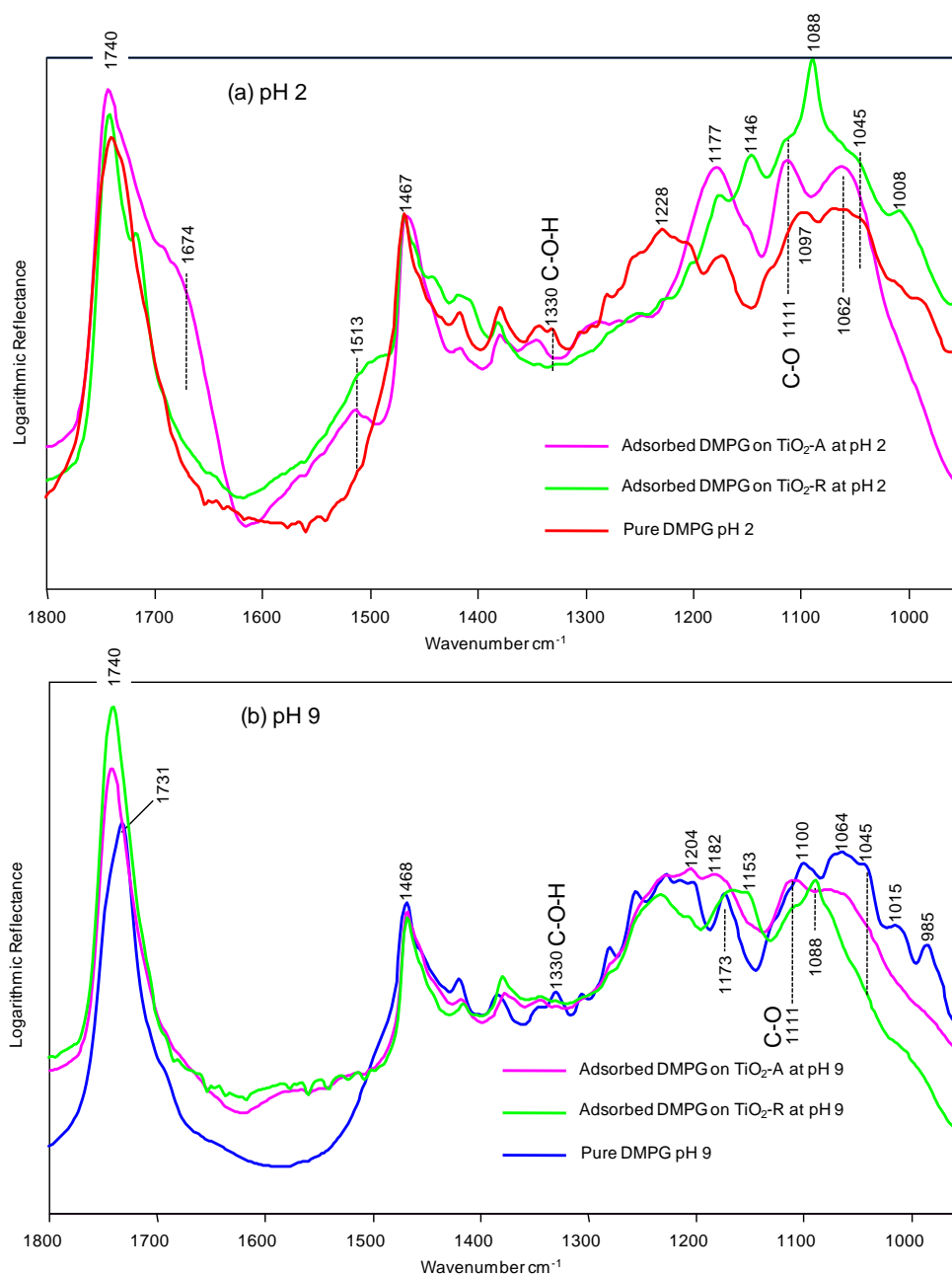


Figure 5.15. IR spectra of adsorbed DMPG on $\text{TiO}_2\text{-A}$ and $\text{TiO}_2\text{-R}$ at (a) pH 2 and (b) pH 9. Pure DMPG at pH 2 and pH 9 are presented for comparison.

Intensity of peaks at 1111 cm^{-1} and 1330 cm^{-1} are significantly altered after the adsorption of DMPG on TiO_2 . The first peak is attributed to stretching of C-O in the secondary alcohol of glycerol and the second is assigned to C-O-H bending. At both pH 2 and pH 9, the intensity of C-O-H peak decreases. This is a clear evidence for the involvement of hydroxyl groups of glycerol in the interaction with TiO_2 .

The behavior of the C-O peak is dependent on crystallinity of TiO_2 . On $\text{TiO}_2\text{-A}$, the intensity of this peak increases, whilst it decreases on $\text{TiO}_2\text{-R}$. This change in intensity

demonstrates that the interaction of glycerol OH groups with $\text{TiO}_2\text{-R}$ is stronger than with $\text{TiO}_2\text{-A}$. Especially, the sharp peak at 1088 cm^{-1} , which may be attributed to the primary OH group in glycerol substituent, interacts with surface $\text{TiO}_2\text{-R}$. The spectral data are apparently in agreement with the adsorption isotherms reported in chapter 4. Indeed, we observed that DMPG adsorbed in greatest amount on rutile than on anatase phases, and that this amount did not depend on pH (2 or 9).

5.5.3 Interaction model

In addition to the presence of terminal (Ti-OH) and bridging ($\text{Ti}_2\text{-OH}$) hydroxyl groups, the surface of TiO_2 in this study is overall covered by multilayers of physisorbed water. At pH 2, the positively charged groups (Ti-OH_2^+) appear because of the protonation of surface hydroxyl groups. At pH 9, negatively charged groups (Ti-O^- and $\text{Ti}_2\text{-O}^-$) are present via the deprotonation processes. At ambient condition, the presence of surface coordinatively unsaturated Ti^{4+} sites is excluded. Figure 5.16 suggests the dominant phospholipid species and surface functional groups on TiO_2 in solution at pH 2 and pH 9.

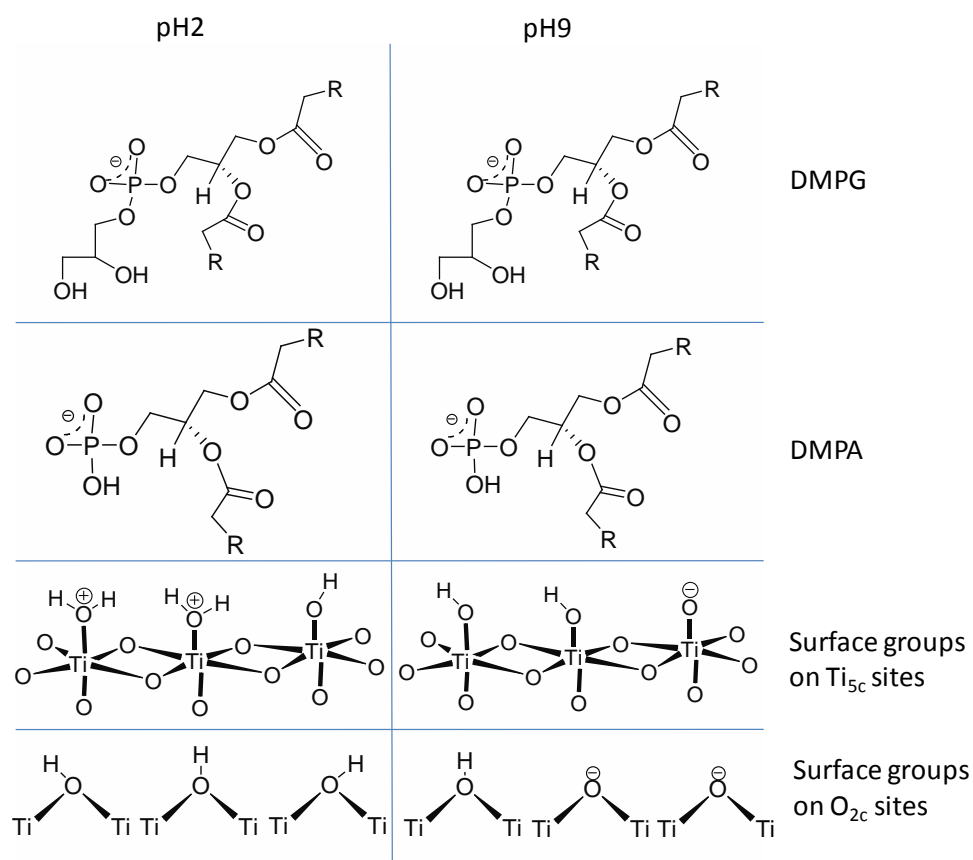


Figure 5.16. Predominant protonation states of DMPA and DMPG at pH 2 and pH 9. Possible surface functional groups existing on TiO_2 according to pH of environment. Reference to Tocanne 1990⁴⁵ for DMPA and DMPG.

It is conceivable that mono-substituted phosphate has two possibilities of binding to TiO_2 surface: monodentate and bidentate, whereas disubstituted phosphate has only one possibility: monodentate. Connor and McQuillan proved that n-butyl phosphate adsorbed on TiO_2 via bidentate binding. Nonetheless, dimethyl phosphate did not bind to TiO_2 in the same condition.² DMPA and DMPG can be considered as monosubstituted and disubstituted phosphate, respectively, as DMPG has an additional glycerol substituent.

As shown by spectroscopic investigations, DMPG is not expected to bind via the phosphate group. The bulky structure in conjunction with intra-hydrogen bonds can hinder the direct binding of DMPG to TiO_2 through the phosphate group. Consequently, there is a higher probability for the chemical bond to be formed between the primary hydroxyl of glycerol substituent and the surface of TiO_2 .

Evidences from Raman, NMR and Infrared spectra show the disturbance of phosphate group in adsorbed species in comparison with pure phospholipids. Furthermore, the removal of surface hydroxyl groups (including $-\text{OH}_2^+$) on TiO_2 upon adsorption gives rise to the evidence of a strong interaction between phospholipids and TiO_2 surface. Nonetheless, it is uncertain to confirm the formation of chemical bonds between phospholipids and TiO_2 . Hereafter, some adsorption modes of DMPA and DMPG onto TiO_2 are suggested.

At low pH, it is likely that phospholipids displace $-\text{OH}_2^+$ groups and create a direct covalent bond between oxygen in phosphate or glycerol and Ti^{4+} sites (Lewis acid). Another possibility is that an electrostatic bond could be established between Ti^{4+} sites and negative oxygen atoms from phosphate moieties. In addition, the formation of H-bonds between phospholipids with residual surface OH groups or with surface oxygen atoms (terminal and bridging) is highly possible.

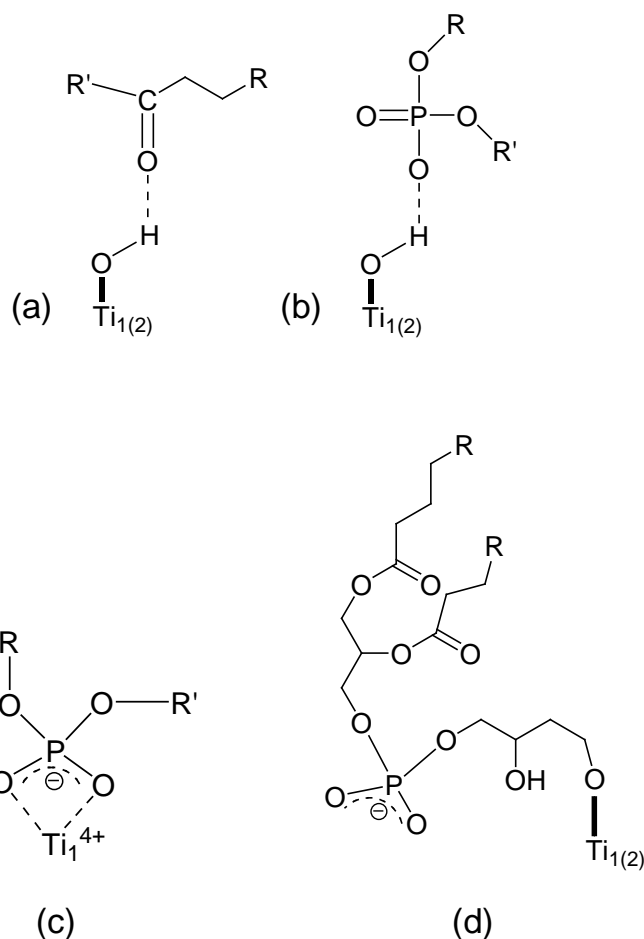


Figure 5.17. Some binding modes of DMPA (a, b, c) and DMPG (a, b, d) at pH 2 to surface of TiO_2 . Ti_1 indicates that only one Ti^{4+} atom in the lattice bind to one oxygen atom (terminal oxygen). Ti_2 denotes that there are two Ti^{4+} atoms in the lattice bind to one oxygen atom (bridging oxygen).

At high pH, the majority of surface hydroxyl groups is deprotonated and results in $\text{Ti}-\text{O}^-$ and Ti_2-O^- groups. In this condition, electrostatic interaction between TiO_2 and phospholipid headgroups is repulsive. This explains why DMPA could not adsorb on TiO_2 surfaces at pH 9. In contrast, DMPG can form H-bonds between OH groups of glycerol function and negatively charged surface oxygen atoms. This binding mode has been proven for the interaction between glycerol and anatase particles.⁴³ In addition, oxygen atoms from the carbonyl group can establish H-bonds with residual surface OH groups as suggested in literature.⁴⁶

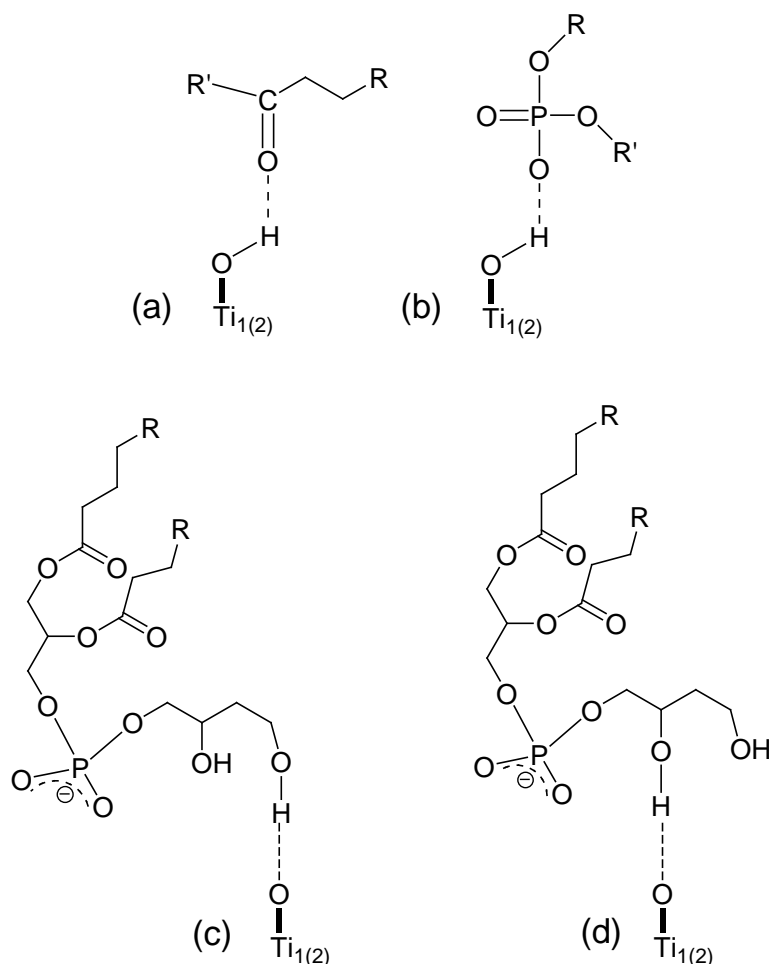


Figure 5.18. Some binding modes of DMPG at pH 9 to surface of TiO_2 . Ti_1 indicates that only one Ti atom in the lattice bind to one oxygen atom (terminal oxygen or Ti_{5c}). Ti_2 denotes that there are two Ti atoms in the lattice bind to one oxygen atom (bridging oxygen).

Although the direct evidence of these binding modes was not observed in this study, the displacement of surface hydroxyl groups on TiO_2 by the adsorption of phospholipids is certain. In order to probe these binding modes, more studies are now required.

5.6 Perspective

This chapter shows at first that the spectroscopic methodology proposed here combining NMR, Raman, MIR and NIR analysis is a good approach to investigate the interactions at the interfaces PL/ TiO_2 in aqueous solutions. The experimental adsorption conditions chosen in a first step to favor the recording of the spectroscopic signals, and not to be perfectly comparable to the experimental conditions of the chapter 4, do not allow us to conclude about the adsorption at low ratio PL/ TiO_2 . Thus, with perhaps too high ratios PL/ TiO_2 , and despite efforts, determining the bond nature of phospholipids onto TiO_2 has not yet been achieved. There is a clear need to further extend this study. For this goal, NMR should

be employed in combination with hydrogen – deuterium exchange method (H/D exchange) in order to follow the signal of ^{31}P . This provides possible insight concerning the involvement of the phosphate moiety into the interaction with surface oxide. In addition, exchange hydrogen by deuterium atom in hydroxyl groups of DMPG can help to determine the implication of these groups into the interaction.

As both phospholipids and TiO_2 surface are very sensitive to the effect of humidity, it would be interesting to follow the adsorption of phospholipids on TiO_2 by controlling H_2O vapor pressure. The role of H_2O has been found to be crucial in the interaction at the solid – liquid interface.

Furthermore, the adsorption of glycerol molecules and phosphate ions (PO_4^{3-}) should be investigated in conjunction with phospholipids by IR spectroscopy in the same conditions. This should bring supplementary information to understand the complex interaction of phospholipids with TiO_2 .

Effect of crystal faces of TiO_2 on the interaction with phospholipids could be investigated through the use of single-crystals. This direction should take advantage of Sum Generation Frequency techniques.

Finally, the effect of ultraviolet light on the adsorbed species can be followed through Diffuse-Infrared spectroscopic study. This step should bring more useful information related to the photocatalytic activity of TiO_2 , particularly towards biomolecules which are directly in contact with the oxide integrated in some commercial products (food, sunscreen...).

References

1. Gong, W. A real time in situ ATR-FTIR spectroscopic study of linear phosphate adsorption on titania surfaces. *Int. J. Miner. Process.* **63**, 147–165 (2001).
2. Connor, P. A. & Mcquillan, A. J. Phosphate Adsorption onto TiO₂ from Aqueous Solutions: An in Situ Internal Reflection Infrared Spectroscopic Study. *Langmuir* **15**, 2916–2921 (1999).
3. Myller, A. T., Karhe, J. J. & Pakkanen, T. T. Preparation of aminofunctionalized TiO₂ surfaces by binding of organophosphates. *Appl. Surf. Sci.* **257**, 1616–1622 (2010).
4. Donnet, J. B. & Muller, F. Properties physico-chimique superficielles des oxides de titane. II. Détermination des sites actifs à la surface des cristaux d'oxyde de titane pigmentaire.. *Bull. Soc. Chim. Fr.* **1**, 9 (1973).
5. Hadjiivanov, K. I., Klissurski, D. G. & Davydov, A. A. Study of Phosphate-Modified TiO₂ (Anatase). *J. Catal.* **116**, 498–505 (1989).
6. Parida, K., Acharya, M., Samantaray, S. & Mishra, T. Studies on Anion Promoted Titania. I: Preparation, Characterization, and Catalytic Activity toward Alcohol and Cumene Conversion Reactions of Phosphated Titania. *J. Colloid Interface Sci.* **217**, 388–394 (1999).
7. Persson, P., Nilsson, N. & Sjöberg, S. Structure and Bonding of Orthophosphate Ions at the Iron Oxide-Aqueous Interface. *J. Colloid Interface Sci.* **177**, 263–275 (1996).
8. Tejedor-tejedor, M. I. & Anderson, M. A. Protonation of Phosphate on the Surface of Goethite As Studied by CIR-FTIR and Electrophoretic Mobility. *Langmuir* **6**, 602–611 (1990).
9. Liu, X., Li, Y., Peng, S., Lu, G. & Li, S. Modification of TiO₂ with sulfate and phosphate for enhanced eosin Y-sensitized hydrogen evolution under visible light illumination. *Photochem. Photobiol. Sci.* **12**, 1903–10 (2013).
10. Bhaumik, a & Inagaki, S. Mesoporous titanium phosphate molecular sieves with ion-exchange capacity. *J. Am. Chem. Soc.* **123**, 691–6 (2001).
11. Lin, L. *et al.* Photocatalytic properties of phosphor-doped titania nanoparticles. *Appl. Catal. B Environ.* **75**, 52–58 (2007).
12. Zhu, B. I. N., Mellander, B. & Chen, J. Cubic alkali orthophosphates with high ionic conductivity. *Mater. Res. Bull.* **28**, 321–328 (1993).
13. Raj, K. J. A., Shanmugam, R., Mahalakshmi, R. & Viswanathan, B. XPS and IR spectral studies on the structure of phosphate and sulphate modified titania – A combined DFT and experimental study. *Indian J. Chem.* **49A**, 9–17 (2010).
14. Takahashi, H., Oi, T. & Hosoe, M. Characterization of semicrystalline titanium(IV) phosphates and their selectivity of cations and lithium isotopes. *J. Mater. Chem.* **12**, 2513–2518 (2002).

15. Jones, D. J. *et al.* High surface area mesoporous titanium phosphate: synthesis and surface acidity determination. *J. Mater. Chem.* **10**, 1957–1963 (2000).
16. Kovalchuk, T. V *et al.* Synthesis, structure, and acidic properties of MCM-41 functionalized with phosphate and Titanium phosphate groups. *J. Phys. Chem. B* **109**, 13948–13956 (2005).
17. Ren, T., Yuan, Z., Azioune, A. & Pireaux, J. Tailoring the Porous Hierarchy of Titanium Phosphates. *Langmuir* **22**, 3886–3894 (2006).
18. Fei, H. *et al.* Facile template-free synthesis of meso-macroporous titanium phosphate with hierarchical pore structure. *Microporous Mesoporous Mater.* **100**, 139–145 (2007).
19. Brow, R. K. Review: the structure of simple phosphate glasses. *J. Non. Cryst. Solids* **263**, 1–28 (2000).
20. Schmutz, C. *et al.* EXAFS, Raman and ³¹P NMR study of amorphous titanium phosphates. *J. Non. Cryst. Solids* **170**, 250–262 (1994).
21. Grussaute, H., Montagne, L., Palavit, G. & Bernard, J. L. Phosphate speciation in Na₂O-CaO-P₂O₅-SiO₂ and Na₂O-TiO₂-P₂O₅-SiO₂ glasses. *J. Non. Cryst. Solids* **264**, 312–317 (2000).
22. Montagne, L., Daviero, D. & Palavit, G. Glass Network Evolution with Bi³⁺/Ti⁴⁺ Substitution in Phosphate Glasses Formulated with a Constant Oxygen/Phosphorus Ratio. EXAFS, XANES, and ³¹P Double Quantum MAS NMR. *Chem. Mater.* **15**, 4709–4716 (2003).
23. Abrahams, I. & Dygas, J. R. Structural and electrical characterisation of Li₂O: TiO₂: SnO₂: P₂O₅ electrolyte glass. *Dalt. Trans.* 3129–3136 (2004).
24. Tiwari, B., Pandey, M., Sudarsan, V., Deb, S. K. & Kothiyal, G. P. Study of structural modification of sodium aluminophosphate glasses with TiO₂ addition through Raman and NMR spectroscopy. *Phys. B Condens. Matter* **404**, 47–51 (2009).
25. Ananthanarayanan, a., Kothiyal, G. P., Montagne, L. & Revel, B. MAS-NMR investigations of the crystallization behaviour of lithium aluminum silicate (LAS) glasses containing P₂O₅ and TiO₂ nucleants. *J. Solid State Chem.* **183**, 1416–1422 (2010).
26. Brauer, D. S., Karpukhina, N., Law, R. V. & Hill, R. G. Effect of TiO₂ addition on structure, solubility and crystallisation of phosphate invert glasses for biomedical applications. *J. Non. Cryst. Solids* **356**, 2626–2633 (2010).
27. Kiani, A. *et al.* Structural characterization and physical properties of P₂O₅-CaO-Na₂O-TiO₂ glasses by Fourier transform infrared, Raman and solid-state magic angle spinning nuclear magnetic resonance spectroscopies. *Acta Biomater.* **8**, 333–40 (2012).
28. Rice, C. V & Wickham, J. R. Heterogeneous Binding of Lipoteichoic Acid to the Surface of Titanium Dioxide as Determined with ³¹P Solid-State NMR Spectroscopy. *J. Am. Chem. Soc. - Commun.* **127**, 856–857 (2005).

29. Wickham, J. R. & Rice, C. V. Solid-state NMR studies of bacterial lipoteichoic acid adsorption on different surfaces. *Solid State Nucl. Magn. Reson.* **34**, 154–61 (2008).
30. Brodard-severac, F. *et al.* High-Field ^{17}O MAS NMR Investigation of Phosphonic Acid Monolayers on Titania. *Chem. Mater.* **20**, 5191–5196 (2008).
31. Humbert, B. Developpements experimentaux et theoriques en spectrometries infrarouge et raman. Application à l'étude des silices divisisées. (1991).
32. Humbert, B., Mevellec, J.-Y., Grausem, J., Dossot, M. & Carteret, C. Spectrométrie d'adsorption dans l'infrarouge. *Tech. l'Ingénieur* 2850 (2012).
33. Scamehorn, R. *Rapid IR Sampling Methods for the Organic Chemistry Laboratory Using a Diffuse Reflectance Accessory.* (1994).
34. Cagnasso, M., Boero, V., Franchini, M. A. & Chorover, J. ATR-FTIR studies of phospholipid vesicle interactions with alpha-FeOOH and alpha-Fe₂O₃ surfaces. *Colloids Surf. B. Biointerfaces* **76**, 456–67 (2010).
35. Tamm, L. K. & Tatulian, S. A. Infrared spectroscopy of proteins and peptides in lipid bilayers. *Q. Rev. Biophys.* **30**, 365–429 (1997).
36. Zhang, X., Borda, M. J., Schoonen, M. A. A. & Strongin, D. R. Adsorption of Phospholipids on Pyrite and Their Effect on Surface Oxidation. *Langmuir* **19**, 8787–8792 (2003).
37. Mendelsohn, R. & Maisano, J. Use of Deuterated phospholipids in Raman spectroscopic studies of membrane structure I. Multilayers of Dimyristoyl phosphatidylcholine (and its -d₅₄ derivative) with distearoyl phosphatidylcholine. *Biochim. Biophys. Acta* **506**, 192–201 (1978).
38. Lippert, J. L. & Peticolas, W. L. Raman active vibrations in long-chain fatty acids and phospholipid sonicates. *Biochim. Biophys. Acta* **282**, 8–17 (1972).
39. Bailey, G. F., Horvat, R. J. & Regional, W. Raman Spectroscopic Analysis of the cis/trans Isomer Composition of edible Vegetable Oils. *J. Am. Oil Chem. Soc.* **49**, 3–7 (1972).
40. Lin-Vien, D., Colthup, N. B., Fateley, W. G. & Grasselli, J. G. *The Handbook of Infrared and Raman Characteristic Frequencies of Organic Molecules.* (Academic Press, 1991).
41. Marcinko, S. & Fadeev, A. Y. Hydrolytic Stability of Organic Monolayers Supported on on TiO₂ and ZrO₂. *Langmuir* **20**, 2270–2273 (2004).
42. Finnie, K. S., Cassidy, D. J., Bartlett, J. R. & Woolfrey, J. L. IR Spectroscopy of Surface Water and Hydroxyl Species on Nanocrystalline TiO₂ Films. *Langmuir* **17**, 816–820 (2001).
43. Copeland, J. R., Santillan, I. A., Schimming, S. M., Ewbank, J. L. & Sievers, C. Surface Interactions of Glycerol with Acidic and Basic Metal Oxides. *J. Phys. Chem. C* **117**, 21413–21425 (2013).

44. Copeland, J. R., Shi, X.-R., Sholl, D. S. & Sievers, C. Surface interactions of C and C(3) polyols with γ -Al₂O₃ and the role of coadsorbed water. *Langmuir* **29**, 581–93 (2012).
45. Tocanne, J. F. & Teissié, J. Ionization of phospholipids and phospholipid-supported interfacial lateral diffusion of protons in membrane model systems. *Biochim. Biophys. Acta* **1031**, 111–42 (1990).
46. Fortunelli, A. & Monti, S. Simulations of lipid adsorption on TiO₂ surfaces in solution. *Langmuir* **24**, 10145–10154 (2008).

General conclusion and outlook

This study investigated the interactions between nanoparticles of TiO₂ and phospholipids in aqueous medium. A first screening step using Laser Doppler Velocimetry and Langmuir films whose organization is highly sensitive to media, was carried out with the popular TiO₂-P25 particles and a large panel of phospholipid molecules. This allowed us to classify phospholipids in two groups.

In the first group, there are the phospholipids that are sufficiently charged and interact with TiO₂-P25 particles solely in acidic media (phosphatidic acid DMPA, phosphatidylserine DMPS), and those which interact with TiO₂-P25 particles on a large pH range (phosphatidylglycerol DMPG and cardiolipin TMCL). The phospholipids DMPA and DMPS interact with TiO₂-P25 particles by electrostatic interactions that are screened by salt in concentrations 10⁻¹ mol/L and 10⁻² mol/L respectively. Obviously, the phosphate group of DMPA is involved in the adsorption on TiO₂-P25 particles, while the carboxylate group in DMPS is at least one of the groups involved in the adsorption on TiO₂-P25 particles. For DMPG and TMCL, the hydroxyl groups of the ending glycerol group are expected to play a role in the adsorption on TiO₂-P25 particles.

In the second group, there are the zwitterionic lipids like phosphatidylcholine DMPC, phosphatidylethanolamine DMPE and sphingomyelin SM, which do not interact with TiO₂-P25 regardless of pH. These phospholipids, widely present in the composition of biological membranes, thus do not favour the anchoring of TiO₂-P25 particles on the membranes.

The different affinities of phospholipids for titanium dioxide help us to understand the separation of only PC, PE and SM phospholipids from milk by chromatography on TiO₂ columns. Indeed, some charged phospholipids that are present in milk were not further identified after the separation and were probably retained on the columns.

Since TiO₂-P25 particles are composed of anatase and rutile phases, the role of the surface crystalline structures was investigated with separated anatase and rutile samples. Surface pressure-area isotherms and batch adsorption experiments performed at pH 2 and pH 9 in aqueous medium showed that DMPA and DMPG, the main adsorbing phospholipids on TiO₂-P25 particles, adsorb on both anatase and rutile surfaces. DMPA adsorbs solely at acidic pH on anatase and rutile, while DMPG adsorbs on rutile and anatase in similar amounts in both acidic and basic media, then by non-electrostatic interactions. The strong interactions

between TiO₂-P25 (85 % anatase + 15% rutile) and DMPA or DMPG at pH 2, as well as the remaining interactions observed between DMPG and TiO₂-P25 at pH 9 and pH 2 in the presence of salt, can be thus understood by the interactions of DMPA and DMPG at pH 2 with both anatase and rutile, and with rutile at pH 9 for DMPG.

The characterization of the bonds by vibrational spectroscopy (infrared and Raman) and ³¹P NMR did not bring a direct evidence of the formation of covalent bonds, as claimed in the literature. Adsorbed phospholipids (DMPA & DMPG) displaced adsorbed H₂O and surface OH groups on TiO₂. They clearly form inner-sphere complexes. While the phosphate group is actually the sole species involved in the adsorption of DMPA on TiO₂, it is less clear for DMPG: the primary and secondary alcohols of the glycerol moiety are mainly involved in the interaction with TiO₂ but also in a less extent, the phosphate group carrying the glycerol group.

In spite of our extensive efforts, there are yet many questions to answer. The effect of ultraviolet light on the interaction is worth studying due to the photo-catalytic activity of TiO₂. The dynamics of phospholipid adsorption on TiO₂ can be followed with H/D exchange method applied in NMR and Infrared spectroscopy. The absence of phospholipid interactions with some anatase samples is quite surprising, thus a fine description of the oxide surface could help us to understand this phenomenon and extend our results to any anatase sample. A single crystal of TiO₂ should be used in the future to investigate the different adsorption behaviors of crystal facets against phospholipids. If humidity can be controlled during IR experiment, the effect of water on the interaction of phospholipids with TiO₂ can be revealed.

Regarding phospholipids, a more complex system (mixture of phospholipids, protein...) can now be studied considering the organization of the phospholipids (that do not mix with each other in any conditions and form lipid rafts with cholesterol). It must be interesting and useful for studying at physiological conditions.

This thesis may have potential implications in biomaterial research considering phospholipids as modifiers, which can render TiO₂ surface biocompatible. Furthermore, understanding the TiO₂-phospholipids interaction can serve as a background to assess the interaction of this oxide with cell, cell membrane or, at larger level, with living beings. This must be useful in toxicology studies in the area of nanomaterials.